

Discovery and characterisation of anti-amyloid beta fibril antibodies from naive phage display VHH libraries

Juan Alberto Fernandez Bonfante, BSc, MSc

Thesis submitted to The University of Nottingham for the degree of
Doctor of Philosophy.

December 2021

Supervised by:

Prof. Kevin Gough (University of Nottingham)

Dr Lisa Chakrabarti (University of Nottingham)

Dr Anthony Scott-Tucker (UCB Celltech)

Dr Patrick Downey (UCB Celltech)

Supervisors previously at UCB Celltech:

Dr Michael Wright

Dr Anastasios Spiliotopoulos

Table of Contents	
Acknowledgements	i
Abstract	ii
Abbreviations	iii
List of Figures	v
List of Tables	viii
1 Chapter 1. Introduction	1
1.1 Protein Misfolding Diseases.....	2
1.1.1 Parkinson’s disease	2
1.1.1.1 Pathology	3
1.1.1.2 Risk factors	6
1.1.2 Alzheimer’s disease.....	8
1.1.2.1 Pathology	10
1.1.2.2 Risk factors	13
1.1.3 Current therapies for PMDs.....	15
1.2 α -synuclein.....	16
1.2.1 Structure	17
1.2.2 Function	18
1.2.3 Pathological Role.....	19
1.3 Different strains (polymorphs) of α -synuclein.....	21
1.4 β -amyloid	25
1.4.1 Structure	25
1.4.2 Function	28
1.4.3 Pathological Role.....	29
1.4.4 Different strains (polymorphs) of Amyloid β	30
1.5 Protein misfolding cyclic amplification (PMCA).....	34
1.6 Thioflavin T Assay.....	36
1.7 Immunotherapy approach to treat protein misfolding diseases.....	37
1.7.1 Therapeutic antibodies targeting α -synuclein	38
1.7.2 Therapeutic antibodies targeting β -amyloid	40
1.8 Use of phage display to develop therapeutically relevant antibodies	43
1.8.1 Passive immunization studies	52
1.8.2 Active immunization studies.....	54

1.9	Aims and objectives.	55
2	Chapter 2: Materials and Methods	56
2.1	Expression of α -syn monomers:	57
2.2	α -syn purification	59
2.3	Preparation of synthetic $A\beta_{42}$ Monomers.....	61
2.3.1	For kinetic studies and characterization studies (at the University of Nottingham)	61
2.3.2	For Biopanning with VHH-phage display library, shaking PMCA and functional assays (in UCB Celltech)	61
2.4	PMCA.....	62
2.4.1	PMCA of α -syn:	62
2.4.2	Amplification of $A\beta$ fibrils:	63
2.5	Other Fibril manipulation procedures	63
2.5.1	$A\beta_{42}$ de novo fibril formation.....	63
2.5.2	$A\beta_{42}$ fibril propagation through incubation.....	63
2.5.3	$A\beta_{42}$ seeded fibril propagation with real time quaking induced conversion (RT-QUIC) 64	
2.5.4	$A\beta_{42}$ fibril fragmentation	64
2.6	Human brain samples	65
2.7	Cerebrospinal fluid samples.....	65
2.8	Thioflavin T assay.	66
2.9	SDS-PAGE gels and western blotting.	66
2.10	Native-PAGE.....	67
2.11	Proteinase K digestion.	67
2.12	Thermolysin treatment.....	68
2.13	Conformational stability assay.....	68
2.14	Densitometry assay.....	68
2.15	Negative stain Transmission Electron Microscopy.	69
2.16	Circular dichroism	69
2.17	Bradford assay.	69
2.18	Phage display biopanning against $A\beta$	70
2.18.1	Target preparation	71
2.18.2	Agar plate preparation.....	71
2.18.3	Biopanning against fibrils.....	71
2.18.4	Colony picking and master plate creation	77
2.18.5	Monoclonal phage enzyme-linked immunosorbent assay (ELISA)	77

2.18.6	Colony polymerase chain reaction (PCR) and sequencing.....	79
2.19	Antibody-FC DNA production	80
2.20	Antibody DNA transfection in Expi™ 293 F cells.....	81
2.21	Small scale purification	82
2.22	ELISA with purified antibodies	83
2.23	Biolayer interferometry (BLI)	84
2.24	Aβ42 functional assays.....	86
2.25	Statistical analysis	86
2.26	MUSCLE sequence alignment and phylogenetic tree	86
2.27	Further methodology used for the amplification and characterisation of fibrils	87
3	Chapter 3. Production and misfolding of recombinant alpha synuclein	89
3.1	Introduction	90
3.2	Purification of α-syn.....	91
3.3	Misfolding experiments using 90 μM α-syn.....	97
3.4	Misfolding experiments using 20 μM α-syn.....	99
3.4.1	Seeding of alpha synuclein misfolding with human samples	100
3.4.1.1	Characterization of human brain samples	100
3.4.1.2	20 μM α-syn PMCA using human seeded samples.....	102
3.4.1.3	Characterization of human seeded samples.....	105
3.4.2	Identifying different polymorphs of α-syn fibrils.....	106
3.4.3	Additional experiments with α-syn.....	111
3.5	Discussion.....	112
3.5.1	<i>De novo</i> misfolding methods	113
3.5.2	Human seeded assays	114
3.5.2.1	Characterization of human brain samples	115
3.5.2.2	PMCA misfolding of seeded samples	116
4	Chapter 4. Production and <i>de novo</i> misfolding of synthetic Amyloid beta.....	120
4.1	Introduction	121
4.2	Solubilization of synthetic Aβ42 and monomer stability analysis	122
4.3	PMCA experiments	124
4.3.1	Parameter optimization tests	124
4.3.2	PMCA with human seeds	129
4.3.3	Using different additives to enhance PMCA	130
4.4	Aβ Incubation experiments.....	135

4.5	RT-QUIC misfolding	138
4.5.1	Synthetic monomer comparison.....	138
4.5.2	Misfolding of monomers with RT-QUIC.....	140
4.6	Fibril fragmentation for phage display.....	143
4.7	Additional experiments with A β 42.	146
4.8	Discussion.....	146
4.8.1	Monomer solubilization	146
4.8.2	PMCA misfolding of Gencust monomers	148
4.8.3	RT-QUIC assays and the misfolding of monomers from two different suppliers	150
4.8.3.1	Misfolding of biotinylated monomers	152
4.8.4	Fibril fragmentation	152
5	Chapter 5. Discovery of Aβ fibril-specific binders through phage display.....	154
5.1	Introduction	155
5.2	Biopanning with a naïve VHH phage display library	156
5.2.1	Panning experiment 1 (P1).....	157
5.2.2	Panning experiment 2 (P2).....	159
5.2.2.1	Panning experiment 2.5 (P2.5).....	160
5.2.3	Panning experiment 3 (P3).....	161
5.3	Sanger sequencing and antibody gene synthesis	163
5.4	Antibody expression, purification and testing.....	168
5.4.1	Binding pattern analysis tin ELISA using purified antibodies	173
5.5	Identification of best fibril binders through BLI.....	175
5.5.1	BLI binding assessment with SA tips	175
5.5.2	BLI binding experiments with AHC tips.....	179
5.6	Discussion.....	181
6	Chapter 6. Discovery of fragmented Aβ fibril-specific binders through phage display and functional assay optimization.....	190
6.1	Introduction	191
6.2	Biopanning against fragmented fibrils.....	192
6.3	Antibody expression and purification	206
6.4	Binding characterization	209
6.4.1	Binding pattern assessment with ELISA.....	209
6.4.2	Identification of best FFB through BLI	211
6.5	Functional assays	215

6.6	Discussion.....	218
6.6.1	Discovery and characterization of FFB.....	218
6.6.2	Functional assay optimization.....	225
7	Chapter 7. Conclusions and future prospects.....	227
7.1	α -syn polymorph generation	228
7.2	A β misfolding and fibril characterization.....	229
7.3	Antibody discovery using UCB's naïve VHH library.....	231
7.4	Future prospects	232
8	References.....	236

Acknowledgements

I would like to thank, first of all, my primary supervisor Prof. Kevin Gough and secondary supervisor Dr Lisa Chakrabarti. I feel honoured to have grown as a scientist following your footsteps, and I have nothing but gratitude for your guidance throughout these years. I hope I was able to keep my initial promise and made you proud.

I would also like to say a big thank you for everyone in ADAS: Ben, Claire, Jon, Keith and Helen, for their kindness. I will carry the skills and techniques learnt under your tutelage for the rest of my career and can only hope to be half as good in teaching them as you have been with me.

To Dr Anthony Scott-Tucker, Dr Anastasios Spiliotopoulos and everybody in the Antibody discovery team (Louise, Aleardo, Cecile, Thomas, Rachel and Matt) I wanted to thank from the bottom of my heart for your patience, friendship and generosity in sharing your vast knowledge. I had the best experience in UCB I could possibly wish for, and thanks to you I have been able to develop both as a scientist but also as a person. To UCB scientists: Olly, Marco and Ilaria, thank you for your support, for your time and teachings.

To my SVMS friends and colleges: Maria, Kate and Anitha, I am thankful for the laughs we shared and grateful for the support given when it was most needed. Working alongside you was a pleasure, and sincerely hope we can collaborate again soon.

To Bethany, Davide, Antonia and Alanna: I feel so thankful for having you as my first flatmates, living together was one of the best experiences I had during my PhD. I feel very lucky to call each one of you my dear friends.

To Rose, thank you for being by my side since the beginning. You made me into a better person and your infinite patience has always kept me grounded. Thank you for your support, company and affection.

Finally, for my family: thank you for always believing in me and for all the support you have given me throughout the years. I will carry your advice in my heart, and I can only hope to keep making you proud during the next chapter of my life.

Abstract

Parkinson's disease (PD) and Alzheimer's disease (AD) are two of the most common incurable neurological disorders affecting the worldwide population over 60 years of age and are characterized by the progressive loss of either motor or cognitive functions in affected individuals. Although the main cause of these diseases remains unknown, genetic, histological and animal models point to the progressive accumulation of misfolded synaptic proteins called alpha-synuclein (α -syn) and amyloid beta ($A\beta$) as the main suspects in, respectively, causing PD or AD. In pathological conditions, α -syn and $A\beta$ have been observed to change their physiological conformations and aggregate into protein polymers, also known as fibrils. These different structures have been directly linked to disease progression, and thus the in depth understanding of these polymers is crucial for future hopes of identifying a cure for PD or AD. Currently, no drugs have been identified with the ability to reverse or reduce the disease burden of these diseases, with available therapies only delaying the inevitable progression of the diseases.

During this project, a way to reproduce these disease-relevant structures was identified through the means of protein misfolding cyclic amplification (PMCA) and real-time quaking induced conversion (RT-QUIC), two methodologies developed for the amplification of protein polymers *in vitro*. By means of different biochemical and imaging methods two distinct α -syn polymorphs and two $A\beta$ conformers were detected.

Next, a naïve VHH library was implemented to discover antibodies against the characterized $A\beta$ fibrils through several rounds of biopanning. This was done for both full-length fibril conformers (or polymorphs) and fragmented fibrils, with the latter strategy targeting the elongation sites responsible for fibril propagation.

Overall, an array of antibodies were discovered that bound to fibrils or fragmented fibrils. The binding properties of these antibodies were then characterized through immunoassays and the measuring of biomolecular interactions with bio-layer interferometry. This was achieved using both fibril

polymorphs, fragmented fibrils, monomers (sourced from one supplier, Genscript) and a mixed solution of monomers, oligomers and protofibrils sourced from another supplier (Gencust). From this analysis it was revealed that fibril binders could be grouped in three categories, depending on their binding affinity to each of the different A β forms tested: 1) binders to all forms tested (including fibrils, monomers, oligomers and protofibrils); 2) binders to both fibril polymorphs and the mixed aggregate solution from Gencust and 3) binders to a single fibril polymorph and Gencust monomers, oligomers and protofibrils. Fragmented fibril binders, on the other hand, could be grouped in 4 categories: 1) binders to fragmented fibrils, both fibril conformers and Gencust monomers, oligomers and protofibrils; 2) binders to fragmented fibrils, one of the fibril polymorphs and Gencust monomers, oligomers and protofibrils; 3) binders to a single fibril polymorph and Gencust monomers, oligomers and protofibrils and 4) binders to all forms of A β tested (including fragmented and both full-length fibril polymorphs, Genscript monomers and Gencust monomers, oligomers and protofibrils).

Functional assays were then attempted for 9 antibodies, producing preliminary data demonstrating that the VHH antibodies identified through phage display might have a protective effect *in vitro* with the inhibition of the formation of fibrils in solution.

Abbreviations

α -syn- α -synuclein

AChE- Acetylcholinesterase

ACID- APP intracellular domain

AD-Alzheimer's disease

AHC- Anti-Human FC kinetic Tips

APP- Amyloid precursor protein

A β - Amyloid β

BLI- Bio-Layer interferometry

BSA- Bovine Serum Albumin

CD- Circular dichroism

CDR- Complementarity-determining regions

CFU- Colony forming units

CH- heavy constant domain

CL- Light constant domain

CNS- Central nervous system

COMT- Catechol-o-methyltransferase

CSF- cerebrospinal fluid
D- Digitonin
DLB- Dementia with Lewy bodies
DS- Dextran sulphate
DMSO- Dimethyl sulfoxide
E. coli- *Escherichia coli*
Fabs- antigen binding fragments
FB-Fibril binders
FF-Genscript fragmented fibrils
FFB- Fragmented fibril binders
FTIR- Fourier-transform infrared spectroscopy
GABA- γ -aminobutyric acid
GCI- Glial cytoplasmic inclusions
GdnHCl-Guanidine hydrochloride
GPe- *globus pallidus externus*
GPI- *globus pallidus internus*
hCMV- Human cytomegalovirus promoter
HFIP- Hexafluoroisopropanol
KO- Knock out
LB- Lewy bodies
LN- Lewy neurites
LTP-Long-term potentiation
MAO- Monoamine oxidase
m/o/pr- Monomers, oligomers and protofibrils (in the context of solubilized Gencust solutions)
MSA- Multiple system atrophy
MSN-Medium spiny neurons
MTL- Medial temporal lobe
Mw-Molecular weight
nACR- Nicotinic acetylcholine receptor
NMDA- N-methyl-D-aspartate
NS-TEM- Negative stain transmission electron microscopy
NTF- Neuro fibrillary tangles
OD- Optical Density
OD630- Absorbance at 630nm (for ELISA)
PEG- Polyethylene glycol
PD- Parkinson's disease
PK- Proteinase K
PMCA- Protein Misfolding Cyclic Amplification
PMD- Protein misfolding diseases
PMSF- Phenylmethylsulfonyl fluoride
PrP-Prion protein
PrP^C- Physiological prion protein
PrP^{Sc}-Pathological prion protein
PS1- Presenilin 1
PS2- Presenilin 2

RT-QUIC- Real Time Quaking Induced Conversion
ROS- Reactive oxygen species
SA- Streptavidin biosensor
scFc-Single Chain-Fc
ScFv- single chain Fv
SN- *Substantia nigra*
SNAP25- Synaptosome Associated Protein 25
SNARE- Soluble NSF attached protein receptors
SNpc- *Substantia nigra pars compacta*
SNpr- *Substantia nigra pars reticulata*
ssDNA- Single stranded DNA
STN- Subthalamic nucleus
SV40 Poly A- Simian virus 40 PolyA
TAE- Tris-Acetate-EDTA
TgM83-Transgenic mice expressing mutated A53T human α -syn
ThT- Thioflavin T
ThLY- Themolysin
TSE- Transmissible spongiform encephalopathies
t-SNARE- Target SNARE
VH- heavy variable domain
VHHFc-Two VHH subunits connected by human FC
VL- Light variable domain
v-SNARE- Vesicle SNARE

List of Figures

Chapter 1:

Figure 1-1: Clinical signs and time course of PD progression:	3
Figure 1-2: Basic anatomy of basal ganglia.	5
Figure 1-3: Schematic representation of the circuits of the basal ganglia.	5
Figure 1-4: Sequence of pathogenic events leading to Alzheimer's disease.	10
Figure 1-5: Structure of α-synuclein.	18
Figure 1-6: Processing of human APP	26
Figure 1-7: Structure of $A\beta$	28
Figure 1-8: Schematic representation of fibril propagation through PMCA	35
Figure 1-9: Schematic representation of M13 bacteriophage	44
Figure 1-10: Different forms of antibody and fragments	47
Figure 1-11: Example of human phage display library construction	49
Figure 1-12: The phage display process in solution	51

Chapter 2:

Figure 2-1: α-syn vector map	57
Figure 2-2: Schematic representation of VHH and VHH-page particle	70

Figure 2-3: VHH phagemid vector.....	72
Figure 2-4: Panning strategies	73

Chapter 3:

Figure 3-1: Analysis of filtered cell culture supernatant.....	91
Figure 3-2: HiTrap™ Q FF filtration step	92
Figure 3-3: Mono Q filtration step	94
Figure 3-4: HiLoad™ 26/600 Superdex™ 75 pg size exclusion chromatography step	96
Figure 3-5: Time course of de novo misfolding of 90 μM α-syn	97
Figure 3-6: Preformed fibril seeding of PMCA reaction	99
Figure 3-7: Misfolding assessment with 20 μM α-syn	99
Figure 3-8: Characterization of human cytosolic brain fractions.....	101
Figure 3-9: Human seeded PMCA experiments.....	103
Figure 3-10: Morphological assessment of the different band patterns with NS-TEM and CD	104
Figure 3-11: Comparison between human and de novo seeded samples	106
Figure 3-12: Proteolytic digestion of cytosolic brain extracts	108
Figure 3-13: Assessing the effects of pre-digested brain samples on α-syn misfolding	109
Figure 3-14: PMCA passage of α-syn polymorphs.....	110
Figure 3-15: Conformational stability assay of α-syn polymorphs.....	111

Chapter 4:

Figure 4-1: Characterization of Aβ42 fibrils.....	123
Figure 4-2: Monomer stability assessment	124
Figure 4-3: PMCA parameter optimization- Amplitude	126
Figure 4-4: PMCA parameter optimization- Sonication time	128
Figure 4-5: PMCA with AD brain	130
Figure 4-6: PMCA with different additives	132
Figure 4-7: Further assessment of the effects of additives on human seeded PMCA	133
Figure 4-8: In-depth comparison of brain-seeded and non-seeded samples.....	134
Figure 4-9: Comparison of incubated and sonicated samples for fibril formation	136
Figure 4-10: Morphological comparison of incubated and sonicated fibrils.....	137
Figure 4-11: Incubation experiment with brain seeding.....	138
Figure 4-12: Comparison of Gencust vs Genscript monomers.....	140
Figure 4-13: RT-QUIC on seeded Genscript monomers	142
Figure 4-14: RT-QUIC on biotinylated monomers	143
Figure 4-15: Fibril fragmentation.....	145

Chapter 5:

Figure 5-1: Biotinylation test on modified fibrils	157
Figure 5-2: Analysis of panning experiment 1 (P1), targeting Gencust fibrils.....	159
Figure 5-3: Analysis of panning experiment 2.5 (P2.5), targeting Gencust fibrils.....	161

Figure 5-4: Analysis of panning experiment 3 (P3), targeting Genscript fibrils	162
Figure 5-5: Fibril-specific binder PCR	163
Figure 5-6: Examples of Sanger sequencing chromatograms of fibril-specific binders	165
Figure 5-7: Different antibody formats and sequence alignment	168
Figure 5-8: Expression test of VHHFc, scFc and control antibodies using AHC tips	169
Figure 5-9: Binding pattern comparison between VHHFc and scFc with ELISA	171
Figure 5-10: Examples of purification of fibril binding antibodies	172
Figure 5-11: In-depth binding pattern analysis of fibril binders of interest.....	174
Figure 5-12: BLI experiments measuring SA tip background binding.....	176
Figure 5-13: BLI experiments-SA tip immobilised Genscript fibril binding to antibodies.....	177
Figure 5-14: BLI experiments-SA Gencust fibril binding.....	178
Figure 5-15: Traces of all antibodies tested with SA tips and Gencust fibrils	179
Figure 5-16: BLI experiments-AHC Gencust fibril binding.....	180
Figure 5-17: BLI experiments-AHC Genscript monomer binding.....	181

Chapter 6:

Figure 6-1: Model of A β aggregation	191
Figure 6-2: Fragmented fibril biotinylation test	193
Figure 6-3: Fragmented fibril biopanning, selection 1, monoclonal ELISA screening of phage antibodies	195
Figure 6-4: Fragmented fibril biopanning, selection 2, monoclonal ELISA screening of phage antibodies	196
Figure 6-5: Fragmented fibril biopanning, selection 3, monoclonal ELISA screening of phage antibodies	197
Figure 6-6: Antibody DNA sequence amplification through PCR	198
Figure 6-7: Protein sequence alignment of FF-specific antibodies	203
Figure 6-8: Alignment of FFB and FB CDR3 sequences.....	204
Figure 6-9: FFB and FB C-terminal phylogenetic tree.....	205
Figure 6-10: Antibody expression test with BLI	206
Figure 6-11: FFB small scale purification with PhyNexus system	207
Figure 6-12: Monoclonal ELISA with purified antibodies.....	211
Figure 6-13: Genscript monomer binding with AHC tips	211
Figure 6-14: Genscript fibril binding with AHC tips.....	212
Figure 6-15: Gencust fibril binding with AHC tips	213
Figure 6-16: biotinylated fragmented Genscript fibril binding with AHC tips.....	214
Figure 6-17: biotinylated fragmented Genscript fibril binding with SA tips	215
Figure 6-18: Functional assay- Assessment of monomer misfolding and control antibody inhibition	216
Figure 6-19: Functional assay- inhibition of fibril forming process through the use of FFB and FB	217

List of Tables

Chapter 1:

Table 1-1: Risk factors for Parkinson's disease	7
Table 1-2: Risk factors for Alzheimer's Disease	14
Table 1-3: α -syn polymorphs/strains	24
Table 1-4: A β polymorphs.....	33
Table 1-5: Characterization of the therapeutic antibodies against α -syn	40
Table 1-6: Characterization of the therapeutic antibodies against A β	43
Table 1-7: Genes and proteins coded by the M13 filamentous phage genome [224, 229]	45
Table 1-8: Genetic makeup of phagemid and helper phage.....	46

Chapter 2:

Table 2-1: Summary of additional experiments performed with α -syn	87
Table 2-2: Summary of additional experiments performed with A β 42.....	88

Chapter 3:

Table 3-1: Brain homogenate protein concentration as measured with Bradford assay.....	100
Table 3-2: Summary of additional experiments performed to misfold α -syn in different conditions	112

Chapter 4:

Table 4-1: Summary of additional experiments performed with A β 42.....	146
---	-----

Chapter 5:

Table 5-1: cfu values throughout three rounds for experiment P1.....	158
Table 5-2: cfu values for the two rounds of panning for experiment P2.....	160
Table 5-3: cfu values for the three rounds of panning for experiment P2.5	160
Table 5-4: cfu values for the three rounds of panning for experiment P3	162
Table 5-5: Protein sequences of fibril-specific antibodies	166
Table 5-6: control scFv antibody sequences	167
Table 5-7: Fibril-binding and control antibody concentration measured with Nanodrop	173

Chapter 5:

Table 6-1: cfu per round of biopanning against FF	194
Table 6-2: FFB amino acid sequences	199
Table 6-3: identification of sequence homologies within the discovered FFB	200
Table 6-4: Unique FFB sequences	202

Table 6-5: Calculation of the extinction coefficient and Molecular weight (Mw) of each VHHFc FFB	208
Table 6-6: Summary of binding properties of all FB and FFB identified through phage display.	223

Chapter 1. Introduction

1.1 Protein Misfolding Diseases.

Most proteins are capable of performing their function thanks to a specific and organized three-dimensional structure specific to each molecule. This structure can either be achieved spontaneously or by the use of molecular chaperones [1]. As the structure of a protein is so intertwined with its function, when the structure of a particular protein is compromised, its activity is also affected. It is now apparent that different diseases are caused by the loss of function of one or more specific proteins and/or the accumulation of the concomitant misfolded proteins within tissue. Further studies have demonstrated that these pathologies were often caused by either genetic or sporadic modifications to a protein sequence/structure, and also that diseases generated by the accumulation of misfolded proteins were more predominant in later stages of life, where the misfolded protein deposits had accumulated over many years [2].

These categories of illnesses have been classified as Protein Misfolding Diseases (PMDs). Well known examples affect the central nervous system (CNS) and include Parkinson's Disease (PD), Alzheimer's Disease (AD) and Transmissible Spongiform Encephalopathy (TSE). PD is caused by the accumulation of misfolded α -synuclein (α -syn) into what are known as Lewy bodies (LB) [3, 4]. AD is characterized by the accumulation of β -amyloid (A β) plaques and Tau fibrils [5]. TSE is caused by the accumulation of the pathological form of the prion protein (PrP^C), designated PrP^{Sc} [6]. PMDs can also cause accumulation of misfolded proteins and pathology outside of the CNS, for example type II diabetes [7] and cystic fibrosis [7, 8], among others.

1.1.1 Parkinson's disease

PD is one of the most common neurodegenerative diseases in the aging population, affecting around 2% of people aged over 65 years of age [9]. The main pathological hallmarks of the disease are the death of a dopaminergic neural population in the *substantia nigra* (SN) and the progressive accumulation of α -syn aggregates, known as Lewy bodies and Lewy neurites (LN) throughout the brain [10, 11]. PD manifests itself as series of motor dysfunctions such as muscle rigidity (resistance to

passive limb movement); bradykinesia (slow movement); hypokinesia (reduced amplitude of bodily movement); akinesia (hindered voluntary movement); hypomimia (reduced degree of facial expression) and resting tremor [9, 12]. With the progression of the disease 80% of patients show signs of falls and freezing and 50% of patients suffer from dysphagia (with concomitant increase in the risk of choking). Alongside the motor symptoms, in later stages of PD, patients can additionally suffer from autonomic symptoms, such as incontinence and increased orthostatic hypotension. Finally, at around two decades post diagnosis, around 83% of patients start to show signs of dementia (figure 1.1) [11].

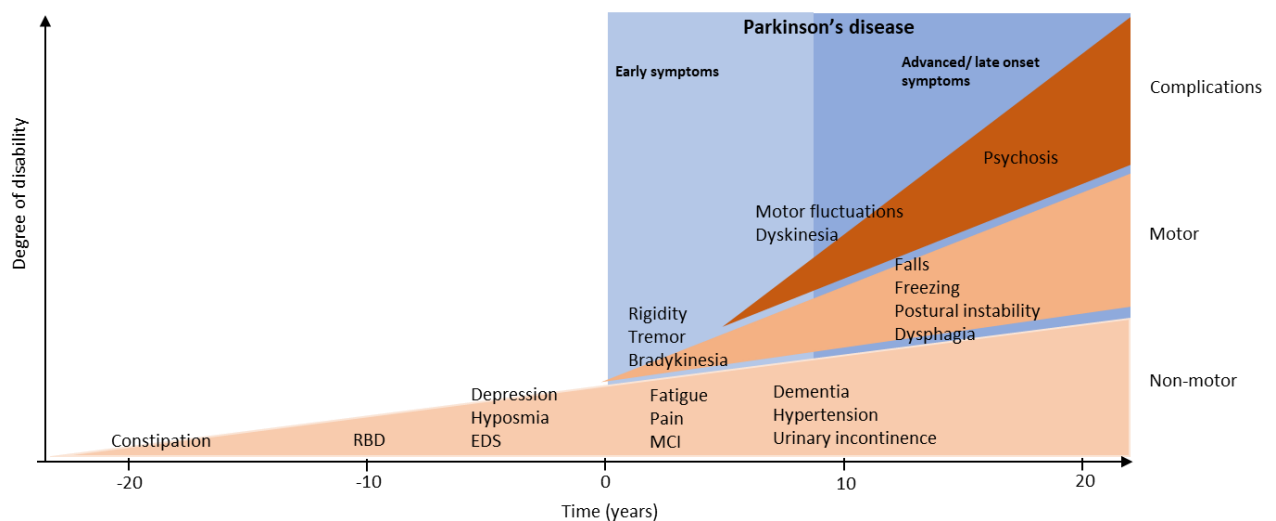


Figure 1-1: Clinical signs and time course of PD progression:

PD diagnosis occurs with the onset of motor symptoms (indicated as year 0) but can be predated by a series of non-motor prodromal symptoms for the 20 years leading to the diagnosis. Non-motor symptoms also develop following the diagnosis and worsen as the disease progresses, causing considerable functional disability. In advanced stages of the disease axial motor symptoms, such as falls, speech difficulties, freezing and postural instability can occur. RBD= REM sleep behaviour disorder; EDS= Excessive daytime sleepiness; MCI= Mild cognitive impairment. Image adapted from Kalia *et al.*, 2015 [11]. License number 5120760680767.

1.1.1.1 Pathology

Although the aetiology of PD is yet to be fully understood, most of the symptomatology can be explained by a severe deregulation of the motor circuits of patients. Among these, the basal ganglia seem to be the most affected by this condition. The basal ganglia are a series of nuclei distributed

between the midbrain, diencephalon and cortex whose main function is the fine regulation of voluntary movement. The basal ganglia are constituted by five interrelated nuclei: SN, comprised of *substantia nigra pars compacta* (SNpc) and *substantia nigra pars reticulata* (SNpr); *globus pallidus*, comprised of the *globus pallidus internus* (GPi) and *globus pallidus externus* (GPe); subthalamic nuclei (STN), caudate nuclei and putamen (figure 1.2). The two latter nuclei, despite being anatomically separated by white matter in the brain of human beings, are effectively interconnected by numerous grey matter links. Due to this close interaction these two nuclei are referred together as the “striatum” [13]. The modulatory function of the basal ganglia is enacted thanks to the differential activation of one of two pathways: the “direct”, and “indirect” pathways (figure 1.3) [14]. In the direct pathway, glutamatergic (excitatory) signals are delivered from the cortex and thalamus to the striatum, the main data collection point for the circuit. The main population of cells within the striatum are known as medium spiny neurons (MSN), they are predominantly inhibitory neurons, as they release γ -aminobutyric acid (GABA). The glutamatergic thalamocortical afferents excite these inhibitory neurons, which in turn project to both the GPi and SNpr. The GPi and SNpr are an important component of the basal ganglia as they serve as the “output nuclei” of the circuit, as they project directly to the ventrolateral nucleus of the thalamus, an important integrative centre for motor control. Prior to the activation of the direct pathway the output nuclei exert a tonic inhibitory control upon the ventrolateral nucleus of the thalamus through release of GABA. Upon the activation of the direct pathway the GABA released by the MSN serves to downregulate the activity levels of the GPi and SNpr, thus releasing the sub thalamic nucleus from the tonic GABAergic inhibition and promoting movement through glutamatergic neurons innervating both the cortex and striatum. In the indirect pathway, on the other hand, another set of MSN project to the GPe. The GPe is characterized by the prevalence of GABAergic neurons that innervate the STN (the only glutamatergic nucleus within the basal ganglia), and the output nuclei. The activation of the indirect pathway determines the inhibition of the GPe that releases the excitatory STN from tonic inhibition resulting in a net excitatory stimulus of the output nuclei; which in turn inhibits the ventrolateral nucleus of the thalamus and prevents the

onset of movement. In this way, the STN play a central role in the regulation of the indirect pathway, as it is able to regulate not only the activity of the output nuclei [12], but also the GPe, through a retrograde excitatory loop [13, 14].

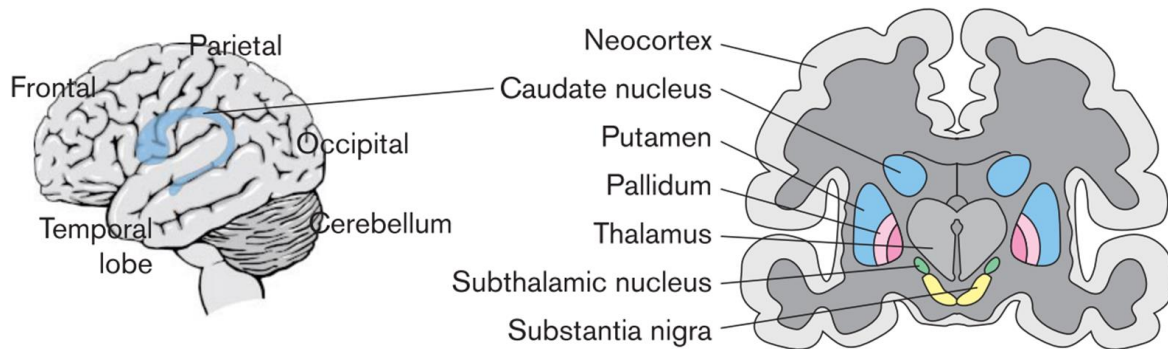


Figure 1-2: Basic anatomy of basal ganglia.

Anatomical localization of the different nuclei within the basal ganglia: the Striatum (in blue), constituted by the caudate nucleus and putamen; the *globus pallidus*, divided in *globus pallidus externus* (in bright pink) and *globus pallidus internus* (in dark pink); Thalamus (in grey) and subthalamic nuclei (in green) and *substantia nigra* (in yellow). Image adapted from Graybiel *et al.*, 2000 [15]. Licence number 5120760413037

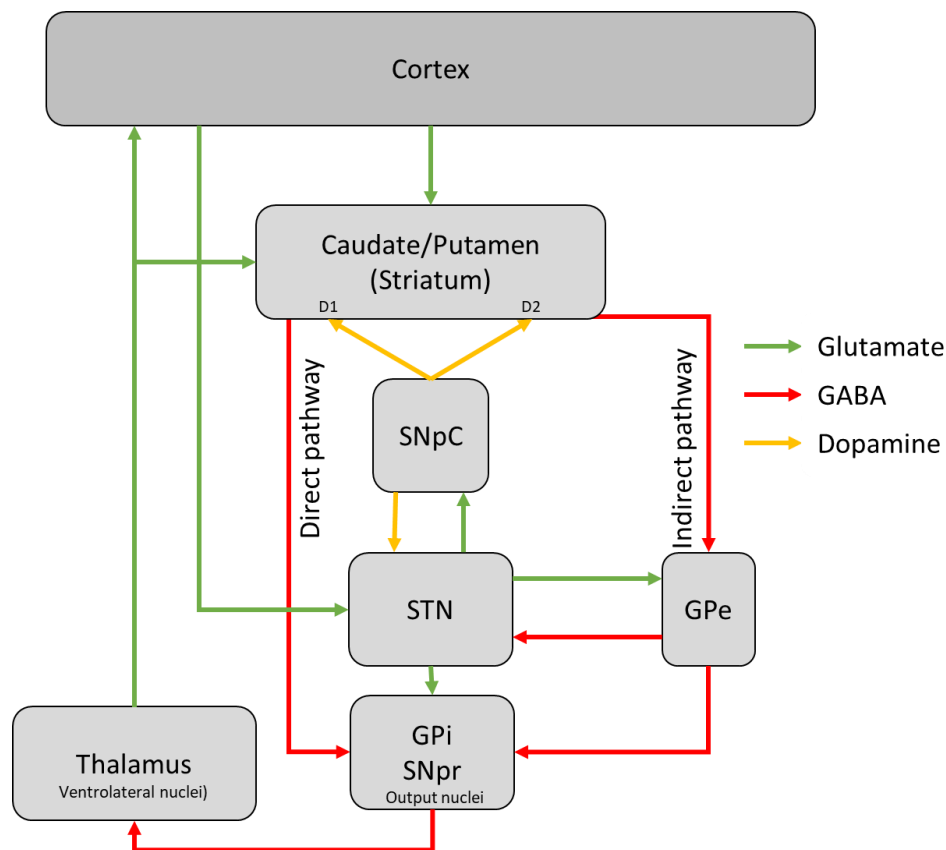


Figure 1-3: Schematic representation of the circuits of the basal ganglia.

The basal ganglia are one of the main hubs for fine motor control in the CNS through the activation of the direct and indirect pathway. In the direct pathway, excitatory stimuli from the cortex and thalamus are integrated in the striatum. The striatum then outputs inhibitory stimuli to the tonically activated output nuclei, this results on the activation of the ventrolateral nuclei in the thalamus, and output of excitatory signals to the cortex and striatum, promoting the generation of movement. In the indirect pathway striatal projections inhibit the activity of the GPe, releasing the STN from tonic inhibition. The STN in turn upregulate the activity of the output nuclei, which results in the inactivation of the sub thalamic nuclei. As the thalamic output ceases, so does movement. Within this process dopamine plays an important role regulating the activation of either pathway through D1 or D2 receptor stimulation; in PD pathological conditions the lack of dopaminergic stimulus determines the tonic activation of the indirect pathway, resulting in the characteristic motor symptoms of PD. SNpC= *Substantia nigra pars compacta*; SNpR= *Substantia nigra pars reticulata*; GPe= *Globus pallidus externus*; GPi= *Globus pallidus internus*; STN= Sub thalamic nuclei. Image adapted from Blandini *et al.*, 2000[13], modified.

In addition to the role of the direct and indirect pathway in the regulation of movement, dopamine is a key factor to ensure the correct function of this circuit. This is evidenced by the fact that within the striatum, the MSN belonging to the direct or indirect pathway can be distinguished by the expression of either the D1 or D2 dopaminergic receptors. These two types of receptors are capable of increasing or decreasing the excitability of MSN, respectively, and thus modulating the activity of these interneurons [16]. The importance of these receptors is evidenced by the fact that beyond the thalamocortical projections, the striatum is innervated by dopaminergic neurons deriving from the SNpc [13]. Under physiological conditions the correct functionality of the basal ganglia is present through the release of dopamine activating the MSN in the direct pathway via the D1 receptors and inhibiting the indirect pathway through the D2 receptors. In pathological conditions, this fine regulation is no longer achieved. As stated, one of the main hallmarks of PD is the chronic loss of dopaminergic cells in the SN, in particular in the SNpc. Lacking a dopaminergic input, D2 inhibitory receptors are no longer stimulated, inducing a striatal MSN response by an over activation of the indirect pathway, that results in the chronic activation of the output nuclei and therefore tonic inhibition of the ventrolateral nuclei of the thalamus leading to reduced mobility and the symptoms found in PD (figure 1.3) [11, 12].

1.1.1.2 Risk factors

Although no clear cause of PD has been identified (table 1.1), it is well known that several environmental and genetic risk factors play a role in the development of the disease. The prevalence of PD has been identified to be higher in Europe, North and South America when compared to other

countries. Other environmental risk factors include exposure to pesticides, rural living, use of β -blockers, head injuries and well water drinking [11]. Among these environmental factors, exposure to pesticides seems to have the strongest correlation to the development of PD. In particular, studies show that the use of pesticides such as paraquat, rotenone and maneb have been found to induce PD symptomatology by interfering with mitochondrial activity through the blockage of the mitochondrial complex I, inducing the generation of reactive oxygen species (ROS) [10]. Genetics also play a fundamental role in the development of PD, as mutations have been observed in both sporadic and familial cases [17]. One of the first studies that recognized the involvement of genetics in the development of PD was the revolutionary work performed by Polymeropoulos *et al.* (1997) in which a missense mutation in the *SNCA* gene found in an Italian cohort was correlated to the early onset of PD [3]. Following these initial discoveries, other missense mutations and gene locus multiplications correlating with an increased risk of developing PD have been discovered. To date, mutations in 5 genes have been directly linked to the autosomal dominant transmission of PD: *SNCA*, *LRRK2*, *VPS35*, *EIF4G1* and *CHCHD2*. An additional 5 genes have been identified to play a role in autosomal recessive transmitted PD: *DJ1*, *parkin*, *PINK1*, *RAB39B* and *DNAJC6* [9] (table 1.1). For an in depth review of the role of genetics in PD please refer to Kallia *et al.*, 2015 [11]; Ferrerira *et al.*, 2017 [9] and Soukup *et al.*, 2018 [17].

Table 1-1: Risk factors for Parkinson's disease

Environmental risk factors					
<ul style="list-style-type: none"> • Country of origin • Pesticide exposure • Rural living • Head injury • B-blocker use • Well water drinking 					
Most prominent genetic risk factors					
Gene	Protein	Function	Mutation	Inheritance	
<i>SNCA</i>	α -synuclein	Neurotransmitter release; cellular respiration; vesicle transport.	<ul style="list-style-type: none"> ❖ A53T ❖ A30P ❖ E46K ❖ H50Q ❖ G51D ❖ Gene duplicates/triplicates 	Autosomal dominant	
<i>LRRK2</i>	leucine-rich repeat kinase 2	Neurite growth, synapsis formation/morphology,	<ul style="list-style-type: none"> ❖ I1371V ❖ N1437H 	Autosomal dominant	

		autophagy, vesicle transport, synthesis of new proteins.	❖ R1441C ❖ R1441G ❖ R1441H ❖ Y1699C ❖ I2020T ❖ G2019S	
<i>VPS35</i>	Vacuole protein sorting 35	Vacuole transport.	❖ D620N	Autosomal dominant
<i>EIF4G1</i>	Eukaryotic translation initiation factor 4-gamma	Binding between mRNA and ribosomes.	❖ R120H substitution ❖ A502V substitution	Autosomal dominant
<i>CHCHD2</i>	Coiled-coil-helix-coiled-coil-helix domain containing 2 protein,	Transcription factor with an influence over mitochondrial respiration.	❖ T61I ❖ R145Q ❖ Splice site alterations	Autosomal dominant
<i>DJ1</i>	Human protein deglycase DJ-1	Regulation of oxidative stress, protein homeostasis. Inhibition of α -syn aggregation [18, 19].	❖ Exon shuffling ❖ Missense mutations ❖ splice site mutations. No specific mutation linked to PD onset	Autosomal recessive
<i>parkin</i>	E3 ubiquitin ligase	Mitophagy.	❖ Missense mutations ❖ Nonsense mutations ❖ Exon shuffling ❖ Splice site mutations ❖ Deletions and insertions. No specific mutation linked to PD onset	Autosomal recessive
<i>PINK1</i>	Phosphate and tensin homolog-induced putative kinase 1	Transcription of kinase protein.	❖ Missense mutations ❖ Altered gene copy number ❖ Exon shuffling No specific mutation linked to PD onset	Autosomal recessive
<i>RAB39B</i>	Rab GTPase	Regulatory proteins involved in vesicle transport and membrane trafficking and synaptic activity.	❖ Gene deletions ❖ Missense mutations No specific mutation linked to PD onset	Autosomal recessive
<i>DNAJC6</i>	HSP40 Auxilin	Regulating chaperone activity and clathrine mediated endocytosis.	A handful of mutation carriers identified worldwide- no specific mutation linked to PD	Autosomal recessive

1.1.2 Alzheimer's disease

Alzheimer's disease is the most common neurodegenerative disease, affecting up to 30% of the aging population. AD is additionally considered to be the current leading cause of dementia worldwide, being responsible for 50-70% of all reported cases. Clinically, AD patients suffer from deteriorated episodic memory and mild cognitive impairment. As the disease progresses the cognitive difficulties and memory loss worsen; patients lose their ability to multitask, recognize their surroundings (topographagnosia) and perform everyday activities. In the final years of the disease, patients present behavioural changes (depression, anxiety and aggression are the most common), hallucinations and motor difficulties. Patients usually succumb to the disease within 8-10 years after the diagnosis [20, 21]. Within the brain, AD does not seem to be localized within a specific brain region or affect a specific

neurotransmitter system. AD pathology promotes widely distributed neurodegeneration in the neocortex of patients, hampering a plethora of neurotransmitter systems including cholinergic, glutamatergic and noradrenergic neurons [22]. Although AD is mainly a sporadic disease, mutations have been linked to familial cases of early onset AD [20]. For a more in depth review regarding the genetics involved in AD please refer to Masters *et al.*, 2015 [22] and Liu *et al.*, 2019 [23].

The two major pathological hallmarks for AD are the accumulation of amyloid β plaques and neurofibrillary tangles (NFT) [22]. These aggregates are distinguished by their protein composition: while plaques consist of amyloid beta peptide with 40 or 42 amino acids ($A\beta_{40}$ and $A\beta_{42}$), NFTs are made up of misfolded hyperphosphorylated Tau. As these aggregates spread within the brain, they induce cell death and an inflammatory immune response within the newly infected areas, representing a widespread neurodegenerative process [24]. Beyond the accumulation of protein deposits, other pathological adaptations are observed. These include mitochondrial dysfunction, synapse loss, calcium and metal homeostasis imbalances and issues in the vascular and lymphatic systems. All of these processes likely contribute in different degrees to the clinical onset and development of the disease [23]. Macroscopically, the AD brain is characterized by the presence of generalized cortical atrophy (with particular emphasis on the medial temporal lobe) and enlargement of the ventricles. The visual, motor and sensory cortex are less affected by the disease. Microscopically, histological sections reveal extensive microglial activation, astrogliosis, dystrophic neurites, neuropil threads and, more prominently, protein accumulation; with extracellular $A\beta$ plaques and intracellular NFTs (figure 1.4). Within the hippocampus, it is also possible to find two lesser known processes, directly linked to AD: Hirano bodies and granulovascular degeneration [20-23].

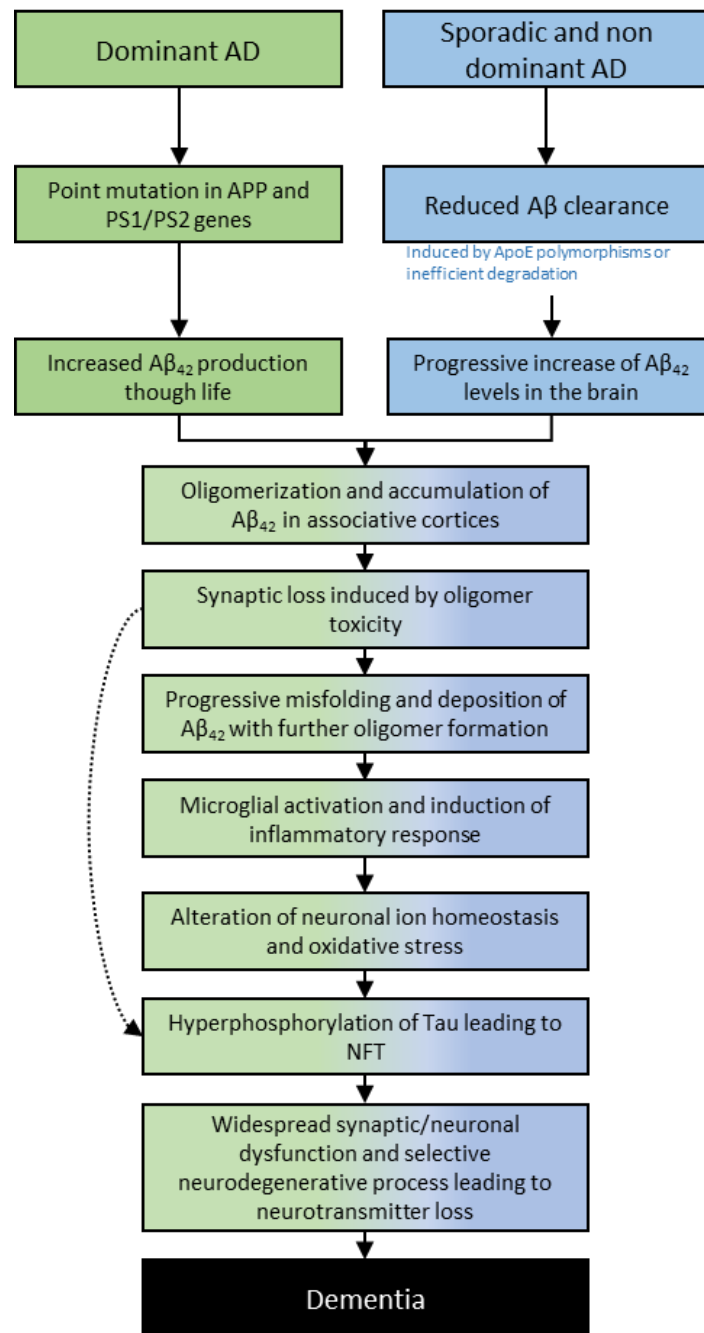


Figure 1-4: Sequence of pathogenic events leading to Alzheimer’s disease.

The dotted arrow indicates that oligomers might directly cause neurodegeneration, synaptic loss and Tau hyperphosphorylation. Dominant AD is characterized by the comparison of symptoms in individuals younger than 65 years of age, and is induced by autosomal inheritable mutations in the genes responsible for the production and processing of Aβ. Sporadic and non-dominant AD on the other hand, is the most common form of AD, and is caused by sporadic mutations in the genome of patients, or the presence of specific polymorphs, such as the ApoE4. Image adapted from Selkoe *et al.*, 2016 [25], modified. Licence under the CC BY 4.0.

1.1.2.1 Pathology

Like PD, the mechanisms that kickstart AD pathology are not yet fully understood. Widespread neurodegeneration is the root cause of cognitive impairment in affected individuals. In particular, the

medial temporal lobe (MTL) is one of the first areas in which AD pathology is observed and consequently one of the most affected areas as the disease progresses. The MTL is comprised of the hippocampus, parahippocampal cortex, entorhinal cortex and perirhinal cortex and is responsible for recollection and familiarity, processing of the “when” and “where” of a memory [26]. MTL impairment explains the initial memory deficiency experienced by patients. One of the main agents of neurodegeneration in the AD brain are A β plaques and NFTs. They have the ability to spread through the brain causing cell death and neuroinflammation, and the A β plaque and NFT burden in the brain directly correlate with the extension and severity of pathology [27]. Therefore, understanding the formation and biological consequences of these protein aggregates is essential to comprehend AD. Starting with A β deposits, two kinds of plaques can be found in the brain: diffuse and core dense plaques; while diffuse plaques are thought to be nontoxic and are present in non-demented aged individuals, dense core plaques are only found in AD cases. Dense core plaques are highly toxic, promoting neurodegeneration, synapse loss and a localized inflammatory response. This toxicity can be attributed to the fact that dense core plaques are mainly constituted of misfolded A β 42 and act as a reservoir for this pathogenic peptide. The concept of toxic “penumbra” or “halo” has been used to describe a 50 μ m ring around dense core plaques with increasing neurodegeneration and synaptic loss [21, 28]. A β 42 assumes a more pathogenic role than other A β isoforms, such as A β 40, due to the addition of two hydrophobic amino acids (isoleucine and alanine) at the C-terminus of the A β 42 peptide. This determines the increased tendency of the A β 42 monomers to aggregate and form oligomers, fibrils and dense core plaques [29]. A β 42 has been found to inhibit normal brain function by promoting cell death, downregulating synaptic activity and hampering neuronal connectivity in affected areas. Plaques have also been found to propagate in the brain following a predictable pattern; this allowed scientist to subdivide the disease progression in three stages, based on A β plaque deposition: stage A, where A β deposits are mainly found in the basal neocortex of patients; stage B where plaques spread in the adjacent neocortical areas and hippocampal formations and the final stage C, in which A β deposits spread throughout the cortex of affected individuals [27]. Interestingly,

regardless of their inherent toxicity, total A β accumulation seems to plateau quite early in the disease, with maximum levels being reached as early as the onset of the symptoms in AD [30, 31], therefore A β accumulation is not used as a marker for disease progression.

NFTs, the other main hallmark of AD, are intracellular protein deposits (consisting of hyperphosphorylated Tau) with a paired helical structure. It is possible to distinguish at least three different stages of Tau fibrillization within the brain of AD patients: i) soluble NFTs with diffuse Tau aggregates localized within otherwise healthy looking neurons; ii) fibrillar NFTs where Tau deposits assume a fibrillar shape and are predominant in the cytoplasm, extending from the axon to dystrophic neurites, and displacing the nucleus to the periphery of the perikaryon; iii) Extracellular NFTs, where the neuron dies leaving behind prominent Tau fibrillar deposits [21]. Tau is a protein involved in microtubule stability and axon transport. The hyperphosphorylation and subsequent aggregation of this protein determines the dysregulation of these systems and leads to the death of affected neurons [23, 32]. Interestingly, like A β plaques, NFTs do seem to follow a predictable deposition pattern that better correlates with disease progression [27]. Tau aggregation can first be detected in the cortical regions of the MTL, as the disease progresses NFTs spread to the brain cortex, mainly affecting the frontal regions of the brain; visual, motor and sensory cortex remain mostly undisturbed throughout the disease.

As previously mentioned, A β deposition seems to have a more prominent role in early stages of the disease, evidenced by the early accumulation of this protein and genetic data [20]. Tau, on the other hand, is more strongly linked to disease progression and cognitive decline, with NFTs slowly spreading throughout the brain as clinical and cognitive symptoms deteriorate [31]. Although mutations in the gene responsible for the production of Tau (MAPT) are linked to the development of a series of neurological diseases termed Tauopathies, very few genetic links have been established between MAPT mutations and AD. So far, only one MAPT point mutation has been identified as increasing the risk of developing AD (mutation A152T) [33, 34]. Overall, genetic and histological findings suggest that

AD is the result of a complex interplay of genetic and environmental factors, that together determine the onset of the disease.

1.1.2.2 Risk factors

As with PD, risk factors for the development of AD can be subdivided into environmental and genetic (table 1.2). As for the environmental risk factors, the most prominent is age, with older individuals being more at risk of developing this condition. Other risk factors include diabetes mellitus, hypertension, obesity, sedentary lifestyle, depression, smoking, cerebrovascular disease and poor educational attainment [22]. Gender also seems to influence the risk, as AD seems to be higher in women [28] and the incidence seems to be the same regardless of the geographical population considerations [22].

Genetic risk factors play a major role in the developing of AD, as around 70% of late onset (sporadic) cases have been directly linked to genetic alterations [20]. Furthermore, inherited forms of AD (causing early onset pathology) are estimated to represent up to 5% of all reported cases [23]. As such, mutations in several genes have been linked to the development of AD (for an in-depth review please see Rosenberg *et al.*, 2019 [35]). Mutations in genes linked to the production, processing and clearance of A β 42 have been found to particularly contribute to the risk of developing AD. The most prominent among these are: the amyloid protein precursor protein (APP), *presilin 1 (PS1)*, *presilin 2 (PS2)* and apolipoprotein E (*ApoE*). APP is a membrane protein mainly involved in signal transduction, synapse formation, synapse plasticity and neuroprotection [36]. As part of the physiological processing of this protein, APP is subjected to cleavage by two proteolytic enzymes, β and γ -secretase which result in the production of A β 40 and A β 42. It has been observed that mutation in the *APP* gene are directly linked with early onset AD. Two mutations in the recognition site for the γ -secretase are of particular interest: the KM670/671NL (Swedish) mutation and the A673T (Icelandic) mutation; as the outcome of the amino acid substitutions produces polar opposite effects. On the one hand, Swedish mutation carriers are characterized by the development of early onset AD, this is due to an overproduction of pathogenic A β 42 peptides which is the direct result of the facilitated recognition of

the APP protein by the γ -secretase. In contrast, Icelandic mutation carriers possess a “protection” against the development of AD, due to the point mutation resulting in a reduced recognition rate of the APP protein by the γ -secretase, with overall reduced A β peptide production [35]. Another example of the important role of the *APP* gene in the development of AD comes from individuals with Down's syndrome: APP is located in chromosome 21, the presence of an extra copy of this chromosome in individuals with this syndrome causes the over production of APP, and as a consequence A β peptides. As a result most individuals suffering from Down's syndrome develop early onset AD [28]. *PS1* and *PS2* are two genes located in different chromosomes (14 and 1 respectively) but together they play a crucial role in the homeostasis of A β peptide, as they are both part of the catalytic subunit of γ -secretase. It has been observed that mutations in *PS1* and *PS2* lead to the overproduction and accumulation of A β 42 peptides, strongly contributing to the onset of the disease [37]. Finally, ApoE mutations are considered to be the most frequent among sporadic AD cases. This is a chaperone protein involved in lipid transport between the plasma and the CNS. Three different isoforms have been identified for this protein, ApoE2 (C112 and C158), ApoE3 (C112 and R158) and ApoE4 (R112 and R158). It has been observed that ApoE4 isoform carriers possess a higher risk of developing AD compared to other isoform carriers (with ApoE2 isoform carriers being the less at risk for developing the disease). ApoE4 carriers have increased accumulation of A β peptides both in the brain and cerebrospinal fluid (CSF), suggesting that the clearance of the peptides is sub-optimal. This inefficiency in clearing the peptides is what is currently thought to lead to the development of AD [22, 38].

Table 1-2: Risk factors for Alzheimer's Disease

Environmental risk factors
Old age
Diabetes mellitus
Hypertension
Obesity
Physical inactivity
Sedentary lifestyle
Depression
Smoking
Cerebrovascular disease
Poor educational attainment

Most prominent genetic risk factors*				
Gene	Protein	Function	Mutation	Inheritance
<i>APP</i>	Amyloid precursor protein	Synaptic function, cell adhesion, transcriptional regulation, membrane receptor (or ligand), apoptosis regulator and axonal plasticity	Missense mutations (most prominent: KM670/671NL (Swedish); E693G (Arctic); 717F; V717I; V717L) Duplications Deletions Insertions	Autosomal dominant
<i>PSEN1 & PSEN2</i>	Presenilin 1 and presenilin 2	γ -secretase activity	Missense mutations Deletions Insertions	Autosomal dominant
<i>APOE</i>	ApoE	Protein chaperone and lipid transport	Different alleles associated with higher risk of AD	Autosomal dominant

*Please refer to Alzforum (<https://www.alzforum.org/mutations>) for a list of all mutations

1.1.3 Current therapies for PMDs

To date, no disease modifying therapies are available for treating PD or AD [39-41]. The main therapeutic approaches for these diseases have aimed to maintain neurotransmitter availability by providing an exogenous source to be used by the brain, or by inhibiting neurotransmitter degradation and processing systems. In the case of PD, levodopa represents the gold standard for treatment [42-44]. Levodopa is a precursor to dopamine, the most severely compromised neurotransmitter in PD, and its main pharmacological function is that of being processed by surviving neurons in the brain allowing the release of increased quantities of dopamine, counteracting the effects of the progressive dopaminergic degeneration in the SN of patients. Other treatments for PD involve the use of monoamine oxidase (MAO) and catechol-o-methyltransferase (COMT) inhibitors; these two enzymes are responsible for dopamine degradation therefore their inhibition results in prolonged stimulation of the available dopaminergic receptors [42-44]. Other, more aggressive, treatments for PD involve the use of surgery, for example deep brain stimulation [40].

In the case of AD, available drugs mainly involve the use of acetylcholinesterase (AChE) inhibitors, to reduce acetylcholine degradation acted upon by this enzyme. This counteracts the effects of progressive loss of acetylcholine neurons in the brain of diseased patients [45, 46]. A further therapeutic option is the use of N-methyl-D-aspartate (NMDA) antagonists. In AD, as in other neurodegenerative diseases, an increased level of extracellular glutamate can be observed, which in

turn is involved in the over-stimulation of glutamate receptor NMDA, an ion channel permeable to Ca^{++} cations. Aberrantly increased levels of extracellular glutamate over-excite the NMDA receptors, producing an excessive inward flow of Ca^{++} ions and inducing the formation of Ca^{++} deposits inside neurons. These deposits then initiate a cascade of events culminating in cell death. NMDA inhibitors protect surviving neurons from the excitotoxic effect of glutamate [47]. Other less used therapeutic approaches involve the use of β and γ secretase inhibitors; α secretase potentiation drugs, metal chelators and anti-inflammatory drugs [41, 47].

Although these therapeutic approaches are currently the most widespread strategies available, they do not provide a viable cure for the diseases but can improve the overall quality of life. However, many of these treatments have unpleasant side effects after prolonged use [39, 43, 47]. Examples include levodopa induced dyskinesia in PD patients [43] and side effects induced when an AD patient switches between different AchE inhibitors can include vomiting, insomnia, nausea and in some instances anorexia [47-49].

1.2 α -synuclein

α -synuclein is part of a family of proteins defined as “synucleins”, together with β -synuclein and γ -synuclein. These proteins are predominantly expressed in the brain, and possess 55-62% structural homology [50]. α -syn is best known for its involvement with neurodegenerative diseases. Indeed, ever since the link between α -syn deposition and PD was discovered in 1997 by Spillantini [4] and Polymeropoulos [3], several other diseases have been linked to the accumulation of α -syn such as multiple system atrophy (MSA), dementia with Lewy bodies (DLB) and Hallervorden-Spatz disease. Together these are known as synucleinopathies. Additionally, the accumulation of α -syn deposits has been found to be a common trait with other non-synucleinopathy related conditions, such as AD, Down’s syndrome, rapid eye movement disorders, pure autonomic failure, several Tauopathies and normal aging (incidental Lewy body disease) [51].

1.2.1 Structure

α -syn is a 140 amino acid long protein coded by the *SNCA* gene [9], with a high degree of conservation between species [52]. It is characterized by an amphipathic N-terminus region, capable of forming α -helices; a hydrophobic middle region, and an acidic C-terminus [50]. In physiological conditions *in vivo* and *in vitro*, α -syn is believed to exist within a range of dynamic configurations that can range from random coil in solution [53] or an α -helix predominant conformation when bound to membranes [53-55]. Recent studies also suggest that α -syn can also be found as a soluble 58-60 kDa tetramer which is resistant to aggregation *in vivo* [56, 57]. In pathological conditions α -syn assumes a predominantly β -sheet structure and interacts with other misfolded α -syn monomers to form oligomers (characterized of possessing an anti-parallel β -sheet structure) and fibrils (with parallel β -sheets) [58]. Each domain within the protein serves a purpose in both physiological and pathological conditions: the N-terminus grants the protein the ability to bind lipid bilayers through the formation of 5 amphipathic α -helices within 11 imperfect KTKEGV repeats; the hydrophobic middle section is necessary for protein aggregation and the C-terminus of the protein is involved in interaction with other proteins and has anti-aggregation properties (figure 1.5) [53, 59, 60].

α -syn has been found to possess several post translational modifications that can affect the protein's functionality and involvement in both physiological and pathological processes. Among the different modifications observed, α -syn has been found to possess several phosphorylation, nitration, oxidation, ubiquitination and sumoylation sites [61]. Post translational modifications have been linked to pathological α -syn, in particular the phosphorylation of S129 and S87 are only be found in LB and other pathological α -syn aggregates. Furthermore, it has been observed that the presence of a phosphate group within the α -syn protein can influence the misfolding tendencies of this protein [62-64]. Alongside phosphorylation, oxidation and nitration have been found to induce covalent links within the α -syn protein, stabilizing pathogenic oligomeric and fibrillar conformers of α -syn [65, 66]. Additionally, ubiquitination and sumoylation have also been linked to pathological conformers of α -

syn *in vitro* [67-69]. For a more detailed review of the structure and different post translational modifications found in α -syn please refer to Beyer *et al.*, 2006 [61], and Ottolini *et al.*, 2017 [53].

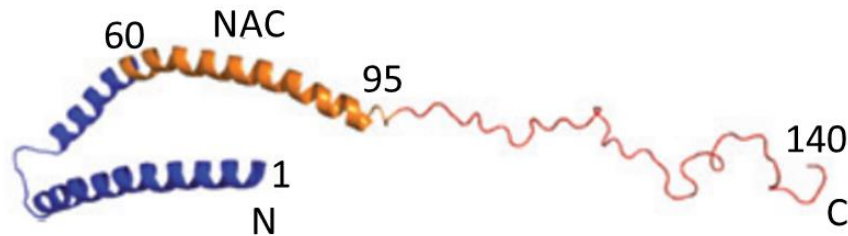


Figure 1-5: Structure of α -synuclein.

The N-terminus (indicated in blue) is capable of forming α -helix through 11 KTEGV imperfect repeats. The highly hydrophobic NAC region (indicated in orange) is mainly involved in protein aggregation in pathological conditions. The acidic C-terminus (indicated in red) is responsible for interaction with other proteins and has anti aggregation properties. Image adapted from Lashuel *et al.*, 2013 [70]. Licence number 5133080493489

1.2.2 Function

α -syn is predominantly expressed in the CNS, in neuronal presynaptic terminals [71]. In these terminals, α -syn plays an important role in the regulation of neurotransmitter release by modulating the activity of the soluble N-ethylmaleimide-sensitive factor attached protein receptors (SNARE) protein complex, a key element necessary for vesicle fusion and neurotransmitter release [72]. α -syn mediated vesicle release is achieved by facilitating the interaction of vesicle SNARE (v-SNARE) proteins, such as synaptobrevin-2 and vesicle-associated membrane protein 2 (VAMP2) with SNARE proteins within the presynaptic plasma membrane, target SNARE (t-SNARE), such as syntaxin and Synaptosome Associated Protein 25 (SNAP25). The continuous cycle of assembly and disassembly of these proteins determines the release of neurotransmitters within the synaptic terminal. This process is heavily controlled by chaperone molecules, such as α -syn, capable of binding the lipid bilayer with its amphipathic N-terminal region and synaptobrevin-2 with its C-terminus. Knock out (KO) models lacking the expression of α , β and γ -synuclein showed reduced neurotransmitter release and SNARE complex assembly in an age dependant manner, suggesting that the synuclein family play an important role to maintain normal synaptic function as age progresses. Additionally, neuronal culture

of α , β and γ -synuclein KO cells showed that this time dependant decrease in SNARE activity was rescued by the introduction of wild type α -syn, evidencing the important role that α -syn plays within this protein complex. Rescue was not achieved with C-terminal truncated α -syn, further cementing the importance of the interaction between α -syn and v-SNARE proteins [72].

In addition to neurotransmitter release and SNARE complex assembly, α -syn has also been found to be involved with mitochondrial health, structure and function. Indeed, in physiological conditions, α -syn has been observed to translocate to the outer mitochondrial membrane in an ATP and mitochondrial membrane potential dependant manner. Within this organelle, α -syn is closely involved in the production of new ATP molecules by modulating complex III and ATP synthase activity [73-75]. Beyond its involvement with proteins in the respiratory chain, α -syn also modulates mitochondrial – endoplasmic reticulum interactions and regulates, among other things, calcium homeostasis and lipid metabolism between these two organelles [76, 77].

1.2.3 Pathological Role

As previously described, α -syn accumulation is the main pathological hallmark of PD, with its misfolding and spread acting as the main driving force behind disease progression [78]. Interestingly, misfolded α -syn is able to enact its pathological role through a gain of pathological function and loss of function of the protein. This has been evidenced by α -syn KO animal models being viable [79] albeit with neurotransmitter impairments during old age, as α -syn has been found to be an important protein in the modulation of the SANRE complex as the mice age [72]. Misfolded α -syn has been found to enact its pathological role through several mechanisms. One is the sequestration of monomeric α -syn from the synaptic terminals by the ever-growing number of oligomers, fibrils and LBs, this hampers the synapse's ability to release neurotransmitters as α -syn mediated SNARE activity is disrupted [72, 80]. It has also been suggested that pathological α -syn can translocate to the nucleus, where it promotes neurotoxicity through the inhibition of histone deacetylase and promotes further aggregation of α -syn molecules [81, 82]. Misfolded α -syn has also been found to have a toxic effect on mitochondria; translocating to the inner membrane of the organelle, where it interferes with

mitochondrial complex I activity (reducing ATP production), promotes cell death and enhances the production of ROS [73-75]. Additionally, α -syn sequestration prevents the communication between mitochondria and endoplasmic reticulum, causing mitochondrial stress due to a lack of lipid and calcium ion supplementation [77]. Another key element of α -syn pathology can be understood through the study of the structural changes the misfolding of this protein brings. Pathological α -syn is characterized by its increase tendency to aggregate with other misfolded α -syn proteins to form oligomers and fibrils. This process is propagated through the recruitment of physiological monomer into the misfolded α -syn structure through templated induced misfolding and/or the interaction of independently misfolded α -syn to form high molecular weight complexes [83-85]. Oligomers possess a wreath shaped cylindrical structure, with predominantly antiparallel β -sheets [58, 86]. Although the diameter and length of these aggregates can vary depending on the number of α -syn monomers associated together to form this pore-like structure, some oligomers possess an average length of 4.5 nm, which can span from one side to the other of the hydrophobic core of the lipid bilayer [86, 87]. In doing so, α -syn oligomers act as a conduit that allows the unregulated transfer of ions between both sides of the lipid bilayer. The permeabilization of the cell membrane and uncontrolled ion traffic leads to cell death, making α -syn oligomers one of the main agents of α -syn toxicity [88, 89]. In particular, two distinct types of α -syn oligomers have been described in the literature: type A and type B oligomers [90, 91]. These forms of aggregated α -syn are mainly distinguished by their secondary structure composition, with type A oligomers being more flexible and unstructured compared to the more rigid β -sheet rich type B oligomers. Interestingly both types of oligomers were also found to have different effects on cells. Indeed, type A oligomers have been observed to tightly bind to lipid bilayers, but not cause any major disruptions in the structural integrity of the membrane itself. Type B oligomers, on the other hand were found to be able to penetrate lipid bilayers with their rigid β -sheet rich domains allowing the depolarization of the membrane [90]. As such, type B oligomers are able to enact their toxic effect in neurons through the deregulation of the intracellular calcium

concentrations, the generation of ROS, mitochondrial dysfunction and apoptosis as discussed above [91].

Insoluble fibrils are the end point of α -syn aggregation, and their involvement with the disease onset and progression has been controversial. The general consensus states that fibrils assume a more protective role, acting as a defence mechanism adopted by the cells to sequester the excess monomeric α -syn and thus preventing the formation of further oligomers [50, 53, 60, 62, 92]. Alternatively, α -syn fibrils may play a more prominent role in inducing pathology, as α -syn fibrils transfected to cells overexpressing α -syn are capable of seeding the formation and propagation of new pathogenic α -syn aggregates, a phenomenon that is not observed when oligomers are used as seed [93], and suggesting the possibility that α -syn fibrils are involved with the spread of the disease [94]. More recently, Cascella *et al.* [91] proposed that under particular conditions, fibrils have the ability to release toxic oligomers from their ends, thus indirectly inducing a toxic effect in the near vicinity of the fibril itself.

1.3 Different strains (polymorphs) of α -synuclein

One of the most interesting properties of α -syn is its ability to form different 'strains'. This is a terminology borrowed from prion biology, another pathology that shares many similarities with synucleinopathies [95, 96]. A strain can be defined as an infectious unit that exhibits distinct disease phenotypes when transmitted to identical hosts. The disease phenotype can include distinct histopathological lesion profiles, target areas of neurodegeneration and incubation time. Serial transmission of a strain results in the propagation of the same pathological phenotype. It is believed that each strain is able to induce distinct pathological profiles due to the structural alterations present within the protein aggregates [97]. Given that different strains result from slightly altered fibril conformations (or polymorphs) [95], different assays can be used to evidence the differences between strains, such as digestion with proteinase K (PK), analysis with Thioflavin T (ThT) [83], cell culture toxicity [98] or inoculation in animal models [99]. In recent years, several techniques have been implemented to discover different strains of α -syn [84, 96] (table 1.3).

For the study of α -syn strains, the most widely used animal model is the transgenic mouse line TgM83, that expresses mutated (A53T) human α -syn through the prion protein promoter [100]. Animals homozygous for this gene (TgM83^{+/+}) show no signs of pathology for the first 7 months of life. After that point, it is possible to see the accumulation of α -syn deposits and onset of motor difficulties that progress with age [100]. Interestingly, the inoculation of young mice with brain derived from old diseased animals results in accelerated development of the disease, providing some of the first evidence for α -syn related pathology transmission. [101]. This model was also applied to investigate the seeding ability of different synucleinopathies: MSA brain homogenate was compared with PD brain and TgM83^{+/+} diseased brain after inoculation into heterozygous TgM83 mice (TgM83^{+/-}). Heterozygous mice, unlike TgM83^{+/+}, do not develop any pathological signs with age. Therefore, any changes seen in the animal model post-inoculum were directly connected to the α -syn pathology injected into the brain. Infection with MSA and TgM83^{+/+} brain homogenates promoted the onset of α -syn pathology, with widespread α -syn deposit formation and motor difficulties; animals inoculated with PD brain homogenate did not show any signs of a successful transmission. Furthermore, histological analysis of brains infected with MSA or TgM83^{+/+} displayed different α -syn deposition patterns in the brain of infected mice. Overall, the data demonstrated that MSA, PD and TgM83^{+/+} represent different strains of α -syn mediated disease [99, 102]. *In vitro* studies using cell cultures mirrored the results found in transmission studies where PD brains possessed a reduced ability to seed α -syn deposition, compared to MSA samples, which showed an aggressive spread of α -syn pathology [98, 103]. Strain differences between MSA and PD are also seen in *in vitro* generated fibrils. CSF extracted from patients carrying these synucleinopathies were used to seed monomeric recombinant α -syn; fibrils were then formed through constant agitation. MSA derived fibrils were more toxic compared to their PD seeded counterpart, and fibril morphology was also different [85]. Further investigation using isolated LB and glial cytoplasmic inclusions (GCI) (characteristic of MSA lesions) inoculated in brains of mice revealed that purified LB α -syn is able to induce pathology, and compared to GCI, LB pathology was milder. LB pathology also showed longer incubation times compared to MSA.

Different incubation times and lesion patterns were suggestive of these two pathologies belonging to different strains. The resulting inclusions did not necessarily show the same kind of pathology as the inoculum, namely, GCI derived α -syn aggregates were able to induce LB-like deposits outside of oligodendroglia cells, suggesting that the cell milieu is able to somehow influence the creation of different strains [104]. Additional evidence of cellular environment being able to influence the generation of strains is seen in immunohistochemistry studies performed on MSA brain sections. Binding patterns of a wide range of antibodies targeting different epitopes of the C or N terminus of the α -syn protein, were able to demonstrate different kinds of aggregates within MSA patients, providing evidence but not conclusive proof that different strains exist within the brain of an individual [105]. In addition, *in vitro* generated fibrils using sonication with either brain or spinal cord samples to seed the misfolding of recombinant α -syn produced fibrils with different morphological properties [106]. Overall, bioassay, cell culture and *in vitro* biochemical analysis experiments provide strong evidence for the existence of different α -syn strains, but this theory is not without controversies.

Although, it is known that α -syn is essential for the spread of the disease, with *in vitro* generated fibrils being capable of inducing pathology both in cell culture, TgM83 mice [107] and α -syn KO mice [108]; transmission is not as straight forward when using CNS derived material to inoculate animal models. A study performed on TgM83^{+/+} mice inoculated with spinal cord homogenate deriving from TgM83^{+/+} mice with motor symptoms; mice carrying the G93A mutation in the superoxide dismutase 1 gene and also presenting motor symptoms unrelated with α -syn pathology; healthy non transgenic mice and healthy α -syn KO mice found that all inoculated mice (except sham injected individuals) presented α -syn pathology and accumulation. This was not observed when instead of spinal cord extracts, brain homogenate of control and α -syn KO mice were used; strongly suggesting that compounds within the spinal cord are able to seed α -syn pathology in the inoculated host, regardless of the diseased or healthy status of the donor [109].

Beyond disease specific strains seen *in vivo*, such as the MSA, PD and TgM83^{+/-}, several other strains have been artificially generated through the use of different *in vitro* incubation methodologies. Most notably, constant shaking of α -syn monomer in buffer with either physiological or low salt concentrations can induce the formation of two distinct strains of α -syn, characterized by possessing different fibril morphologies. These structural differences were evidenced through the PK assay, able to highlight conformational differences (and concomitant cleavage sites) in the core of fibrils and the ThT assay, capable of measuring the presence of distinct levels of β -sheets in solution. Differences in structure were further demonstrated through the use of direct imaging techniques (negative stain transmission electron microscopy (NS-TEM)) and also spectroscopic techniques, circular dichroism (CD) and Fourier-transform infrared spectroscopy (FTIR), that measure the secondary structures within the aggregates. All of the techniques revealed differences between the conformers. Beyond physicochemical differences, high vs low salt fibrils were also distinguishable by their ability to promote disease in cell cultures. In addition, the inoculation of both strains in the TgM83^{+/-} model resulted in the spread of different pathological profiles in the brains of infected mice, confirming the idea that these aggregates are indeed two distinct strains [107, 108, 110].

Other compounds have been identified as being capable of inducing different polymorphs. For example, endotoxins (LPS in particular) were able to dramatically influence the morphology and toxicity of fibrils generated *in vitro* [111]. Beyond the use of additives, the methodology implemented to form fibrils *in vitro* has also been noted to direct the misfolding pathway of α -syn towards different polymorphs. Indeed, α -syn monomers subjected to different cycles of shaking and incubations have been observed to induce distinct levels of Tau hyperphosphorylation in cell cultures. Samples subjected to prolonged seeding and propagation passages were able to cross seed the highest amount of Tau hyperphosphorylation [112].

Table 1-3: α -syn polymorphs/strains

In vivo generated strains	
Study of a-syn strain type	Strain characteristics

Brain homogenate from TgM83 ^{+/+} mice with motor symptoms [101].	Brain from diseased TgM83 ^{+/+} are able to accelerate pathology when inoculated into the brain of asymptomatic TgM83 ^{+/+} mice.
Human MSA and diseased TgM83 ^{+/+} brain homogenate [102].	MSA and diseased TgM83 ^{+/+} brain homogenate produced different pathological profiles when injected in TgM83 ^{+/-} mice.
Human MSA, PD and diseased TgM83 ^{+/+} brain homogenate [99].	Human PD and MSA brain homogenate were inoculated in TgM83 ^{+/-} mice. While MSA was able to propagate in the new host, PD did not induce any pathological changes.
Spinal cord homogenates from: 1) TgM83 ^{+/+} mice with α -syn pathology, 2) Mice carrying the G93A variant in the superoxide dismutase-1 gene, with motor difficulties. 3) Healthy mice. 4) Healthy α -syn KO mice [109].	TgM83 ^{+/-} were inoculated with spinal cord homogenate samples. The injection of spinal cord material in a new host always produced α -syn pathology (except sham injection).
MSA brain sections [105].	Multiple antibodies were used to demonstrate different α -syn strains within the brain of an MSA patient.
α -syn aggregates from LB and oligodendroglia inclusions [104].	LB and glial cytoplasmic inclusions were precipitated and inoculated on WT mice, resulting in different α -syn deposition patterns depending on the sample used.
<i>In vitro</i> generated strains	
Study of α -syn strain type	Strain characteristics
Human MSA and PD brain homogenate [98].	MSA brain homogenate was able to infect cell cultures and mouse models, with decreasing incubation times over several passages; PD brain homogenates on the other hand were not able to induce pathology.
Human MSA and PD brain homogenate [103].	Brain homogenates from MSA and PD patients were separated into detergent insoluble and soluble fractions. They show that both MSA fractions are able to seed pathology in cell cultures, while for PD only the detergent insoluble fraction is able to seed pathology.
CSF from MSA and PD patients [85].	RT-QUIC was used to misfold synthetic α -syn with MSA and PD derived CSF. The resulting fibrils possessed different physicochemical properties and different toxicity in cell cultures.
Synthetic fibrils generated with different buffer conditions [110].	Fibrils generated with physiological ('fibrils') or low salt concentrations ('ribbons') possessed different morphologies, physicochemical properties and toxicity in cell cultures.
Synthetic fibrils generated with different buffer conditions [108].	Synthetic fibrils generated with physiological vs low salt concentrations inoculated into TgM83 ^{+/-} produced different pathological profiles.
Synthetic fibrils generated through several amplification passages [112].	Synthetic fibrils generated through several passages of seeded-propagation in vitro could cross-seed Tau deposits while <i>de novo</i> fibrils could only seed the formation of new α -syn aggregates (assessed in primary neuron cell cultures and Tau transgenic mice).
Synthetic fibrils generated with different additives [111].	Synthetic fibrils generated with and without endotoxin (LPS) possessed different morphology, physicochemical properties and toxicity in mice.
<i>In vivo</i> like fibrils generated through PMCA, using different sections of the central nervous system as seeds [106].	α -syn fibrils were generated through PMCA. Fibrils seeded with brain homogenate possessed different structural properties than spinal cord seeded samples
Synthetic fibrils generated with different buffer conditions [107].	Synthetic Fibrils and ribbons were generated using different salt concentrations. These aggregates not only possessed different physicochemical properties and morphology, but they were able to promote different aggregates in cell cultures and possessed characteristic transmission patterns in TgM83 ^{+/-} mice.

1.4 β -amyloid

1.4.1 Structure

A β encompass a range of peptides between 37 to 49 amino acids. Among these A β 40 and 42 are the isotypes most often found in the brain of AD patients as plaques, and are therefore thought to be the

most pathologically relevant [113, 114]. A β originates from the consecutive proteolytic cleavage of APP. The cleavage is performed by a group of enzymes: α , β and γ secretase [115]. APP is a complex membrane protein characterized by a large extracellular domain, a single pass transmembrane domain, and a short cytoplasmic domain [116]. In physiological conditions, APP cleavage follows one of two possible pathways: the non-amyloidogenic and amyloidogenic pathways. In the non-amyloidogenic pathway, α -secretase cleaves the extracellular domain of APP in position 83, producing the SAPP α fragment, released in the extracellular medium and CTF α , anchored to the plasma membrane. CTF α , is then recognized and cleaved by γ secretase, producing P3 and the APP intracellular domain (AICD). The amyloidogenic pathway starts with the proteolytic cut of the extracellular domain of APP by β -secretase in position 99, producing the extracellular sAPP β and the membrane bound CTF β . CTF β is then cleaved by γ -secretase, producing AICD and A β . Although both A β 40 and 42 are produced by this method, the proportion of A β 40 generated is higher than A β 42 in physiological conditions, and lower in an AD related pathological condition (figure 1.6) [114].

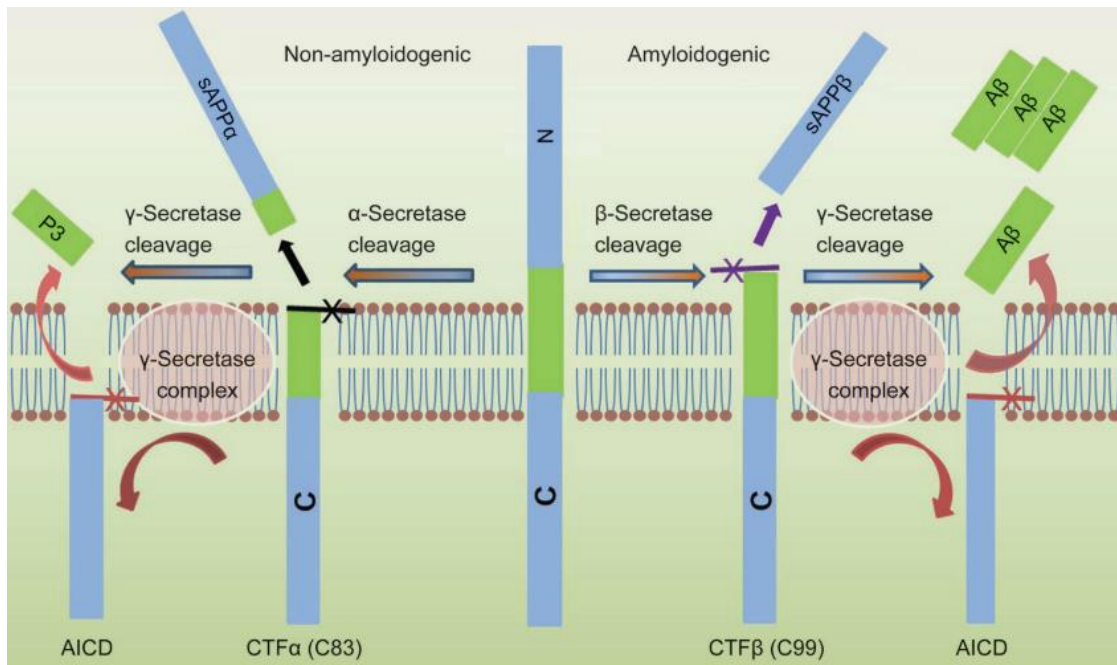


Figure 1-6: Processing of human APP

APP cleavage process for the non-amyloidogenic and amyloidogenic pathways. The non-amyloidogenic pathway starts with the proteolytic cut of APP by α -secretase, producing the release of the N-terminal SAPP α and membrane bound CTF α (or C83). CTF α is subsequently cleaved by the γ -secretase complex releasing P3 and AICD. The amyloidogenic pathway involves

the initial cut of APP by β -secretase, releasing sAPP β and the membrane bound CTF β (or C99). Next, CTF β is cleaved by the γ -secretase complex releasing A β 40/A β 42 and ACID. Image from Chen *et al.*, 2017. Licence number 5120780443645.

Unlike α -syn, once in solution A β peptides can assume an array of isoenergetic conformations, the prevalence of which depend on the particular conditions of the environment (such as temperature, pH, ionic concentration and hydration). Due to the tendency of these peptides to form spontaneous aggregates in solution, most of our understanding in regard to A β monomer morphology has been obtained through the use of NMR-based simulations [114, 117-119]. A β 40 monomers are generally characterized by the presence of a structured N-terminal region with a 3_{10} helix and γ -hairpin in residues 12-18; a central hydrophobic region spanning residues 17-21 and a flexible C-terminal stabilized by β -turns and transient polyproline II type structures in residues 24-40. As for A β 42, the presence of the two additional hydrophobic amino acids at the C-terminal confer the peptide an increased conformational variability compared to A β 40. Structurally, A β 42 monomers are generally characterized by the presence of an unstructured N-terminal (residue 1-7), the central region of the peptide assumes a collapsed coil structure, with several loops and turns between residues 8 and 29; the hydrophobic amino acids within the central regions have also been observed to form hydrophobic pockets within the peptide. The C-terminal of A β 42 is structured, with the presence of β -hairpins and β -turns, reducing the overall flexibility of this domain [120] (figure 1.7). Recent studies have focused on understanding the conformation of A β units once they associate into fibrils. These studies were performed using cryo-electron microscopy methodologies and reveal an interesting pattern. A β 42 fibrils extracted from the brain of AD patients were revealed to be highly polymorphic structures, with at least three different subtypes: type I and Ib, more commonly found in sporadic AD patients and type II fibrils, found in the familiar AD cases. These aggregates were found to be made of "S" shaped protofilaments that interact in different ways to produce the different fibril polymorphs, and confer the overall structure a left-handed twisted motif [121]. Furthermore, A β 40 fibrils extracted from the meninges of AD patients possessed a different conformation, with protofilaments assuming characteristic "C" shaped fold and fibrils displaying a right-handed twisted motif [122]. Interestingly, *in vitro* generated fibrils seem to have an altogether different structure from *in vivo* fibrils, as

recombinant A β 42 aggregates were recorded to be constituted by “LS” shaped protofilaments and an overall right-handed twisted motif for fibrils [123]. The different polymorphs identified throughout these studies evidence the importance of understanding the structure of A β fibrils in pathological conditions, as differentially shaped structures could be associated with different disease pathways [121-123] and could potentially be targets of interest for the development of therapeutics.

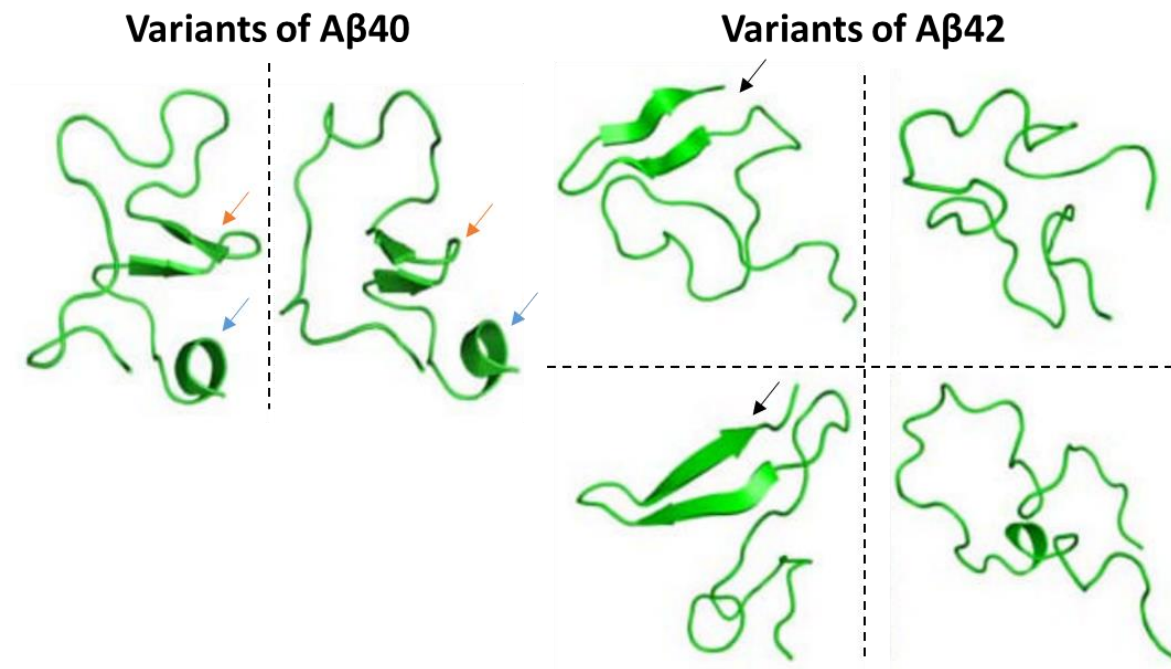


Figure 1-7: Structure of A β

Examples of the different monomeric conformers of both A β 40 and A β 42, obtained through NMR based simulations. Each A β 40 structure is represented with both the N-terminal and C-terminal facing down, while A β 42 structures is displayed with the C-terminus up and the N-terminus down. For A β 40 it is possible to see the predominantly collapsed structure with short α -helix (blue arrows) and γ -hairpin (orange arrows) in the structured N-terminal. A β 42 display a bigger repertoire of conformers. The N-terminal is generally unstructured and most of the peptide presents a collapsed coil structure with exception of the C-terminus that possessed either a β -hairpin (black arrow), loops or turns. Each conformer possesses the same energy and stability as the others, within each peptide, but with different probabilities of manifesting. Image adapted from Sgourakis *et al.*, 2007, modified. Licence 5120780710236.

1.4.2 Function

A β peptides are present in both physiological and pathological conditions in the brain, albeit at different concentrations. Within the CNS, A β peptides have a physiological function in healthy individuals. This is evidenced by APP KO animal models showcasing an array of cognitive and motor difficulties, together with an increased propensity to suffer from seizures [124]. The study of both A β 40 and A β 42 within the physiological context has led to the discovery that both monomeric and

oligomeric forms of these peptides possess a neurotrophic effect on young neurons and are able to regulate synapse activity of mature synapses [124, 125]. Synaptic regulation is achieved through the implementation of a negative feedback loop that is dependent on synapse excitation: neuronal activity promotes the upregulation of CTF β production through the increased β -secretase activity; higher concentrations of CTF β are then cleaved by the γ -secretase complex, resulting in the overall increased concentration of A β peptides. Higher levels of A β peptides in the synaptic button induce a synaptic depression, ceasing the synaptic stimulus. In doing so, A β is able to be part of the fine tuning and modulation of synaptic activity within the physiological context [126, 127]. Through the use of animal models and cell cultures, it was also possible to discover that A β has a direct role in memory and long-term potentiation (LTP) functionality. This phenomenon seems to be directly correlated to the concentrations of the peptides within the synaptic terminals, with picomolar levels of the peptides being able to promote these effects. Memory potentiation and increased LTP seem a direct result of A β activation of the α 7 subunit of the nicotinic acetylcholine receptor (nAChR), a fundamental receptor involved in learning and memory formation in physiological conditions [124, 128]. Beyond being involved in roles relates to synaptic plasticity and memory formation, A β is also known to participate in an array of functions in physiological conditions. These include the modulation of the response of different neurotransmitters [129], acting as an antimicrobial peptide, and acting as a response mechanisms to environmentally induced inflammatory processes [114]. For in depth reviews about A β functionality please refer to Chen *et al.*, 2017[114].

1.4.3 Pathological Role

Similar to α -syn, A β toxicity is mainly enacted by the formation of oligomers and fibrils. These aggregates have been found to induce cell death and toxicity through different mechanisms. Firstly, oligomers are able to form pores in the plasma membrane, disrupting ionic homeostasis and leading to cell death and altered synaptic activity [130, 131]. A β fibrils, in a similar manner to α -syn fibrils, possess a controversial role in AD pathology. While some studies suggest that fibrils are protective entities, acting through the sequestering of more toxic lesser aggregated species; other studies

provide evidence of a toxic effect. Fibrils have been observed to be destabilized by lipids in the brain (such as sphingolipids and gangliosides) towards the formation of more toxic protofibrils and oligomers, promoting further degeneration in affected areas [132]. Furthermore *in vitro* studies with cell cultures have demonstrated that fibrils have intrinsic cytotoxic effects that are inversely correlated with the length of the polymers themselves [133]. Also, A β is able to accelerate lipid peroxidation, overproducing two specific oxidative stress markers in neurons and astrocytes: 4-hydroxynonenal and malondialdehyde; as shown by the increased CSF levels of these markers in AD patients. The membrane depolarization caused by the pore like structures that are formed, and the oxidative stress caused by increased levels of ROS also lead to deregulation of mitochondrial functions, this then causes the depolarization of the organelle, and induces the release (among other things) of cytochrome C, prompting the onset of an apoptotic process through the caspase cascade [134]. Mitochondrial dysfunction is additionally promoted by morphological changes induced in the organelle [135] and the deregulation of the peptidosome responsible for the cleavage of the N-terminal prepeptide present in proteins destined to be transported to this organelle, causing further protein aggregation and organelle stress [136]. Higher concentrations of monomeric and aggregated A β found in pathological conditions have an increased toxic effect on synaptic plasticity, LTP and memory. This is thought to be the result of increased A β being able to act as an antagonistic ligand for many neuronal receptors, such as the previously mentioned α 7-nAChR [125, 128, 131, 137]. In addition, the misfolding of A β is able to cross seed the misfolding of Tau, promoting the hyperphosphorylation and subsequent aggregation of this protein in both *in vitro* and *in vivo* models [138-140]. For an in depth review, please refer to Benilova *et al.*, 2012 [141] ; Angelova *et al.*, 2017 [134] and Lanni *et al.*, 2019 [129]

1.4.4 Different strains (polymorphs) of Amyloid β

A β is a small hydrophobic peptide with a high propensity to form aggregates. Aggregation often leads to fibril formation (going through the oligomeric and protofibril stages), as these structures are more thermodynamically stable than the unstructured monomer [142]. In the case of A β , it has been reported that fibrils are highly polymorphic, with both A β 40 and 42 peptides being able to produce a

wide variety of fibrils with different toxicity, physicochemical properties and morphologies both *in vitro* and *in vivo*. *In vitro*, reports have shown that the formation of fibril polymorphs is strongly correlated to the conditions (temperature, pH, agitation, additives) used to form the fibrils. Synthetic A β 40 fibrils generated either through shaking or static incubation produced two different fibril populations, each with a specific morphology and toxicity. Fibril conformation was stable within different sub passages [143]. Buffer selection, pH and temperature are also important: fibrils generated in PBS (pH 7.2 at 37 °C) or in sodium borate (pH 7.8 at 22 °C) were highly polymorphic in nature with fibrils formed in PBS being the most widely variable in conformation compared to those produced in sodium borate. Interestingly, although fibrils produced in PBS were highly irregular and displayed a wide variety of conformations, those produced in sodium borate were longer, with a more consistent morphology and fewer polymorphs were present in solution [144].

Although the study of A β fibrils *in vitro* can produce insights into the properties and behaviour of different polymorphs, the analysis of the effects of A β fibril conformers *in vivo* reveals the true intrinsic complexity of A β polymers. Studies with misfolded synthetic A β 40 and A β 42 fibrils possessing different physicochemical properties (differential ThT binding profiles and fibril morphology as evidenced with TEM) showed that intracranial inoculation in transgenic mouse models produce different pathological phenotypes in infected animals. A β 42 peptides induced a greater number of smaller plaques consisting almost exclusively of misfolded A β 42 compared to the larger, less numerous plaques in A β 40 injected mice [145]. As for the analysis of human fibrils, the *in vitro* propagation of brain derived fibrils from confirmed AD cases resulted in the formation of specific conformers that differed between patients [146]. For each patient, a specific polymorph seems to dominate over others. These polymorphs possessed specific morphologies (evidenced with TEM and ThT binding profiles) leading to speculation that specific polymers were linked to a more aggressively progressive AD pathology [147]. Interestingly, the in-depth analysis of *in vivo* fibril polymorphs highlighted the ability of these aggregates to act as seeds for the propagation of new fibrils with the same structural properties.

Similarly, *in vivo* co-infection studies of two transgenic mouse models possessing two distinct age-dependant A β depositions patterns: APP23 (carrying the Swedish mutation) and APPPS1 (carrying both Swedish and PS1 mutations) revealed that the infection with older diseased brain from animals belonging to the same transgenic category resulted in the acceleration of the disease in the inoculated mice. Interestingly, the inoculation of younger mice with brain from the other transgenic line resulted in the propagation of the proteinase K resistant band patterns characteristic of the seed used in SDS-PAGE assays, suggesting a strain-dependant transmission of the plaque deposition [148]. This phenomenon was also observed through the inoculation of APP23 mice with brain homogenate derived from diseased human Swedish and Arctic mutation carriers (APP E693G), with different mutation carriers being able to induce differential A β deposition patterns in infected mice, and isolated fibrils possessing different stability as evidenced with the guanidine hydrochloride (GdnHCl) assay. This evidence strongly suggest that these two different mutations are responsible for the production of two different human AD strains [149]. Moreover, the presence of different AD strains in the human brain was additionally proven by the direct analysis of plaques from familial forms of AD and sporadic AD. The comparison revealed the presence of different structural polymorphs [150]. Furthermore, it has been suggested that the number of A β 42 polymorphs in comparison to A β 40 have been correlated with different subtypes of AD pathology. For example, rapidly progressing AD has been observed to possess a higher number of A β 42 polymorphs compared to slowly progressing AD. Additionally, the predisposition of the strains to deposit in specific areas of the brains were also correlated with disease progression, with rapidly progressing AD presenting major A β 42 accumulation in the posterior cingulate cortex compared to slowly progressing AD [151, 152]. Overall, data from *in vitro* and *in vivo* studies with both animal models and human derived fibrils show that within the brain of AD patients there is a plethora of A β conformers that are often specific to each individual. A β 42 seems to be more polymorphic and toxic than A β 40 and the presence of higher numbers of A β 42 polymorphs was correlated with more aggressive forms of AD. Transmission revealed that prevailing polymorphs within the brain of both humans and mice models, carrying different mutations, can be

propagated within a susceptible host. This, together with different TEM, GdnHCl and ThT assay data suggests that AD pathology, in all of its complexity is also characterized by the presence of strains, represented by different A β polymorphs [84, 147-151].

Several studies have attempted to understand the mechanisms behind the polymorph formation. Current theories agree that different fibril conformers arise from a differential organization of the β -sheets. Several simulations and crystallography studies have shown that A β fibrils consist of two β -sheets closely interacting with one another. Different interactions formed by these “zippers” would then repeat themselves as the fibrils grows, granting a specific morphology to the growing polymer [142, 153, 154]. The structure of the different polymorphs is controlled by the complex interplay forces that shape the zippers and as a consequence the growing fibrils [155]. These interactions are most likely defined by the conditions through which the fibrils are formed (temperature, pH, agitation, buffers used, etc) [142, 143, 154], but studies suggest that amino acid composition of the A β monomer also plays an important role in the propensity to form specific polymorphs, as evidenced by the Arctic and Swedish mutations acting as different strains [148], together with deletions having a destabilizing and anti-amyloidogenic effect [156]. More recently, it has also been suggested that monomers in solution exist within a gradient of energetic levels, and possessing higher or lower energy levels (conferred by extrinsic factors such as pH, concentration and temperature but also intrinsic factors such as primary sequence of the peptides) could determine the propensity of the monomers to associate into different protein aggregates [157] (table 1.4).

Table 1-4: A β polymorphs

<i>In vivo</i> generated strains	
Studies on strain type	Strain characteristics
Diseased APP23 and APPS1 brain homogenates [148]	Brain homogenate from diseased APP23 and APPS1 mice were able to accelerate pathology when inoculated into younger individuals. When inoculated in the other model, the disease phenotype induced corresponded to that of the seed.
Brain homogenate from different AD patients [147]	Within the AD brain, a single polymorphism has been found to prevail, but A β 40 fibrils derived from the brain of two distinct AD patients presented two different structures.
Brain homogenates from AD patients with the Swedish or Arctic mutation [149]	Inoculation of brain homogenate from the two-mutation carrier resulted in a different pathology in transgenic mice.

AD brain samples with different disease durations [151]	Rapidly progressing AD demonstrated a higher number of A β 42 polymorphs than slowly progressing AD.
Synthetic peptide seeded with fibrils derived from AD patients [152]	Differently progressing AD pathologies possess different numbers of A β 42 polymorphs. As for A β 40, a single morphology seems to dominate across the brain of different patients.
Brain section from AD patients with different disease progressions and transgenic mice models inoculated with human brain [150]	Different forms of AD pathology possess a different “cloud” of A β fibril polymers that are able to propagate in animal models.
<i>In vitro</i> generated strains	
Studies on strain type	Strain characteristics
Synthetic A β 40 fibrils grown with shaking or static incubation [143]	Fibrils grown with shaking vs incubation conditions possess different morphologies, evidenced with TEM and atom force microscopy and toxicity for neural cell cultures.
Synthetic fibrils generated through different buffer conditions [144]	A β 40 fibrils were generated through static incubation of monomers in either PBS (pH 7.4, 37 °C) or sodium borate (pH 7.8, 22 °C). Although both buffers were able to induce fibrils, PBS fibrils possessed the highest number of polymorphs in solution but were also shorter and more irregular than sodium borate fibrils.
Synthetic peptide seeded with fibrils derived from AD patients [146]	Synthetic A β 40 fibrils seeded with fibrils derived from AD patients displayed different morphologies to synthetic fibrils, indicating that specific conformers are predominant in the AD brain.
Synthetic A β 40 and A β 42 peptides [145]	Synthetic A β 40 and A β 42 fibrils possessed different structural morphologies, but also different toxicity in mouse models

1.5 Protein misfolding cyclic amplification (PMCA)

Protein Misfolding Cyclic amplification is a highly sensitive and efficient tool for the propagation of protein fibrils. This technique was initially developed for the amplification of misfolded prion proteins, and has allowed scientist to further the understanding of the behaviour of prions, such as advancing knowledge of the existence of different prion strains and assessing the effects of the PrP transmission barrier [158, 159]. PMCA is now used for the propagation and characterization of prion strains and disease management/control. This includes the testing of animals for asymptomatic carriers [160], the analysis of soil derived from farmlands and woodlands to control the presence of prion pathogens [161] and to develop new decontamination methodologies [162].

PMCA consists of the incubation of a seed containing pathological misfolded proteins in an excess of physiological monomeric protein. Samples are sonicated to fragment the protein aggregates in solution, that in turn will act as seeds to recruit more monomeric protein to form fibrils. The cycle is then repeated, and the formation of more seeds results in the formation of more fibrils, exponentially

increasing the pathological protein in solution [159]. Although originally created for prions, in recent years the method has been adapted for the propagation of several other proteins involved in PMDs, including α -syn, obtaining fibrils that closely resemble the fibrils found *in vivo*. Through the use of human derived samples such as brain homogenate and CSF to direct the aggregation of synthetic α -syn monomers through templated misfolding, PMCA has been applied for therapeutic screening, diagnostics and the characterization of different strains of α -syn [106, 163-165] (figure 1. 8).

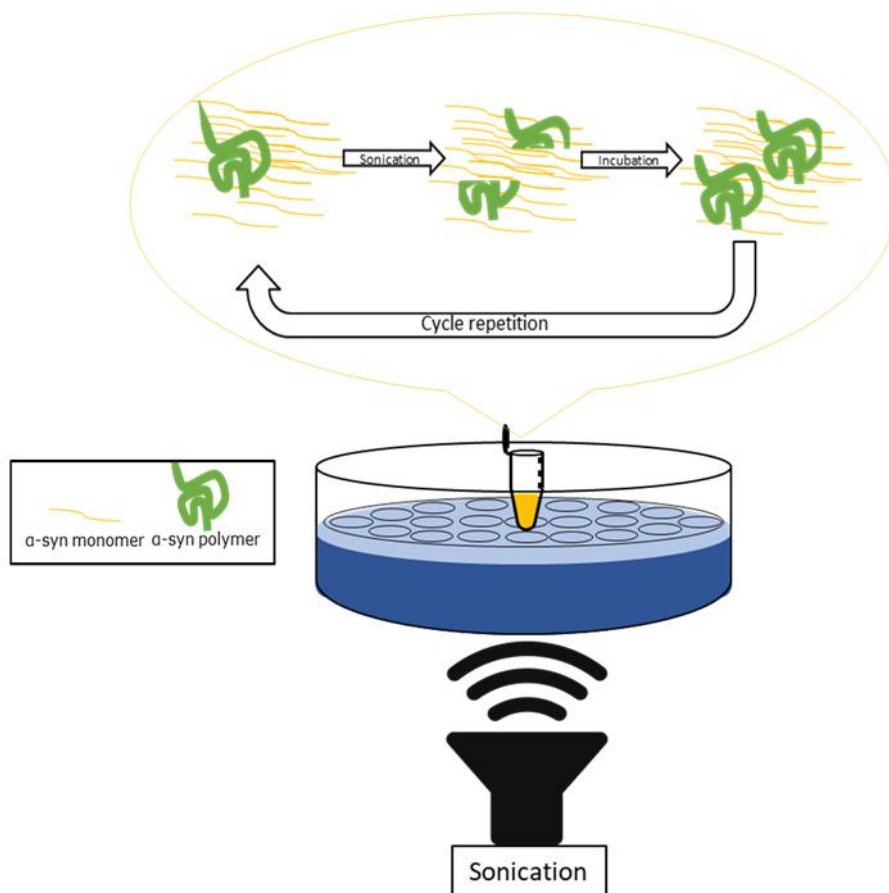


Figure 1-8: Schematic representation of fibril propagation through PMCA

PMCA is a methodology developed for the amplification of protein polymers *in vitro*. This is achieved through the repetition of a cyclical process consisting of two steps. First, small amounts of misfolded protein polymers are incubated in an excess of monomers; this allows the polymers to grow through the recruitment of the monomers in solution. Then, samples are subjected to mechanical stimuli (sonication with ultrasounds) that fragments the polymers and creates new polymerization sites. Repeating these two steps results in an exponential increase in the number of polymers in solution

To date, PMCA through sonication has not been reported for the propagation of $A\beta$ fibrils. Alternative methodologies include the incubation of synthetic or recombinant $A\beta_{40/42}$ peptides with preformed

fibrils, derived either from CNS tissue or produced *in vitro*. Propagation is achieved through the use of intervals of high intensity shaking and incubation [166], constant gentle agitation [133, 143, 145] or quiescent incubation [143, 146, 167]. As with α -syn, the propagation of A β fibrils *in vitro* has been utilized for furthering the understanding of amyloid fibril formation, diagnostics and screening for therapeutics, for an in depth review please refer to Singh *et al.*, 2019 [168]. Throughout this thesis, the term “misfolding” and “aggregation” in relation to the formation of protein aggregates with the aid of methodologies such as sonication or shaking are used interchangeably, as these two phenomena go hand in hand to propagate fibril aggregates *in vitro* [168].

1.6 Thioflavin T Assay

Thioflavin T (ThT) is a fluorescent dye that found widespread use in the studying of fibril forming proteins in solution, in particular A β [169]. ThT contains three structural sections: i) a benzothiazole ring, ii) a benzyl ring and iii) a diethylamino group. In solution, the ThT molecule assumes a non-linear conformation, due to intra-molecular Van der Waals repulsive forces; but upon the introduction of β -sheets (such as fibrils) in solution, ThT is able to bind these structures with high affinity and specificity [170]. This binding results in the transition of ThT from a weakly fluorescent molecule when unbound, to a highly fluorescent compound if excited when bound to fibrils (440-450 nm excitation). Interestingly, ThT fluorescence is proportional to the number of aggregates in solution, making this an ideal compound to probe for β -sheet rich protein aggregates in solution [171-181]. This remarkable property can be attributed to ThT being a “molecular rotor”: when excited in an unbound state, energy acquired through 440-450 nm excitation is usually dispersed through intra-molecular movements (rotation, twisting and intra-molecular charge transfer) that result in the ThT molecule returning to the non-linear ground state. When fibrils are present in solution, ThT binds to pockets, or grooves within the repetitive β -sheet stands, known as “cross-strand ladders”. This interaction with cross-strand ladders, locks the ThT molecule in such a way that the energy acquired through photoexcitation can no longer be dissipated, and results in the emission of intense fluorescent signals at around 490 nm [182].

Drawbacks of this methodology include reports of ThT interfering with the aggregation pathways of some fibril forming proteins [183], and the presence of ThT insensitive aggregates which do not interact with this molecule, and are therefore undetectable with this probe [184].

A typical ThT assay consists in adding a diluted amount of dye to a solution containing β -sheets, and monitoring fluorescence with excitation at 440-450 nm and emission at 490 nm, as seen in paragraph 2.8.

1.7 Immunotherapy approach to treat protein misfolding diseases

One strategy in PMD therapeutics is immunotherapy. Immunotherapy consists of the use of antibodies to treat specific disease causing targets, in the case of PMDs antibodies would target protein aggregates [185]. Immunotherapy can be divided into two subcategories: active and passive immunization. In active immunization (vaccination), the immune system of an individual is instructed to produce antibodies against a specific target. Passive immunization, on the other hand, consists of the administration of exogenous antibodies targeting a specific molecule [186]. For active immunization, an advantage is the creation of a vast array of polyclonal antibodies capable of generating a prolonged immune response whilst a potential disadvantage is the variability of antibody response between patients and the generation of adverse effects due to the vaccinations. For passive immunization, advantages include the capacity to deliver consistent amount of a known antibody with therapeutic effects, and the quick withdrawal of such molecules if side effect should arise; however, the approach necessitates continuous doses in order to maintain a therapeutic effect [187].

For PMDs, circulating antibodies may act by three main mechanisms to interact with the pathological targets to effectively reduce the disease burden: the catalytic modification of conformation of the target, phagocytosis and the “peripheral sink” effect. The catalytic modification of the target’s conformation, as the name suggests, consists of the alteration of the target’s secondary structure, into a conformation that is less prone to forming aggregates, this mechanism is possible even when the levels of available therapeutic antibodies crossing the blood brain barrier (BBB) are low, and does not

require the activation of other cellular populations (like macrophages) to take effect. The second mechanism, phagocytosis, relies on the more classic humoral response of opsonizing antigens triggering macrophage phagocytosis through complement activation. This would result in localized protein aggregate clearance; but this approach relies on the assumption that enough antibody is able to cross the BBB to bind the protein aggregates in the brain and trigger the activation of the resident microglial population without inducing an overactivation of the microglial population itself, thus causing harm. Finally, the peripheral sink effect is a clearance mechanism that doesn't rely on the antibodies crossing the BBB to take effect. The peripheral sink model assumes that circulating antibodies are able to bind free misfolded proteins in plasma, altering the BBB equilibrium towards the efflux of low molecular weight forms of the misfolded proteins to the periphery. With lower amounts of low molecular weight misfolded protein in the brain due to this "clearance", protein plaques are not able to proliferate, and no new protein deposits are formed. Antibodies capable of triggering this phenomenon are characterized by having a high affinity for their epitope [188].

1.7.1 Therapeutic antibodies targeting α -synuclein

In terms of passive immunotherapy, the monoclonal antibody, Prasinezumab (PRX002) has shown promising results, as injections of this molecule are able to induce a dose dependent decrease of aggregated α -syn in the serum of PD patients, when compared to controls [189]. Of note is that increased free α -syn in the serum is indicative of PD pathology. PRX002 was reported to reduce 96.5% of free α -syn in the serum of treated patients when compared to placebo treated individuals [190]. PRX002 is a humanized monoclonal antibody targeting α -syn and is currently under study in phase II clinical trials (NCT03100149/ NCT04777331). BIIB-054 is a human derived antibody directed towards α -syn with the ability to prevent α -syn misfolding in *in vitro* misfolding assays, prevent misfolded α -syn transmission in cell culture experiments and prevent dopaminergic loss in transgenic mice models [191]. Although showing promising results in clinical trials [191, 192] BIIB-054 was ultimately terminated as both primary objective (measurement of a dose-dependent improvement of the clinical symptoms of treated patients measured with Movement Disorder Society-Unified Parkinson's Disease

Rating Scale [MDS-UPDRS]) and secondary objectives (assessment of dose-dependent safety of the drug and pharmacokinetics of the drug) failed to be met (NCT03318523), resulting in the discontinuation of the drug. MEDI1341 is a monoclonal antibody initially discovered through phage display and optimized via several rounds of CDR optimization and reformatting into an IgG1 frame; MEDI1341 was initially found to inhibit fibril formation *in vitro*, to stop fibril conversion in cell culture studies and reduce pathological α -syn burden in mouse and primate models [193]. MEDI1341 recently started phase 1 clinical trial studies with an estimated completion date of May 2022 (NCT04449484).

Finally, new clinical trials to test the efficacy of passive immunization against α -syn has also been set up by several companies in recent years, but information about the mode of action and chemistry of these molecules is not yet available. This is the case for:

- UCB7853, set up by UCB, currently in phase I; the outcome of this trial is expected to be concluded on April 2023 (NCT04651153).
- Lu AF82422, set up by Lundbeck, currently in phase I; expected to be concluded on August 2021 (NCT03611569).
- ABBV-0805, set up by AbbVie, currently in phase I; concluded and withdrawn on June 2020 for strategic reasons (NCT04127695).

A list of all current and past clinical are summarized in table 1.5.

The pursuit of further antibodies to suppress α -syn pathology is on-going, and new molecules are continuously being developed; for a more detailed review discussing the historical and current research into immunotherapy in PD, please refer to Brundin *et al.*, 2017 [194]; Wan *et al.*, 2019 [195]; Fields *et al.*, 2019 [196] and Jamal *et al.*, 2020 [197].

Table 1-5: Characterization of the therapeutic antibodies against α -syn

Antibody	Epitope	Specificity	Conformational Specificity	Class	Antibody format
Most recent clinical trials					
PRX002* ¹	118-126	Linear	Aggregates* ²	Humanized	IgG1
BIIB-054	1-10	Conformation	Aggregates* ²	Human	IgG1
MEDI1341	Around 103-129	Linear	Monomers and Aggregates* ²	Human	IgG1
ABBV-0805	Not specified	Not specified	Not specified	Humanized	Not specified
LU AF82422	C-terminal (No further details available)	Not specified	Not specified	Humanized	IgG1
UCB7853	Not specified	Not specified	Not specified	Not specified	Not specified

*¹PRX002 was derived from the humanization of 9E4

*² Aggregates refer to elements including fibrils; protofibrils and oligomers

1.7.2 Therapeutic antibodies targeting β -amyloid

A β has been the main molecular target in AD immunotherapy for many years, and thus extensive pre-clinical research has allowed the discovery of several therapeutically relevant antibodies (shown in table 1.6). Indeed, several studies in the past have shown how immunization with synthetic A β peptides had neuroprotective effects in younger mice, and increased A β clearance from the brain of older treated subjects [198]. In other instances, administration of anti-A β antibodies in the periphery of mice could reduce the A β plaque burden, and even reverse the formation of cerebral A β plaques [199]. A β immunotherapy is therefore arguably in a more advanced stage than that for α -syn, ptau or PrP. Indeed, several molecules have been proposed as potential treatments for AD from animal models, and many have been tested in clinical trials. Examples include AN1792 (the first ever AD vaccine) and Bapineuzumab, both clinical trials which were halted due to adverse effects (such as microhaemorrhages, meningoencephalitis and increased vascular A β deposition [188, 199, 200]), or not achieving the desired clinical targets [187, 201]. Currently, five passive immunization clinical trials are ongoing [187, 202-206].:

Solanezumab, an anti-A β humanized monoclonal antibody with high affinity for soluble monomers, is currently undergoing phase III clinical trial studies (NCT02008357). Initial results revealed a modest positive effect in ameliorating A β deposition and slowing cognitive decline. Phase III clinical trials are expected to be concluded in December 2022. Controversially, preclinical studies with animal models showed no clearance of A β deposits from treated diseased transgenic mice (PDAPP model), but found a statistically significant improvement in the cognitive decline of treated animals [207]; further analysis using a different transgenic line (J20) not only showed no real changes in the cognition and protein deposition patterns of treated individuals but found an increased mortality rate of J20 treated mice compared to controls [208].

Gantenerumab, is a fully human anti-A β monoclonal antibody with high affinity for fibrillar A β , currently undergoing phase III clinical trials (NCT03444870; NCT03443973). This anti A β drug showed early promising results for A β clearance in treated patients [209]. Phase III clinical trials are expected to be concluded in November 2023. Gantenerumab was discovered through phage display and was found to bind epitopes both in the N-terminal and central portions of A β , and through this binding promote A β clearance via phagocytosis in cell culture and animal models [210].

Lecanemab is a humanized monoclonal antibody capable of binding large A β fibrils, also undergoing phase III clinical trials expected to be concluded in August 2024 (NCT03887455). Studies in humans and transgenic animal models showed an effective reduction in A β deposition in the brain of treated subjects (with actual prevention of further deposition seen in mice models [211]).

MEDI1814 is a human monoclonal antibody capable of targeting the C-terminal region of A β 42. Studies in animal models (mice and primates) showed a reduction in soluble A β [212]. Phase I clinical trials have recently been concluded, with results showing good tolerability and bioavailability of the drug in treated individuals (NCT02036645).

SAR228810 is a humanized monoclonal antibody with an affinity to fibrils and protofibrils. The drug was found to possess protective effects in cell culture *in vitro* studies. Further experiments in mouse models showed good tolerability and the antibody showed effective binding to pathological A β in human brain slices [213, 214]. SAR228810 completed phase I clinical trials in February 2015, with no follow-up clinical trials being performed (NCT01485302).

Several reviews have discussed the subject of AD immunotherapy, with particular emphasis on clinical trials throughout the years, for a more detailed description on the subject refer to Vaz *et al.*, 2020[205], Tolar *et al.*, 2020 [204] and Zampar *et al.*, 2020 [203].

To date, a single antibody, Aducanumab, has been given Food and Drug Administration (FDA) approval to be used to treat AD. This first of a kind drug was found to significantly improve AD pathology in animal models and patients, as evidenced by positron emission tomography images measuring A β deposition and cognitive tests [215]. Although initial analysis of Phase III clinical trial data found the antibody to be inefficient in successfully treating AD (NCT02477800), follow-up data analysis found a statistically significant improvement in A β clearance and cognition of patients, prompting the drug to be granted approval. These events led many members of the scientific community question the real efficacy of aducanumab, mainly with the recruitment and data analysis processes, and several prominent figures have called to perform re-tests on this drug [216].

Overall, 20 years of human studies with anti-A β immunotherapy have produced studies that showed a clear delay in the onset of the disease in treated subjects [217] as evidenced by the reduction of A β deposition in the brain of treated patients 18 months post injection [188] and the onset of dementia, but only a slight improvement in cognitive decline in later stages of the disease [217]. Recent studies focusing on alternative immunotherapy against other proteins of interests in AD, such as tau have demonstrated overall improvements in both A β deposition and cognitive decline in affected patients, showing very promising results for the treatment of AD affected patients [217-220].

Table 1-6: Characterization of the therapeutic antibodies against A β

Antibody	Epitope	Specificity	Conformational Specificity	Class	Antibody format
Most recent clinical studies					
Solanezumab	13-28	Conformation	Monomer	Humanized	IgG1
Gantenerumab	N-terminal (aa 3-12) and C-terminal (aa 18-27)	Conformation	Oligomer /Protofibril	Human	IgG1
Lecanemab	Large A β fibrils and protofibrils	Conformation	Protofibrils	Humanized	IgG1
MEDI1814	C-terminal (no further data available)	Not specified	Monomers	Human	IgG1
SAR228810	4-20	Not specified	Fibrils /Protofibrils	Humanized	IgG4
Approved drugs					
Aducanumab	3-7	Conformation	Aggregates* ¹	Human	IgG1

*¹ Aggregates refer to elements including fibrils; protofibrils and oligomers

1.8 Use of phage display to develop therapeutically relevant antibodies

Phage display is a high throughput methodology that allows for the discovery of antibody binders to a vast array of targets. This methodology has been implemented for different purposes such as: the identification of therapeutics, inhibitors of target activity or protein structure stabilizers, to find binders to inorganic materials and nanostructures, and to identify novel methods for cell targeting and enzyme design [221]. The versatility of this methodology makes it a desirable tool for the exploration of antibody binders capable of targeting fibril forming proteins, such as α -syn and A β , with the hopes of identifying a therapeutically relevant antibody with the ability of halting the progression of the disease. Phage display exists in conjunction with other display methodologies, such as ribosome display, mammalian cell display and bacterial display, among others, each with their own pros and cons. For detailed review discussion the different kinds of antibody discovery strategies refer to Ministro *et al.*, 2020 [222] and Chan *et al.*, 2014 [223].

Phage display is centred around the M13 filamentous bacteriophage, a single stranded DNA (ssDNA) viral vector possessing around 6500 bp [221, 224] (figure 1.9). M13 targets a specific subtype of *Escherichia coli* (*E.coli*) that possess the F plasmid, allowing it to express the fertility F pilus (a structure used for bacterial conjugation). The presence of the pilus is necessary as infection occurs through the interaction of one of the viral coat proteins (pIII) with the pilus; this causes the retraction of the pilus and the dragging of the virus to the proximity of the bacterial body. Once in contact with the bacterial cell membrane, the viral pIII interacts with the bacterial TolA. This interactions kickstarts the disassembly of the viral protein coat and transport of the ssDNA into the bacterial host. M13 infection does not result in the lysis of the bacterial host, but rather the establishment of a chronic infection that results in the continuous production and extrusion of viral particles from the infected cell [224] For an in depth review of M13 phage biology and *modus operandi* please refer to Kehoe *et al.*, 2005 [221] and Ledsgaard *et al.*, 2018 [224].

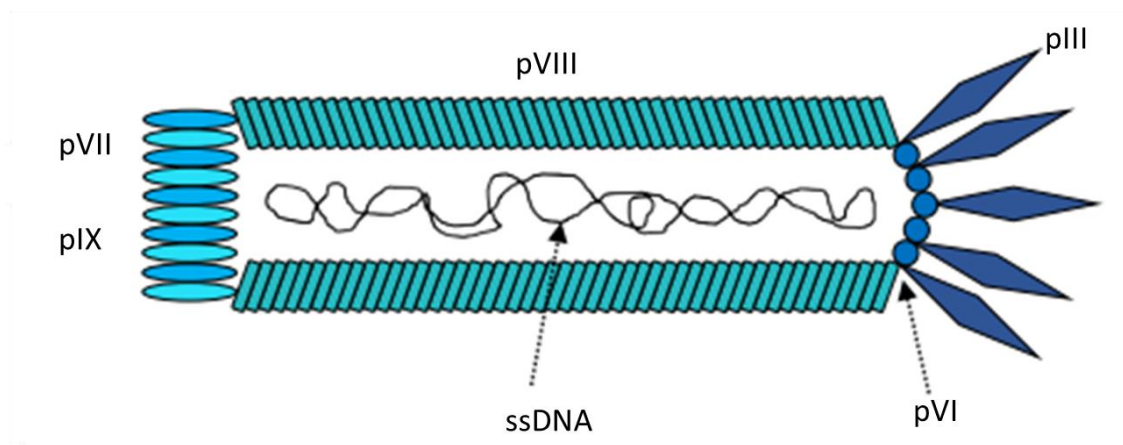


Figure 1-9: Schematic representation of M13 bacteriophage

The M13 filamentous phage possessing a ssDNA chromosome with nine genes, capable of producing eleven proteins. Five of these proteins are expressed to coat the phage (pIII, pVI, pVII, pVIII and pIX), while the remaining 6 proteins are involved in DNA replication, assembly and extrusion of the phage. Image adapted from Ledsgaard *et al.*, 2018 [224]. Licence under the CC BY 4.0.

In essence, this methodology revolves around the phage coat proteins, and the genetic engineering of these polypeptides for the display of a desired protein, such as antibody fragments as a coat protein fusion [221, 225-228]. Indeed, the wild type M13 virus produces 11 proteins, five of which (pIII, pVI,

pVII, pVIII and pIX) are coat proteins (table 1.7) [221, 224]. Some of these coat proteins can be genetically engineered to express a fused antibody fragment. Antibody fragments come in different forms (figure 1.10); amongst the most common ones are: i) Fragment antigen binding (Fabs) domains, where heavy and light variable domains (VH and VL respectively) interact through their heavy and light constant domains (CH and CL respectively) to form an antigen binding unit; ii) single chain Fv (scFvs), in which the antigen binding VH and VL domains are linked through a poly-peptide linker; and iii) nanobodies, small antibodies that are the equivalent of VH domain in an IgG. Nanobodies can be further divided into VHH (from camelids) and Vnar (new antigen receptor, from sharks) [228]. Antibody fragments (Fabs, scFvs and VHHs) are most commonly expressed as a pIII phage protein fusion, to allow the display of the antigen binding domains (see figure 2.2).

Table 1-7: Genes and proteins coded by the M13 filamentous phage genome [224, 229]

Gene	Protein	Function
I	Gene protein 1 (pI) Gene protein 11 (pXI)	Assembly
II	Gene protein 2 (pII) Gene protein 10 (pX)	Replication
III	Attachment protein(pIII)	Extrusion and coat protein adsorption
IV	Virion export protein (pIV)	Extrusion and assembly
V	DNA binding protein (pV)	Replication
VI	Head virion protein (pVI)	Budding and coat protein infection
VII	Tail virion protein (pVII)	Budding and coat protein assembly
VIII	Capsid protein (pVIII)	Coat protein
IX	Tail virion protein (pIX)	Budding and coat protein assembly

Phage display is usually performed using a vector called a “phagemid”. A phagemid only contains the genetic information for the coat protein fusion, for instance pIII-antibody, an antibiotic resistant gene to allow for the selection of bacteria containing this vector, and an origin of replication to propagate in the bacterial host. This strategy is used as it allows for the creation of large libraries and high efficiency during transformation [224]. A “helper phage” is then used to rescue the phagemid from the bacterial host. This helper phage is able to provide the missing genes necessary for assembly and extrusion and allows the propagation of the ssDNA phagemid itself. Unlike the phagemid, helper phage lacks an efficient origin of replication. When the helper phage infects a cell, the replication is

enough for the production of high amounts of helper phage, but when phagemid (with an intact origin of replication) is also present in the host *E.coli* cell, this will out-compete the helper phage packaging and results in the packaging of phagemid itself (table 1.8) [224].

Table 1-8: Genetic makeup of phagemid and helper phage.

Table adapted from Ledsgaard et al., 2018 [224].

Gene	Phagemid	Helper Phage
I		✓
II		✓
III		✓
IV		✓
V		✓
VI		✓
VII		✓
VIII		✓
IX		✓
Gene III + antibody fragment (Fab, scFv, VHH)	✓	
Origin of replication	✓	
Inefficient origin of replication		✓
Antibiotic resistance	✓	✓

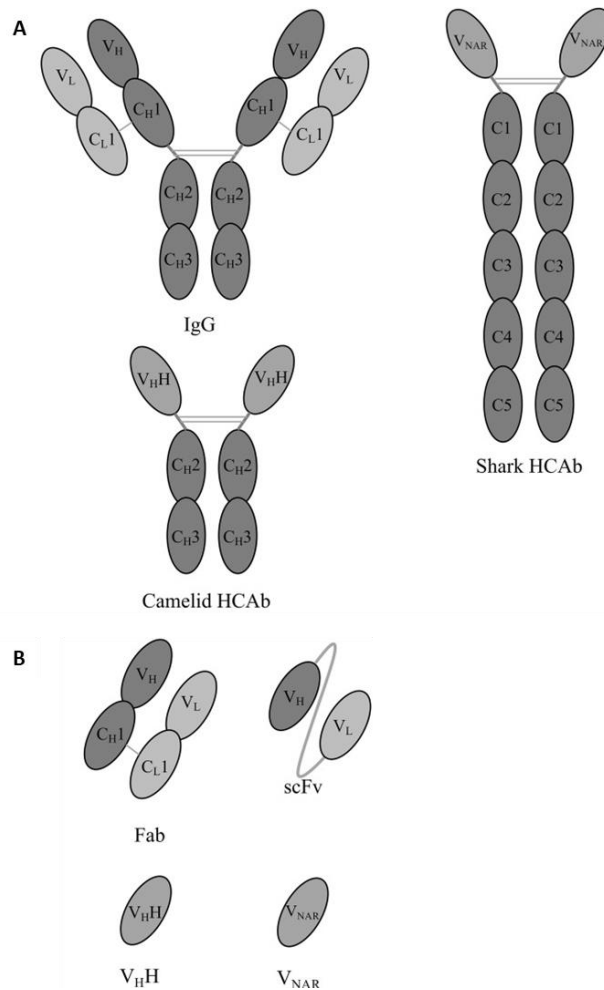


Figure 1-10: Different forms of antibody and fragments

A: Structure of multidomain conventional IgG and heavy chain antibodies (the latter expressed in shark and camelids). B: Different antibody fragments capable of being displayed on M13 phage. These can be Fabs, scFvs or nanobodies (either VHHs or Vnars). C: constant domain, V: variable domain, H: heavy chain, L: light chain. Image adapted from Reader *et al.*, 2019 [228], modified. Licence under the CC BY 4.0.

Phage-antibody complexes are produced as “libraries”. Libraries of antibody fragments displayed on the phage’s coat protein can be highly diverse. This variability within the binding regions of the antibodies can be introduced through different sources: animals immunized against specific targets, non-immunized animals, semi-synthetic or synthetically produced antibodies [226-228]. In the first method, animals are immunized against a target and their antibody-producing cells used to create the phage display library. As antibodies within the library are enriched *in vivo* for specificity for the immunization target, libraries produced with this methodology have the advantage of possessing high affinity antibodies even from relatively small diversity libraries ($\sim 10^6$ binders). This specificity is also a

drawback for these types of libraries, as a lack of diversity prevents the use of the same library for different targets, together with the ethical concerns derived from immunizing animals [226, 227]. Non-immunized animals (or human donors) can also be used to form what are known as naïve libraries [226-228], these libraries have the advantage of being more widely applicable than immunized libraries. Whilst they lack the target dependant specificity and affinity introduced by the immunization process, they can possess the range of antibody diversity present in the natural immunity of the animal used. However, these libraries are not completely unbiased, as previous immune responses accumulated through the donor's life prior to the library construction would shape the diversity of the library itself [226, 227]. Another approach is to use molecular biology techniques to artificially introduce variability to the binding regions within the antibodies, in what is known as a synthetic library [226-228]. Often, antibody templates, or cassettes, are used, and variability is introduced within the complementarity-determining regions (CDRs), regions within VH and VL defined as hypervariable regions where most of the diversity within the antibody molecule is found. This technique can produce a wide variety of antibodies capable of binding different targets. This approach offers the advantage of providing an unbiased library, able to be used against almost any target, but at the price of obtaining antibody binders with often lower affinity compared to immunized libraries and also the need to produce a very high diversity library (usually 10^9 to 10^{12} binders). Finally, semi-synthetic libraries are a mixture of the naïve and synthetic approach, whereby the natural immune diversity of the donor is enhanced using molecular biology techniques [226, 227]. For a more detailed exposition of phage display library types, please refer to Hoogenboon *et al.*, 1998 [227]; Hoogenboon *et al.*, 2002 [226]; Kehoe *et al.*, 2005 [221]; Ledsgaard *et al.*, 2018 [224] and Reader *et al.*, 2019 [228].

Most commonly, phage display libraries can be generated through the isolation and amplification of the VH and VL domains from B-cells of immunized or naïve donors through PCR. Alternatively, the different VH/VL fragments can be assembled *in vitro*, also through PCR for the generation of synthetic libraries. The generated amplicons are then cloned into the phagemid vector in frame with the phagemid pIII coat protein and rescued in preparation for biopanning [227], a human library

construction example can be found in the figure below (figure 1.11), the same process applies for libraries generated from non-human sources. Details of the VHH library used for the purpose of discovering antibodies towards fibrils for this thesis can be found in the methods section (paragraph 2.18)

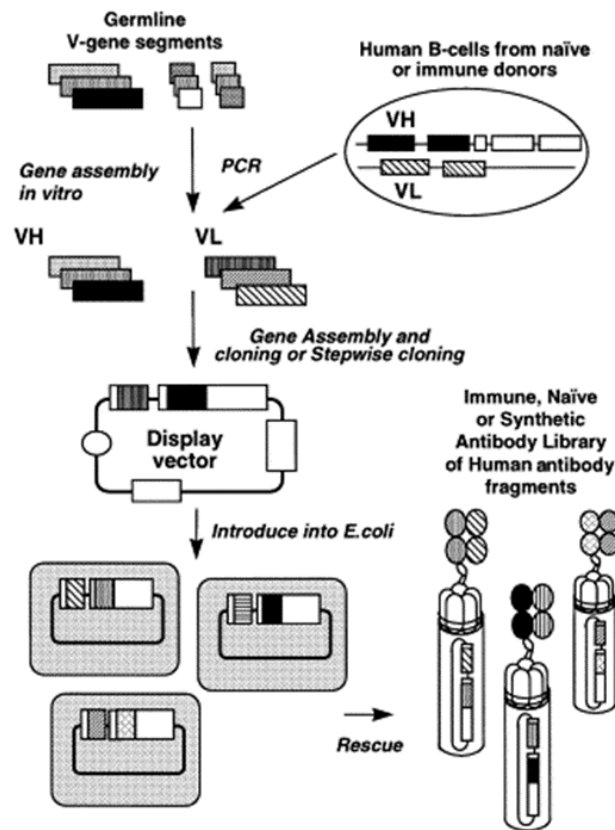


Figure 1-11: Example of human phage display library construction

Construction of human phage display library. VH and VL gene fragments are either assembled *in vitro* (for synthetic libraries) or amplified from B cells of immune or naïve donors (for immune or naïve libraries, respectively) through PCR. These genes are then cloned into the phagemid vector, in frame with the pIII phage coat protein and transformed into *E.coli* cells. Using a helper phage, the phagemids are rescued from the bacterial cells to produce phage particles expressing different antibody fragments fused to the pIII protein. The combination of the different variations of the antibody fragments makes up the diversity of the libraries. Image modified from Hoogenboom *et al.*, 1998 [227], licence number 5276391506849.

The phage display methodology is based on the binding of the phage library to a target molecule. This allows the binding of a subset of the antibodies expressed by the phage particles to the target. Binding is followed by several washes, aimed at eliminating non-bound viral particles; and then elution of the phage from target molecules, through the cleavage of the bond between antibody and target (usually

by a shift in pH or enzymatic treatment). The eluted phage is then propagated in *E.coli* and a second cycle of antibody selection or “panning” is performed. The aim of this procedure is to increase the number of high affinity binders against a specific target (figure 1.12). Generally, 3-5 rounds of panning are performed prior to the analysis of antibody binders [221, 225-227]. Once panning is concluded, several methodologies can be used to assess the presence of antibody binders, such as monoclonal ELISA, and then sequencing to assess the nature of the antibody binders. Phage display can be performed in solution (as seen in figure 1.12) using biotinylated proteins, or on a solid matrix, i.e. a 96 well plate, with proteins attached to the well’s surface [225-227].

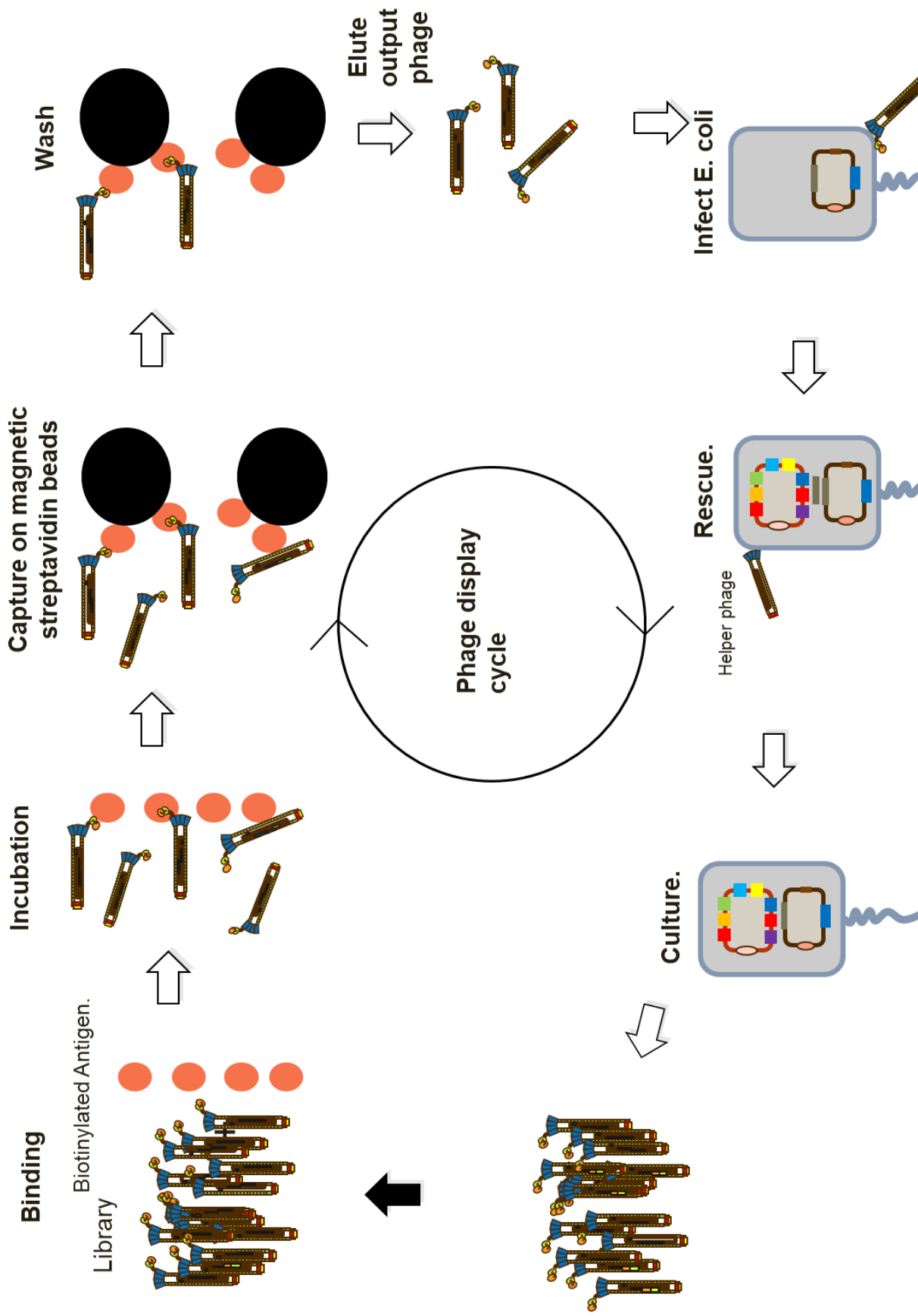


Figure 1-12: The phage display process in solution

DNA possessing the genetic information of a high number of ligands (antibody fragments) is cloned into the viral genome fused to a coat protein (most commonly pIII but also in pVI or pVIII). Libraries are generated through the use of phage to infect *E. coli* cells. From the libraries, phage containing the genetic information to produce a target specific binder is isolated through the repetition of a cyclical process including binding to the target, wash of non-specific molecules incapable of forming a bond with the target, elution, through the separation of the antibody fragment from the phage particle, using the eluted phage to infect new *E. coli* cells, rescue of phage through the use of a helper phage, and culture.

As mentioned above, phage display is an attractive methodology to facilitate the discovery of A β and α -syn binders, due to this technique's versatility and efficacy. Previously, several attempts have been made to identify an antibody binder with potential therapeutic applications, using both the passive and active immunization approaches.

1.8.1 Passive immunization studies

One of the first studies using phage display as a tool for the discovery of anti-A β antibodies for potential passive immunization was the work performed by Manoutcharian *et al.*, 2003 [230]; where common albino mice were immunized with A β ₄₂ fibrils, phage scFvs were then generated from the mRNA from the spleen of immunized animals, producing the first ever anti-A β fibril scFv library. From these early discoveries, several different approaches have been attempted:

Naïve and synthetic libraries (scFv and VHH [173, 177, 180, 231, 232]) have been used for the discovery of antibodies capable of reducing disease burden in APP transgenic mice [231]. Antibodies have been shown to identify differentially sized oligomers and reduce the toxicity of these aggregates [177]; and halt the spread of A β fibrils through the inhibition of secondary nucleation sites [180]. Such antibodies could also reduce amyloid burden in human brain tissue through the targeting of the oligomeric subpopulation larger than 60 kDa. Within the treated tissue, reduction of amyloid burden was accompanied by lower levels of Tau hyperphosphorylation and reactive oxygen species production [232].

Immunized libraries have also been used to target A β oligomers and have been shown to produce functional high affinity antibodies [173, 233]. Using an scFv library generated from the immunization of non-human primates with A β oligomers resulted in the discovery of antibodies capable of reducing overall fibril aggregation *in vitro* [173]. Additionally, a human derived scFv library was generated using blood samples derived from AD patients (with higher titres of peripheral A β oligomers compared to non-pathological controls). This library was used to discover a antibody that bound a conformational

epitope that was capable of binding A β oligomers with high affinity and specificity, and that could rescue cognitive behaviour when injected into APP transgenic mice [233].

In addition to naïve and immunized libraries, other approaches have also been utilized to intentionally or accidentally discover molecular binders to A β fibrils; for example the use of a semi-synthetic scFv library (Tomlinson) to generate antibodies against insulin fibrils able to cross react with fibrillar A β species [234]. Moreover, antibodies capable of indirectly inhibiting the spread of AD have also been successfully produced. This was achieved through the use of β -secretase immunized llamas, to create a VHH library. Through this approach, antibodies capable of binding this enzyme were discovered, and functional testing showed a dose dependant reduction of β -secretase activity, in both biochemical and cellular assays, demonstrating the viability of this approach as a potential therapeutic [235]. Finally, an entirely synthetic method to generate computationally designed antibodies has also been implemented [179]. Antibodies generated in this way were used to target Zinc²⁺ stabilized A β oligomers (with increased toxicity compared to non-stabilized aggregates), and antibodies capable of altering the physicochemical properties of these aggregates were identified.

As discussed, several attempts have been made to discover a functional antibody capable of halting the spread of AD via passive immunisation. Out of all of the drugs currently on trial, only one was discovered through phage display: the previously mentioned Gantenerumab [210]. This binder is currently half way into its phase III clinical trial, and was discovered using the human combinatorial Fab library-1, a Fab library [209] generated through the recombination of a previously generate scFv library [236]. Ganterenumab is capable of binding the N-terminal and central region of A β and promotes the clearance of aggregated peptides through the activation of the macrophage response [210].

In the case of targeting α -syn through antibody phage display; naïve (Griffin library [175]) and semi-synthetic (Tomlinson [174]) libraries have been used to target monomeric and oligomeric α -syn species, respectively. Antibodies raised against these targets showed inhibition of α -syn fibril

formation [175] and a dose-dependent protection against oligomeric species in cell-based assays [174]. Camelids immunized with monomeric α -syn have also been utilized to create a VHH library from which an antibody (NbSyn2) capable of binding the C-terminal of monomeric α -syn was identified. Interestingly, initial findings indicated this antibody did not seem to alter the structure of the target protein, and kinetic studies confirmed that bound monomers were undisturbed in the formation of fibrils; therefore this antibody did not prevent fibril formation but was capable of labelling the protein without altering its properties [172]. However, further analysis of NbSyn2 together with another nanobody identified with a similar method (NbSyn87) revealed their ability to redirect the misfolding pathway of α -syn monomers and oligomers towards a less toxic and unstable form, making them potential candidates for further developments as therapeutics [237, 238].

Finally, the genetic manipulation of a conformational antibody (Syn-F2) capable of binding α -syn fibrils [239] led to the discovery of an engineered scFv antibody, called scFv-pC, with the ability of inhibiting fibril formation *in vitro*, reducing the spread and phosphorylation of serine 129 in cell culture studies and possessing a facilitated cell absorption rate through the use of a fused cell-penetrating peptide, making this a potential candidate for further studies in animals [240].

1.8.2 Active immunization studies

Active immunization strategies focused around phage display have been attempted mainly in mouse models, and to my knowledge, no vaccination candidate resulting from these tests has been attempted in human clinical trials. In most studies, immunization is achieved by the inoculation of transgenic animal models (London [APP V717I] [241-243] and Swedish [242, 243]) with phage expressing the peptide sequence EFRH in their coat protein (most commonly pVIII, due to the high number of copies of this protein in the phage's capsule). The tetrapeptide EFRH was chosen as this same sequence is present in the A β peptide, and studies showed the strong influence of this region in the regulation of A β misfolding. The infection with phage expressing this sequence serves the purpose of introducing (in a controlled manner) a high number of specific antigens, with the aim of raising specific immunity against this particular sequence in the host, effectively producing anti-EFRH

antibodies [241-243]. Interestingly, infected transgenic mice showed a rescue of cognitive behaviour (not present in sham injected animals). Surprisingly, the protection offered by the phage was longer than expected in infected mice; this was believed to result from the chronic infection of the *E.coli* cells naturally present in the gut of these animals, chronically expressing the phage and thus providing a long-term immunization against the tetrapeptide [243]. To my knowledge, no active immunization studies have been attempted with anti- α -syn compounds.

In addition to antibody-phage display, peptide-phage display has been used in numerous studies to isolate therapeutic candidates to PMDs with varied success. Examples include the anti-aggregation peptides discovered by Orner *et al.*, 2006 with the ability of binding the N-terminal sequence of A β [181]; or the anti-A β oligomeric pentapeptide discovered by Kawasaki *et al.*, 2010 [178]. This antibody free approach offers another possibility of the discovery of anti-aggregation compounds and shows the versatility of phage display as a methodology. As peptide libraries are outside of the scope of this research, they will not be discussed in detail.

1.9 Aims and objectives.

The main goal of this project is the production of potentially clinically relevant antibodies to be used in the treatment of PMDs like PD and AD. To do so, firstly, fibrils will be produced from recombinant and synthetic monomers *in vitro* and the resulting aggregates characterised in terms of their biochemical and physical properties. Secondly, antibodies with the ability to bind said fibrils will be identified using phage display methodologies. And finally, these antibodies will be tested for their abilities to inhibit fibril formation, shifting the equilibrium towards the stabilization of monomers.

Fibril production and characterization will focus on both recombinant α -syn and synthetic A β ; fibril-specific binders would then be raised only against A β aggregates.

Chapter 2: Materials and Methods

2.1 Expression of α -syn monomers:

The α -syn vector was a kind gift from UCB Celltech. This plasmid (4974 bp) was an in-house vector expressing the wild type (140 amino acid) human α -syn protein (gene bank number: NG_011851) under the transcriptional control of the human cytomegalovirus promoter and a kanamycin resistance gene under transcriptional control of the bacterial pUC origin of replication (figure 2.1).

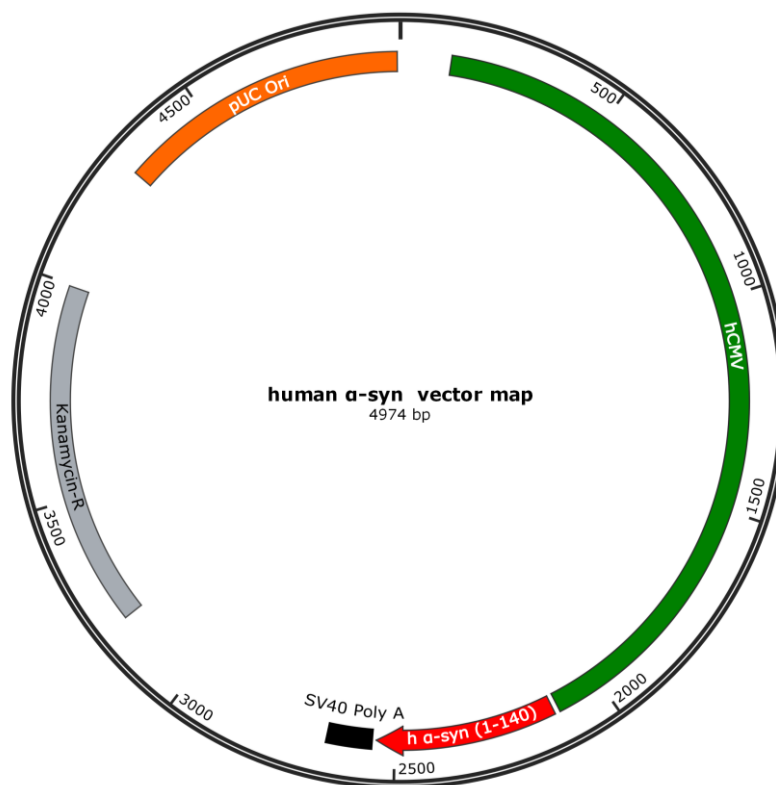


Figure 2-1: α -syn vector map

Vector showing the kanamycin resistance gene under the transcriptional control of the pUC origin of replication and α -syn regulated under the human cytomegalovirus (hCMV) promoter. The α -syn gene was inserted into the vector using the *HindIII* and *XhoI* restriction enzymes at the 5' and 3' site respectively. A Simian virus 40 PolyA (SV40 Poly A) stop signal is present at the end of the α -syn gene to stop the transcription.

XL Blue 1 cells (Fisher, 50125058) were transformed with the α -syn plasmid. Transformation was achieved through a 4 °C to 42 °C heat shock for 50 seconds. The cells were then incubated with S.O.C medium (ThermoFisher, 15544034) (0.5% (w/v) yeast extract, 2% (w/v) tryptone, 10 mM NaCl, 2.5 mM KCl, 10 mM MgCl₂, 10 mM MgSO₄ and 20 mM glucose) for 1 hour at 37 °C in a shaking incubator (200 rpm orbital shake). The transformed cells were then plated on LB-agar+kanamycin petri dishes (15 g/L agar, 10 g/L tryptone, 10 g/L NaCl, 5 g/L yeast extract, 50 μ g/ml kanamycin [ThermoFisher, J17924.14]), and incubated at 37 °C overnight. A single colony was then picked and grown in 2 YT

growth media (16 g/L tryptone, 10 g/L yeast extract, 5 g/L NaCl) overnight, with 50 µg/ml kanamycin in a shaking incubator (200 rpm orbital shake) at 37 °C.

The cells were transferred to a 200 ml Falcon tube. Growth media and cells were separated through a 30 minute centrifugation with 3,649 g (Beckman Coulter, Avanti J-20 centrifuge, fitted with fixed angle JLA 16.250 rotor), at 20 °C. The plasmids were isolated using the Qiagen Plasmid Plus Giga kit, following the in-kit instructions. A final 2 ml yield of α-syn plasmid DNA concentrated at 3 µg/µl was obtained and stored at 4 °C until ready to be used; long term storage was performed by freezing the DNA at -20 °C.

Expi™ 293 F cells (ThermoFisher, A14527) were used for the transfection of the plasmids. Expi™ 293 F are a derivative of human embryonic kidney 293 cells, a highly stable cell line that is characterized by the constitutive expression of the SV40 large T antigen. This antigen drives the expression of proteins coded in vectors with the SV40 promoter (as in the case of the human α-syn vector) thus allowing high titres of proteins to be produced. This, in combination with the fact that Expi™ 293 F cells are propagated in solution, highly tolerant to transfections and would allow the human α-syn to be expressed in a human-derived system contributed to the decision of using this cell line to produce proteins for this project.

Cell culture was performed by the UCB cell culture laboratory staff. Cells were ready to be transfected when a density of 3×10^6 cells/ml with 95% viability in 1 L was achieved. Transfection was performed using the ExpiFectamine™ 293 Transfection Kit (ThermoFisher, A14524): α-syn plasmid DNA (1 mg) and 2.7 ml of Expi™ 293 Reagent were mixed separately with Opti-MeM™ I Reduced Serum Media, to a final volume of 50 ml for each solution. Both solutions were incubated for 5 minutes at room temperature and then mixed together, making a final volume of 100 ml and then incubated again for an additional 30 minutes. Next, the DNA and reagent mixture were added to the litre of cells and incubated for 16 hours in a shaking incubator (125 rpm) at 37 °C in a humidified atmosphere and 8% CO₂. Next, 150 µl of ExpiFectamine™ 293 Transfection Enhancer I and 1.5 ml of ExpiFectamine™ 293

Transfection Enhancer II were added to the flask containing the cells following by a 96 hours incubation in a shaking incubator (125 rpm) at 37 °C in a humidified atmosphere and 8% CO₂, in order to express recombinant α -syn.

2.2 α -syn purification

α -syn was purified following a standard protocol developed by UCB Celltech. The α -syn expressed by the Expi™ 293 F cells was secreted into the transfection medium. A crude separation of the proteins of interest from the cells was performed by an initial centrifugation at 3,064 g (Beckman Coulter, Avanti J-HC centrifuge, fitted with fixed angle JLA 8 1000 rotor) for 45 minutes at room temperature. A second separation was then achieved by the use of two filters: Sartobran P (Sartorius Stedim, 5232507H1) with a pore size of 0.45 μ m followed by a Millipack® 60 Gamma gold filter (Millipore, MPGL06GH2), with a filter size of 0.22 μ m. The end result of this two-step filtration process was 1 L of cell-free supernatant with α -syn in solution.

α -syn was purified on an AKTA Pure (GE Healthcare) FPLC machine with a four-step chromatography purification process. For this purpose, buffer solutions were prepared: Buffer A: 20 mM Tris/HCL, pH 8.0 (Trizma® TRIS base, Sigma) in ultrapure water; Buffer B: 20 mM Tris/HCL + 1 M NaCl (Sigma) and Buffer C: 100 mM NaOH (Sigma) in ultrapure water.

The cell free supernatant (1 L) was mixed with 1 L of Buffer A and slowly loaded onto two conjoined 5ml HiTrap™Q FF (Scientific Laboratory Supplies, 17515601) anion exchange columns, washed and equilibrated in buffer A, through the sample line. Bound protein was eluted with a NaCl gradient achieved by mixing 40% Buffer B in Buffer A, over 16 column volumes. The eluted fractions (2ml) were collected in Nunc® 96 DeepWell™ plates (Sigma, Z717274). From these plates, small volumes (10 μ l) were analysed with 4-12% Bis-Tris gels (200V for 35 minutes) in order to confirm the presence of α -syn as a band of 14 kDa. Gels were stained with 20 ml InstantBlue (Expedeon) for at least 15 minutes. Once fractions containing α -syn were identified, they were pooled together (final volume of 70 ml). The pool of proteins were then concentrated using Centriprep Ultra 10 kDa MWCO (Millipore), by

loading 15 ml of protein solution and spinning at 4415 g for 15 minutes (Thermo multifuge X3R, fitted with TX-750 rotor body and 750mL swinging buckets); this step was repeated until the initial 70 ml volume was reduced to 20 ml. The concentrated product was then desalted using a HiTrap™ 26/10 Desalting column (Sigma, GE17-5087-01) that had been equilibrated and run in Buffer A, manually loading 10 ml into the columns using a syringe. Fractions were collected in 8ml Falcon™ round-bottom polystyrene tubes (FisherScientific). Following the desalting step, protein solutions were pooled together (around 80 ml) and loaded onto a second anion exchange column, a Mono Q (Sigma, GE17-5166-01) ion exchange column equilibrated in buffer A, manually loading 10 ml of pooled desalted product at a time. As for the previous anion exchange column, elution of the bound proteins was achieved with a 40% Buffer B gradient | Buffer A, over 20 column volumes with a flow rate of 2 ml/min. The resulting fractions (2ml) were collected in Nunc® 96 DeepWell™ plates and analysed with 4-12% Bis/tris gels, to identify fractions with the most α -syn content. This step allowed the additional separation of the initial α -syn pool into two distinct species: α -syn A and α -syn B, distinguished by different peaks in the chromatogram. These two populations were pooled separately (36 ml α -syn A and 40 ml α -syn B). Next, each population was concentrated to a final volume of 5 ml, using protein concentrators as described above. The 5 ml of concentrated α -syn A and B pools were then loaded separately (5ml at the time) into a HiLoad™ 26/600 Superdex™ 75 pg size exclusion column (Sigma, GE28-9893-34), pre-washed with Buffer C and equilibrated with PBS. The resulting fractions (2ml) were collected in a 96 deep well plate and analysed by SDS-PAGE. Fractions with the highest amount of monomeric α -syn were then pooled and concentrated to a final value of 2.69 mg/ml for α -syn A and 3.71 mg/ml for α -syn B. The final α -syn solutions in PBS were filtered through a Millex-GP 0.22 μ m (Sigma, SLGPB5010) syringe filter before snap freezing in dry ice and storage at -80 °C.

2.3 Preparation of synthetic A β ₄₂ Monomers

2.3.1 For kinetic studies and characterization studies (at the University of Nottingham)

The synthetic A β ₄₂ peptide (DAEFRHDSGYEVHHQKLVFFAEDVGSNKGAIIGLMVGGVVIA) was purchased from Gencust and was delivered as 2 mg aliquots in 1.5 ml Eppendorf tubes. Monomeric A β ₄₂ solutions were created by following a two-step solubilization protocol that includes the resuspension of the monomers in different highly alkali solutions, to minimize the presence of pre-formed aggregates in solution [244-246]. First, the 2 mg aliquots were carefully dissolved into 4 ml of chilled 10% (v/v) NH₄OH in PBS (pH > 11); creating 4 ml of a 0.5 mg/ml solution of A β ₄₂. Unnecessary pipetting or manipulation of the peptides in solution was avoided, so as to prevent the formation of aggregates. Samples were then incubated on wet ice for 10 minutes and then frozen in dry ice. Once frozen, the NH₄OH was removed through an overnight re-lyophilization step using a freeze drier unit (Labogene Coolsafe) attached to a Vacuubrand RZ2.5 vacuum pump. This process yielded 0.5 mg of a white fluffy powder known as “fairly floss” [244]. This alkali-treated re-lyophilized powder was stored at -80 °C. For use, 0.5 mg aliquots of re-lyophilized A β ₄₂ peptides were dissolved in 200 μ l of a 60 mM NaOH solution and incubated at room temperature for 10 minutes, creating a 554 μ M solution of A β ₄₂. This A β ₄₂ monomer stock solution was then dissolved in PBS to create the required concentrations of A β ₄₂.

2.3.2 For Biopanning with VHH-phage display library, shaking PMCA and functional assays (in UCB Celltech)

Synthetic peptides A β ₄₂ peptides (DAEFRHDSGYEVHHQKLVFFAEDVGSNKGAIIGLMVGGVVIA) were ordered from both Gencust and Genscript. Due to unavailability of a freeze dryer, an alternative method to dry the 10% (v/v) NH₄OH from the resuspended peptide pellet was carried out. For this, a GreenHouse Plus Parallel Evaporator™ (Radleys) was used. A β ₄₂ samples were resuspended in 10% (v/v) NH₄OH in PBS (pH > 11) and incubated in wet ice for 10 minutes, as previously described; then 1ml of the 0.5 mg/ml A β ₄₂ solution was placed into small 7 ml round bottom greenhouse glass test

tubes (Radleys), and positioned within a 48-space test tube rack within the evaporator. Gaseous N₂ was then flowed at a rate of 10-20 L/min to the samples within the tubes. The chamber containing the tubes with solubilized peptides was placed on top of a heated plate set at 30 °C and samples (1 ml) were then allowed to evaporate with a constant N₂ flow for at least 3 hours. The process was stopped when all the liquid within the tubes was evaporated, leaving a uniform layer of dried A β 42 peptides. Dried monomers were treated in the same as freeze-dried samples.

In order to capture any potential contaminants raised during the drying process (A β 42 particles and evaporated NH₄OH) the evaporator chamber was connected to the upper port of a greenhouse blowdown condenser, topped up with dry ice. The air was then made to flow through the frozen condenser, and contaminants captured in a sealed round bottom collection flask attached to the condenser. As an additional precaution, the gas flowing from the lower port of the condenser was redirected to a gas bubbler, with around 200 ml 1M NaOH aqueous solution.

2.4 PMCA.

2.4.1 PMCA of α -syn:

Protein misfolding was achieved by the repeated sonication and incubation cycles. Two different settings were used to misfold α -syn over the course of the study: one more closely resembling the method described by Herva *et al.*, 2014 [163], for the production of *de novo* α -syn fibrils; and the other following the methodology implemented in Jung *et al.*, 2017 [106] for the amplification of α -syn fibrils in reactions seeded with brain material. Throughout the PMCA experiments, α -syn A was preferentially used, due the higher level of purity found in this sub population. For the first method, α -syn was diluted to a final concentration of 90 μ M in conversion buffer (1% Triton X-100 (v/v) from Fisher Bioreagents in 1X PBS). This dilution was then aliquoted into 200 μ l PCR tubes (Sigma, AXYPCR02C) and placed within the water bath of a Misonix ultrasonic liquid processor S-4000. For PMCA, samples were sonicated for 40 seconds (70 % amplitude) every 29:20 minutes of incubation at 37 °C for 48 cycles (24 hours). Where indicated, samples were additionally seeded with preformed α -syn fibrils at a dilution of 1:100. The second method used 20 μ M recombinant α -syn in conversion

buffer. Samples were placed in the water bath and sonicated for 20 seconds (50% amplitude) every 29:40 minutes of incubation at 37 °C, for 96 cycles (48 hours). PMCA reactions were either non-seed or, whenever specified, seeded with 2 µl of human cytosolic brain extracts derived for 10% (w/v) brain homogenates from PD and control individuals (further described in 2.6) in 200 µl of conversion buffer.

2.4.2 Amplification of Aβ fibrils:

Aβ42 PMCA was attempted by implementing a range of different conditions (further described in the result section). Briefly, solutions of Aβ42 monomers (200 µl with 20 µM monomer in PBS buffer) were seeded with either 1% (v/v) pre formed Aβ42 fibrils, 10% (v/v) pre formed Aβ42 fibrils, 2 µl of brain cytosolic extract (as is, or as part of a 10-fold dilution series) or not seeded at all; samples were sonicated with 20 second pulses at 10% amplitude every 29:40 minutes of incubation at 37 °C. For PMCA reactions with additives, the following molecules were dissolved in PBS and added to PMCA tubes prior to the addition of the monomers and seeds (final concentrations are given): Heparan sulphate (100 µg/ml), Heparin (20 µg/ml), Digitonin (500 µg/ml), Saponin (500 µg/ml), α-crystallin (0.1 µg/ml) and Dextran sulphate (5mg/ml); all sourced from Sigma (respectively, H7640-1MG, H3393-10KU, D141-100MG, 47036-50G-F, C4163-5MG and 42867-5G).

2.5 Other Fibril manipulation procedures

2.5.1 Aβ42 de novo fibril formation

De novo fibrils were generated by dissolving 50 mg of the synthetic peptides (without any prior treatment) into 3.75 ml of a 1% (v/v) NH₄OH solution in ultrapure water (pH>11). Once the peptides were dissolved, the solution was adjusted to a final concentration of 1 mg/ml by adding 46.25 ml of PBS. The final product was gently agitated, aliquoted, and stored at -80 °C for further analysis and use. For positive controls in fibril monitoring assays including fluorescence measurement experiments, fibrils were either used as is (1 mg/ml ≈ 222 µM) or diluted to the desired concentration.

2.5.2 Aβ42 fibril propagation through incubation.

Monomeric Aβ42 solutions (20 µM) were prepared in PBS buffer. Aliquots (200 µl) were placed in different wells of a black Nunc™ MicroWell™ 96-Well Optical-Bottom Plates with Polymer Base (Fisher,

265301). Wells were then either not seeded or seeded with a final volume of 10% (v/v) preformed synthetic A β 42 fibrils. The plates were sealed with a clear sheets of adhesive PCR sealing tape (ThermoFisher, AB0558) and incubated for 72 hours at 37 °C with no agitation. Fibril propagation was assessed through the thioflavin T (ThT) assay. Where indicated, incubation experiments were also performed with AD and HC brain seeded samples, at a final concentration of 1:100 per well analysed.

2.5.3 A β 42 seeded fibril propagation with real time quaking induced conversion (RT-QUIC)
RT-QUIC (referred also as shaking PMCA throughout this manuscript) was performed using a FLUOstar Omega plate reader. N₂ dried and reconstituted solution of A β 42 (200 μ l per well at 20 μ M) in PBS were seeded with 1%, 10% or no fibrillar material from either Genscript or Gencust. ThT was added to each well to a final concentration of 30 μ M. Fibril formation was accelerated by 1 minute of orbital shaking (500 rpm) every 29 minutes of incubation at room temperature (25 °C). At the end of each shaking/incubation cycle, ThT emission was measured at 450 nm excitation and 492 nm emission.

Synthetic A β 42 peptides derived from N₂ dried Genscript batch E6379020H monomers needed an additional filtration step after resuspension, as a fibrillar contamination was observed. Following the addition of 200 μ l of 60 mM NaOH and 10-minute incubation in wet ice, the monomers were further diluted in PBS, reaching a final volume of 1 ml. Aliquots (500 μ L) were then placed on the outer chamber of two Microcorn DNA Fast Flow Centrifugal Filter Units (Merck), with a 100 kDa molecular weight cut-off. The tubes were then centrifuged at 500g for 10 minutes using a benchtop centrifuge. After the filtration process was concluded, the 'clean' flowthrough found in the inner chamber was used to seed the PMCA reactions at 20 μ M.

2.5.4 A β 42 fibril fragmentation

Genscript A β 42 fibrils (500 μ l) at 1 mg/ml in PBS were placed in a safety lock 1.5 ml Eppendorf tube (Fisher, 16439009) and subjected to ultrasonic degradation with 7x 10 second incubation-sonication (20 microns) cycles using a Soniprep 150 probe ultrasonic disintegrator (MSE). Fragmentation was confirmed with native gel electrophoresis (see section 2.10).

2.6 Human brain samples

Human brain samples were obtained from Parkinson's UK brain bank (Imperial College London). The tissue bank granted use of the tissue as end users. The Biobank had NRES approval, REC reference: 08/MRE09/31 + 5. This study was granted specific ethical approval by the School of Veterinary Medicine and Science Local Ethics Committee at the University of Nottingham and the ethics committee serving the biobank. For the purpose of this project, cell-free cytosolic brain extracts were used as human seeds to spike our PMCA reactions. These samples were kindly provided by Dr Lisa Chakrabarti, and produced using the methods described in Pollard *et al.*, 2016 [247]; briefly: brain samples from PD or AD patients were placed in GentleMACS C tubes with mitochondrial extraction buffer (50 mM Tris-HCl pH7.4, 50 mM HEPES, 100 mM sucrose, 1.5 mM MgCl₂, 100 mM KCl and 1 mM EGTA) and homogenized with a GentleMACS Dissociator. Samples were then spun at 4 °C in a benchtop centrifuge at 850 g for 10 minutes. The resulting supernatant was then centrifuged again at 1000 g for 10 minutes (precipitating the nuclear fraction). This process was repeated for a third centrifugation step at 10000 g for 30 minutes to precipitate the mitochondrial fraction and resulting in the brain cytosolic extract as the supernatant. α -syn PMCA was seeded using the *substantia nigra of 9* PD and 11 age and sex matched controls. A β 42 on the other hand, was seeded with the frontal cortex (Brodmann area 9) of 10 AD and 10 age and sex matched controls. Seeded reactions were performed at a final seed to buffer ratio of 1:100.

2.7 Cerebrospinal fluid samples

Human CSF samples were obtained from Human Tissue Authority approved biobanks, Oxford Parkinson's Disease Centre and BioMOx. The tissue bank granted use of the tissue as end users. The Biobank has NRES approval, REC references: South Oxfordshire REC 08/H0605/85; OPDC NRES: 10/H0505/71. All samples had been previously processed to render them cell-free. This study was granted specific ethical approval by the School of Veterinary Medicine and Science Local Ethics Committee at the University of Nottingham.

2.8 Thioflavin T assay.

ThT was purchased from Sigma (T3516-25G). A concentrated stock of 1 mM ThT in sterile PBS was produced, filtered through a 0.22 μm syringe filter (Sigma, SLGL0250S), aliquoted and stored at $-20\text{ }^{\circ}\text{C}$. Prior to use, aliquots were thawed and stored at $4\text{ }^{\circ}\text{C}$; defrosted vials were not kept for more than a week. For our experiments, 3 μl of the 1mM solution of ThT were added for every 100 μl of the fibril product tested, making a 30 μM ThT solution. Fluorescence was then measured with a TECAN, GENios Plus plate reader or a FLUOstar Omega plate reader using 450 nm excitation and 492 nm emission wavelengths. Measurements were taken every 10 minutes for 1 hour. ThT data was analysed and plotted using GraphPad Prism version 9.2.0.

2.9 SDS-PAGE gels and western blotting.

Electrophoresis was performed on 12-well NuPAGE 4-12% Bis-Tris gels (ThermoFisher, NP0322BOX) run with 1X MES running buffer (ThermoFisher, NP0002) in XCell SureLock Mini-Cells (ThermoFisher, EI0001). For each run, 10 μl of sample were mixed with 10 μl of sample buffer (NuPage LDS[®] sample buffer 2X [ThermoFisher, NP0008], with 5% (v/v) β -mercaptoethanol), boiled for 10 minutes and loaded into the gel. Electrophoretic separation was achieved with a 35-minute run at 200 V. Protein bands were detected either by coomassie blue staining or western blotting. Coomassie blue staining was achieved through an overnight incubation with 20 ml of a 1:1 dilution of InstantBlue (Expedeon, ISB1L-EXP-1L) in ultrapure water; SeeBlue[™] Plus2 Pre-stained Protein Standard (ThermoFisher, LC5925) was used as the protein ladder of choice for coomassie stained gels.

For western blotting, the proteins were transferred from the gels onto a PVDF membrane (Life technologies) using the XCell II[™] Blot Module (ThermoFisher, EI9051) with 30V for 75 minutes. The membrane was then blocked overnight with a 5% (w/v) skim milk in TBS-T (20 mM Tris-HCl, 150 mM NaCl, pH 8.0, 0.05% (v/v) Tween-20) solution. Next, the membrane was treated with 0.5% milk TBS-T buffer containing a primary antibody (5G4 1:500, Merck [MABN389]; MJFR1 1:10000, abcam [ab138501]; syn33, 1:500, Merck [ABN2265-25UG]) and incubated with mild agitation for 90 minutes at room temperature. Secondary antibody binding was achieved using 1:2000 dilutions of either goat

anti-rabbit (ThermoFisher, 31460) or goat anti-mouse (Dako, P044701-2) HRP conjugated antibodies in 0.5% milk TBS-T buffer and incubated for 1 hour at room temperature with mild agitation. Chemiluminescent signal was obtained by pre-treating membranes with 1 ml of HRP substrate EZ-ECL (Sartorius, 20-500-120). For image acquisition while at the University of Nottingham, both gels and western blots were sealed in clear plastic and visualised using the ChemiDoc™ Imaging System (BioRad); the same system was used in UCB Celltech, without the clear plastic seals. MagicMark™ XP (ThermoFisher) or WesternSure Chemiluminescent Pre-stained Protein Ladder (Licor) were used as protein standards for western blots.

2.10 Native-PAGE

Native-PAGE was performed using 12-well 7% Tris-acetate gels (ThermoFisher, EA03552BOX). Samples (10 µl of fragmented and non fragmented Aβ42 fibrils at 1 mg/ml) were mixed with 10 µl of 2x Tris-Glycine Native Sample buffer (ThermoFisher, LC2673) and loaded onto the pre-casted gel. HiMark™ Pre-stained Protein Standard (ThermoFisher, LC5699) was used as a reference molecular ladder. Gels were run in 1x Tris-Glycine Native running buffer (ThermoFisher, LC2672) for 2.5 hours at constant 150 V and stained overnight with a 1:1 dilution of InstantBlue in distilled water. Native gels were also run with 4-12% Bis-Tris gels, following the methods above indicated, with the only difference being the omission of the boiling step and the omission of reducing agents such as 5% (v/v) β-mercaptoethanol.

2.11 Proteinase K digestion.

Aliquots of the PMCA sonicated samples (20 µl) were incubated for 30 minutes at 37 °C with 5 µl of an 83 µg/ml solution of proteinase K (PK) (ThermoFisher, 25530031) in PBS + 0.4% (v/v) sodium dodecyl sulphate (SDS, Sigma L3771-25G). Protease activity was terminated by mixing 10 µl of the PK digested product and 10 µl of LDS sample buffer and incubating for 10 minutes at 100 °C. The PK digested samples were then separated on 4-12% Bis -Tris gels and stained overnight with a 1:1 dilution of InstantBlue in distilled water.

2.12 Thermolysin treatment

Human cytosolic brain extracts were digested with either 25 µg/ml or 200 µg/ml of thermolysin (Sigma, P1512-25MG) in a final volume of 25 µl. This was achieved through a 1 hour incubation at 70 °C. The proteolytic reaction was subsequently stopped by transferring the reaction tubes to wet ice and by the addition of 1 mM EDTA (Sigma, E9884) in distilled water. Digested brain material was then used to seed PMCA reactions (2µl in 200 µl conversion buffer)

2.13 Conformational stability assay.

Conformational stability assay (CSA) was performed with increasing molar concentrations of guanidine hydrochloride (GdnHCL, Sigma, 5010-1KG) in distilled water. PMCA products (40 µl) were incubated with an equal volume of a 100 mM Tris-HCL + 4% (w/v) sarcosyl (Fisher Bioreagents) solution for 1 hour at 37 °C. The resulting 80 µl were then aliquoted onto four 20 µl fractions in four different tubes containing progressively more concentrated solutions of GdnHCl (final concentration of 0.25 M, 0.5 M, 0.75 M and 1 M) and incubated for 1 hour at 37 °C. Next, samples were brought to a final concentration of 0.4 M GdnHCl in 400 µl and then digested with 17 µg/ml PK for 1 hour at 37°C. PK activity was blocked with 5 mM PMSF (Phenylmethylsulfonyl fluoride, ThermoFisher). Samples were then precipitated overnight in methanol at -20 °C. Precipitated samples were resuspended in LDS sample buffer and analysed on a 4-12% Bis-Tris gel with a 1:1 dilution of InstantBlue in distilled water.

2.14 Densitometry assay

Densitometry analysis was performed using the Analyse gel tools on ImageJ. Greyscale images of SDS-PAGE gels were opened in the software; the square tool was then used to delimit a rectangular zone between the 3 and 17 kDa regions of the gels. This first rectangular area was used as a standard to create a series of rectangles with the same dimensions delimiting each lane of the gel. The plot lanes tool was then selected to transform the band intensity of the gels to curves in a graph. Next, the area of each curve was measured, and the values were used to analyse the data using GraphPad Prism version 9.2.0.

2.15 Negative stain Transmission Electron Microscopy.

Carbon film on Copper 200 mesh grids (EM Resolutions) were glow discharged using an Agar Turbo carbon coater machine for 10 seconds at 10 mV, to change the polarity of the grids. Small volumes (13 μ l) of sonicated sample were pipetted onto the disks and incubated at room temperature for 15 minutes. Next, liquid sample was removed from the disk with filter paper and 13 μ l of an aqueous 2% (w/v) uranyl acetate solution was pipetted onto the disks. An initial 13 μ l of this solution was used to wash the disks, and promptly removed with filter paper and then a second application of the same volume was used to stain the fibrils for 1 minute at room temperature. The grids were examined using a FEI Tecnai BioTwin-12 TEM with a power setting of 100 kV.

2.16 Circular dichroism

Samples (200 μ l) of α -syn fibrils (20 μ M) in conversion buffer or A β fibrils in PBS (111 μ M, unless otherwise specified) were placed on a Zeba 7 kDa cut off desalting centrifuge column (Fisher, 10056033) and buffer exchanged with a 1X phosphate-buffered fluoride solution, pH 7.4. Next, fibrils (200 μ l) were placed in a rectangular quartz cuvette with 10 mm path length (Hellma[®] absorption cuvette, Merck Z800015-1EA). Spectra was measured on a Chirascan spectrophotometer CD spectrophotometer (Applied PhotoPhysics) at room temperature. CD spectra were measured between 250-190 nm for each sample. An average of three scans were taken and developed, with each sample measured three times. Time courses were also performed by taking a scan every 2 hours.

2.17 Bradford assay.

Bovine serum albumin (BSA) was used to generate a standard curve, from which the protein concentration of the brain samples could be measured: a stock of 2 mg/ml BSA was produced in mitochondrial extract buffer (50 mM Tris-HCl, 100 mM KCl, 1.5 mM MgCl₂, 1mM EGTA, 50 mM HEPES and 100 mM Sucrose, pH 7.4). The stock was then used to create four BSA dilutions: 1.4 mg/ml, 1 mg/ml, 0.5 mg/ml, 0.25 mg/ml and 0 mg/ml (buffer only). Small volumes of each dilution (5 μ l) were mixed with 200 μ l of Bradford reagent (Sigma, B6916-500ML) in duplicate within a clear flat bottom Nunc-Immuno Maxisorp ELISA 96 well plate. The absorbance of the standards was measured by

reading the plate at 595 nm using a Tecan plate reader. The obtained absorbance values were then plotted against their concentration and a curve was obtained. The best fit line between the absorbance points was calculated using Microsoft Office Excel 2016, the r^2 was confirmed to be ≥ 0.99 and the trendline equation was calculated. An aliquot of brain material (5 μ l) was then mixed with 200 μ l of Bradford reagent in duplicate, within the same 96 well plate used to create the standard curve; absorbance was measured for each sample. The trendline equation obtained from the standards was then used to calculate the protein concentrations within the brains.

2.18 Phage display biopanning against A β .

Phage display biopanning was performed in solution, using established proprietary VHH naïve libraries generated in UCB Celltech. For this, the VHH sequences from the heavy chain antibodies were isolated (diagram in figure 2.2, A) from llama B cell DNA, and inserted into phage, linked to the pIII coat protein, producing a viral particle expressing a VHH antibody within its surface (figure 2.2, B). For these experiments, both full length fibril and fragmented fibrils were targeted for antibody discovery. Although the used library (and the process behind its creation) are proprietary to UCB Celltech, an excellent example of naïve VHH library construction can be found in Sabir *et al.*, 2014 [248]

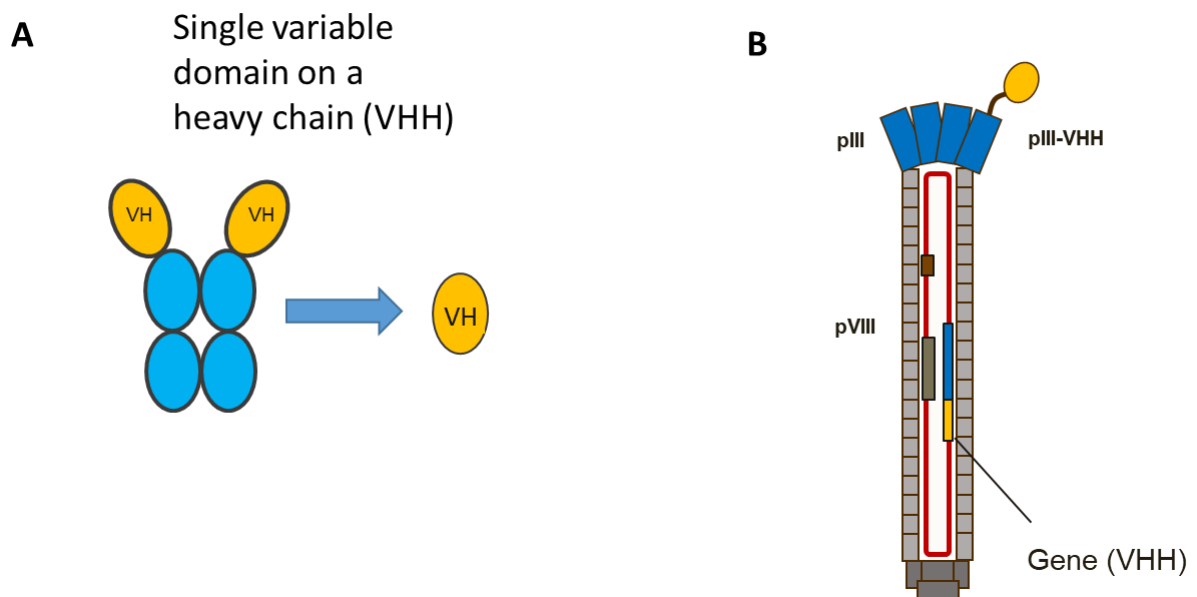


Figure 2-2: Schematic representation of VHH and VHH-phage particle

A: Camelid heavy chain antibody, the VH domain is isolated to form the VHH antibody; **B:** The VHH antibody is linked to the pIII phage coat protein. Different VHHs are expressed in different phage particles to form the VHH-Phage library.

2.18.1 Target preparation

As part of the experimental setup, A β monomers, fibrils and fragmented fibrils were pre-treated with Lightning-Link[®] Biotin Conjugation Kit (Fast, Type B, abcam ab201796). Chemical biotinylation was performed following the in-kit instructions; in short: monomers, fibrils or fragmented fibrils were mixed with Lightning-Link[®] modifier. For this, 1 μ l of modifier was added every 10 μ l of target solution used. Next, the A β -modifier solutions were pipetted into the vial containing the lyophilized Biotin-conjugation mix and incubated for 15 minutes at room temperature in the dark. To conclude the reaction, 1 μ l of quencher solution was added for every 10 μ l of target solution used. With fibrils, the solutions were then incubated at 4 °C in the dark overnight; monomers and fragmented fibrils on the other hand, were incubated for 5 minutes (or up to 1 hour) at room temperature, in the dark, prior to use.

2.18.2 Agar plate preparation

For each selection, 1x 150 mm and 3x 90mm petri dishes were prepared. Solidified 2YT-agar (1.6 % (w/v) tryptone, 1.0 % (w/v) yeast extract, 0.5 % (w/v) sodium chloride, 1.5 % (w/v) agar) was melting using a microwave. The liquid agar (400 ml) was placed in an incubator set at 60 °C for at least an hour in order to cool. Next, 8.8 ml of a 45% glucose solution in water (Sigma, G8769-100ML) were added, to create a final dilution of 2% (v/v) glucose in agar. Next, carbenicillin (Merck) was added at 1:1000 dilution from a 100 mg/ml stock solution; once ready the 2% (v/v) glucose, 100 μ g/ml carbenicillin agar was poured onto the plates to solidify.

2.18.3 Biopanning against fibrils

The naïve VHH library used for biopanning experiments was a UCB proprietary library, based on a pUC119-backbone phagemid vector (figure 2.3).

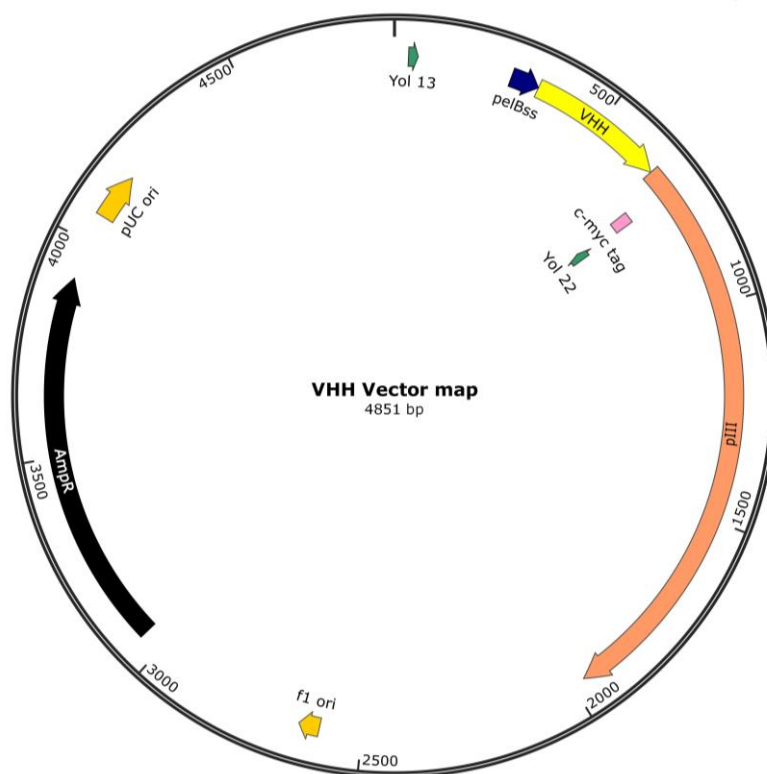


Figure 2-3: VHH phagemid vector

Vector map describing the different features of the VHH phagemid vector: pelBss, the leader peptide needed for protein expression in the bacterial system; VHH-pIII fusion, expressing the antibody linked to the coat protein; F1 signal (f1 ori) for ssDNA packaging; ampicillin resistance gene (AmpR), expressing β -lactamase and finally, the origin of replication (pUC ori). In addition to these major features, the vector also illustrates the position of Yol 13/Yol 22, the two primers used for the propagation of the VHH sequence during PCR and the c-myc tag. Once expressed, c-myc produces a linear peptide between the VHH and pIII domains translated to EQKLISEEDLS which is trypsin sensitive (unlike all other capsid proteins), a feature exploited during phage elution; further described below.

For Biopanning experiments, ten sub-libraries derived from ten different non-immunized llamas were pooled together, in order to maximize diversity. A total of 3 rounds of panning were performed for each experiment, using 10 μ g of biotinylated fibrils (from either Genscript or Gencust) or fragmented fibrils (from Genscript) per round. During round 2 of each panning experiment, a subtraction step with an unrelated biotinylated protein mix and monomers was performed on some selections, in order to remove non-specific binders. For experiments targeting fibrils, two selections were used: one with subtraction, labelled “S” (subtracted) and one without “NS” (non-subtracted). Experiments targeting fragmented fibrils were performed with three different selections: “1”, non-subtracted selection; “2”, monomer and biotin-protein subtraction and “3”, monomer, biotin-protein and full-length fibril

(Genscript) subtracted. All centrifugation steps were done using Thermo multifuge X3R, fitted with TX-750 rotor body and 750mL swinging buckets. A flow diagram explaining the panning strategy is described in figure 2.4.

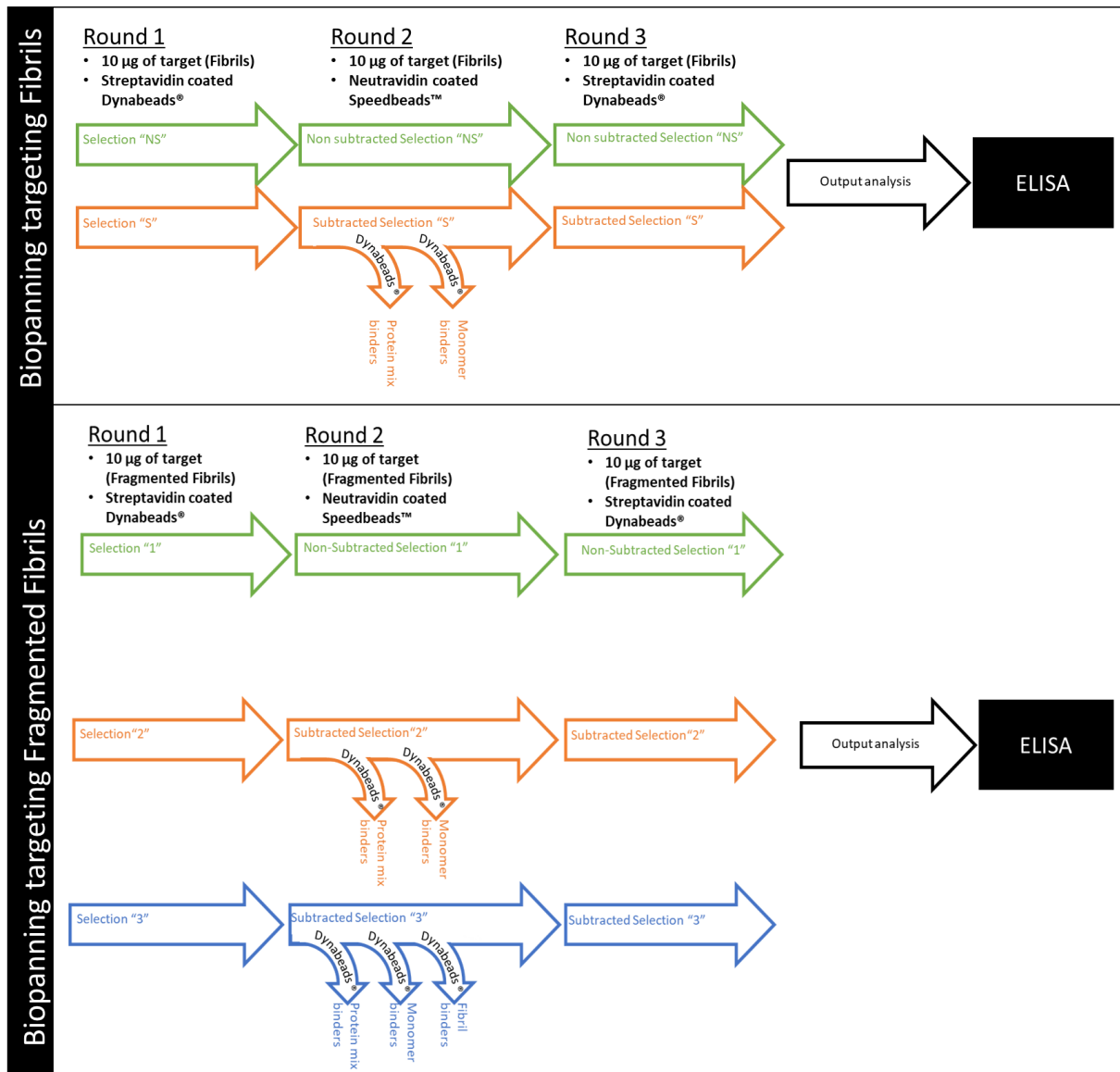


Figure 2-4:Panning strategies

Flow chart describing the panning strategies used to target both fibrils (top) and fragmented fibrils (bottom). Round 1 of panning consisted of the introduction of 10 µg of target to the blocked library tubes. Streptavidin coated beads were then used to remove the antibody-target complexes from the solution and phage was then eluted with trypsin. For round 2, selected libraries were subtracted of binders to nonrelated biotinylated proteins and monomer (and also fibrils during panning targeting fragmented fibrils) through the use of streptavidin coated beads (as indicated). Then, the target was added (10 µg) and the antibody-protein complexes isolated with neutravidin coated beads. The phage was then eluted with trypsin. Finally, round 3 was carried out in the same way as in round 1. Subtraction was performed in round 2, in order to allow a further round of enrichment after removing non-specific binders. For all 5 panning strategies, output antibody-phage particles were then further analysed by ELISA.

A typical round of panning was performed as follows:

The naïve library was diluted 1:1 with 6% (w/v) skim milk PBS (mPBS) in a 1.5 ml Eppendorf tube (selection tubes), to block non-specific phage-antibody binders; this was then incubated with constant mixing for 1 hour at room temperature. As biopanning was performed in solution, magnetic beads coated with streptavidin (Dynabeads® M-280, Thermofisher 11205D) were also prepared. A total of 150 µl of Dynabeads® were used per selection. Prior to use, the beads were washed by aliquoting the volume of beads needed and pipetting this into a 1.5 ml Eppendorf tube. The tube was then placed in a magnetic rack, that allowed the concentration of beads to a side of the tube; the supernatant was then removed, and the beads resuspended in the desired buffer. Beads were prepared through three washes in PBS and a final resuspension in 3% (w/v) mPBS prior to an hour-long incubation with constant shaking at room temperature.

The target (10 µg of protein) was the directly added to the 1.5 ml Eppendorf selection tubes containing the blocked library with 0.1 % (v/v) Tween 20 in PBS and incubated statically for 1 hour at room temperature. Concurrently TG1 *Escherichia Coli* (*E.coli*) cells [*F'' traD36 ProAB lacIqZ ΔM15*] *supE thi-1 Δ(lac-proAB) Δ(mcrB-hsdSM)5(rK-mK)* (Lucigen) were grown. These cells were also used for phagemid manipulation and reuse. For this 100 ml of 2YT media (16 g/L Tryptone, 10 g/L Yeast Extract and 5 g/L NaCl) + 1% (v/v) glucose were inoculated with 15 µl of a frozen aliquot of TG1 cells in a sterile 250 ml vented Erlenmeyer flask. Bacterial propagation was achieved by incubating the flasks at 37 °C with constant shaking at 230 rpm. Every 30 minutes, bacterial growth was checked using an absorbance spectrophotometer (Ultrospec 3100 Pro, Amersham Biosciences); TG1 cells were deemed ready to be used when optical density (OD) reached 0.5.

Next, the mPBS was washed from the Dynabeads® through 3x washes in PBS and 150 µl of these beads were added to each selection, in order to capture the biotinylated target-antibody-phage complex.

The binding reaction was performed for 5 minutes. The selection tubes were then placed on magnetic racks and the supernatant removed. The bead-target complex was then washed three times with 3% (w/v) mPBS and two times with 0.1% (v/v) Tween20 in PBS. The phage particles were then eluted by treatment with 100 µg/ml trypsin (1.2 ml; Sigma) in TBSC buffer (10mM Tris, 137 mM NaCl, 1mM CaCl, pH 7.5) for 30 minutes at room temperature and then 15 minutes at 37 °C. The tubes were then placed on a magnetic rack and the phage containing supernatant was used to infect TG1 cells. Infection was achieved by the inoculation of 600 µl of eluted phage with 10 ml of mid-log phase TG1 cells (at OD 0.5) per selection (the remaining 600µl of eluted phage was stored at -20 °C) and incubated statically for 30 minutes at 37 °C. Infected cells were then plated onto the agar plates. For the 90 mm petri dishes a 1:10 serial dilution of the infected bacteria was made in 2TY media + 1% (v/v) glucose, 50 µl of each dilution (usually 10^{-2} , 10^{-3} , 10^{-4}) were then dispensed onto each petri dish and a cell spreader was used to ascertain complete coverage of the plate with the infected bacteria, plates were incubated a 37 °C overnight. The remainder of the cells from each selection were then centrifuged at 4536 g for 10 minutes. The supernatant was then discarded, and the cell pellet resuspended in 300 µl of 2YT media with 1% (v/v) glucose. The resuspended cells were plated onto the 150 mm petri dishes, using a cell spreader; these plates were incubated at 30 °C overnight.

The next day, colonies were counted on the smaller petri dishes (also known as titration plates), in order to verify the colony forming units (cfu) related to each selection, to check for enrichment. The larger plates were used to make glycerol stocks of the output phagemid by adding 5 ml of 2YT media + 1% (v/v) glycerol + 100 µg/ml carbenicillin and 10% (v/v) glycerol and scraping off the lawn of bacteria. Glycerol stocks were used to inoculate 100 ml of 2YT media + 1% (v/v) glucose in 250 ml vented Erlenmeyer flasks, until a final cell density reached an OD of 0.5. Next, the MK13K07 helper phage (Stratagene) was added, at a ratio of 10 helper phage units per bacterial cell. Helper phage infection was achieved through static 30-minute incubation at 37 °C. Helper phage-infected cells were then centrifuged at 4536 g for 15 minutes, the supernatant was discarded and cells were resuspended

in 100 ml of 2YT media + 50 µg/ml Kanamycin (Sigma, K0254-20ML) + 100 µg/ml carbenicillin (Fisher, 12737149) in a 250 ml vented Erlenmeyer flask and incubated at 30 °C overnight at 200 rpm.

The next day, phage particles were precipitated using a solution of 20% (w/v) polyethylene glycol-8000 + 2.5 M NaCl (PEG, VWR RC-078) used at a final concentration of 3.3% (w/v) and incubated on ice for 1 hour. The phage was pelleted at 4536 g for 15 minutes, resuspended in PBS and then sterilized through a 0.22 µm stericup filter.

For some selections, a subtraction step was performed in round two of panning. The subtraction step was performed before the addition of the target. For fibril targeted panning, subtraction followed a two-step process: first, 10 µg of freshly resuspended and biotinylated monomers (Genscript) were added to the blocked phage library tube and incubated for 1 hour at room temperature; then 150 µl of blocked and washed streptavidin-coated magnetic Dynabeads® were introduced to the solution. The streptavidin-monomer-phage complex was then removed from the solution using a magnetic rack and the supernatant moved to a new clean 1.5 ml tube. Next, a mix of unrelated proteins were used for the following subtraction step; this was achieved by mixing 5 µg of three different biotinylated proteins (Rat lumican, interferon 1- α and tissue transglutaminase 2; these proteins were chosen as they were unrelated to Aβ and were readily available in our fridge stocks), creating a final 15 µg of mixed protein. Next, 5 µg of this mix were added to the phage library tubes and incubated statically for 1 hour. As before, binding phage was removed by adding 150µl of streptavidin beads per selection tube, incubating for 5 minutes and pulling out bound phage through the use of a magnetic rack. The phage libraries left after subtraction was then processed alongside the non-subtracted selection following the previously described protocol above (addition of target, phage elution, infection of TG1 cells and plating). N.B during round 2 of panning, SpeedBeads™ Magnetic Neutraavidin Coated particles (Merck, GE78152104010150) were used on all selections (subtracted and non) after the addition of target (instead of streptavidin coated Dynabeads®). This was done with the purpose of removing potential Dynabeads® binders in the library.

Subtraction for the fragmented fibril panning was done in the same way as with the fibril panning, with the additional step of a further subtraction with 10 µg of full-length fibrils (Genscript), followed by an hour-long incubation at room temperature and capture with streptavidin coated beads.

2.18.4 Colony picking and master plate creation

After three rounds of panning, the titration plates were used to pick individual colonies. Each colony was then placed in a single well of a sterile 96 well plate containing 100 µl of 2YT media + 1% (v/v) glucose + 100 µg/ml carbenicillin. A well was left empty (usually H12) as blank control. This plate was incubated for 2.5-4 hours with constant 1000 rpm shaking at 37 °C, until visual inspection of bacterial density reaching an estimated OD of 1. A full 96 well plate was used per selection. To create a master plate, 50 µl of a 50% (v/v) glycerol in 2YT media was added to each well, prior to flash freezing with dry ice and storage at -80 °C.

2.18.5 Monoclonal phage enzyme-linked immunosorbent assay (ELISA)

From the master plates, 5 µl of monoclonal culture were used to seed a new 96 deep well plate, containing 200 µl of 2YT media + 1% (v/v) glucose + 100 µg/ml carbenicillin per well. This new plate incubated for 2.5 hours with constant shaking at 1000 rpm at 37 °C, or at least when visual inspection of the wells revealed an estimated OD of 0.5. Next, MK13K07 helper phage was added, at an estimated final concentration of 10 helper phage unit per bacterial cell and the deep well plate was incubated statically for 1 hour at 37 °C. The plates were then centrifuged at 3600 g for 10 minutes, the supernatant removed from each well, and the infected cell pellets were resuspended in 400 µl of 2YT media + 50 µg/ml kanamycin + 100 µg/ml carbenicillin. The blocks were then incubated at 30 °C with constant shaking at 900 rpm overnight.

Nunc Maxisorp™ (ThermoFisher) plates were coated with 100 µl of a 5 µg/ml solution of streptavidin (Fisher, 10700995) in PBS. The streptavidin coated Maxisorp™ plates were also allowed to incubate overnight in a fridge.

Antibody- phage were harvested from the deep well plates by centrifugation at 3600 g for 10 minutes. Supernatants were then pipetted into a new 96 deep well plate containing 400 μ l of 6% (w/v) mPBS per well and antibodies were blocked for 1 hour at room temperature. The Maxisorp™ plates were washed two times by removing the streptavidin and adding 300 μ l of PBST + 0.1% (v/v) Tween 20. Next, the biotinylated proteins were added to the wells of the coated Maxisorp™ plates. Binding assessment of each antibody was carried out against biotinylated targets or controls as appropriate for each panning experiment. These were fibrils from either Genscript or Gencust, Genscript monomers, the control protein mix and fragmented fibrils. For this, 100 μ l of 2 μ g/ml solution of biotinylated protein was pipetted into the wells. A streptavidin-coated plate was left untreated to act as blank streptavidin control. The streptavidin-biotin reaction was allowed to proceed for 20 minutes at room temperature; after which, the plate was washed for twice with PBS + 0.1% (v/v) Tween 20. Then, the plates were blocked for 1 hour at room temperature with 300 μ l of 3% (w/v) mPBS. The blocking solution was then removed and 100 μ l of the phage-antibodies from the deep 96 well plates were added to each well of the Maxisorp™ plates; antibodies were then incubated for 1 hour at room temperature. Following phage-antibody incubation, the plates were washed four times in PBS + 0.1% (v/v) Tween 20 and 100 μ l of anti-M13 bacteriophage HRP antibody (Sino Biological) at a concentration of 73 ng/ml was added to each of the wells. Binding was performed over 1 hour at room temperature; the wells were washed, and 100 μ l of 1-Step™ Ultra TMB-ELISA substrate solution (ThermoFisher) were added. Incubation was allowed for 5 minutes prior to plate imaging and scanning using a Synergy 2 microplate reader, fitted with a 630 nm absorbance filter with Gen5 version 3.08.01. Antibodies were deemed to be specific for either fibrils or fragmented fibrils, when the absorbance measured at 630 nm was three-fold higher in the target plate (fibril or fragmented fibril) than in the monomer, protein mix and streptavidin plates.

N.B. for monoclonal phage ELISAs, initial screenings (with high numbers of clones) were performed by adding a single biotinylated protein type per plate, therefore analysing the binding patterns of each clone separately. Further, more in-depth studies were performed by adding all the relevant

biotinylated proteins and controls to a single plate, therefore analysing the binding pattern of each clone without potential plate-to-plate variation. Negative controls were not used for these assays

2.18.6 Colony polymerase chain reaction (PCR) and sequencing

PCR followed by sequencing was performed on those colonies that were revealed to possess antibodies of interest through monoclonal ELISA. A PCR reaction master mix was created by adding 20.75 µl DEPC-treated water (Fisher, AM9937); 2.5 µl of 10x standard Taq buffer (Merck, MO273X); 0.5 µl of deoxyribonucleotide triphosphate (dNTPs, Merck, MO273X); 0.5 µl of 10 µM forward primer YOL13 (sequence: GTTGGCCGATTCATTAATGCAG); 0.5 µl of 10 µM reverse primer YOL22 (sequence: CATTGAGATCCTCTTCTGAGATGAG) and 0.25 µl of Taq polymerase (Merck, MO273X) for a final master mix reaction of 25 µl per tube (figure 2.3). This was scaled up to provide a master mix for all required reactions. Master mix (25 µl) was aliquoted into individual 0.2 ml dome cap tubes (Fisher), and 1 µl of monoclonal colony from the master plate was used to seed the reaction.

A PCR cycle consisted by 6 steps: 300 second incubation at 95 °C, 40 second incubation to 95 °C, 40 second incubation at 55 °C and 100 second incubation at 68 °C; this was repeated for 35 cycles. After the last cycle was concluded, a final 120 second step was performed at 72 °C.

PCR efficacy and product purity was checked by resolving amplicons on a 1% (w/v) agarose gel in 1x Tris-Acetate-EDTA (TAE) buffer (ThermoFisher, B49). This was performed by dissolving 1 g of ultrapure agarose (ThermoFisher, 16500500) in 100ml 1x TAE buffer through the use of a microwave. Once the powder was melted, 6 µl of SYBR Safe DNA gel stain (Life Technologies) were added directly to the mix. The melted agarose was then poured onto an agarose gel cast fitted with a 12-well comb. Then, 7 µl of PCR product were mixed with 4 µl of 6x purple gel loading dye (New England Biolabs); then 10 µl of this mixture were loaded into the gel, using 10 µl of Quick-Load® Purple 1 kb Plus DNA Ladder as standard (Merck, N0550S). Gels were run at 80V for 40 minutes and visualized using the blue light settings on an E-gel™ Imager camera hood kit.

Sanger sequencing was performed by an external company, MacroGen Europe BV. Samples were pre-processed with Illustra ExoProStar 1-step (VWR, US77705), by mixing 3 µl of DNTP-treater water and 1 µl of Illustra ExoProStar 1-step directly into a tube containing 7 µl of PCR product. The enzyme was activated through incubation at 37 °C for 40 minutes, then deactivated through an 80 °C step for 15 minutes. Samples were then shipped and sequenced using the LMB3 primer (CAGGAAACAGCTATGAC).

2.19 Antibody-FC DNA production

DNA sequences obtained through sanger sequencing were analysed using DNADynamo (BlueTractorSoftware). Sequences were aligned, the quality of sequencing was checked and then translated to obtain the antibody protein sequences. Whenever necessary, manual corrections were performed (e.g. removal of extra amino acid due to align due to sequencing error), whenever corrections were not possible, sequences were excluded altogether. Protein sequences were further characterized using Vector NTI (ThermoFisher), through the alignment using the AlignX tool; by alignment of the whole sequence and CDR3 sequence only. Phylogenetic trees were created using the default settings of AlignX.

DNA sequences were synthesized by Twist Biosciences. Fibril binding antibodies were ordered in two antibody formats: dimeric VHH subunits connected by two human FC regions (VHHFc) or monomeric VHH subunit connected by two linked human FC regions, also known as single chain-FC (scFc) format. Sequences listed in results chapter 5.3 and 6.2. For VHHFc antibodies, the BspHI/NotI insertion points were selected, in the scfcFC_human vector; for scFc antibodies, the start of Hinge Proline was used as the insertion point, with the pMA_HuScFc_(tool_reagents) vector (sequence proprietary to UCB). Additionally, for the scFc antibodies, a C-terminal flanking sequence was specified for all inserts: ATGGAATGGAGCTGGGTCTTTCTTCTTCTCCTGTCAGTAACTACAGGAGTCCATTCT; and all VHHFc sequences were designed to start with an alanine. Fibril binders were ordered as 23 scFv antibodies and 23 VHHFc antibodies and were delivered as pure lyophilized DNA in a 96 well plate, together with the glycerol stocks of the bacteria containing the insert for further DNA production. Together with the

fibril specific antibodies, 6 antibodies from the Munke *et al.*, 2017[180] paper were ordered (I2, I48, I68, J48, J57 and J7) as controls, in the scFc format.

Fragmented fibril binders were ordered only in the VHHFc format, using BspHI/NotI site as insertion points in the scFc_human vector (sequence proprietary to UCB). DNA was delivered as lyophilized DNA in a 96 well plate, no glycerol stocks were ordered for this batch of DNA synthesis.

2.20 Antibody DNA transfection in Expi™ 293 F cells

Antibodies were produced through the transient transfection of DNA into the Expi™ 293 F cells system, using the Expi293™ Expression system kit. For antibody protein expression, cells were transfected in 48 well blocks. For each construct, 1 µg of lyophilized DNA from the Twist Bioscience order (resuspended in ultrapure water) was diluted with 50 µl of OptiMEM™. In the meantime, 2.66 µl of ExpiFectamine™ 293 was slowly dripped into 50 µl of OptiMEM and incubated for a maximum of 5 minutes. Next, the DNA and ExpiFectamine™ 293 in OptiMEM™ were mixed together and incubated for 30 minutes at room temperature. During this incubation, the Expi™ 293 F cells were prepared. For the purposes of transfections, a concentrated cell stock was available within UCB Celltech, cells were taken from this stock and counted through the use of a haemocytometer. For 1 µg of DNA used, 850 µl of cells at $3 \cdot 10^6$ cells/ml per well were needed; therefore, the required amount of cells were taken from the stocks, centrifuged at 400 g in a Thermo multifuge X3R, fitted with TX-750 rotor body and 750mL swinging buckets for 10 minutes and resuspended to the required volume of warm Expi293™ expression medium. After pipetting 850 µl of cells at the right concentration into each well, the DNA/ExpiFectamine™ 293 mixture related to each construct was added. The blocks were then incubated at 37 °C at 255 rpm in a Kuhner shaker with 8% CO₂ and 95% humidity overnight. For each transfection experiment, a blank (mock) well with no DNA was present, to act as a non-transfected control.

The following day 5 µl of Enhancer 1 and 50 µl of enhancer 2 were added to each of the transfected wells of the 48 well block and incubated for an additional 6 days in a Kuhner shaker with 8% CO₂ and 95% humidity overnight.

Following the week-long incubation, the supernatant was harvested through a 10 minute centrifugation at 300 g in a Thermo multifuge X3R, fitted with TX-750 rotor body and 750 mL swinging buckets. Expression levels of antibodies were tested using Biolayer interferometry (BLI), to assess successful transfection. For this, a Fortebio Octet HTX system was implemented, fitted with Anti-Human FC kinetic tips (AHC) tips (Sartorius, 18-5064) were soaked for 10 minutes in a “kinetic buffer” solution consisting of PBS + 0.05% Tween 20, then a 100 µl of 1:4 dilution of the harvested supernatants in kinetic buffer was pipetted into a black bottom Greiner 96 well plate (Sigma). BLI was performed through a 60 second baseline step in kinetic buffer with 1000 rpm shaking, followed by a 300 second association with 1000 rpm shaking in the 1:4 supernatant dilution and a final 300 second dissociation step at 1000 rpm in kinetic buffer. The BLI sonogram was then analysed using Octet Data Analysis High Throughput software version 11.1. Using this software, the blank well trace was subtracted from all the other transfected traces, the association and dissociation steps aligned to baseline and labelled using the sample ID.

2.21 Small scale purification

Expressed antibodies were purified using the PhyNexus MEA 2 Fully Automated Protein Purification Robot (Biotage), together with 1ml Protein A Protein A PhyTip® columns (Biotage, PTT-91-10-01) containing 10 µl of affinity media per column, compatible with Rainin system and Buffer kit for 96 x 40 µl ProA/ProPlus columns (containing 5x wash 1, wash 2, elution and neutralization buffer). Sample purification was performed on 96-deep well plates. Wash 1 was diluted 1:5 in distilled water, and 1 ml loaded into wells A 1-12 and C 1-12; 1 ml of crude supernatant containing the antibodies was loaded into wells B 1-12; 1 ml of Wash 2 was loaded into wells D 1-12, and finally, 40 µl of Elution buffer were pipetted into wells E 1-12 and F 1-12. The program run by the protein purification robot was a propriety protocol owned by UCB and programmed by PhyNexus (Biotage) that resulted in the elution

of the purified antibodies in wells E and F. Once the purification protocol was concluded, the 40 μl of eluted antibody from both wells E and F were transported to a new clean plate, and 20 μl of Neutralization buffer was added, reaching a final volume of 100 μl per sample.

Protein concentration was measured using a ThermoFisher Nanodrop™ 2000/2000c. The machine was blanked using a mix of 80 μl of Elution buffer and 20 μl of Neutralization buffer. Small volumes of purified protein (2 μl) were loaded into the machine's pedestal and protein concentration was measured using the Protein A280 function, obtaining an estimated concentration in mg/ml. In order to increase the accuracy of the measured concentrations for fragmented fibril binders, the extinction coefficient ($\epsilon_{/1000}$) and molecular weight were calculated using the ProtParm tool from Expasy (<https://web.expasy.org/protparam/>).

2.22 ELISA with purified antibodies

The methodology to perform an ELISA with purified antibodies was similar to the procedure described in section 2.18.5, with the main difference being the preparation of the primary antibodies and the secondary antibodies used. In short: Maxisorp™ 96 well plates were coated with 100 μl of 5 $\mu\text{g}/\text{ml}$ of streptavidin in PBS overnight. The next day, the streptavidin solution was removed, and the plates washed twice with 300 μl of PBS + 0.1% (v/v) Tween 20. 100 μl of biotinylated fragmented fibrils (Genscript), fibrils (Genscript or Gencust), freshly resuspended monomers (Genscript or Gencust) and a protein mix (biotinylated Rat lumican, interferon 1- α and tissue transglutaminase 2) were added to the different wells of the streptavidin-coated plates. As before, some wells were left untreated to act as streptavidin binder controls. After a 20 minute incubation at room temperature, the biotinylated protein solutions were removed from the plates and the wells blocked with 300 μl of 3% (w/v) mPBS for 1 hour. Next, the blocking solution was removed and 100 μl of 100 nM (or around 8 $\mu\text{g}/\text{ml}$) of primary VHHFc or scFc antibodies in 3% (w/v) mPBS were added to the wells. Commercial rabbit polyclonal primary antibodies were also used as controls, these were the Anti-Amyloid Fibril OC antibody (AB2286, Merck), diluted 1:1000 and the Anti-Beta-Amyloid 1-42 antibody (AB5078P, Merck), diluted 1:10000, both antibodies were diluted in 3% (w/v) mPBS, 100 μl of which were loaded

into the different wells. Primary antibodies were incubated for 1 hour prior to washing 4x with 300 μ l of PBS + 0.1% (v/v) Tween 20. Two types of secondary antibodies were then used: Goat Anti-Rabbit IgG Fc-HRP antibody (ThermoFisher), targeting the commercial rabbit polyclonal control antibodies; and Peroxidase AffiniPure Goat Anti-Human IgG, Fc γ fragment specific (Jackson ImmunoResearch), for recombinant antibody targeting fibril and fragmented fibrils. Both secondary antibodies were used at a dilution of 1:5000 in 3% (w/v) mPBS, loading 100 μ l per well. After a 1-hour incubation at room temperature, the HRP-conjugated antibodies were removed, and the plates washed 4x in 300 μ l of PBS + 0.1% (v/v) Tween 20. During the final step of the ELISA, 100 μ l of 1-Step™ Ultra TMB-ELISA substrate solution (ThermoFisher, 34029) was added to each well; incubation was allowed for 5 minutes prior to plate imaging and scanning using a Synergy 2 microplate reader, fitted with a 630 nm absorbance filter with Gen5 version 3.08.01.

2.23 Biolayer interferometry (BLI)

BLI was performed on purified antibodies. This methodology is based on the measurement of interference patterns generated by the reflection of white light from a layer of molecules immobilized within the biosensor tip (defined) bio-layer and an internal reference present within the tip itself. As molecules in solution bind to the bio-layer, the interference patterns change, allowing for the visualization of the binding kinetics in real time (expressed as shift in nm) [249-254].

AHC tips (also used in section 2.20) were used in conjunction with streptavidin (SA) biosensors (Sartorius, 18-5021). Both SA and AHC tips were activated by a 10-minute hydration step in 200 μ l of kinetic buffer (by placing the biosensor holder on top of a Greiner black polypropylene 96 well plate, making sure the biosensors were aligned with each well). Sample plate preparation and the program used to obtain kinetic data varied depending on the biosensor used:

For SA biosensors, two plates were prepared, a Greiner black polypropylene 384 well containing the biotinylated target for biosensor capture, kinetic buffer for baseline and dissociation steps and antibody dilutions for association step (sample plate); and a Greiner black polypropylene 96 well plate

containing 200 μl per well of a 1% (v/v) sodium dodecyl sulphate in distilled water per well for decontamination (decontamination plate). For the sample plate preparation 100 μl volumes were loaded in columns, following a “skipping stone” motif (skipping the adjacent wells immediately next to the one just loaded for substance of the same kind). Biotinylated Fragmented fibrils, fibrils and monomers were used at a concentration of 25 $\mu\text{g}/\text{ml}$ in kinetic buffer; antibodies were used at a 30 $\mu\text{g}/\text{ml}$ dilution in kinetic buffer. Generally, a single sample plate was used per biotinylated protein analysed. The number of biotinylated protein wells matched the number of antibodies analysed. Buffer wells containing kinetic buffer were also present in the sample plates, in double the number of antibody wells used per plate (buffer wells 1 and 2). The programme used for SA tip kinetic assessment consisted in a 60 second baseline in buffer wells 1; a 1200 second loading step where the biosensors were lowered into the biotinylated protein wells (until the sonogram showed saturation of the tips); a second baseline step for 60 seconds in buffer wells 1; a 900 second association step in the antibody wells; a 900 second dissociation in buffer wells 2 and a final 1800 second incubation in the decontamination plate. The plates were not shaken during the experiment, so as to avoid potential spillage of fibrillar material.

For AHC tips, two Grainer 384 well plates were used, one containing the biotinylated protein, buffer and decontamination wells, and another containing the antibody dilution wells. As before, 100 μl volumes were used to load 25 $\mu\text{g}/\text{ml}$ of biotinylated proteins in kinetic buffer and 30 $\mu\text{g}/\text{ml}$ of antibodies in kinetic buffer. The program for AHC kinetic measurement started with a 60 second baseline step in buffer wells 1; a 1200 second loading step of the antibodies in the antibody plate; a 300 second baseline in buffer wells 2; a 900 second association step in the biotinylated protein wells; a 900 second dissociation in the buffer wells 2 and a final 1800 second dip in the wells containing the decontamination solution.

For both SA and AHC biosensor experiments, a control antibody that did not bind either fibrils or monomers was used.

All data was analysed using the Octet Data Analysis High Throughput software version 11.1. All traces were subtracted to the control antibody trace, and association and dissociation steps aligned to the baseline. The traces were then labelled to reflect the antibody used and binding was compared. At the same concentration both fibril and fragmented fibril binders showed a shift ranging from 0.1 to 1 nm after subtraction to the control antibody, indicating the effective binding of the molecules to the biosensors.

2.24 A β 42 functional assays

A β 42 functional assays were based on the misfolding methodology developed in section 2.5.3: in short; freshly resuspended Genscript monomers were diluted to a final concentration of 10 μ M in PBS. 100 μ L of this dilution were then added to the wells of a black-optic bottom 96 well plate. While some wells remained unseeded, to act as A β misfolding (no inhibition) controls, other wells were treated with the addition of purified VHHFc fibril or fragmented fibril binding antibodies. The concentration of these antibodies varied between experiments, initial experiments added antibody at a final concentration of 30 nM; further experiments used a dilution range of antibodies at 1 μ M, 5 μ M and 10 μ M. As a control, the Anti-Amyloid Fibril OC antibody (AB2286, Merck) diluted 1:1000 in a final volume of 100 μ l was used as an inhibition control antibody. ThT was added at a final concentration of 30 μ M and the plates sealed before placing them in FLUOstar Omega plate reader. Plates were incubated for 29 minutes at 37 °C before a 60 second orbital shaking step (500 rpm). ThT emission data was analysed using GraphPad Prism version 9.2.0.

2.25 Statistical analysis

Statistical analysis was performed using GraphPad Prism version 9.2.0. Data was subjected to a normality test prior to being analysed for statistical significance. If non-parametric, the data was assessed using the test recommended by the software.

2.26 MUSCLE sequence alignment and phylogenetic tree

MUSCLE sequence analysis and phylogenetic tree were performed with Geneious Prime version 2022.1 created by Biomatters. MUSCLE alignment was set for 30 as the maximum number of

iterations. Phylogenetic tree was created using the Jukes-Cantor Genetic Distance Model, with Neighbour-Joining tree building method and no outgroups selected.

2.27 Further methodology used for the amplification and characterisation of fibrils

In addition to the methodologies described in this section, several other techniques were

attempted; but due to the negative outcome of these experiments these results were not expanded

upon. The techniques were for the amplification and characterisation of α -syn (table 2.1) or $A\beta_{42}$

(table 2.2) fibrils.

Table 2-1: Summary of additional experiments performed with α -syn

PMCA with PTFE beads	Herva <i>et al.</i> , 2014 [163]	Three 3 mm PTFE beads were placed in a PMCA tube together with a 90 μ M recombinant α -syn solution. Samples were sonicated for 24 hours, with 20 second pulses at 70% amplitude and 29:40 second incubation.
Testing different sonication times	Optimization step	A 90 μ M solution of recombinant α -syn was sonicated for 24 hours with either 20, 30 or 40 seconds (70% amplitude) and incubated for 29:40, 29:30 or 29:20 seconds, respectively.
PMCA seeded with CSF	Optimization step	9 μ M α -syn dilutions (200 μ l) were spiked with CSF from PD patients and age-matched HC, at a final concentration of 1:100. A non seeded sample acted as an internal control. PMCA consisted in 20 second pulses at 70% amplitude and 29:40 second incubation at 37 $^{\circ}$ C for 24 hours. Fibril formation was assessed with the PK assay.
PMCA with 9 μ M α -syn substrate	Optimization step	PMCA was performed with 70 % amplitude, 20 second sonication pulses and 29:40 second incubation for 72 hours, with a time point being taken every 24 hours. Samples were seeded with a PD and HC brain, and a non seeded sample was used as control.
PMCA with different detergents	Optimization step	PMCA with 70% amplitude, 40 second pulses and 29:20 second incubation at 37 $^{\circ}$ C was performed on an array of α -syn samples (10 μ M) dissolved in different buffers: PBS; PBS+1% SDS; PBS+1% sarcosyl; PBS+1% (v/v) Triton X-100; 1M urea in PBS, 4 M urea in PBS and 8 M urea in PBS. Samples were sonicated for 24 hours, after which fibril formation was assessed with both the PK and ThT assay.
PMCA with increasing concentrations of Triton X-100	Optimization step	PMCA with 70% amplitude, 40 second pulses and 29:20 second incubation at 37 $^{\circ}$ C was performed on an array of α -syn samples (10 μ M) dissolved in buffers with increasing concentrations of Triton X-100 (1%, 2.5%, 5%, 10% and 20%, v/v). Samples were sonicated for 24 hours, after which fibril formation was assessed with both the PK and ThT assay
Static incubation of samples spiked with 1% brain or CSF	Optimization step	200 μ l aliquots of 9 μ M recombinant α -syn in PBS were spiked with 2 μ l of brain cytosolic extract or CSF material derived from PD or HC subjects. The samples were incubated at 37 $^{\circ}$ C for 21 days. Following incubation, samples were analysed with both ThT and the PK assay.
Static incubation of samples spiked with 1% of increasingly sonicated preformed α -syn fibrils.	Optimization step	200 μ l aliquots of a 9 μ M solution of recombinant α -syn in PBS were spiked with 1% (v/v) increasingly sonicated preformed α -syn fibrils (0 pulses, 1 pulse, 2 pulses, 4 pulses, 8 pulses, 16 pulses and 48 pulses). Samples were then incubated at 37 $^{\circ}$ C for 21 days. Following incubation, samples were analysed with both ThT and the PK assay.
Static incubation of brain seeded samples in different concentrations of ApoE	Emamzadeh <i>et al.</i> , 2016 [255]	Recombinant α -syn was diluted to a final concentration of 50 μ M. Different aliquots of this solution were prepared in one of two different working concentrations of ApoE (50 nM and 10 nM) while others were prepared in PBS alone to act as controls. Samples were spiked with 2 μ l of PD or HC brain cytosolic extract; one sample was not spiked, to act as

		controls. Fibril formation was assessed over 6 days of static incubation at 37 °C with 0.05 mM ThT.
Static incubation of increasingly sonicated seeded samples.	Optimization step	Different aliquots (200 µl) of a 9 µM solution of α-syn in PBS were seeded with 2 µl of either a PD brain or a HC brain. These samples were then sonicated with an increasing number of 20 second pulses (70% amplitude): from 0 pulses to 1 pulse then 2, 4, 8, 16 and 48 pulses. These samples were then transferred to a 96 well plate with 10 µM ThT and analysed over 21 days at 37 °C.
Static incubation of 1:200 diluted <i>de novo</i> fibril seeded samples	Optimization step	Several PMCA tubes were loaded with 200 µl of a 90 µM dilution of α-syn. Preformed fibrils were added to the tubes, at a final concentration of 1:200. As soon as the fibril were added, some samples were frozen, while others were incubated at room temperature for either 10, 30 or 60 minutes prior to freezing. 24 and 48 hour sonicated samples with a 1:200 spike of preformed fibrils were also assessed as controls.
Shaking PMCA with 1% brain extract spike	Shahnawaz <i>et al.</i> , 2017 [165]	PMCA was carried out with shaking rather than sonication. 200 µl aliquots of a 9 µM dilution of α-syn were placed in a single well of a 96 well plate, with 5 µM ThT. Samples were spiked with 2 µl PD and HC brain samples. A non seeded well was also used as a control. Every 29 minutes of incubation at 37 °C, the plate was subjected to 60 seconds of “intense” orbital shaking (rpm not specified by manufacturer).

Table 2-2: Summary of additional experiments performed with Aβ₄₂

Experiment	Reference / Purpose	Method
Shaking PMCA	Salvadores <i>et al.</i> , 2014 [166]	Different concentrations of Aβ ₄₂ monomeric solutions were prepared (100 µM, 50 µM, 10 µM and 2 µM) in PBS buffer with 5µM ThT and transferred into a 96 well plate. The differentially diluted samples were then seeded with different concentrations of an AD or HC brain (1:5, 1:20 and 1:100 seed). Some wells were not seeded, to act as controls. PMCA was performed through “intense” orbital shaking (rpm not specified by manufacturer) for a minute every 15 minutes, and ThT fluorescence measured every 30 minutes for 7 days.
PMCA misfolding with different temperatures	Optimization step	PMCA was performed on 111 µM non seeded Aβ ₄₂ samples. Sonication as performed with 20 second pulses at 50% amplitude and 29:40 seconds of incubation for 72 hours. Two PMCA machines were used, one of them set at 37 °C and the other at 22 °C. After the final sonication, fibril formation was measured with ThT. Following this, samples were divided into two groups: frozen and incubated samples. The frozen group was placed in dry ice for 1 hour, and the incubated group was placed in an incubator at 37 °C for 1 hour. ThT was measured again after this step.
PK titration of digestion	Optimization step	A PK titration was performed on a 222 µM solution of Aβ ₄₂ fibrils in PBS. The concentrations of PK tested were: 50 µg/ml, 40 µg/ml, 30 µg/ml, 20 µg/ml, 10 µg/ml, 1 µg/ml, 750 ng/ml, 500 ng/ml, 250 ng/ml, 125 ng/ml, 31 ng/ml, 62 ng/ml and 15 ng/ml. Fibrils were incubated with PK for 30 minutes at 37 °C prior to their analysis on SDS-PAGE gels

Chapter 3. Production and misfolding of recombinant alpha synuclein

3.1 Introduction

PD is a multifactorial disease, influenced by both environmental [10] and genetic [9] factors. Since the discovery of α -syn as one of the major contributors to disease onset and progression [3, 4] great efforts have been made to better understand this protein and its gain of pathological function; this has been done through the use of human derived samples [27, 78]; animal models and *in vitro* misfolding assays [12]. One of the most successful techniques to propagate fibrils *in vitro* has been found to be PMCA. This methodology was borrowed from prion biology [161, 256] and takes advantage of the property of pathological α -syn to be propagated through templated misfolding [257] (making α -syn a “prion-like” protein [83, 95, 99, 258-260]). Given the high sensitivity and specificity of PMCA for the propagation of small quantities of fibrils, this method is highly appealing for the study of PD [168]. Indeed, studies have successfully used PMCA for both *de novo* [163] and CNS seeded misfolding of recombinant α -syn; allowing for the study of the underlying mechanisms of misfolding, pathogenicity and toxicity of the misfolded protein, but also the discovery of different strains of α -syn [106, 165, 261, 262]. PMCA has also been studied as a potential diagnostic tool [165].

Here, the PMCA approach was used to better understand the kinetics and misfolding capabilities of α -syn, both *de novo* and also after seeding with human brain. At the outset of the study the aim was to generate misfolded α -syn as an antigen for the generation of recombinant monoclonal antibodies that may be able to prevent misfolding. The hypothesis being tested was that PMCA seeded from PD patients’ brain would generate fibrils and protofibrils with distinct phenotypes compared to non-seeded misfolding, providing targets for antibody generation that mimic *in vivo* fibrils. The steps involved were the generation of recombinant α -syn, optimization of the PMCA parameters for both seeded and *de novo* conditions followed by the thorough characterization of the biophysical properties of the generated fibrils. For this, ThT was used together with TEM and CD to confirm the presence of fibrils. TEM was also used to investigate any polymorphs of the fibrils. Furthermore, protein separation techniques such as SDS-PAGE and western blot were used in conjunction with proteolytic enzymes, such as PK, to better understand the conformation of the produced fibrils; as

distinct proteolytic cleavage sites indicate distinct conformations. Results show that PMCA was able to produce fibrils *in vitro*. Also, when reactions were seeded with human brain derived extracts, misfolding of α -syn was directed towards the generation of 'human derived' polymorphs (or strains) that were never present in *de novo* generated fibrils.

3.2 Purification of α -syn

Following transient expression of the α -syn in the Expi™ 293 F cell culture system, the cells were pelleted, and the protein-rich supernatant was harvested and filtered (as seen in section 2.2). The clean supernatant was then resolved on a 4-12% Bis-Tris gel, to determine expression (figure 3.1). The gel clearly showed the presence of α -syn monomer in solution, evident at the 14 kDa band; but the presence of several other proteins in solution highlighted the necessity of further purification steps.

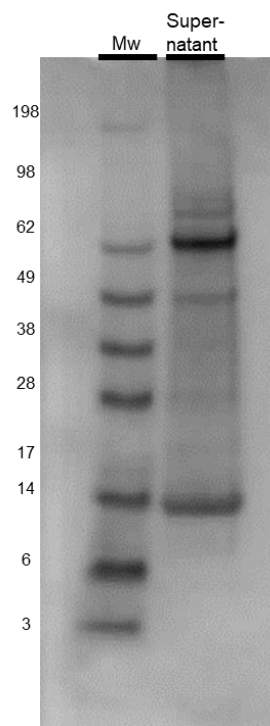


Figure 3-1: Analysis of filtered cell culture supernatant.

The α -syn construct was transiently expressed in Expi™ 293 F cells in a 2 L vented Erlenmeyer flask using the ExpiFectamine™ 293 Transfection Kit. After 6 days, the cell culture supernatant was harvested and filtered through a 0.45 μ m Sartobran P filter and 0.22 μ m Millipack® 60 Gamma gold filter. The flowthrough supernatant (10 μ l of 1 L) was then analysed with SDS-PAGE through a 4-12% Bis-Tris gel. Seeblue Plus 2 (3 to 198 kDa resolution) was used as molecular weight marker (Mw). The supernatant contained α -syn corresponding with the 14 kDa mark together with other contaminating proteins.

α -Syn was further purified on Hitrap Q columns (figure 3.2), eluate fractions (B12-H12, with 2 ml each) contained α -syn at 14 kDa but were still contaminated with other proteins.

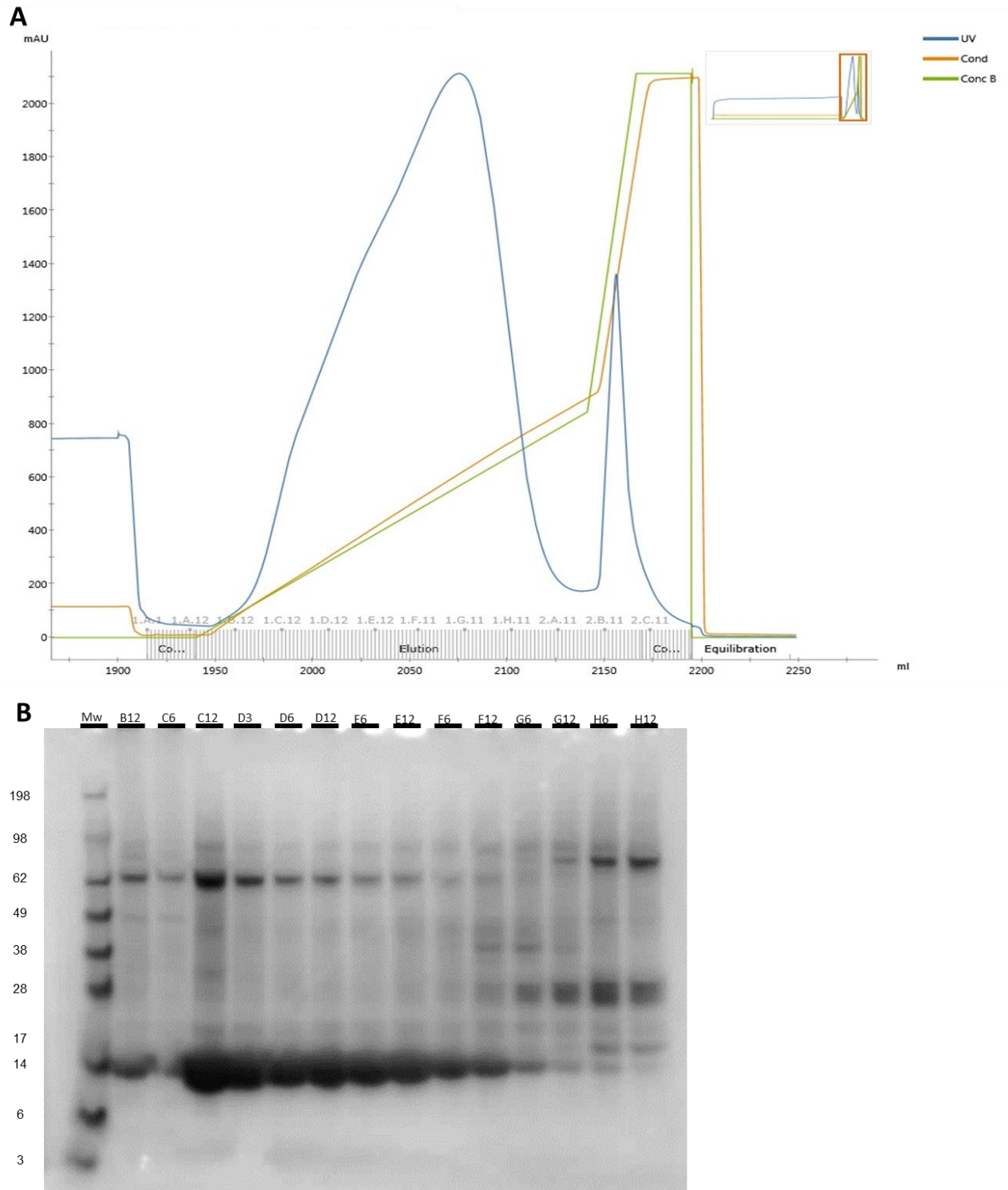


Figure 3-2: HiTrap™Q FF filtration step

The filtered supernatant (1L) was mixed with 1L of protein purification buffer A (20 mM Tris/HCL, pH 8.0). The α -syn in solution was purified through the use of 2x 5ml HiTrap™Q FF columns. Samples are shown from a representative purification. Fractions (around 2 ml) were collected in 96 deep-well plates. **A:** Chromatogram showing the elution of α -syn as a function of milli-absorbance units over time. Blue line indicates UV absorbance at 280 nm. α -syn is eluted the concentration of salt increases (evidenced by the green line, showing the gradient of protein purification buffer B and the orange line, indicating the increase of conductivity). There was a peak of UV absorption around fraction 1-B12 until 2-A12; α -syn can be usually found from 1-B12 to 1H12. **B:** Purification was then assessed by resolving the fractions (10 μ l of 2 ml) on 4-12% Bis-Tris gels. Fractions were analysed from well B12 to H12, picking a sample every 6 wells to confirm the presence of α -syn within each fraction. Fraction C12 to F12 were chosen for further purification, resulting in around 70 ml of purified product. Seeblue Plus 2 (3 to 198 kDa resolution) was used as molecular weight marker (Mw).

The selected fractions were pooled, concentrated, and excess salt (from NaCl gradient needed to elute proteins) removed through a desalting column, the α -syn remained in solution during this procedure. Next, the desalted α -syn was further purified on a second anion exchange column, Mono Q. Fractions were collected and analysed on 4-12% Bis-Tris gels (fractions D2-G2 with 2 ml each; figure 3.3). From the second anion exchange column, it was possible to notice an initial peak from fraction D3 to E5, followed by a slump and an additional shoulder of increased absorbance at 280 nm from fraction E7 to G4. These two peaks corresponded both to α -syn, henceforth labelled as α -syn A and α -syn B respectively. These two populations seemed to possess different biophysical properties as α -syn B was found to possess a slightly bigger and more charged than the α -syn A population as evidenced by the chromatograms. The difference between the two populations could further be evidence with SDS-PAGE as gels revealed the presence of higher molecular weight contaminants (at around 17 kDa) in α -syn B samples.

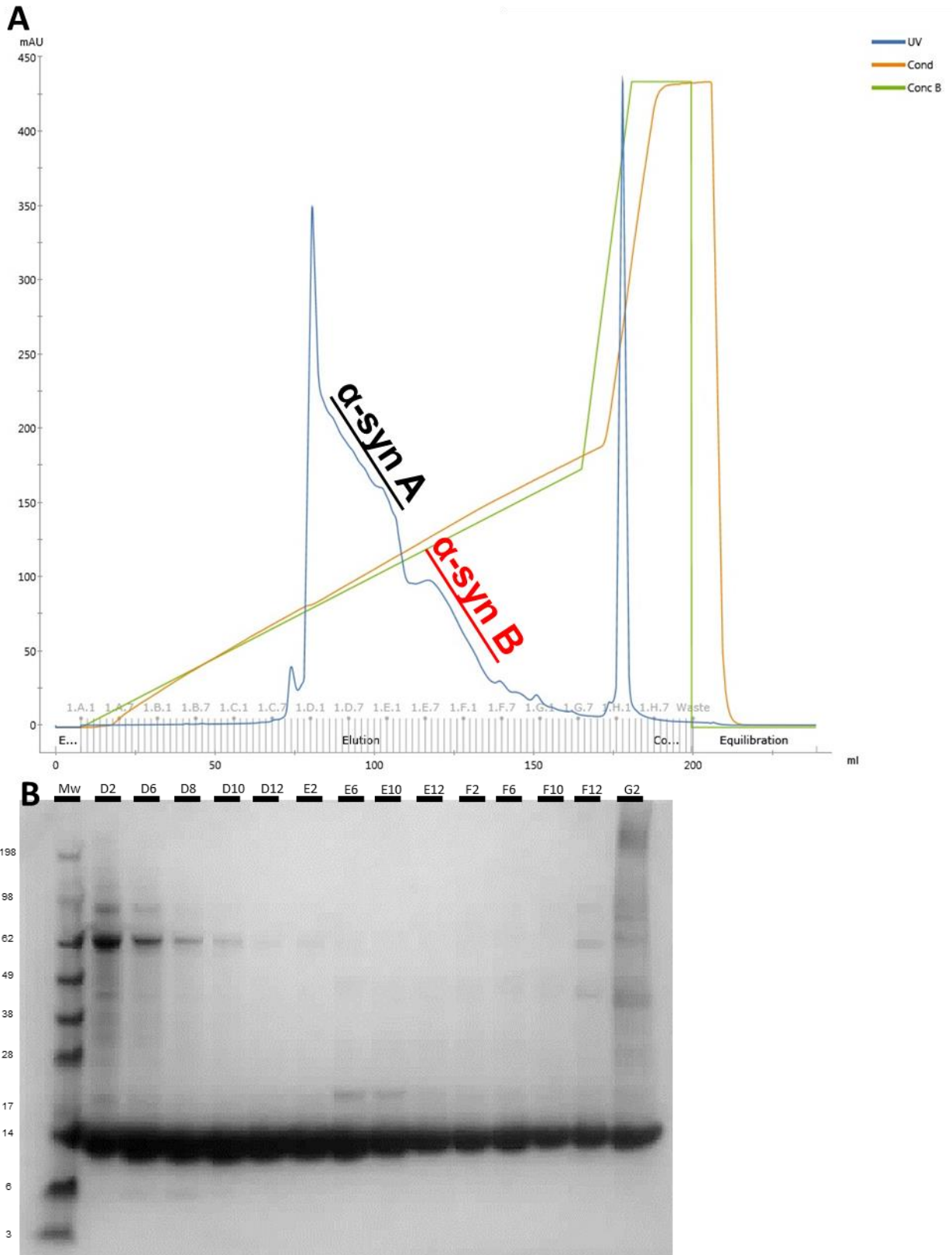


Figure 3-3: Mono Q filtration step

Following the first purification step, the supernatant was concentrated to 20 ml (from 70 ml) and run on a HiTrap™ 26/10 Desalting column. The desalted flowthrough (around 80 ml) was then run on a Mono Q anion exchange column. Fractions (around 2 ml) were collected in 96 deep-well plates. **A**: Chromatogram showing the elution of α -syn (blue line indicates

absorbance at 280 nm) as the concentration of salt increases (evidenced by the green line, showing the gradient of protein purification buffer B and the orange line, indicating the increase of conductivity). There is an increase of UV (at 280nm) absorption from fraction 1-C8 until 1-G7, with an addition peak 1-G10 to 1H5; α -syn can be usually found from 1-D2 to 1-G7. Furthermore, within the chromatogram, it is possible to distinguish two sections within the UV absorption curve, one ranging from D2 to E5 (black line/label) and E7 to G4 (red line/label); these two different sections correspond to the population known as α -syn A and B, respectively **B**: Small volumes (10 μ l) of fractions from wells within the D2-G2 range were resolved on 4-12% Bis-Tris gels. The gel confirmed the presence of α -syn within the selected wells, with strong staining around 14 kDa. It is possible to distinguish both types of α -syn as population B possessed a higher molecular weight contaminant at around 17 kDa. The fractions were then pooled resulting in around 36 ml of α -syn A and 40 ml of α -syn B. Seeblue Plus 2 (3 to 198 kDa resolution) was used as molecular weight marker (Mw).

The final step in the purification of α -syn was size exclusion chromatography. The fractions isolated from the anion exchange Mono Q column were concentrated and loaded onto a HiLoad™ 26/600 Superdex™ 75 pg size exclusion column. The elution profile shown in the chromatogram (figure 3.4, A) allows the distinction of two peaks, which corresponds to α -syn A, found in the main peak and a low level of α -syn B in the secondary peak. Fractions (around 10 μ l from 2 ml, from fractions A4-C4) were resolved by SDS-PAGE (figure 3.4, B). Gels revealed a highly pure α -syn at around 14 kDa, with the characteristic higher molecular weight contaminants for α -syn B samples. α -syn was pooled and filtered through a 0.22 μ M syringe filter and stored at -80 °C until use. Proprietary protocols in UCB confirmed that α -syn A was indeed a purer form of monomeric α -syn, and therefore was the population of choice for future misfolding experiments. Regardless both populations were purified as indicated in the protocols developed by UCB.

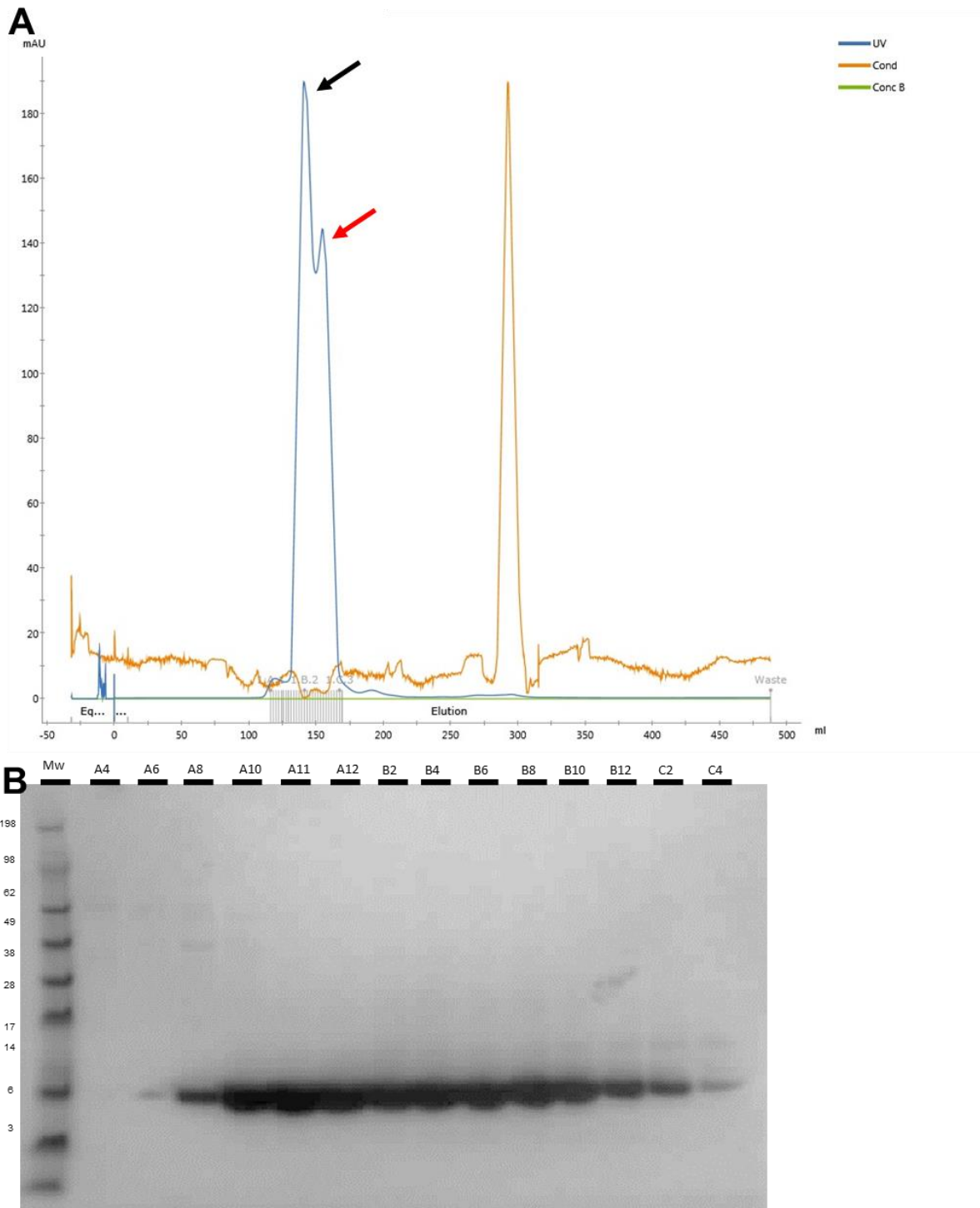


Figure 3-4: HiLoad™ 26/600 Superdex™ 75 pg size exclusion chromatography step

For the final step in the α -syn purification process, both population of α -syn (A and B) were concentrated to a final volume of 5 ml. Each population was then loaded separately into a HiLoad™ 26/600 Superdex™ 75 pg size exclusion column. **A:** Chromatogram evidencing the presence of α -syn within the two peaks of the UV absorption trace at 280 nm. The first peak was constituted of α -syn A (black arrow) and the second peak of α -syn B (red arrow). Fractions (2ml) were collected a 96 deep-well plate. **B:** Fractions A4 to C4 were resolved on a 4-12% Bis-Tris gel. Samples (10 μ l) were collected every 2 wells in order to assess the full range of fractions chosen. α -syn can be found at a high degree of purity within fractions A8 to C2, as shown by the strong staining at 14 kDa. Seeblue Plus 2 (3 to 198 kDa resolution) was used as molecular weight marker (Mw).

3.3 Misfolding experiments using 90 μM $\alpha\text{-syn}$

De novo misfolding was assessed using PMCA. Initial experiments were performed following the methods developed by Herva *et al.*, 2014 [163] in which 90 μM of $\alpha\text{-syn}$ was used. Within the PMCA reaction, samples were sonicated for 20 seconds with 70% amplitude and incubated for 30 minutes at 37 °C for 24 hours. In order to better understand the kinetics of the misfolding of $\alpha\text{-syn}$, samples were taken every 2 hours, and analysed both with the PK assay on SDS-PAGE and using 30 μM ThT staining and measuring fluorescence. The $\alpha\text{-syn}$ was misfolded into a PK-resistant, ThT binding form (Fig 3.5). Prior to 4 hours, no misfolding was evident but following this timepoint, it was possible to see PK-resistant bands appearing until 24 hours. ThT signal (Fig. 3.5, B) mirrors the presence of PK-resistant protein, with none seen at 0 and 2 hours. Interestingly, ThT also reveals that at increasing PMCA cycles, more fluorescence was produced, as there was a progressive increase between 4 hours and 24 hours of sonication. The increase in fluorescence corresponded to an increase of β -sheets in solution, an indication of an increase in the number of fibrils in solution.

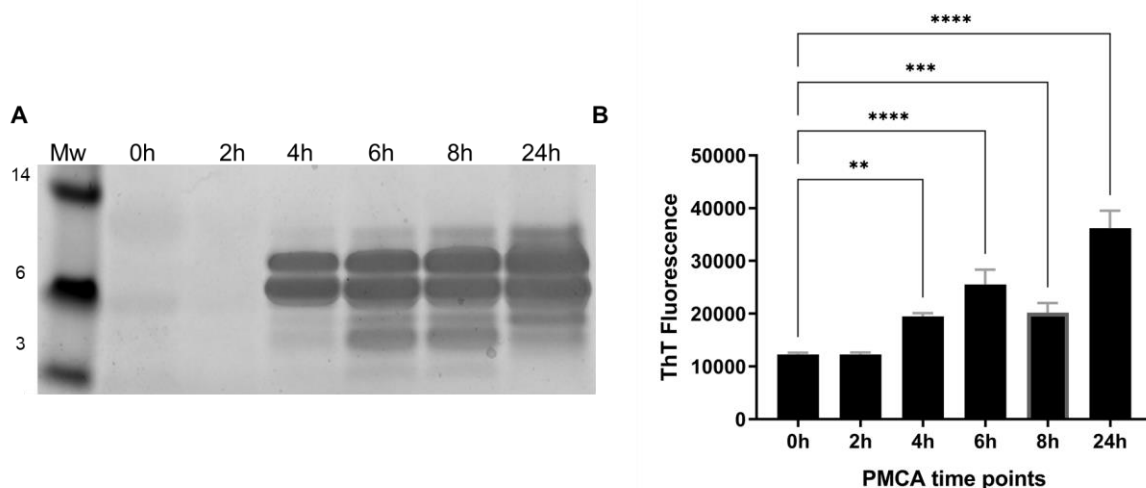


Figure 3-5: Time course of *de novo* misfolding of 90 μM $\alpha\text{-syn}$

A, a 90 μM $\alpha\text{-syn}$ solution sonicated with 70% amplitude, 20 second sonication and 29:40 minute incubation at 37 °C. A time point was taken every 2 hours during the run. PK digested bands show the gradual misfolding of $\alpha\text{-syn}$ over time. **B**, ThT fluorescence emitted by the samples. Fluorescence is emitted in those samples that also present PK resistant bands. Additionally, it is possible to see the trend that the longer the samples are sonicated the more fibrils are generated, as ThT fluorescence increases over time for most timepoints. Statistical analysis was performed with Friedman test with Dunn's multiple comparisons post-hoc analysis revealed statistically significant differences between samples and blank controls (P values indicated in graph as asterisks: P<0.01 [**]; P<0.001 [***]; P<0.0001 [****])

The PK digested patterns on the gels and the increase in fluorescence were strong indicators that PMCA was successful in producing *de novo* fibrils with recombinant α -syn. Next, the effects of the introduction of preformed *de novo* fibrils on the PMCA reaction was tested, to assess if the presence of fibrillar seeds could accelerate the misfolding process [256]. For this purpose, small volumes of 4 hour, 8 hour and 24 hour sonicated α -syn fibrils were used to seed a new PMCA reaction; as increasingly sonicated samples were expected to possess higher amounts of fibrils. The introduction of 1% (v/v) of preformed fibrils into the PMCA reaction was able to enhance the formation of PK-resistant bands (Fig 3.6). Indeed, while the banding pattern of the 4h sonicated seeded samples was comparable with the non-seeded experiment illustrated in figure 3.6; 8-hour and 24-hour sonicated seeds are able to induce dramatic changes to the profiles of the gel. Indeed, an extreme acceleration in the formation of fibrils was observed, with band patterns present without sonication (0h samples). This data suggests first of all, that PMCA reactions can be successfully seeded, accelerating the misfolding rate of monomers. Secondly, by virtue of the presence of PK resistant fibrils even without sonication (0 hours) it indicates that sonication for longer periods of time correlates with higher amounts of fibrils formed that can act as seed.

It is important to notice that the band pattern intensity from samples 4h, 8h and 24h are quite similar (albeit for the presence of additional bands in the latter two samples), as seen in figure 3.5. If the signal seen at 0h of the 8h and 24h sonicated seeds from figure 3.6 was indeed attributed to the seeds themselves, then there should also be band patterns present at 0h of the 4h sonicated seeds. Therefore, the signal seen at 0h in the 8h and 24h sonicated seed samples must be attributed to spontaneous misfolding. Further experiments are needed to confirm this, mainly by introducing 1% (v/v) of these different seeds in solutions with plain buffer and resolving the PK digested bands by SDS-PAGE. An interesting prospect is that the additional band patterns seen in the 8h and 24h sonicated samples in figure 3.5 are indeed the ones responsible for the spontaneous misfolding of α -syn, as these additional bands seem to be lacking at 4 hours of sonication.

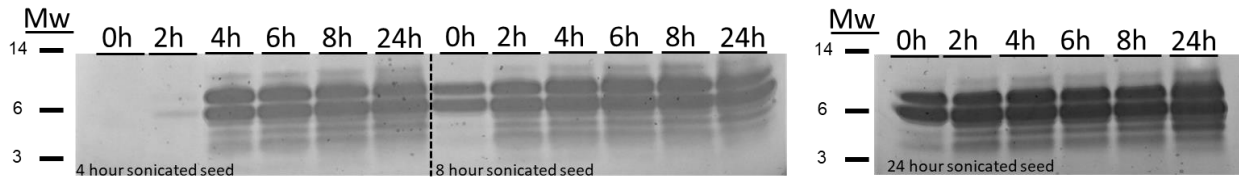


Figure 3-6: Preformed fibril seeding of PMCA reaction

90 μ M α -syn PMCA seeded with *de novo* fibrils formed after either 4 hours, 8 hours or 24 hours of sonication. Following the introduction of the seeds, a time point was taken every 2 hours. The introduction of *de novo* fibrils to the PMCA reaction accelerates the misfolding of α -syn. Seeds subjected to more sonication cycles are able to further accelerate the misfolding of the new PMCA.

3.4 Misfolding experiments using 20 μ M α -syn

Following the successful misfolding of α -syn using the conditions listed in Herva *et al.*, 2014 [163], a new protocol was attempted based on the findings of Jung *et al.*, 2017 [106]. This new approach was tested due to less substrate being used per PMCA reaction (20 μ M as opposed to 90 μ M) and due to the protocol used by Jung *et al.*, also include the implementation of CNS-derived material to seed the misfolding of α -syn. To test this method, misfolding was attempted with 20 μ M of α -syn as substrate in PMCA; with a timepoint being assessed at 24 and 48 hours. Analysis of the sonicated samples on 4-12% Bis-Tris gels after PK digestion revealed the presence of protease-resistant bands within 48 hours of sonication (figure 3.7).

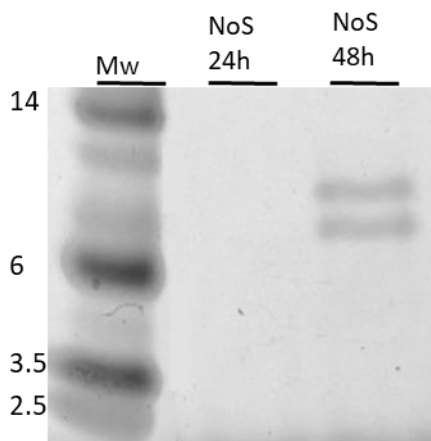


Figure 3-7: Misfolding assessment with 20 μ M α -syn

Time course experiment showing the successful misfolding of α -syn. Lower concentrations (20 μ M) of substrate together with 50% amplitude and 20 second sonication time resulted in a delay in the formation of PK resistant bands (compared to the method by Herva *et al.*, [163]), as no misfolding was observed in the first 24 hours (Nos 24h) but within 48 hours (Nos 48h) misfolding was observed. Molecular weight standard used was Mark12™ Unstained Standard. In this particular gel the band patterns from the non-seeded samples seem to have a higher molecular weight compared to previous observations.

This is most likely to Mark12™ migrating differently from the otherwise used Seebule Plus 2, giving the impression that the bands are heavier than what they really are.

3.4.1 Seeding of alpha synuclein misfolding with human samples

3.4.1.1 Characterization of human brain samples

Human brain samples were characterized prior to being used as seeds for PMCA. This was performed with the aim of assessing the presence and state of the α -syn found within samples. This would confirm if there were any intrinsic differences between samples and also, to determine the presence of α -syn aggregates. The first steps were to measure total protein concentration using the Bradford assay. The quantity of protein present varied between subjects, but overall, all samples had protein content of at least around 1 mg/ml (table 3.1).

Table 3-1: Brain homogenate protein concentration as measured with Bradford assay.

PD	PD 1	PD 2	PD 3	PD 4	PD 5	PD 6	PD 7	PD 8	PD 9		
Average OD	0.4135	0.5571	0.50125	0.2404	0.3223	0.5878	0.3575	0.62145	0.65665		
Concentration (mg/ml)	1.633397	2.184645	1.97025	0.968906	1.283301	2.302495	1.418426	2.43167	2.566795		
HC	HC 1	HC 2	HC 3	HC 4	HC 5	HC 6	HC 7	HC 8	HC 9	HC 10	HC 11
Average OD	0.57075	0.5605	0.66985	0.23405	0.73165	0.51435	0.57835	0.5978	0.643	0.4321	0.6063
Concentration (mg/ml)	2.237044	2.197697	2.617466	0.94453	2.854702	2.020537	2.266219	2.340883	2.514395	1.704798	2.373512

PD stands for Parkinson's Disease and HC stands for Healthy control

Next, cytosolic fractions of the brain samples were analysed by SDS-PAGE and western blotting. Band patterns upon coomassie staining did not reveal any clear distinctions between PD and HC groups (figure 3.8, A). For western blotting, three antibodies were used: Rabbit Anti-Recombinant- α -syn antibody MJFR1 (figure 3.8, B), Rabbit Anti-Oligomeric- α -syn antibody Syn33 (figure 3.8, C) and Mouse Anti-Aggregated- α -syn antibody 5G4 (figure 3.8, D). These different antibodies were chosen due to their ability to target different α -syn populations within the brains. It was possible to see that within each of the PD and HC brains, the monomeric α -syn population is present as evidenced by the strong staining on the 14kDa band when using MJFR1. Variations in signal are present, in particular levels of α -syn were relatively low for subjects 4 and 7 in the PD group and subjects 4 and 10 in the HC group. However, there were no obvious differences between the two cohorts. The analysis of both oligomeric and aggregated α -syn revealed the presence of these compounds within the PD and HC samples analysed, and again no clear distinction was observed between groups. Overall, the analysis of brains

revealed the presence of α -syn present in different aggregation states in brain samples from both PD and HC cohorts. These findings were in agreement with current literature, as no major differences have been recorded in the soluble fractions of brain homogenates from diseased and control individuals using similar methodologies [263-265]. Further studies using different fractionation techniques, such as ultracentrifugation and resuspension with SDS and urea buffers might reveal further insights into the different α -syn aggregate populations presents in both PD and control cohorts [260, 263].

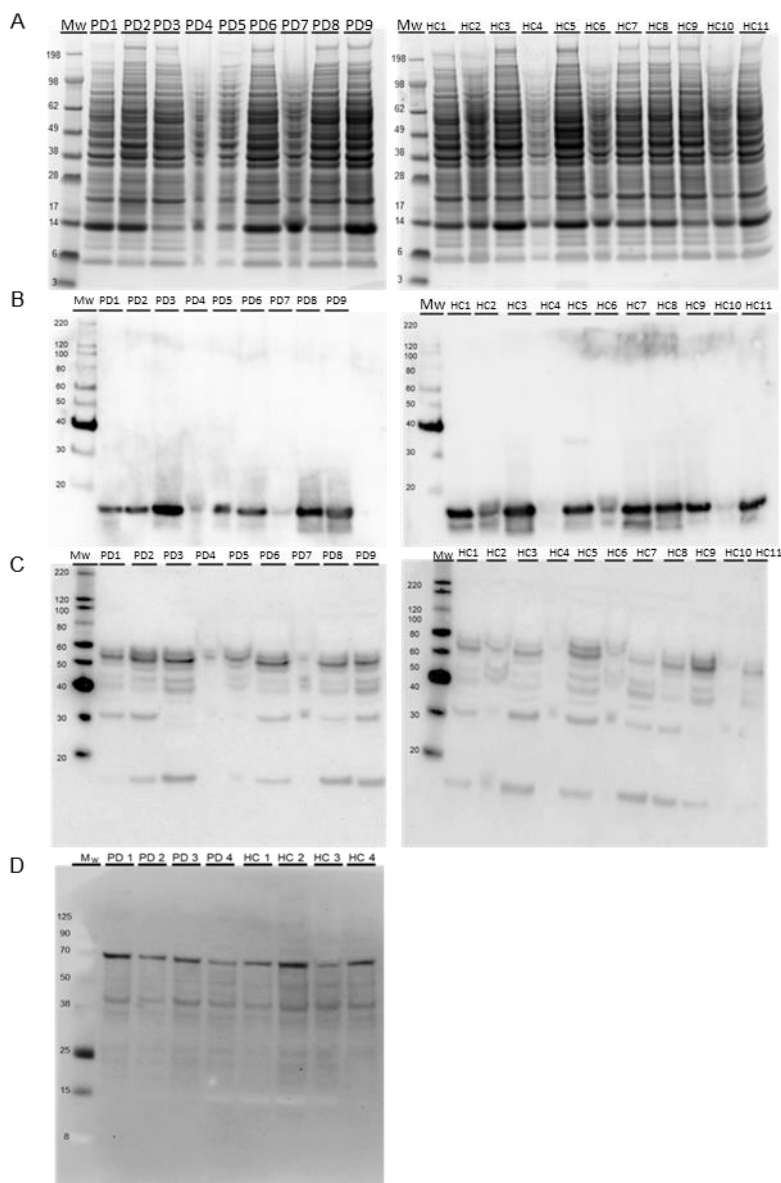


Figure 3-8: Characterization of human cytosolic brain fractions

Characterization of human brain derived samples. **A**, SDS-PAGE of human brain samples stained with Coomassie. Marker used is Seebule Plus2 prestained molecular weight marker. **B**, western blot of human brain samples using primary rabbit monoclonal antibody MJFR1, to evidence full length monomeric (14kDa) α -syn. Marker used is MagickMark. **C**, Western blot of human brain samples using oligomeric-specific primary rabbit polyclonal antibody Syn33. Marker used is MagickMark. **D**, Western blot of human brain samples using aggregate-specific primary mouse monoclonal antibody 5G4. Marker used is WesternSure prestained protein ladder.

3.4.1.2 20 μ M α -syn PMCA using human seeded samples

PMCA seeded with human brain cytosolic extract was performed using the Jung *et al.*, 2017 method [106]. For this, a single PD brain and an age matched HC sample were used, together with a non-seeded 20 μ M recombinant α -syn solution acting as a control for *de novo* misfolding. Within the 48 hours of total run time, a time point was taken every 24 hours to assess the misfolding rate of the samples. Following PMCA, samples were analysed with the PK and ThT assay coupled with NS-TEM imaging to assess both the presence and morphology of fibrils. No fibrils were formed within 24 hours of sonication for all the analysed groups, suggesting that these new PMCA parameter settings were less efficient in the creation of *de novo* fibrils compared to the method from Herva *et al.*, 2014 [163]. After 48 hours of sonication, it was possible to detect the presence of PK-resistant bands for the PD, HC and non-seeded samples. Interestingly, the band patterns differed between groups as non-seeded samples produced low molecular weight two-band pattern; while PD and HC seeded samples seem to possess a higher molecular weight two-band pattern or three band patterns respectively (figure 3.9, A). ThT values (figure 3.9, B) mirrored the PK assay results, with low binding for the 24 hour sonicated samples, and higher binding for the 48 hour sonicated groups, indicative of fibrils. NS-TEM was also performed, in order to assess the presence and morphology of fibrils. Initial NS-TEM experiments on the single PD seeded sample (figure 3.9, C) revealed the presence of fibrils only after 48 hours of sonication, confirming the PK and ThT results. These fibrils were straight and unbranched, with a diameter of around 10-20 nm and a varied length between 500 nm and 1 μ m. The data indicated that seeding with human brain cytosolic extract occurred and produced PK-resistant proteins with molecular weight band patterns that differed between groups, indicating the presence of a different conformation of α -syn being present within the fibrils being induced by different seeds (or lack of seeding).

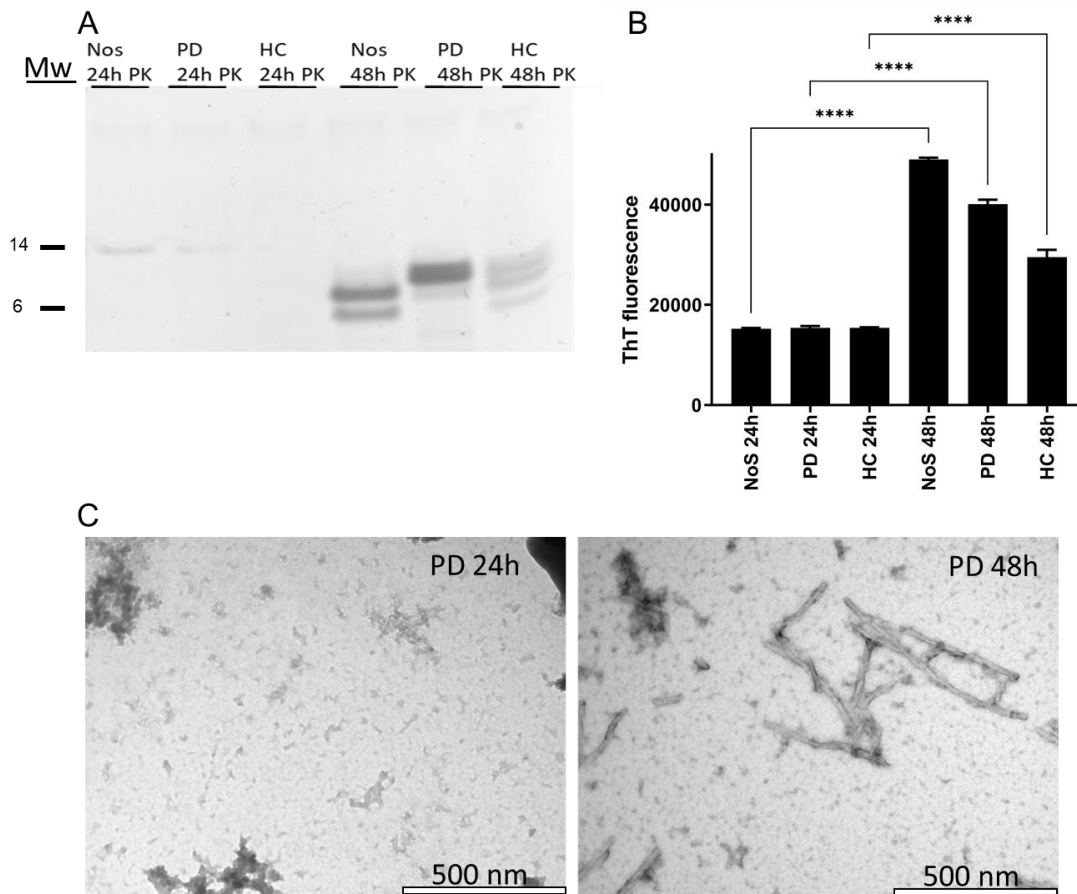


Figure 3-9: Human seeded PMCA experiments

20 μ M α -syn PMCA with no seed (NoS), or seeded with either a PD brain, a HC brain and sonicated for 48 hours, with a time point taken every 24 hours. **A**, SDS-PAGE of PK digested samples, PK resistant bands are only present in 48 hour sonicated samples. **B**, ThT fluorescence readings; as seen in the SDS-PAGE, only 48 hour sonicated samples possess high ThT fluorescence, indicating the presence of fibrils. **C**, NS-TEM with 2% UA, confirming the presence of fibrils in 48 hour sonicated samples seeded with PD brain extract. Statistical analysis was performed with T- test, this revealed statistically significant differences between samples at 24 and 48 hours of PMCA treatment (P values indicated in graph as asterisks: P<0.0001 [****])

To assess if the different band patterns observed during PMCA with either PD, HC or no seed correlated to a different fibril morphology. NS-TEM images of PD and HC seeded samples were compared to the *de novo*, non-seeded fibrils (figure 3.10, A). Although it was possible to detect fibrils in all of the samples analysed, no major morphological differences were observed between groups. Consistent with previous observations, all samples presented long, unbranched fibrils with around 10-20 nm in diameter and around 500 nm to 1.5 μ m long. Additional testing was performed with CD (figure 3.10, B), showing that, as expected, samples derived from PD and HC seeding and *de novo*

fibrils had high β -sheet content as evidence by the peak absorption around 218 nm. Monomeric α -syn, on the other hand, presented the typical absorption pattern displayed by random coil proteins, with a peak absorption at around 190 nm.

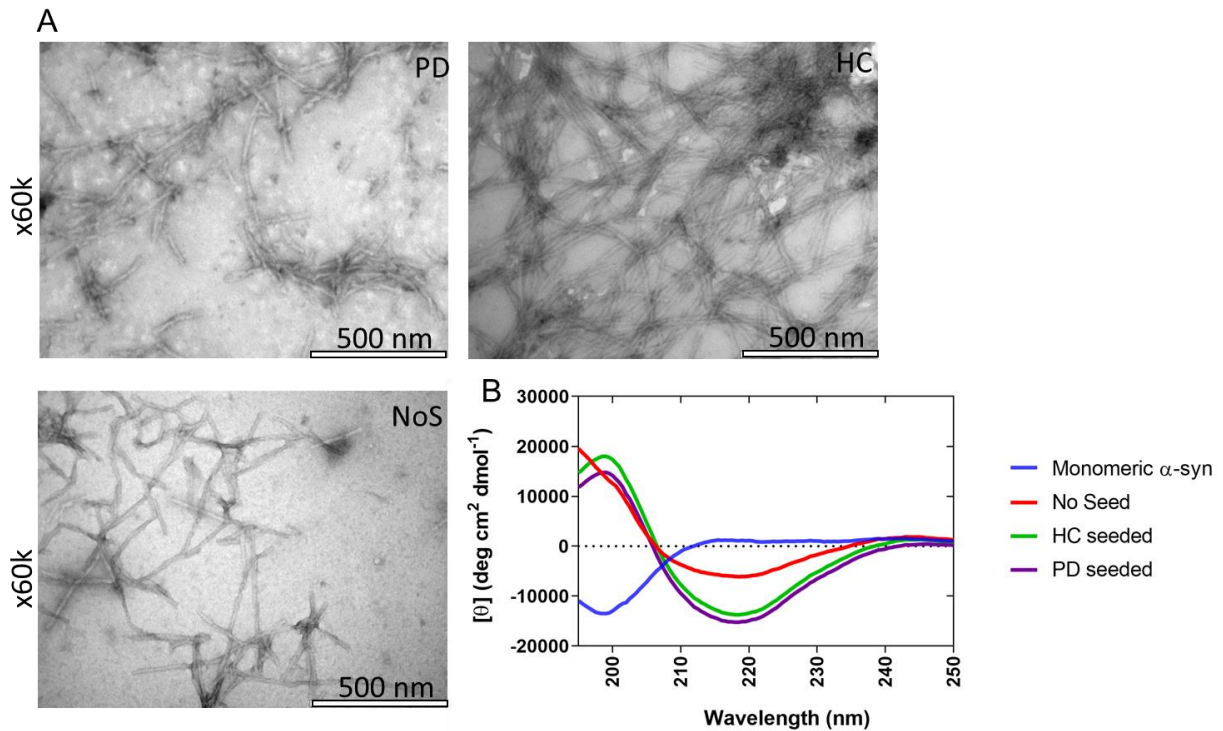


Figure 3-10: Morphological assessment of the different band patterns with NS-TEM and CD

A, NS-TEM images of a PD seeded, HC seeded and no seeded sample. Images show the presence of fibrils in all sample. No major morphological differences were detected when comparing the different groups. **B**, CD spectra detailing the absorption pattern of monomeric α -syn (20 μ M) and PD, HC seeded and non seeded fibrils. While monomeric α -syn possesses the typical random coil absorption pattern (190 nm), all of the fibril samples possess typical β -sheet absorption patterns (218 nm).

Out of the different methodologies used, only the PK assay revealed differences between the human seeded and non-seeded samples, with the discovery of at least three banding patterns. The next step was to analyse higher numbers of brain samples as seed for PMCA reactions and compare the products with more *de novo* fibril samples, in order to better understand the consistency of the misfolding into fibrils with distinct PK-resistance patterns.

3.4.1.3 Characterization of human seeded samples

Human brain cytosolic extract was obtained from 9 PD patients and 11 age matched HC; 9 non-seeded samples were also used as controls. PMCA was carried out using the Jung *et al.*, 2017 method [106]. The analysis of the PMCA products was performed using the PK assay and densitometry was performed on the resulting gels, in order to better evidence the differences between the observed band patterns (figure 3.11). Again, there was a distinction between brain seeded and non-seeded samples in terms of the band patterns of PK-resistant α -syn. While PD and HC seeded samples always produced either a three-band pattern in the gels, consisting of a high, medium and low molecular weight band or they produced a two higher molecular weight band pattern. Non-seeded samples, on the other hand, consistently displayed a pattern where the two lower molecular weight bands were dominant, and the highest molecular weight band was either not detected or detected at relatively low levels.

Densitometry analysis on the PK digested band patterns was displayed as ratios by dividing the values for high and medium bands and the low and medium bands (Fig. 3.11, B). The human seeded versus the *de novo* fibrils were distinct, as the latter was found to form a cluster of values around the y axis, due to the low levels of high molecular weight band. PD and HC seeded samples, on the other hand populate a slightly wider area of the graph, with no major characteristics that would distinguish between these groups. Densitometry analysis allowed the distinction between the high molecular weight conformers (defined as High) present in human seeded samples and low molecular weight conformers (defined as Low) from *de novo* fibrils. Within the High polymorphs, two distinct band patterns could be seen, one with a more prominent high molecular weight band and another with a more prominent mid and low molecular weight band. Several repeats confirmed that brain samples able to induce one or the other band patterns within the High category were able to consistently produce the same banding patterns between experiments.

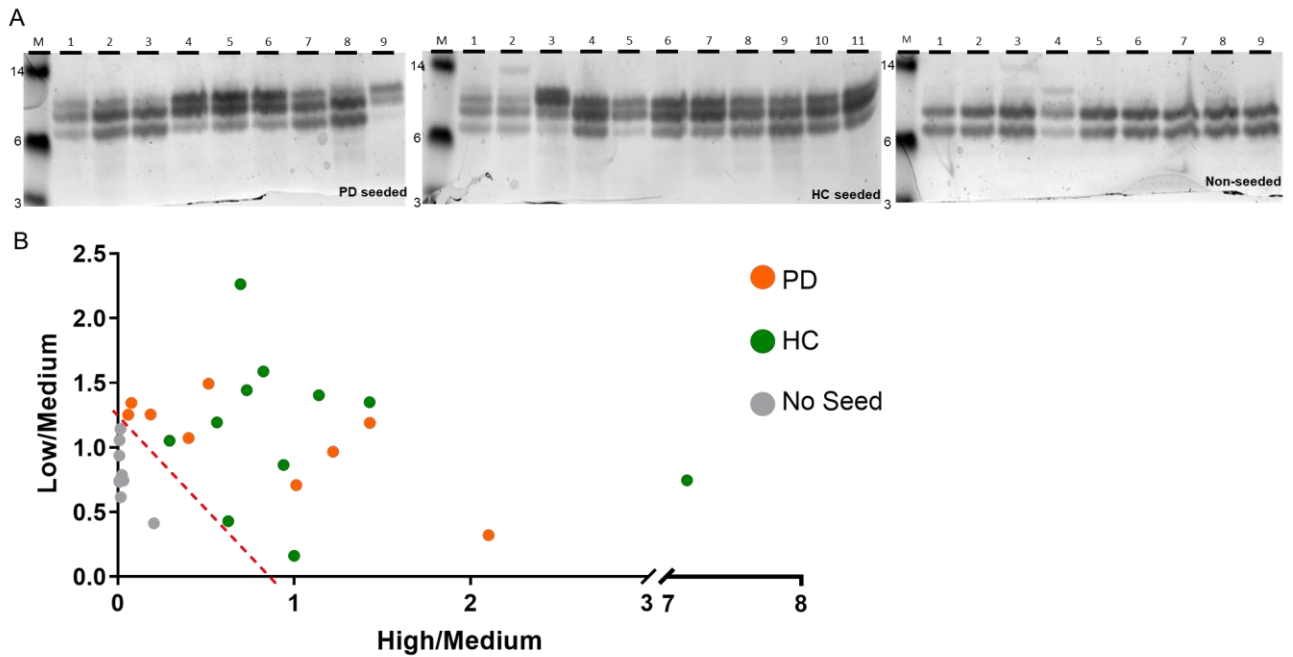


Figure 3-11: Comparison between human and de novo seeded samples

A, 20 μ M α -syn PMCA was carried with 9 non-seeded samples, and 9 PD seeded samples and 11 age and sex matched HC seeded samples; 9 non seeded samples were used as controls. While non seeded samples always showed a characteristic pattern of 2 low molecular weight dominant bands, PD and HC seeded samples displayed either a pattern with 3 dominant bands or a pattern dominated by the 2 higher molecular weight bands. PD and HC seeded samples display both High conformer variations, with no prevalence of either one pattern per group. **B**, Densitometry was measured for each sample and a ratio was obtained by dividing the intensity of the top band by the middle band (High/Medium) and the bottom band by the middle band (Low/Medium) for each sample. The resulting data points were plotted. The plotted data show a clear distinction between the non-seeded ratios (separated by red dotted line) and the PD and HC ratios, further distinguishing the non-seeded groups versus the human seeded groups.

3.4.2 Identifying different polymorphs of α -syn fibrils.

In an attempt to further understand the driving force behind the different PK band patterns induced by the brains, seeds were pre-treated with two different proteolytic enzymes, PK and thermolysin (ThLY). This was done to verify one of two conflicting potential outcomes: Either the pre-digestion of the seeds resulted in i) the complete elimination of all protein populations within the brains, thus removing the suspected fibrils/protofibrils and oligomers responsible for the formation the different band patterns; or ii) the effective degradation of the protease sensitive populations present in the brains, such as monomers, oligomers and protofibrils, leaving only the more resistant aggregates with the ability to act as seeds for further fibril propagation.

PK and ThLY were used in particular, as studies have shown that these enzymes interact differently with fibril forming proteins due to their distinct cleavage sites [266, 267], therefore allowing for the analysis of differently treated seeds for PMCA. Initial studies focused on analysing the effects of these enzymes on brain samples. A set of three PD brains (PD 2, PD 3 and PD 4) were pre-treated with 16 $\mu\text{g}/\text{ml}$ PK or 200 $\mu\text{g}/\text{ml}$ ThLY prior to being run in native 4-12% Bis-Tris gels. The concentration of ThLY was chosen on the findings of Owen *et al.*, 2007 [266] where high concentration of ThLY were capable of preserving pathological aggregates of PrP while digesting the physiological proteins. Enzyme-inactivated lanes were used as controls, by adding a PK inhibitor (5 mM PMSF) or ThLY inhibitor (1 mM EDTA) to the protein-enzyme mix. Gels (Figure 3.12) revealed that PK and ThLY pre-treatment do indeed differentially alter the proteins detected, as seen with PK-digested samples possessing a low molecular weight smear at the bottom of the gel and almost no high molecular weight components, compared to the enzyme-inactivated control. Similarly, ThLY treated brains also dramatically altered the protein migration profile, removing almost all protein components from the brain, leaving behind bands that were most likely the same ThLY in solution, (at around 35 kDa) as seen in Owen *et al.*, 2007 [266] and lower molecular weight elements from digested CNS material (or possibly contaminants within the ThLY enzyme itself). Enzyme-inactivated controls reversed the band patterns seen in enzyme-treated samples, revealing a pattern similar to the untreated brain (figure 3.8, A).

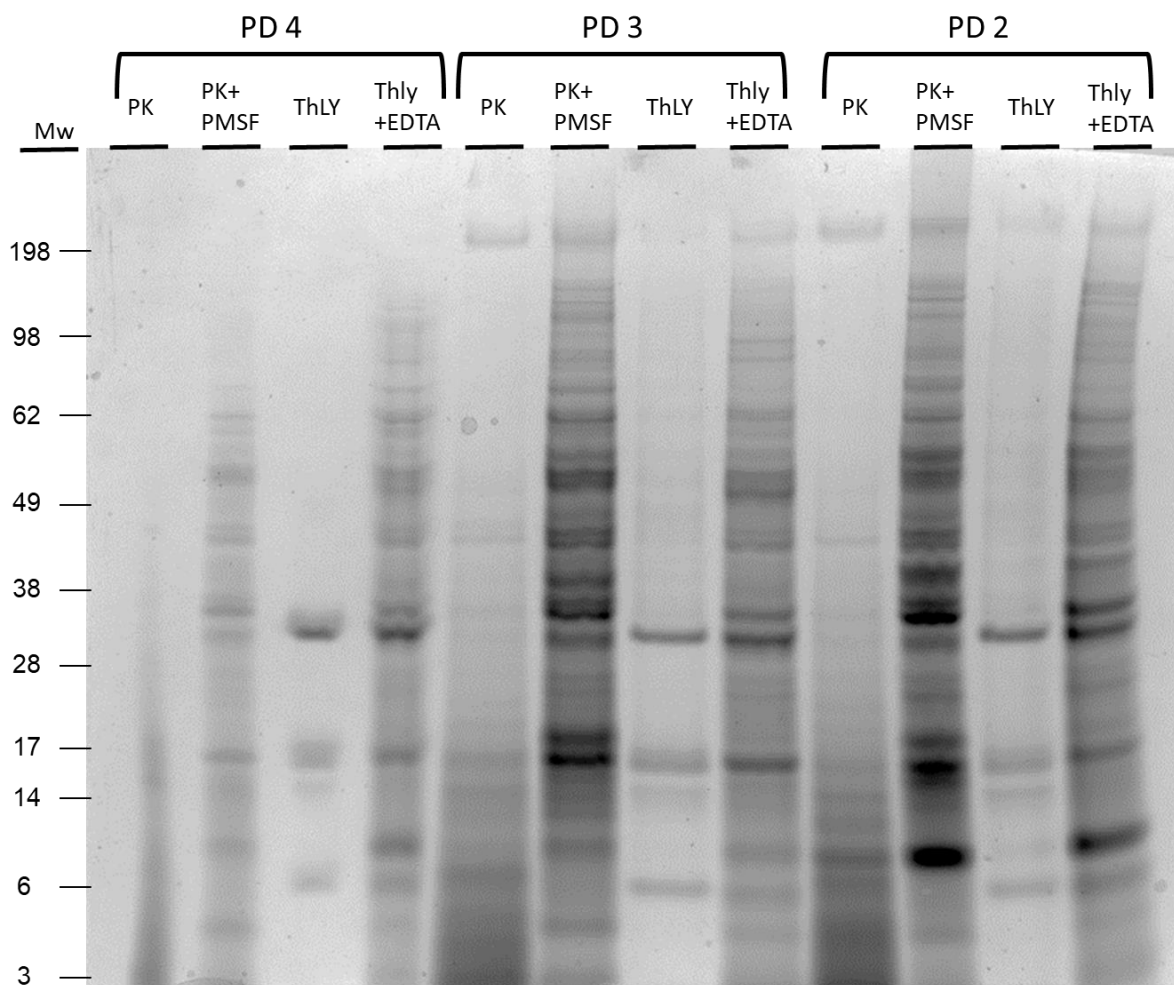


Figure 3-12: Proteolytic digestion of cytosolic brain extracts

Three PD brain samples were pre-treated with PK (16.6 μ g/ml); PK (16.6 μ g/ml) + PMSF (50 mM); ThLY (200 μ g/ml); and ThLY (200 μ g/ml) + EDTA (1 mM). Samples treated with PK seem to possess a smear of lower molecular weight elements around the bottom of the gel. PMSF seemed to prevent this. ThLY treatment was also found to successfully digest the brains, producing a different banding pattern to PK, with only some bands present in the gel attributed to ThLY and lower molecular weight brain elements. Like with PMSF, the use of EDTA reverse the digestion.

After successfully confirming the effects of proteases PK and ThLY on the seed protein content, the next step was to assess how the digested brains would influence the misfolding of α -syn in a PMCA experiment. For this, a brain sample was selected (PD4) and pre-treated with ThLY (25 μ g/ml ThLY or 200 μ g/ml ThLY). For PMCA reactions, 2 μ l of the digested brain were added to 200 μ l of conversion buffer. ThLY was chosen as the resulting treated brain had less fragmented protein samples than PK digested brain. Enzyme-inactivated controls were also assessed with 1 mM EDTA added to the brain-

enzyme mix prior to PMCA start. Further to this, the effects of equimolar concentrations of the EDTA was also tested on its own on the PMCA reaction, to control for potential misfolding-altering effects of EDTA. Finally, a non-seeded and untreated PD4 seeded tube was also tested. Following PMCA; all samples were PK digested and resolved on 4-12% Bis-tris gels. Band pattern analysis (figure 3.13) revealed that proteolytic pre-treatment of the brain dramatically altered the outcome of the PMCA experiment. The non-seeded and PD4 seeded samples displayed the expected banding patterns characteristic of their respective seeds. Similarly, the reaction containing inhibitor all produced the *de novo* formed fibril banding pattern, indicating these reagents did not inhibit this folding pathway. ThLY pre-treatment of the brain affected misfolding into the high molecular weight protease-resistant form. While lower concentration of this enzyme produced a band pattern similar to that found with untreated PD4 seed, treatment of the brain with higher concentrations of this enzyme prior to PMCA resulted in a new banding pattern, with a single dominant high molecular weight band. EDTA inhibition of the enzyme before addition to the brain sample resulted negated the effects of the enzyme on the seeding ability of PD4.

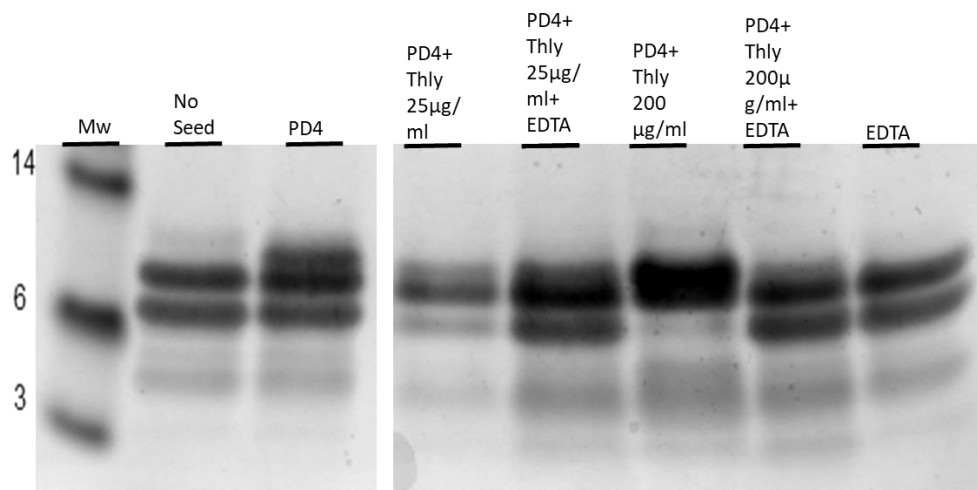


Figure 3-13: Assessing the effects of pre-digested brain samples on α -syn misfolding

Recombinant α -syn was misfolded on its own (No Seed); or seeded with a PD brain (PD4); with PD4 brain pre-digested with 25 μ g/ml ThLY; with PD4 brain and inactivated 25 μ g/ml ThLY; with PD4 brain pre-digested with 200 μ g/ml ThLY; with PD4 brain and inactivated 200 μ g/ml ThLY and EDTA (1mM). Following PMCA, the resulting samples were PK digested and run on 4-12% Bis-Tris gels. The gel confirms the characteristic banding pattern of the non-seeded and PD4 seeded sample. EDTA seeded sample, as expected, produce a non-seeded banding pattern, confirming that the enzyme inhibitors (EDTA) do not alter the *de novo* misfolding pathway of α -syn. ThLY pre-treated samples on the other hand, showed an altered banding pattern depending on the concentration of enzyme used. The expected banding pattern was present within the ThLY-inactivated brain seeded samples. N.B. the displayed image is from a single blot. MW markers are shown (kDa)

The next set of experiments focused on further characterizing the patterns as potential stable polymorphs that could be further passaged. This was achieved through sequential rounds of PMCA (sub-passages), in which small volumes of misfolded material from the previous round was used to seed the next: The first round of PMCA were either non seeded or seeded using PD and HC brains, the second round used 1% (v/v) of the previously round sample to seed monomers. The final sub-passage was performed by repeating this process (figure 3.14, A). Analysis of the PK digested patterns from the different samples revealed consistent patterns between passages, which were characteristic of the seed used (figure 3.14, B).

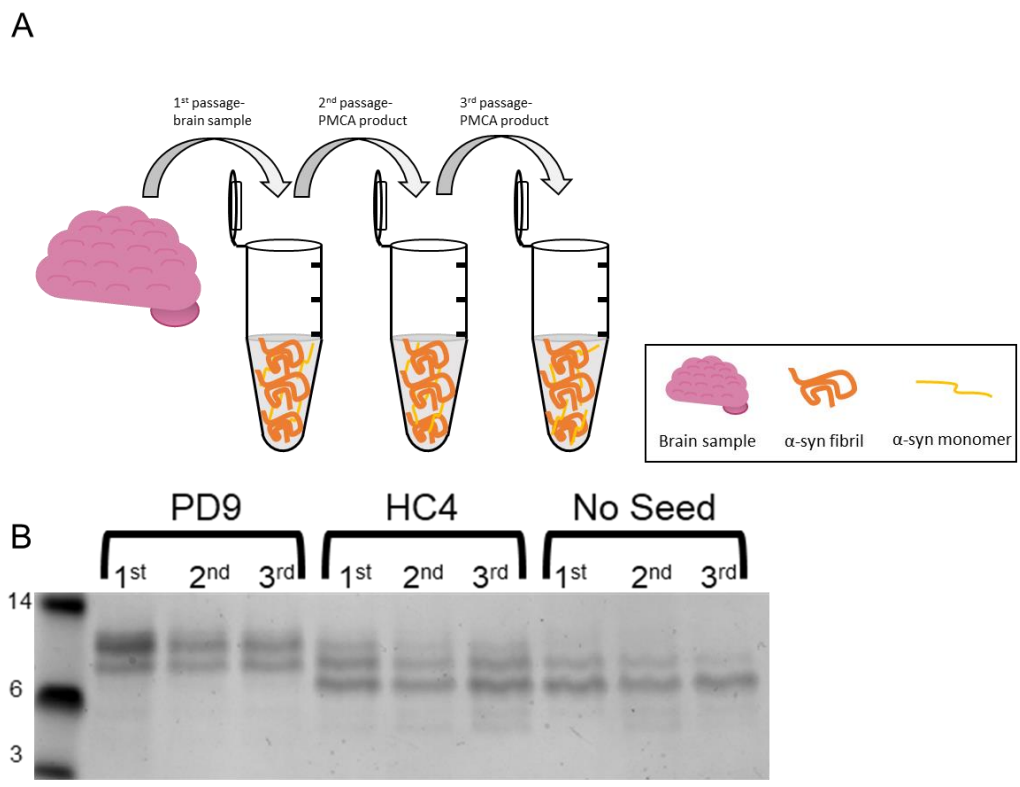


Figure 3-14: PMCA passage of α -syn polymorphs

A, Passage study diagram detailing the process. The first passage used brain sample to seed a PMCA reaction (or a no seed control); the second and third passages used PMCA product obtained from the previous round to seed the next. **B**, PK digestion patterns of a PD, HC and No seed sample over three different PMCA rounds. The stability of the conformations over the passages indicate that the conformation is stable, and the PMCA propagates a specific conformer.

The final experiment was a CSA assay which subjected the fibrils to increasing concentrations of a chaotropic agent, GdnHCl. *De novo* fibrils were compared with samples seeded with PD 2 and PD 9.

Increasing concentration of GdnHCl (from 0.25 M to 1 M) were used to partially denature the fibrils followed by PK digestion (figure 3.15). It was noted that for all 3 samples the band patterns in the GdnHCl treated samples were distinct from untreated samples (Figure 3.11) and the higher molecular weight species were lost or reduced for each sample before the lower molecular weight species. Overall, fibrils had different levels of stability: PD2 and PD9 seeded fibrils showed resistance to the 0.25-0.75 M concentrations, but was mostly or completely denatured at 1 M. In contrast, fibrils from non-seeded samples were the most stable, showing a consistent resistance to GdnHCl denaturation within the range of GdnHCl used.

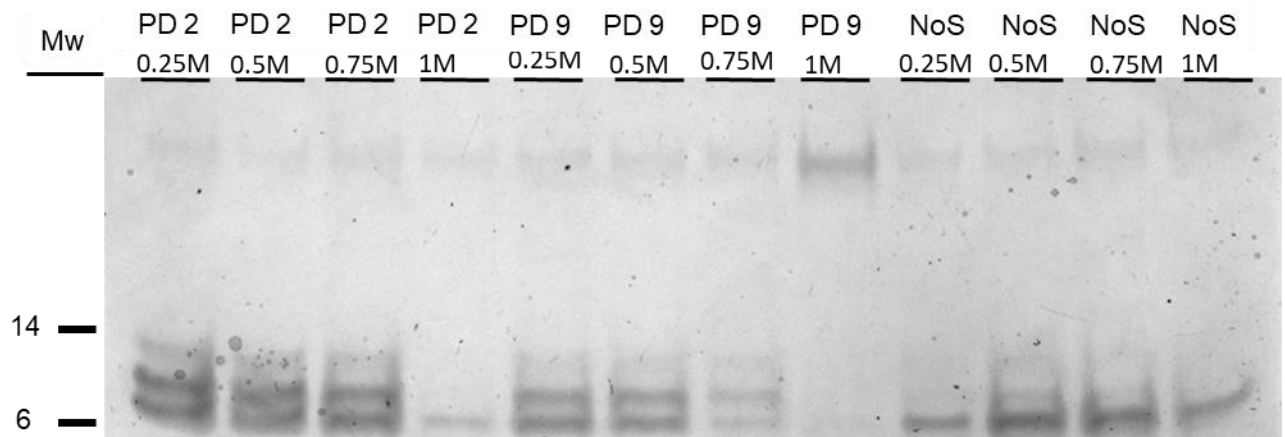


Figure 3-15: Conformational stability assay of α -syn polymorphs

CSA was performed on fibrils produced by either non seeding or seeded with PD 2 or PD 9. PD 2 and 9 were chosen based on their ability to produce different band patterns. Incubating with increasing molar concentrations of GdnHCl prior to PK digestion reveal that the different band patterns possess different stabilities, supporting the presence of different α -syn polymorphs being induced by seeding using brain samples. Molecular weight markers illustrated under Mw

3.4.3 Additional experiments with α -syn.

Beyond the experiments described in this section, several others were performed to optimise the misfolding of α -syn, but due to their inconclusive or negative result or because they did not improve the misfolding, they were not expanded on in the result section (summarised in table 3.2).

Table 3-2: Summary of additional experiments performed to misfold α -syn in different conditions

Experiment	Outcome
PMCA with PTFE beads	The beads did not provide any advantages in terms of increased misfolding rates compared to samples with no beads.
Testing different sonication times	Increasing the sonication time produces a slight increase in the number of α -syn fibrils in solution (measured with densitometry analysis of the PK digested patterns). But it did not accelerate the misfolding rate of fibrils.
PMCA seeded with CSF	Non-seeded samples revealed the characteristic two band pattern typical of <i>de novo</i> fibrils; CSF seeded samples possessed bands similar to the “high Mw” patterns present in brain seeded samples.
PMCA with 9 μM α-syn substrate	PMCA following the Jung <i>et al.</i> , method [106] but using 9 μ M of α -syn substrate was successful, as ThT and PK assays reveal the presence of fibrils. However, the band patterns were faint due to the dilution of the monomers, making interpretation difficult. ThT assays clearly displayed increases in fluorescence.
PMCA with different detergents	1% Triton X-100 buffer produced the typical two band pattern observed in <i>de novo</i> fibrils (produced in PBS) after PK digestion. A faint band was also present with 1% SDS buffered sample, at around 3 kDa. ThT confirmed fibrils in PBS (control) and 1% TritonX-100 buffered samples but not for samples in 1% SDS. Inclusion of sarcosyl and urea were characterized by a lack of fibrils being produced.
PMCA with increasing concentrations of Triton X-100	<i>De novo</i> misfolding with 2.5% Triton X-100 displayed both high ThT emission and a three band pattern after PK digestion similar to the pattern seen in some of the human seeded samples. 1% Triton X-100 buffer again produced the typical two band pattern observed in <i>de novo</i> fibrils (produced in PBS) after PK digestion. Higher concentrations of Triton X-100 did not produce any band pattern after PK digestion and there was an inverse correlation between ThT signal and Triton X-100 concentration.
Static incubation of samples spiked with 1% brain or CSF	No misfolding was observed.
Static incubation of samples spiked with 1% of increasingly sonicated brain seeds.	No misfolding was observed.
Static incubation of samples spiked with 1% of increasingly sonicated preformed α-syn fibrils.	No misfolding was observed.
Static incubation of brain seeded samples in different concentrations of ApoE	No misfolding was observed.
Static incubation of increasingly sonicated PMCA product (from seeded reactions).	No further misfolding was observed over that with the non-sonicated starting material.

3.5 Discussion

PD, the second most common neurodegenerative disease affecting the ageing population, is believed to be the results of the misfolding, aggregation and subsequent propagation of α -syn [9]. Emerging evidence has demonstrated how α -syn shares many similar properties with prion diseases, with some authors even dubbing α -syn a “prion-like” protein [83, 99, 258, 260, 268]. As a prion like protein, one of the most fascinating properties associated with α -syn is its ability to produce different strains; with each strain inducing a different pathological phenotype (mainly evidenced in MSA and PD prions) [84, 99]. Currently, the nature of the different strains and how the same amino acid chain can induce

different pathological phenotypes is unknown, with the most prominent model being the “conformational theory”, where pathological α -syn can self-aggregate in slightly different ways, resulting in fibrils with different structures. These conformers are then able to interact with the host in different ways resulting in differential pathological profiles. If this is true, then different α -syn strains can be distinguished (among other things) by their biophysical properties, such as their aggregation kinetics, band patterns after proteolytic digestion, chemical and thermal stability, and fibril morphology [95, 269]. Furthermore, as a prion-like protein, α -syn was found to be able to be propagated *in vitro* using fragmentation techniques such as PMCA and Real-Time Quaking Induced Conversion [270].

3.5.1 *De novo* misfolding methods

In this chapter, recombinant α -syn monomers were misfolded *in vitro* and the misfolding kinetics were analysed together with the physical properties of the newly produced fibrils. Mirroring protocols optimized by Herva *et al.*, 2014 [163], *de novo* fibrils were produced through the sonication of high concentrations (90 μ M) of recombinant monomeric α -syn (figure 3.5,A). This assay confirmed that the α -syn A produced through the proprietary methods optimized by UCB Celltech could indeed be misfolded with PMCA. Furthermore, misfolding as early as 4 hours was seen. Interestingly, the band patterns in these early experiments were consistent with the classic Low Mw two-band pattern seen in all non-seeded samples in later experiments. But, given the higher concentrations used, samples sonicated for longer periods were also seen to possess additional bands; most likely indicating the presence of a higher number of fibrils, fibril networks or different conformers being generated. This was also confirmed by ThT binding as the 24-hour sonicated samples possessed higher signals than all of the earlier time points analysed (figure 3.5, B). To test whether the misfolding of α -syn could be accelerated by the introduction of preformed fibrils, seeding experiments were attempted, using small volumes (1% [v/v]) of *de novo* fibrils sonicated for different times to seed monomeric solutions (figure 3.6). The presence of seeds greatly accelerated the formation of fibrils, as evidenced by the strength of the different PK digested bands. Beyond the characteristic two-band pattern, several other bands

were present. Interestingly, seeding with 8 and 24 hour sonicated fibrils resulted in the presence of PK resistant bands even without sonication (time point 0h); this could most likely be attributed to particular fibrillar conformers induced by longer sonication times being able to kickstart the misfolding process as soon as the seeds are introduced to the monomeric solutions. This is particularly evident as 4h sonicated seeds (although possessing similar band intensities to 8h and 24h sonicated seed, and therefore similar aggregate counts) lacked any PK resistant bands at time point 0. Further experiments are needed to confirm these findings, such as the implementation of SDS-PAGE on 1% (v/v) seeds in PBS buffer.

3.5.2 Human seeded assays

With evidence that the recombinant α -syn used could misfold *in vitro* through PMCA, and that the addition of preformed fibrils altered the misfolding kinetics; the next step was to assess if human-derived aggregates could also induce the formation of fibrils. The use of human derived samples in the context of PMCA is highly advantageous, as the presence of small amounts of pathological α -syn within the brains can themselves be propagated through templated misfolding [271]. This not only allows for the isolation of disease relevant conformers, but it also allows for PMCA to act as a potential diagnostic tool. In fact, PMCA has been already been successfully implemented for the identification of different α -syn strains from fixed human brain samples [261] and from the CNS of diseased animal models [106, 163], obtaining fibrils with different biophysical and infective properties. Additionally, a related technique, called Real-Time Quaking Induced Conversion (RT-QUIC) which uses vigorous agitation rather than sonication to promote the fragmentation and propagation of fibrils has been developed. This variant of PMCA has found great success in the propagation of fibrils using human-tissue such as CSF [85, 165, 272-274], brain homogenates [257] and even skin [263, 275] or gut [265] homogenates. RT-QUIC has also been successful in producing morphologically distinct conformers of α -syn using samples from subjects affected from different synucleinopathies, and only diseased tissue was seen to induce misfolding, opening up the possibility of using this technique as a potential diagnostic tool [85, 165, 257, 272-275]. Although possessing many strengths, one of the main

weaknesses of RT-QUIC is its inability to produce infectious aggregates. This was first observed in prion diseases, and as of yet, no study has reported *in vivo* infection of animal models with RT-QUIC generated aggregates [276].

In this chapter, PMCA was implemented to propagate misfolded aggregates within human cytosolic brain extracts. This allowed, for the first time, the identification of distinct human brain-derived (High) conformers which were different from another (Low) polymorph that was only present in *de novo* formed fibrils.

3.5.2.1 Characterization of human brain samples

The initial in-depth characterization of the human seeds used for PMCA was a crucial initial step, especially when comparing a diseased group (PD) to a control group (HC); as potential differences highlighted during this process could then translate to different α -syn conformers after misfolding. For this, all of the PD and HC samples were first subjected to SDS-PAGE and then western blotting analysis, using antibodies targeting α -syn at different stages of its aggregation process. Side-by-side comparison of the PD and HC groups did not reveal any major differences and samples contained monomeric (figure 3.8, B), oligomeric (figure 3.8, C) and aggregated (figure 3.8, D) α -syn in both groups. This was in agreement with previous reports in the literature, where soluble brain homogenates from diseased and control cohorts lacked major distinctions evidenced with western blotting [263-265]. This lack of distinctions between brain samples might be the reason why PD and HC seeded reactions both produce the “human-derived” band patterns, but the fact that different human samples were able to produce slightly different High banding patterns underlined the presence of undiscovered distinctions between samples. Further studies were needed to confirm the presence of effective differences between cohorts. Additionally, the way in which the human cytosolic brain samples were processed [247] could also be a factor in determining a more homogenous population of α -syn within the two groups, as the potential contribution of extracellular α -syn aggregates [50] are excluded, by virtue of using only the cytosolic brain fractions of the brains.

The fact that CSF seeded PMCA resulted in the same high Mw band pattern being present across samples from PD and HC groups could indicate a limitation within the methodologies used to propagate fibrils *in vitro*, as similar assays with RT-QUIC seem to produce amplification of α -syn only with seed from PD patients [85, 165, 272-274]; or this could also be a consequence of the presence of inhibitory compounds within the CNS itself [165, 270].

3.5.2.2 PMCA misfolding of seeded samples

Notwithstanding, PMCA seemed to be successful in the propagation of human-derived aggregates *in vitro*, represented by the High Mw band patterns present after PK digestion, which was different from the Low Mw band pattern always seen in the non-seeded or *de novo* fibril seeded samples (figure 3.9, A). Parallel analysis of these aggregates with ThT revealed that these protein structures were rich in β -sheets (figure 3.9, B). These findings were later confirmed with CD, as the spectra of the ThT positive and PK resistant bands matched the typical absorption pattern of a compound with a high proportion of β -sheets in solution; monomers, on the other hand, possessed a spectra matching random coils (figure 3.10, B) [277, 278]. Finally, these same aggregates were ultimately confirmed to be fibrils, as NS-TEM showed characteristic elongated and unbranched structures (figure 3.9, C; figure 3.10, A). Interestingly, although PK digestion revealed the presence of different band patterns, which in turn are indicative of differential fibril structures, NS-TEM analysis did not reveal major differences between samples in terms of fibril morphology. Further analysis with other techniques such as cryo-electron microscopy, could potentially highlight differences that NS-TEM does not [85].

Further PMCA analysis of all available PD and HC brains revealed the ubiquitous presence of two subtypes of High Mw band patterns: one with a more prominent high Mw band and another with more prominent mid and low Mw bands; each sample corresponded with one of the patterns and consistently produced the same result across experiments (figure 3.11, A). Densitometry analysis of the different band patterns allowed the clustering of human-derived samples that was distinct from the non-seeded samples, further confirming the differences between these two groups (figure 3.11, B).

Next, in order to investigate the influence of the protein components within the cytosolic brain extracts in seeding PMCA reactions, experiments were designed in which the protein milieu of the brains were altered by the use of proteolytic enzymes (PK and ThLY). These digested brains would then be used to seed new PMCA reactions. Resolving the digested brains on 4-12% Bis-Tris gels (figure 3.12) revealed that the presence of the enzymes, as expected, resulted in a dramatic change to the brain's protein migration patterns: PK produced a smear of low molecular weight elements around the bottom of the gel, while ThLY seemed act in a different way, by digesting most proteins and only leaving some lower Mw bands from digested CNS material (or ThLY itself). This is to be expected as the PK and ThLY do indeed possess different modes of action, and have been seen to digest prions to produce distinct cleavage patterns [266, 267]. When ThLY digested brain material was introduced to the PMCA reaction (figure 3.13), an interesting phenomenon is observed: ThLY treated brains were able to produce fibrils, and brains treated with higher concentrations of the enzyme produce a different band pattern to the lower concentration-treated brains. There are very interesting results that draw attention to the potential variability induced by the modification of the protein components of the brains used as seeds, but further repeats were needed to draw conclusive remarks about the effects of PK and ThLY on α -syn fibril formation

Further evidence that oligomers and fibrils within the brain seeds are responsible for the formation of the different band patterns was produced by serial PMCA (figure 3.14, A); with this procedure, the protein aggregates responsible for the formation of the High band patterns are isolated from the context of the brains through serial dilution, leaving the preformed α -syn aggregates as the driving force behind the misfolding. With the band patterns being consistent over three sub-passages (figure 3.14, B), it indicates that the misfolded α -syn aggregates in the brain were able to recruit monomers towards the formation of a particular band patterns, and then these *in vitro* formed α -syn fibrils recruited further α -syn monomer to produce the same band pattern. A similar behaviour is also seen in the non-seeded samples. This demonstrated that the different conformers, likely produced by distinct folding pathways, are stable over different sub-passages.

Throughout this chapter, α -syn has been observed to differentially misfold depending on whether or not human or preformed *de novo* fibrillar material is used as seeds. These fibrils have been confirmed by NS-TEM, are bound by ThT and possess confirmed β -sheet structure; additionally, they possess distinct band patterns after digestion with PK which is stable over different PMCA sub-passages. To confirm any biochemical differences between fibrils, a stability assay was performed, using an increasing concentration of GdnHCl to treat the different kinds of fibrils in solution prior to PK treatment (figure 3.15). This revealed that the Low Mw binding pattern, induced by *de novo* formed fibrils was the most stable, as evidenced by the presence of PK resistant bands at higher molar concentrations of the chaotropic agent. These experiments add to the evidence that the different band patterns do indeed correlate with fibrils that possess different biophysical properties to one another [107]. Following prion biology, these properties would strongly suggest that the High and Low Mw band patterns correspond to distinct types of α -syn fibrils with different biophysical properties [161, 256, 269].

In summary throughout this study, recombinant α -syn was misfolded both *de novo* and with human seeds to produce three distinct types of fibrils with different biophysical properties. Through the analysis of these conformers using protein resolution techniques, spectroscopy, fluorescent assays, conformational stability assays and electron microscopy, together with PMCA passage studies it is revealed that these different structures are likely different conformers of α -syn. This first of a kind of study provides firsthand evidence that human brains can seed the formation of different strains of α -syn when using PMCA (with sonication). Further studies are needed to confirm the pathological relevancy of these different aggregates, most likely by toxicity assays in cell line and animal models. Additionally, a bigger sample size should be tested to confirm the presence of these same band patterns in other subjects (and/or the presence of further types). Furthermore, future experiments should include human tissue prepared in different ways (for instance whole brain cell homogenates as opposed to cytosolic brain extracts) as this could add another dimension to the pathological aggregates present for PMCA seeding, potentially allowing for the identification of disease-associated

strains of α -syn. Regardless, this study provides very promising the basis for future antibody discovery efforts, targeting human specific aggregates. These antibodies could then be tested in cell line models to assess for therapeutic function and binding could be further tested by the implementation of immunohistochemistry with disease derived brain material.

Chapter 4. Production and *de novo* misfolding of synthetic Amyloid beta

4.1 Introduction

AD, the current most common neurodegenerative disease affecting the aging population [22, 279], is characterized by the accumulation of two misfolded proteins, tau and A β [25], the latter of which has been shown to accumulate in a predictable manner following three stages (defined as A, B and C as the disease advances) [27]. Beyond progressing in a stereotyped manner, the A β within the diseased brain seems to accumulate following a sigmoidal pattern in early stages of the disease [30] meaning that most if the A β deposits within the diseased brain are already formed by the time the symptomatology of the disease starts to manifest. This early accumulation of A β deposits together with the intervention of other factors, such as tau accumulation are thought to be the driving force behind the onset and propagation of the disease [20, 22-24, 31]. The understanding of the behaviour A β and its misfolding kinetics is therefore an important step for the in-depth understanding of early AD pathology. A β can be induced to misfold *in vitro*, but unlike α -syn, the higher number of hydrophobic amino acids within the structure of the A β peptide determines a higher instability for monomers in aqueous solutions with a high propensity to spontaneously self-aggregate [244, 245]. Currently, only one study has successfully implemented PMCA for the controlled formation of fibrils: Salvadores *et al.*, 2014 [166], where CSF from diseased patients were successful in seeding the propagation of fibrils in solution through shaking PMCA (RT-QUIC) while control CSF did not produce such an increase. Most commonly for A β , *de novo* fibril formation is either induced by static incubation [144, 155, 184, 280, 281] or constant stirring [133, 282]. Regardless of the approach taken, A β fibrils are known to be highly polymorphic, both *in vitro* [144, 155, 184] and *in vivo* [283].

In this chapter, synthetic peptides were used to perform an in-depth analysis of the misfolding kinetics of A β . The aim was to control the fibril formation process in such a way that different stages of the aggregation process of A β could be produced (such as monomers and fibrils), for the purpose of performing antibody discovery techniques. For this, initial experiments focused on the identification of a protocol to consistently produce monomers or fibrils in solution, followed by the implementation of different misfolding techniques such as PMCA or static incubation to attempt to control the

misfolding process. Finally, an RT-QUIC methodology based on the protocols seen in Salvadores *et al.*, 2014 [166] was implemented, and peptides from different suppliers were compared. A β misfolding was analysed with ThT (either by single measurements or time point analysis for RT-QUIC), together with NS-TEM and CD. Through these techniques, a methodology to reliably produce both monomers and fibrils was identified, and their aggregation states were confirmed by both CD or NS-TEM. Monomers and fibrils were then chemically biotinylated in preparation for antibody discovery. Finally, fibrils were fragmented with sonication with the purpose of increasing the number of elongation sites in solution. These fragmented fibrils were characterized with the purpose of using them as targets for further antibody discovery.

4.2 Solubilization of synthetic A β 42 and monomer stability analysis

Synthetic A β 42 peptides were purchased from Gencust; initial solubilization methods were provided by the supplier. Following the resuspension step, the solution was analysed with NS-TEM and CD to confirm the aggregation state of the peptides in solution. Analysis revealed the presence of fibrils rather than monomers from this solubilization method (figure 4.1). Fibrils produced in this way were flash frozen in dry ice and preserved for future use as preformed fibrils to seed misfolding experiments, and also for use as fibril controls.

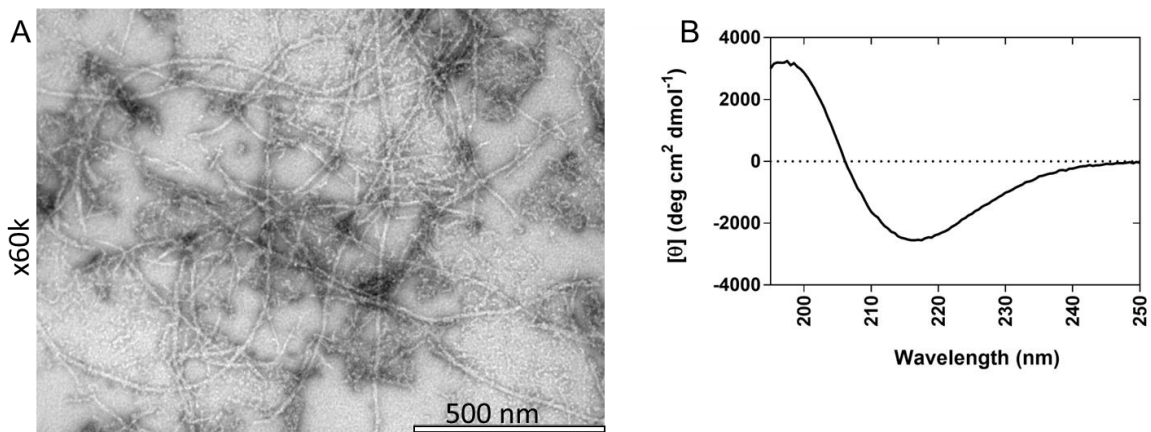


Figure 4-1: Characterization of A β 42 fibrils

Synthetic Gencust peptides (1 mg) were resuspended in small volumes of 1% (w/v) NH_4OH (80 μl) followed by neutralization with sterile PBS (920 μl), making a final 1 ml solution at 1 mg/ml. This solution was characterized with microscopy and spectroscopic techniques. **A:** NS-TEM image of the resuspended A β 42 solution. The image clearly shows the presence of a rich network of *de novo* fibrils. **B:** CD spectra confirming the presence of β -sheets in the *de novo* formed fibrils.

An alternative approach based on the methods described by Teplow *et al.*, 2006 [246], Ryan *et al.*, 2012 and 2013 [244, 245] was attempted. Monomers produced in this manner were tested in a series of conditions, using static incubation and ThT to measure the emission of fluorescence over time (figure 4.2). First, three repeats of a low concentration of peptide (5 μM) were assessed (figure 4.2, A); the measurement of ThT over 48 hours revealed no misfolding throughout the experiment, with fluorescence emissions matching the background fluorescence levels measured with a blank sample. Next, an increasing concentration range of peptides, from 5 to 160 μM were tested (figure 4.2, B); no misfolding was observed over 48 hours of analysis. Finally, human-derived cytosolic brain extract from AD and HC samples were tested (figure 4.2, C and D respectively) as 2 μl seeds introduced to the monomeric solution (200 μl); the presence of human brain did not seed the misfolding kinetics of the peptides, as no increase in ThT was observed in the 48-hour time course.

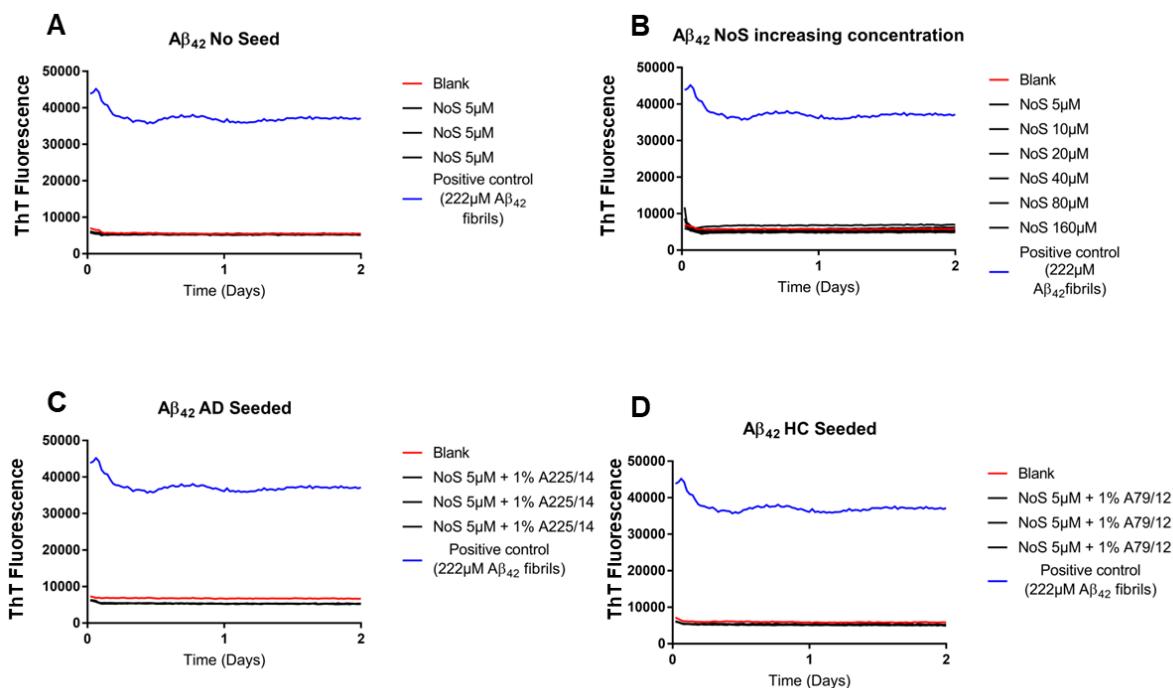


Figure 4-2: Monomer stability assessment

Synthetic peptides (1mg) were resuspended in 2ml of 10% NH_4OH and incubated on ice for 10 minutes. NH_4OH was removed by freeze-drying. The resulting dried pre-treated powder was then resuspended in 60 mM NaOH (200 μ l) and incubated for another 10 minutes in wet ice, making a 554 μ M solution, ready to use. Monomers treated in this way were analysed within a 48-hour time-course, measuring ThT (30 μ M) emissions every 10 minutes. A well was left blank (PBS + 30 μ M ThT) to act as a negative control and measure background fluorescence together with a 222 μ M solution of $A\beta_{42}$ preformed fibrils to act as a positive control. A: Comparison of three repeats of 5 μ M $A\beta_{42}$ solutions, no emission of fluorescence was observed over time. B: Increasing concentrations of $A\beta_{42}$ monomers (5, 10, 20, 40, 80 and 160 μ M) were incubated for 48 hours. No misfolding was observed within the timeframe analysed. C: Three repeats of 5 μ M $A\beta_{42}$ incubated with 2 μ l of AD brain cytosolic extract; no misfolding was observed. D: Three repeats of 5 μ M of $A\beta_{42}$ incubated with 2 μ l of HC brain; no misfolding was observed.

4.3 PMCA experiments

4.3.1 Parameter optimization tests

Following the discovery of a suitable method to produce stable monomers in solution, the next step was to attempt misfolding through PMCA. For this, a series of experiments were designed to pinpoint the optimal settings (amplitude and sonication time) to induce $A\beta$ misfolding. Samples (at 20 μ M) were either non-seeded, to assess *de novo* misfolding, or seeded with preformed fibrils (at 1% or 10% [v/v]) to assess whether the introduction of fibrils in solution could accelerate misfolding. In these experimental conditions, the ideal parameters would minimize *de novo* misfolding and promote seeded misfolding. PMCA products were analysed with ThT, using 20 μ M of preformed fibrils (equivalent to 10% [v/v] preformed fibrils in PBS) in solution and a blank sample as controls to assess

the ThT emission of the highest proportion of seed used (10% [v/v]) and background fluorescence respectively.

The comparison of the effects of amplitude (responsible for the intensity of the ultrasonic signal) revealed no major differences between samples (figure 4.3). For all of the samples analysed, seeded monomers possessed the highest ThT emission values, with 10% (v/v) seeded samples possessing the highest value among all groups and controls, suggesting that fibril seeding successfully induced the formation of further fibrils. Non-seeded samples for 20%, 30% and 40% amplitude possessed higher ThT values than the fibril controls, suggesting the formation of *de novo* fibrils. Only 10% amplitude sonicated samples displayed non-seeded values close to the background fluorescence levels seen in the blank controls. This data suggested that 10% sonication is the optimum condition for future PMCA experiments, as these settings seem to promote the misfolding of seeded samples (as evidence by the high fluorescence of the 1% and 10% seeded samples) while minimizing *de novo* misfolding.

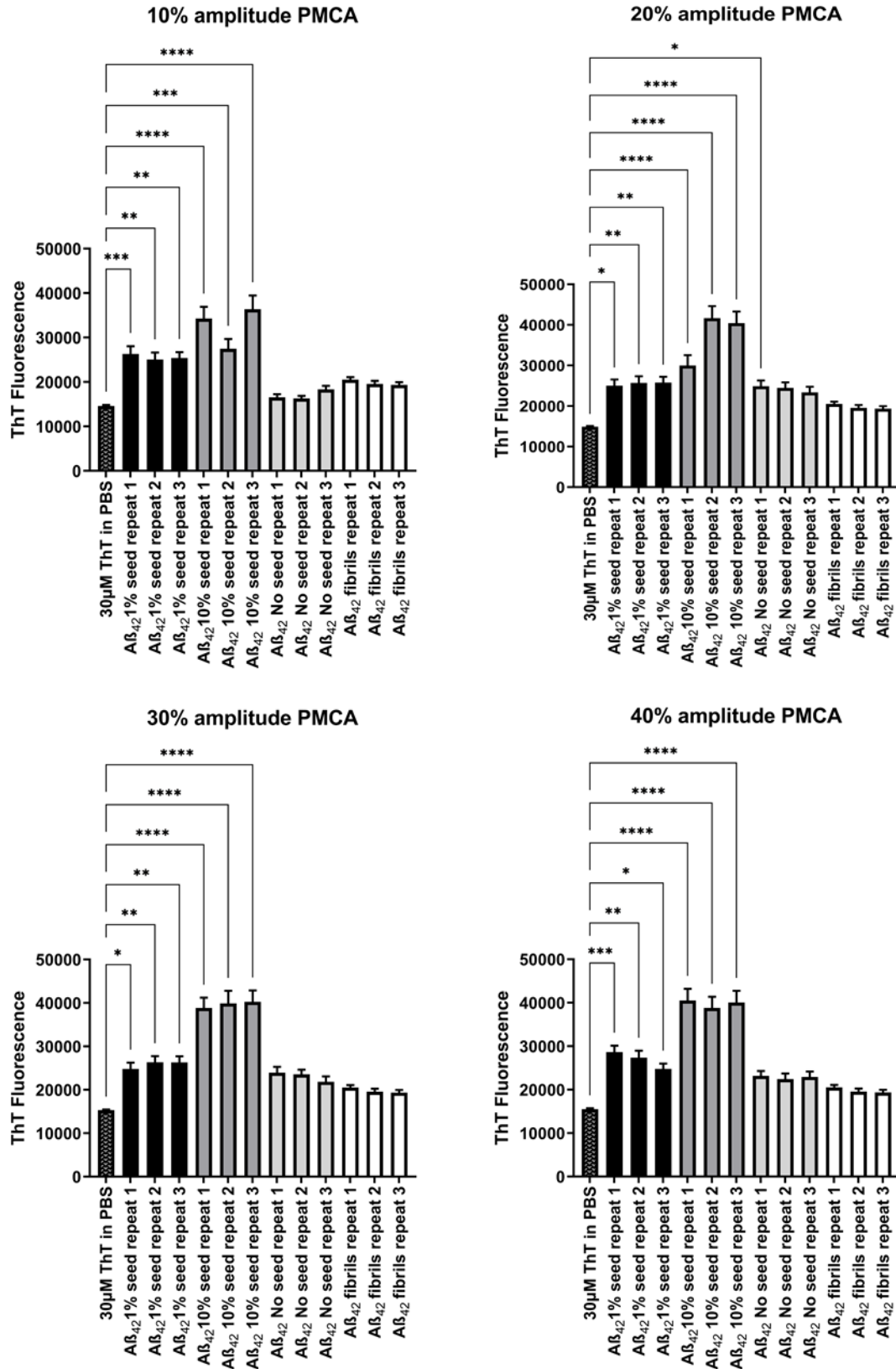


Figure 4-3: PMCA parameter optimization- Amplitude

Aβ₄₂ solutions (200 µl at 20 µM) were seeded with 1% (v/v) or 10% (v/v) preformed fibrils or were not seeded at all. Samples were subjected to 72 hours of sonication with either 10%, 20%, 30% or 40% amplitude for 20 seconds and 29:40 minutes of

incubation at 37 °C in between each sonication. All samples were assessed in triplicate. Following PMCA, the presence of fibrils was confirmed with ThT, using a blank samples (30 μM ThT in PBS) as negative control to measure background fluorescence. Preformed fibrils (222μM) in PBS were used as positive controls. A direct correlation between the presence of preformed fibrils and ThT was observed, with 10% (v/v) seeded samples possessing higher overall fluorescence levels in all experimental conditions, followed by 1% (v/v) and then non-seeded samples. With 10% amplitude it was possible to see less fluorescence in the non-seeded samples compared to the fibril controls, beyond this observation, no major differences seem to be introduced by the variation of the amplitude. Statistical analysis was performed with Kruskal–Wallis test with Dunn's multiple comparisons post-hoc analysis revealed statistically significant differences between samples and blank controls (P values indicated in graph as asterisks: P<0.05 [*]; P<0.01 [**]; P<0.001 [***]; P<0.0001 [****])

With 10% amplitude as the most suitable setting for further PMCA experiments, the next parameter to optimize was the sonication time. For this, the same 10% (v/v) and 1 % (v/v) preformed fibril seed in 20 μM Aβ42 monomer, the 20 μM Aβ42 monomer non seeded samples and 20 μM pre formed fibril in PBS positive control were sonicated with 10 % amplitude and either 10 second, 20 second, 30 second and 40 second sonication pulses. Incubation was always performed at 37 degrees, but the time the samples were incubated for varied depending on the pulse time (29:50, 29:40, 29:30 and 29:20 minutes respectively). For this experiment, beyond having 20 μM fibril and blank controls, a solution of freshly resuspended monomers was also analysed together with the PMCA products to assess fibril formation. The assessment of ThT fluorescence emissions (figure 4.4) revealed a similar outcome to the amplitude optimization tests, where no major differences were observed between samples. As seen before, seeding with preformed fibril produced the highest ThT fluorescence compared to the other samples. Upon closer inspection, 40 second sonication was discarded as the *de novo* misfolding observed in the non-seeded samples seemed to outmatch the ThT background control. 10, 20 and 30 seconds, on the other hand, almost always showed non seeded samples possessing similar values to background fluorescence, and lower ThT binding than the positive controls, making them suitable parameters to use. Due to the fact these three settings produced comparable results; 20 seconds were chosen for future experiments.

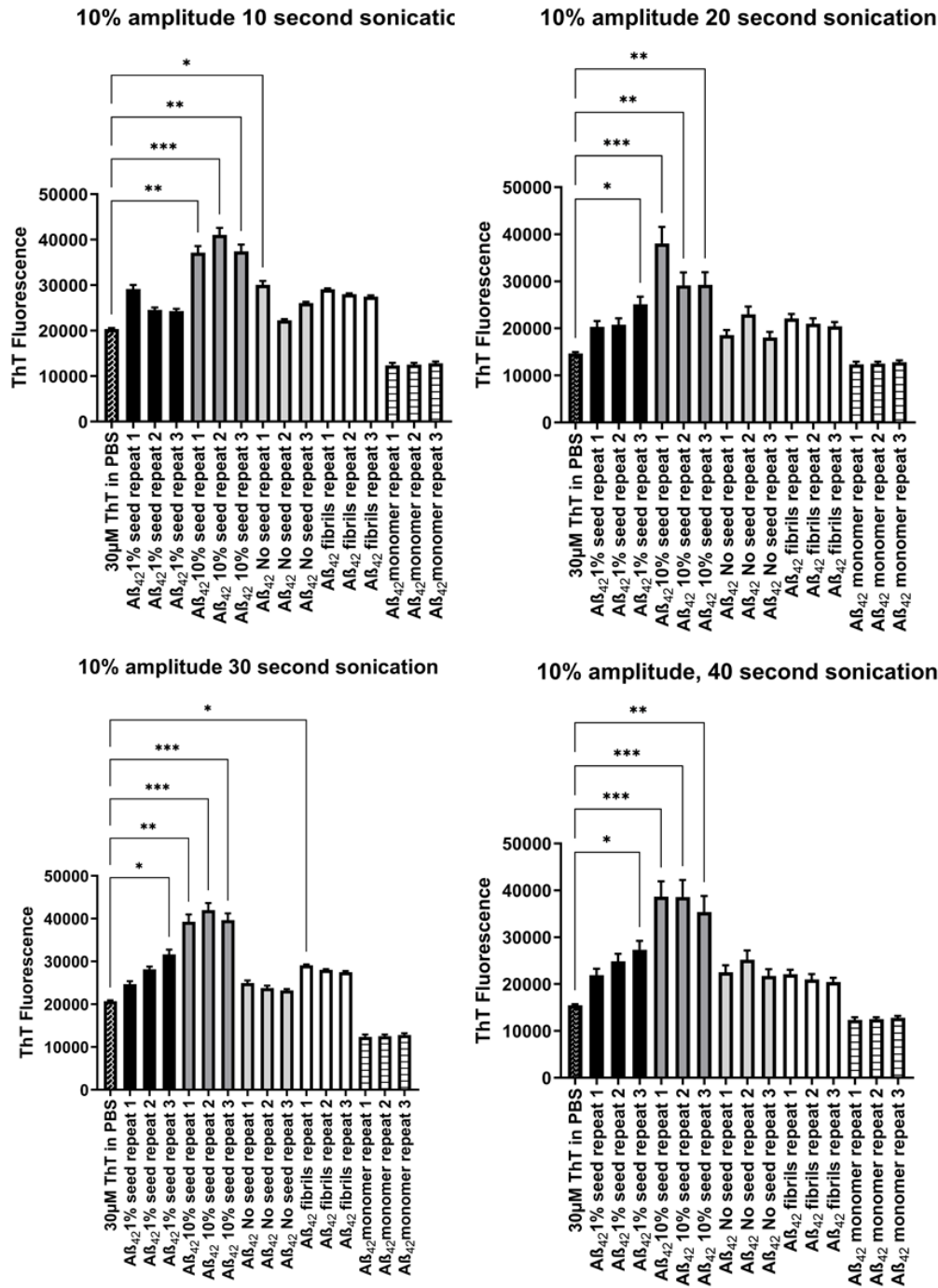


Figure 4-4: PMCA parameter optimization- Sonication time

Aβ₄₂ solutions (200 µl at 20 µM) were seeded with 1% (v/v) or 10% (v/v) preformed fibrils or were not seeded at all. Samples were then sonicated for 72 hours with set 10% amplitude but increasing sonication time (10, 20, 30 or 40 seconds). Following PMCA, fibril formation was assessed with ThT (30 µM), using a blank well (30 µM ThT in PBS) as negative control, and preformed fibrils (20 µM) as positive controls. Additionally, freshly resuspended monomers (200 µl at 20 µM) were also tested with ThT, to measure monomer fluorescence emission. As seen in the amplitude optimization step, there is a direct correlation with amount of preformed fibril introduced in solution and the emission of ThT signal, with 10% always being the highest followed by 1%, 20 µM fibril control, non-seeded sample, and finally monomer control. No further differences were observed, and misfolding seemed to be independent of the sonication time. Statistical analysis was performed with Kruskal–Wallis test with Dunn's multiple comparisons post-hoc analysis revealed statistically significant differences between samples and blank controls (P values indicated in graph as asterisks: P<0.05 [*]; P<0.01 [**]; P<0.001 [***])

4.3.2 PMCA with human seeds

The analysis of the optimal sonication parameters described in the previous section revealed the set of conditions which seemed to be the most promising to induce seeded fibril formation while maintaining low levels of *de novo* misfolding. Within these conditions, an interesting pattern emerged: both the 1% (v/v) and 10% (v/v) preformed fibril seeded samples always possessed higher ThT binding compared to the other samples analysed. This was particularly evident for the 10% (v/v) preformed seeded samples, as they always presented the highest fluorescence amongst all of the different conditions tested, suggesting that PMCA could enhance the formation of fibrils when seeds are present, and that the more seeds are introduced in solution, the more overall fluorescence we will be produced. Next, an attempt was made to introduce human seeded samples obtained from both AD patients and age matched HC into the PMCA reactions, to assess whether human-derived fibrils could seed misfolding. For this, a PMCA experiment was set up, using the newly identified parameters to sonicate samples (10% amplitude and 20 second sonication pulses, with 29:40-minute incubation). The cytosolic brain extracts from the 10% (w/v) brain homogenate samples were added as 2 μ l in 200 μ l of PMCA reaction (20 μ M A β 42 in PBS 1X), making a final concentration of 0.1% (w/v) brain; or as 2 μ l of a 10-fold dilution series of cytosolic brain extract; making a final concentration of brain material of 0.01% (w/v) [in 10^{-1} diluted sample], 0.001% (w/v) [in 10^{-2} diluted sample], 0.0001% (w/v) [in 10^{-3} diluted sample], 0.00001% (w/v) [in 10^{-4} diluted sample], 0.000001% (w/v) [in 10^{-5} diluted sample], and 0.0000001% (w/v) [in 10^{-6} diluted sample]. This was done, as evidence in the literature would suggest that the use of undiluted CNS material has inhibitory effects on the formation of fibrils [270]. As before, 1% (v/v) and 10% (v/v) preformed fibril seeds were also tested, together with non-seeded samples and 20 μ M of preformed fibrils in PBS, acting as controls. Results (figure 4.5) show no major increase in fluorescence for any of the brain seeded samples, at any of the seed concentrations tested, and they possess lower ThT emissions than both 1% and 10% preformed fibril seeded samples, which showed the highest overall binding values. All of the brain seeded samples possessed similar ThT binding values as the blank control; indicating that brain seeds failed to produce fibrils during PMCA.

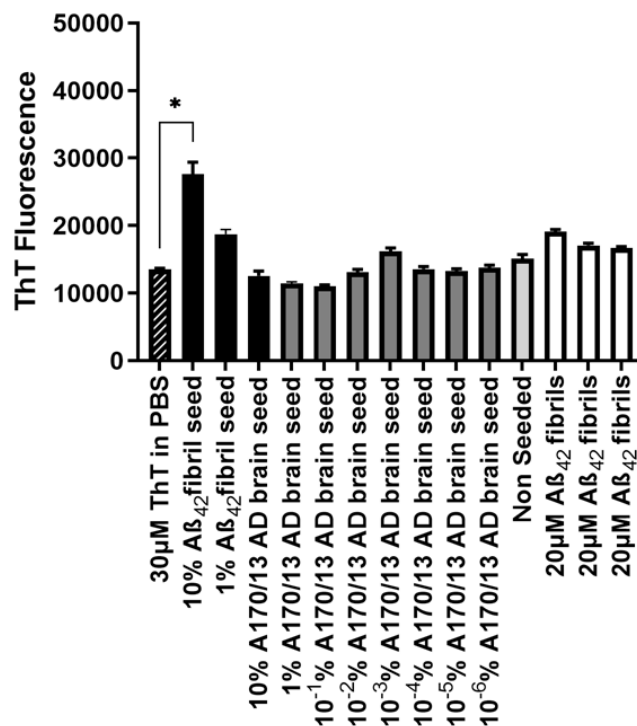


Figure 4-5: PMCA with AD brain

Different proportions of brain homogenate deriving from an AD patient were introduced to the PMCA reaction (200 µl of 20 µM Aβ₄₂): 10% (v/v), 1% (v/v) or 1% (v/v) of serially diluted brain in PBS (from 10⁻¹ to 10⁻⁶). A non-seeded sample was used as negative control for seeded misfolding; 10% (v/v) and 1% (v/v) preformed seeded samples were additionally used for *de novo* fibril seeding controls. Following PMCA (10% amplitude, 20 second pulses with 29:40 minute incubation at 37 °C, for 72 hours), fibril formation was assessed with ThT, using three repeats of 20 µM preformed fibril solutions as positive controls. Emission analysis revealed that preformed fibril samples possessed the highest fluorescence. Statistical analysis was performed with Friedman test with Dunn's multiple comparisons post-hoc analysis, only one sample (10% Aβ₄₂ fibril seed) showed a statistically significant difference to blank control (P<0.05).

4.3.3 Using different additives to enhance PMCA

In an attempt to promote the formation of human-derived fibrils from the aggregates in the brain samples, different additives with fibril-stabilizing properties were tested. These additives were chosen based on their ability to enhance PMCA sensitivity in prion diseases, with the working hypothesis being that these compounds could also enhance Aβ misfolding, being a prion-like protein [96]. The chosen molecules were: Saponin (0.05% v/v) [284]; Digitonin (D) (0.05% v/v) [285]; Dextran Sulphate (DS) (0.5% v/v) [286], α-crystallin (0.1 µg/ml) [287]; Heparin (20 µg/ml) and Heparan Sulphate (100 µg/ml) [288-290]. Of particular interest were Heparin and Heparan sulphate, as these molecules have been

found to directly bind A β , and potentially influence the formation of new aggregates [291]. Additives were dissolved in the PMCA reaction mix (20 μ M A β 42 in PBS) and tested with an array of seeds: either 10% (v/v), 1% (v/v) synthetic preformed fibrils. Additionally, 2 μ l of AD cytosolic brain extract were added as is, or as part of a 10-fold dilution series (10^{-2} or 10^{-6} diluted brain in PBS, as seen in section 4.3.2). Non-seeded samples were also assessed with the range of additives. At the conclusion of the PMCA run, fibril formation was assessed with ThT (30 μ M) using a blank sample to measure background fluorescence and three-repeats of 10% (v/v) preformed fibrils (20 μ M) in PBS to monitor the fluorescence levels without any added monomer. The analysis of the ThT emission of each sample (figure 4.6) show similar patterns emerging within all the different additives used. As expected, 10% (v/v) synthetic fibril seeds always showed higher ThT binding compared to all the other samples analysed within the same group; 1% (v/v) synthetic seeded samples, on the other hand, possessed higher values to background fluorescence and non-seeded samples, but less intensity than the 10% (v/v) seeded samples. The DS group was an exception, as in these samples similar ThT emission values could be found between the 1% (v/v) synthetic seeded samples and non-seeded controls. As for the human seeds, no significant misfolding was observed in any of the groups, except from 10^{-6} diluted brain in the DS treated reaction. Further testing revealed these results were not reproducible, as the analysis of additional samples revealed the effects of DS to be non-specific (figure 4.7). Additional repeats with 10% (v/v) pre formed fibril seeded and non-seeded samples in D and PBS showed that the apparent increase in misfolding induced by D is the result of the additive itself inducing an increase emission of ThT, as the ratio of signals for seeded and non-seeded samples was similar for PBS and D. These results strongly suggest that the use of additives do not provide any additional enhancement to A β 42 PMCA misfolding.

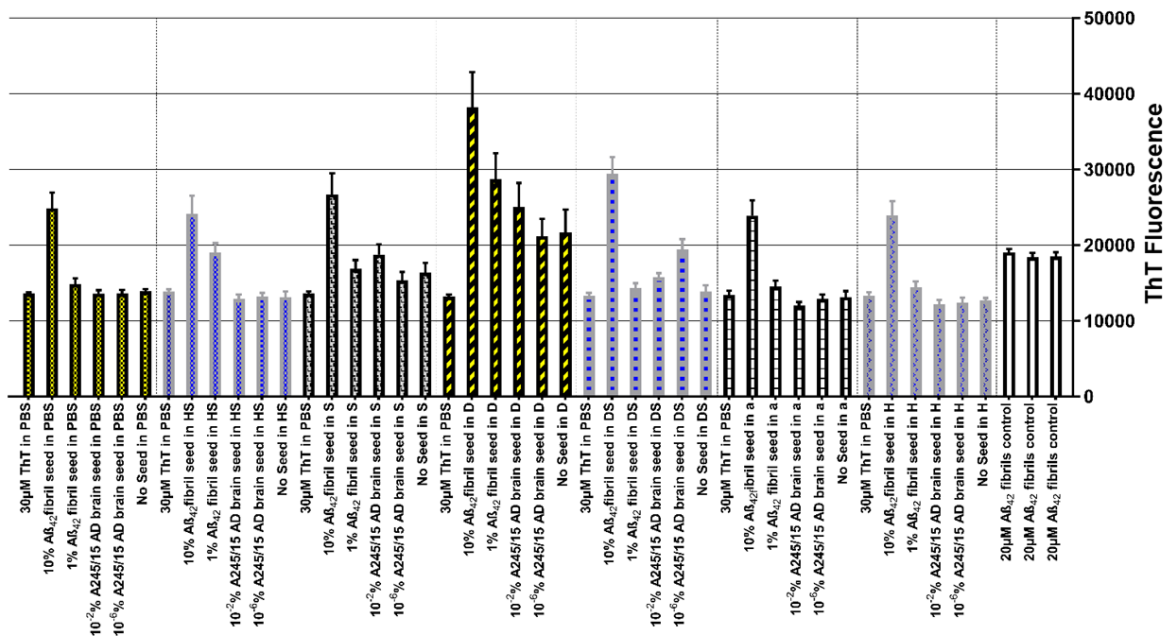


Figure 4-6: PMCA with different additives

PMCA was performed on Aβ₄₂ solutions (200µl at 20 µM) seeded with either 10% (v/v) preformed fibrils, 1% (v/v) preformed fibrils, 0.001% (w/v) diluted AD brain (10⁻² A245/15 AD brain), 0.0000001% (w/v) diluted AD brain (10⁻⁶ A245/15 AD brain) or no seed at all. Also, within the PMCA reaction, different chemical additives were added (as indicated). Following PMCA, fibril formation was assessed with ThT (30 µM). Background fluorescence was measured through a blank sample (30 µM ThT in PBS) and 20 µM of preformed fibril in PBS were used as positive controls. ThT emissions show that overall, preformed fibril seeded samples always possess the highest fluorescence, regardless of the additive used. Additionally, 10% preformed fibril always overperformed all other samples within the group. Out of all of the additives analysed, only D and DS seemed to possess a noticeable effect of fibril formation, with D enhancing the emission values of all samples analysed; and DS enhancing values for the 20 µM preformed fibril control and the sample seeded with 10⁻⁶% brain homogenate. HS: Heparan sulphate, S: Saponin, D: Digitonin, DS: Dextran sulphate, a: α-crystalline, H: Heparin.

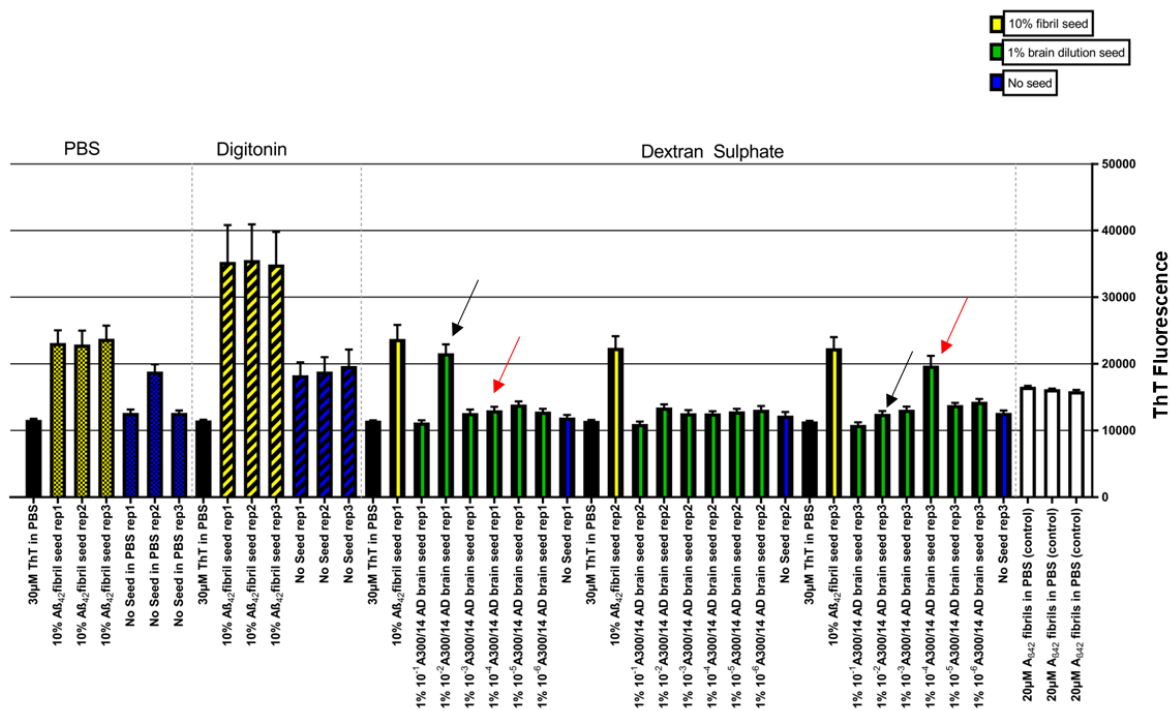


Figure 4-7: Further assessment of the effects of additives on human seeded PMCA

PMCA was carried out on samples in PBS, in PBS+ D buffer and PBS+ DS buffer. For the first two, 10% (v/v) preformed seeded samples were compared to non-seeded samples. For the reactions containing DS, in addition to the 10% (v/v) and non-seeded sample, a range of serially diluted AD brain (from 10^{-1} to 10^{-6}) were also introduced as 1% (v/v) seeds (A300/14 AD brain). At the conclusion of PMCA; fibril formation was assessed with ThT, with a background fluorescence control (30 μ M ThT in PBS) and positive control (20 μ M preformed fibril in PBS). Samples in PBS acted as expected, with 10% preformed seeded samples possessing higher ThT values than non-seeded samples throughout the three repeats. As seen before, the introduction of D to the reaction mix is able to enhance the emission signals of both the seeded and non-seeded samples; interestingly although the overall ThT emission values were higher in the samples with D, the ratio of signals with the pre formed fibril and non-seeded sample seemed to be similar to samples in PBS. The analysis of three-repeats of samples in DS revealed an interesting pattern: in one repeat, a 10^{-2} diluted brain seeded sample possessed similar ThT emission values to 10% (v/v) preformed fibril samples (black arrow), in the second repeat, no misfolding was observed and in the third repeat, it is the 10^{-4} diluted brain seeded sample which is seen to misfold (red arrow), while no misfolding is observed in the 10^{-2} seeded sample (black arrow).

To assess the stochastic nature of A β misfolding during PMCA, a final experiment was designed in which twenty 1% (v/v) 10^{-6} diluted brain seeded samples were compared with twenty non seeded controls; in addition, three-repeats of 10% (v/v) preformed seeded samples in PBS (20 μ M fibril controls) were used as positive controls. As the presence of additives did not provide any immediate benefit to the misfolding of A β , monomers were diluted in PBS (20 μ M final concentration). Following PMCA, samples were analysed using 30 μ M ThT. Blank wells were also used (30 μ M ThT in PBS) to assess the levels of background fluorescence (figure 4.8). Within the 20 repeats of each condition, five human seeded samples and 6 non seeded samples were seen to misfold. The fluorescence emitted by

4.4 A β Incubation experiments

Samples (200 μ l at 20 μ M) were seeded with 10% (v/v) preformed fibrils and either incubated or sonicated for 72 hours. After the seed was introduced to the monomer solution, some samples were frozen in dry ice prior to storage at -80 °C; these frozen samples acted as non-amplified controls. At the end of the 72-hour period, fibril formation was assessed with ThT, with blank wells to assess background fluorescence (figure 4.9). Interestingly, the ThT fluorescence emitted by both incubated and PMCA samples was very similar, with incubated samples possessing slightly higher average values than their sonicated counterparts, but no statistically significant differences as measured with the Kruskal–Wallis one-way analysis of variance. Non-amplified controls showed slightly higher but still not statistically significant values than background fluorescence ($P > 0.99$ in all three repeats), as expected, but slightly lower values than both incubated and PMCA samples. All incubated and sonicated samples possessed significantly different values than background fluorescence (data not shown), but among all repeats analysed, only incubated sample 2 possessed statistically significant differences compared to non-amplified sample 2 ($P = 0.0124$) and non-amplified sample 3 ($P = 0.0033$). Non-amplified sample 3 was also significantly different than PMCA sample 2 ($P = 0.0151$).

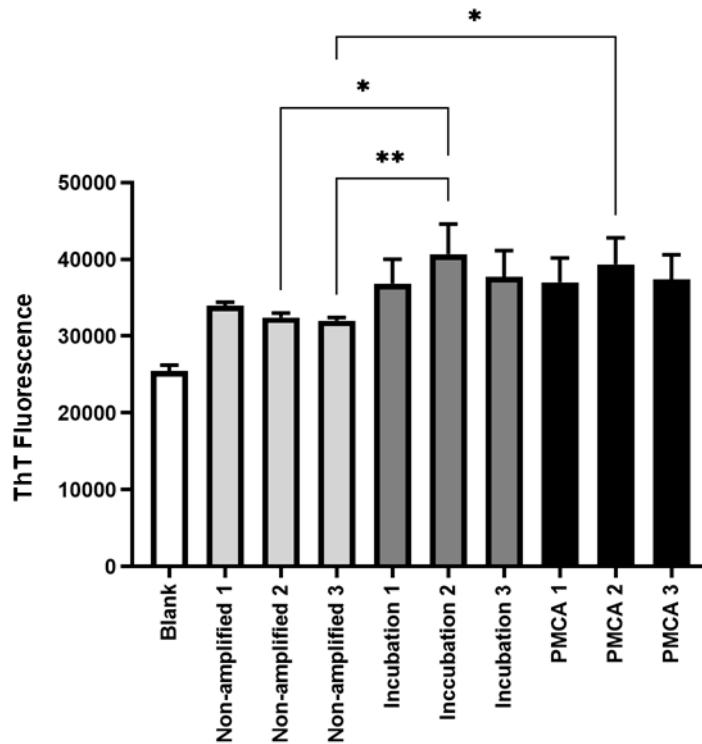


Figure 4-9: Comparison of incubated and sonicated samples for fibril formation

A β 42 monomers were prepared (200 μ l at 20 μ M) and seeded 10% (v/v) preformed fibrils. Some samples were then frozen as soon as the seeds were introduced (non amplified controls, light grey bars); other samples were statically incubated for 3 days at 37 $^{\circ}$ C (dark grey bars) and the final group was subjected to 3 days of sonication (PMCA, black bars). Following the 3-day incubation/sonication treatment, fibril formation was assessed with ThT, using a blank to control for background fluorescence (30 μ M ThT in PBS). Three repeats of each group were compared; statistical analysis was performed with the Kruskal-Wallis test with Dunn's multiple comparison post-hoc test. PMCA and incubated samples possess almost identical ThT fluorescence value, with no statistically significant differences revealed with the Kruskal-Wallis test. Incubated sample 2 though showed a statistically significant difference with non-amplified sample 2 ($P=0.124$) and non-amplified sample 3 ($P=0.0033$). Non amplified sample 3 also showed a statistically significant difference with PMCA sample 2 ($P=0.0151$)

NS-TEM was implemented to validate the ThT emission results, and reveal any morphological differences between the PMCA, incubated and non-amplified groups. The images (figure 4.10) revealed that non-amplified samples presented very little fibrils upon staining with 2% UA; incubated samples, on the other hand presented numerous fibrils with 10-20 nm in diameter and up to 1 μ M in length. Sonicated samples also possessed fibrils, but these appeared to be fragmented, overall shorter and with possibly smaller diameter compared to their incubated counterparts.

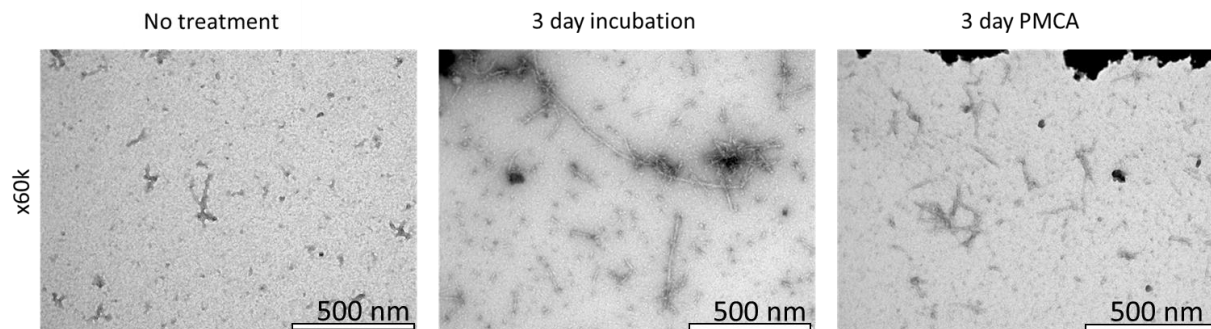


Figure 4-10: Morphological comparison of incubated and sonicated fibrils

A no-amplification sample (frozen as soon as 10% (v/v) seed is introduced) was assessed together with a 3-day incubated sample and a 3-day PMCA sample, using NS-TEM. No-amplification samples were seen to possess small fibrils in lower quantities; incubated samples showed a high number of long unbranched fibrils, with smaller aggregates surrounding the larger structures. PMCA-treated samples, on the other hand, were characterized by a high number of smaller fibril-like structures, with smaller diameters to the fibrils seen in the incubated samples.

An additional experiment was performed to better elucidate the effects of static incubation on the misfolding of A β : a second attempt to create human seed-specific fibrils.

Although previous incubation experiments revealed no misfolding for AD and HC brain seeded samples (figure 4.2) a new attempt was made using a longer incubation period (72 hours) and higher concentrations of monomer (200 μ l at 20 μ M). Cytosolic brain extract from four AD patients were pooled together and used as is (2 μ l acting as seeds) or after a 10-fold dilution series (from 10^{-1} to 10^{-6} [producing a respective dilution range of 0.01% w/v brain to 0.0000001% w/v brain in solution], always using 2 μ l of each dilution to seed 200 μ l of 20 μ M A β , as seen in section 4.3.2). Following incubation, the presence of fibrils was assessed using a final concentration of 30 μ M of ThT per sample (figure 4.11; N.B. as with the previous experiment, the scale of this graph is different from previous ThT data collected as the plate reader used was different, additionally background fluorescence [PBS+30 μ M ThT] was automatically subtracted from all samples). No major misfolding event occurred within the human seeded samples, and statistical analysis with Kruskal-Wallis and Dunn's multiple comparison failed to evidence significant differences between groups (p values were 0.25, 0.66 or >0.99). This mirrors the results found in prior incubation and PMCA experiments, and altogether

strongly suggests that incubation or seeding (with human brain or preformed fibrils) of Gencust monomers was unable to enhance the formation of fibrils.

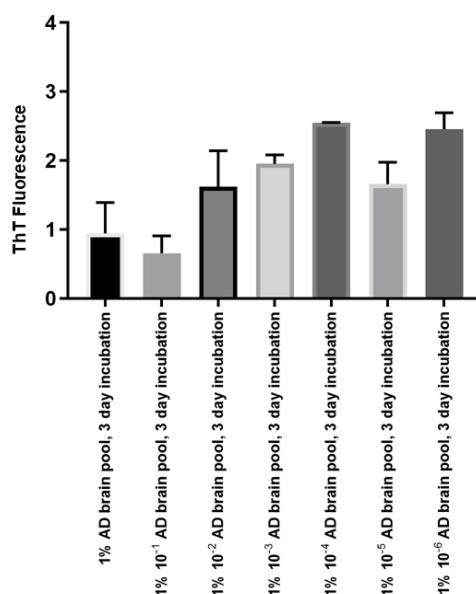


Figure 4-11: Incubation experiment with brain seeding

Brain cytosolic extracts derived from AD patients were pooled (four subjects). The pooled brain material was then serially diluted (from 10^{-1} to 10^{-6}) and used to seed (1% [v/v]) A β monomeric solutions. Seeded reactions were then statically incubated for 72 h at 37 °C. ThT was implemented to assess the rates of fibril formation in each sample. Brain seeded samples did not seem to have an effect on the misfolding rate of each sample, as evidenced by the low ThT emission signals seen in each sample. Interestingly, higher brain dilutions seemed to progressively induce higher ThT emission values, but median comparison with Kruskal–Wallis one-way analysis of variance and Dunn’s multiple comparison post-hoc test revealed no statistically significant differences between groups.

N.B. The scale of ThT emissions is different from previous data due to this experiment being run in a FLUOStar Optima plate reader. As a functionality of the plate reader, an average of the background fluorescence in blank PBS wells were automatically subtracted from all groups.

4.5 RT-QUIC misfolding

4.5.1 Synthetic monomer comparison

With evidence that the experimental conditions tested were unable to reproducibly induce the templated misfolding of Gencust monomers in the presence of seeds; a new approach was attempted with the acquisition of monomers from a different supplier, Genscript. Both monomers were pre-processed and handled as described in paragraph 2.3.2. Initial experiments compared the freshly resuspended monomers (200 μ l at 20 μ M) from both suppliers in a 168 h incubation at 37 °C. ThT was introduced in the monomer reaction to follow the formation of fibrils in real time. Remarkably, the comparison of equimolar solution of Genscript and Gencust monomers revealed no misfolding in the Gencust solution, but a time-dependant sigmoidal increase of β -sheets in solution from Genscript

monomers, with a 96 hours lag-phase followed by an exponential increase of fluorescence over time (figure 4.12, A). Further analysis with CD granted insight into the structural makeup of both solutions (figure 4.12, B). Genscript monomers were seen to possess a typical random coil spectrum, both at 0 and 6 hours after the start of the experiment, indicative of the presence of monomers in solution. Gencust monomers, on the other hand, displayed a spectrum that was not indicative of any particular secondary structure, hinting at several aggregation states coexisting in solution. These findings were further confirmed by running the samples in 4-12% Bis-Tris gels (figure 4.12, C); where a solution of Genscript monomers were seen to accumulate around 4.5 kDa and 12 kDa, respectively hinting to the presence of monomers and trimers, at a concentration of 0.5 mg/ml (111 μ M). Like Genscript monomer, Gencust monomers possessed bands at 4.5 kDa and 14 kDa, but with the addition of a smear of proteins with high molecular weight from 28 kDa to the top of the gel, most likely indicating the presence of oligomers, protofibrils and potentially fibrils. Through this assay, Gencust solutions were defined as Gencust monomer/oligomer/protofibril (m/o/pr), to indicate the intrinsic heterogeneity of the compounds in solution.

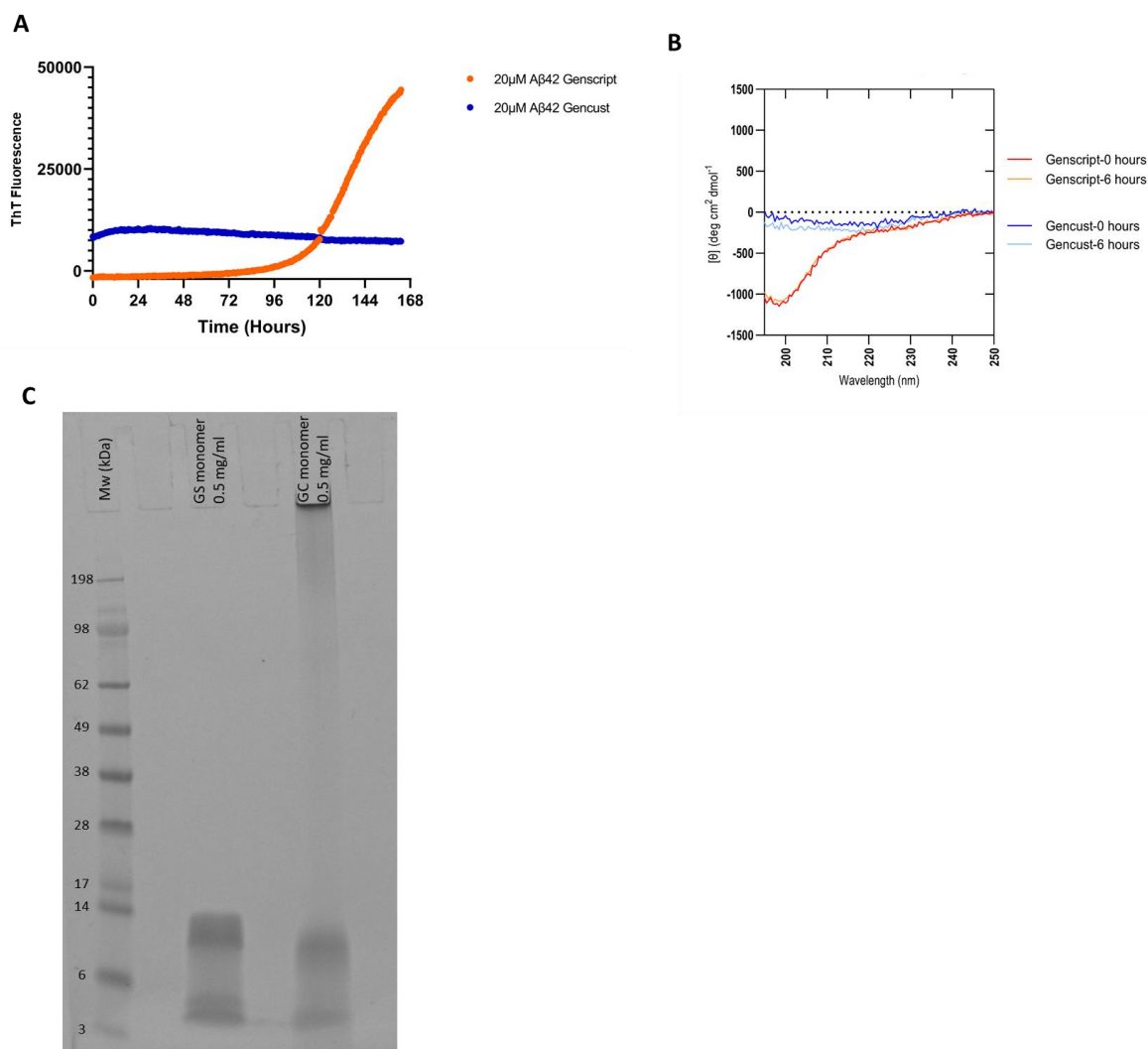


Figure 4-12: Comparison of Gencust vs Genscript monomers

Aβ42 peptides were purchased from both Genscript and Gencust. Both peptides were solubilized in aqueous 10% NH₄OH and incubated in wet ice for 10 minutes prior to drying with N₂ gas, as described in section 2.3.2. A: Fibril formation was assessed through the emission of ThT fluorescence over time. For this, monomeric solutions (20 µM) were statically incubated for 7 days (168 hours), within a FLUOstar Omega plate reader, with a measurement being taken every 30 minutes. Monomer analysis revealed that while Gencust monomers (blue line) show a time-dependant decrease of ThT emission, Genscript monomers (orange line) possess an absorption pattern with a 96-hour lag phase followed by an elongation phase for the next 72 hours. B: CD spectra of the Genscript and Gencust monomeric solutions, at 0 and 6 hours of static incubation. Gencust monomers are seen to possess a non-specific spectrum at both time points; Genscript monomers, on the other hand, are seen to possess a typical random coil absorption pattern, characteristic of monomers in solution. C: Native gel run on 4-12% Bis-Tris gels of both Genscript (GS) and Gencust (GC) monomers in solution (0.5 mg/ml). While the Genscript solution is seen to possess elements mostly around 4.5 kDa (monomers) and 12 kDa (trimers); the Gencust solution is characterized by monomers at 4.5 kDa and trimers, but also elements at higher molecular weights (oligomers, protofibrils and possibly fibrils), as evidenced by the smear at the top of the gel and the strong band in the well itself, representing elements that were too big to be resolved by the gel.

4.5.2 Misfolding of monomers with RT-QUIC

With the identification of Genscript monomers as potential candidates for seeded misfolding, due to their ability to misfold over time in a controlled manner and proven random coil structure in solution; the next step was to attempt accelerating the misfolding of the monomers, and attempt seeded

misfolding. Due to closure of the University facilities during the COVID-19 pandemic, the following experiments were performed after relocating to the labs in UCB Celltech, where no PMCA machine was available. RT-QUIC methodologies were trailed instead. The protocol tested for this was based on the methods described by Salvadores *et al.*, 2014, in which synthetic A β monomers are misfolded through RT-QUIC, evidenced by the sigmoidal increase of ThT [166]. An experiment was designed where solutions of Genscript monomers (200 μ l at 20 μ M) were subjected to intermittent cycles of vigorous agitation and incubation every 30 minutes. A non-seeded sample was compared to a 1 % (v/v) preformed fibril seeded sample, to assess *de novo* misfolding and seeded misfolding within the same experiment. A 20 μ M preformed fibril in PBS solution was used as control (the same fibrils obtained through the resuspension of monomers in PBS, as seen in section 4.2), to assess the effects of incubation/agitation on the of fibril seeds in solution. The formation of fibrils was followed in real-time through the analysis of ThT emissions, measured at the end of each agitation-incubation cycle. The resulting curves (figure 4.13) show a sigmoidal increase of ThT fluorescence for the non-seeded sample, as typically seen with the formation of fibrils in solution. Agitation accelerated the formation of fibrils in the non-seeded samples, with a lag phase lasting 72 hours compared to the previously observed 96 hours in the incubated samples (figure 4.12, A). Seeding with preformed fibrils greatly accelerated the misfolding kinetics, as the lag phase was seen to be reduced by a further 24 hours by the presence of seed, now misfolding at around 48 hours. Seeding also produces a sigmoidal curve, indicative of the formation of fibrils; interestingly, the overall fluorescence emitted by the seeded sample was less than that with the non-seeded sample. The fibril control showed a slight increase in ThT emission in the first 24 hours, followed by a steady emission of fluorescence, with no further increase over time.

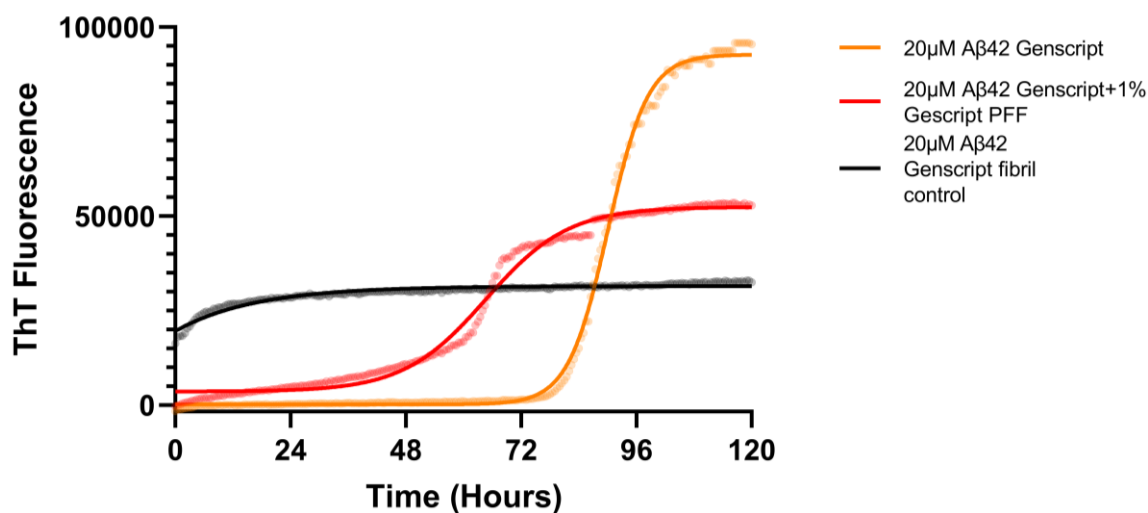


Figure 4-13: RT-QUIC on seeded Genscript monomers

RT-QUIC was performed on Genscript monomer solutions (200 µl at 20 µM) either with 1% (v/v) of Genscript preformed fibrils or no seeding. An equimolar solution of Genscript preformed fibril solution was implemented as a control. Fibril formation was followed in real-time by the measurement of ThT emissions. Samples were shaken for 1 minute at 500 rpm with orbital shaking and incubated for 29 minutes at room temperature, ThT fluorescence was measured at the end of each agitation-incubation cycle. The non-seeded Genscript monomer solution (orange line) possessed a sigmoidal emission pattern, with a 72 hour lag phase, a 24 hour elongation phase and a plateau of ThT emissions from 96 hours onwards. Seeding this solution with preformed fibrils (PFF, red line) greatly accelerated the misfolding kinetics, with a 48 hour lag phase, a 48 hour elongation phase and plateau from 96 hours onwards. Interestingly, although seeding did indeed accelerate the formation of fibrils, the overall fluorescence emitted was lower than in the non-seeded sample. Both the non-seeded and seeded samples possessed higher fluorescence values than the fibril control.

Having identified conditions to observe the fibril forming kinetics of Genscript Aβ monomers with either shaking or preformed fibril seeding, a further step involved the study of the potential changes induced by the chemical biotinylation of the monomers. This was performed with the aim of assessing monomer stability after chemical modification with biotin, as both biotinylated monomers and fibrils would be use for antibody discovery through phage display of VHH antibodies (seen in the next chapter). For this assay, monomeric solutions of both Genscript and Gencust peptides (200 µl at 18.5 µM, slightly more diluted due to biotinylation process- described in paragraph 2.18.1) were analysed with RT-QUIC in both their unmodified and biotinylated form. RT-QUIC was performed for 120 hours (figure 4.14); unmodified Genscript monomers were seen possessing the expected sigmoidal ThT emission pattern, with a 48-hour lag phase and plateau from around 80 hours onwards (N.B. the slightly different kinetics seen between experiments indicate an intrinsic variability in the use of synthetic monomers, as slightly different experimental conditions can results in slightly different

results, albeit preserving the relative misfolding kinetics within any single experiment). Strikingly, biotinylation seemed to have an effect on monomer stability, as the modified Genscript sample was characterized by an accelerated fibril formation process, with a 24-hour lag phase, followed by a slow growth phase, and final plateau reached at 72 hours. Both the modified and unmodified Gencust solution with monomers/oligomers/protofibrils lacked any increase of misfolding over time. These findings strongly suggest that Genscript monomers are not only able to be misfolded in a controlled manner, but that the chemical biotinylation of the monomers results in a product that is stable for around 24 hours prior to fibrilization.

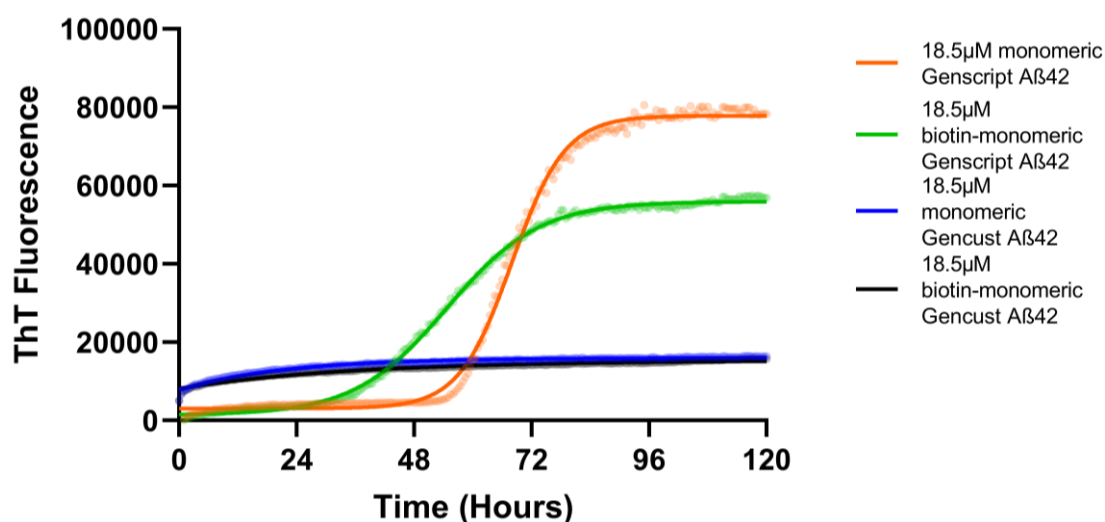


Figure 4-14: RT-QUIC on biotinylated monomers

Genscript and Gencust m/o/pr were chemically biotinylated using the Lightning-Link® Biotin Conjugation Kit (described in paragraph 2.18.1). Modified monomers (200 μl at 18.5 μM) were compared with their unmodified counterparts, to assess protein stability. Genscript monomers (orange line) displayed a typical sigmoidal pattern, with a 48 hour lag phase; modified Genscript monomers (green line), also displayed a sigmoidal pattern, but interestingly, the kinetics of misfolding seemed to be altered by the addition of biotin groups to the peptides, with a lag phase lasting only 24 hours. As expected, both unmodified and modified Gencust m/o/pr (blue and black lines, respectively) did not display an increase of ThT emission over time, with the emission patterns being mostly flat for both samples throughout the experiment.

4.6 Fibril fragmentation for phage display

With the completion of the studies into the behaviour of Aβ monomers in solution from two different suppliers, the final step was understanding the effects of ultrasonic fragmentation on fibrils. This was performed to develop a methodology to increase the number of elongation sites from fibrils in solution through the shattering of the fibrils themselves, with the aim of discovering antibodies with

the ability to bind to these sites and therefore prevent the elongation of fibrils (figure 4.15, A) [133, 180]. Full length fibrils were fragmented as described in paragraph 2.5.4; fragmented fibrils and full-length fibrils were then resolved in native conditions on a gel capable of separating large molecular weight elements (7% tris acetate gel) and analysed under NS-TEM. Protein separation with electrophoresis revealed full length fibrils accumulating in the upper regions of the gel, with most elements not being able to penetrate the gel and therefore concentrating in the well itself (figure 4.15, B); fragmented fibrils, on the other hand showed the presence of a more prominent smear of proteins with different molecular weights, ranging from the middle of the gel and reaching the well itself where unresolved proteins were also found. NS-TEM revealed similar results (figure 4.15, C), with fibrils presenting widespread elongated and unbranched structures, reaching 1 μm in length and 20 nm in diameter; as for the fragmented fibrils, microscopy revealed the presence of smaller fibril-like structures that still possessed around 20 μm in diameter but with a dramatically reduced length, with the observed elements barely reaching 500 μm in length. These results strongly suggest that the protocol implemented was successful in generating fragmented fibrils.

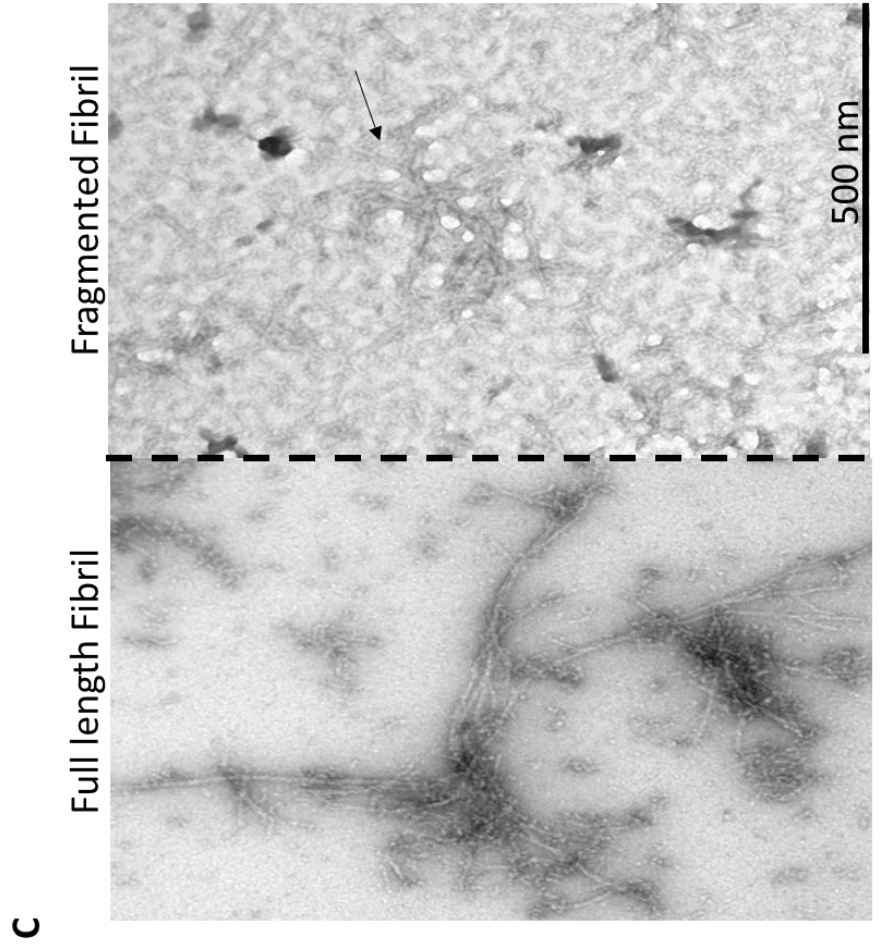


Figure 4-15: Fibril fragmentation

Genscript fibrils were fragmented through sonication. A: Schematic representation of the effects of ultrasonic fragmentation with sonication; the number of elongation sites through the shattering of the fibril itself. B: Comparison of full-length versus fragmented fibril on a 7% tris acetate gel, run in native conditions; fibril samples tend to accumulate on the upper regions of the gel and the well itself, signifying the presence of high molecular weight elements in solution. With fragmented fibrils, it is possible to see a smear of protein elements at different molecular weights. Additionally, with fibril fragmentation it is also possible to see protein accumulation at the bottom of the gel, indicating the presence of low molecular weight elements that were too small to be resolved on a 7% tris acetate gel. C: Comparison of full-length fibrils and fragmented fibrils on NS-TEM; while fibril samples possessed a typical unbranched and elongated structure, the ultrasonic fragmentation produced a wide array of smaller fibril-like structures (arrows).

4.7 Additional experiments with A β ₄₂.

As with α -syn, additional experiments were performed on A β ₄₂. These experiments were omitted from the result section as they were either inconclusive or had negative results. Table 4.1 summarises these experiments.

Table 4-1: Summary of additional experiments performed with A β ₄₂.

Experiment	Reference / Purpose	Method	Outcome
PMCA misfolding with different temperatures	Optimization step- To assess the influence of different temperatures during PMCA and if freezing had any detrimental effects on fibrils.	PMCA was performed on 111 μ M non seeded A β ₄₂ samples. Sonication as performed with 20 second pulses at 50 % amplitude and 29:40minutes of incubation for 72 hours. Two PMCA machines were used, one of them set at 37 °C and the other at 22 °C. After sonication, fibril formation was measured with ThT. Following this initial measurement, samples were divided in two groups: frozen and incubated samples. The frozen group was placed in dry ice for 1 hour, and the incubated group was placed in an incubator at 37 °C for 1 hour. ThT was measured again after this step.	High ThT was present in all of the samples, regardless of the temperature set during PMCA. Additionally, freezing the samples did not seem to have any negative effects on the fibrils, as ThT values were almost identical between the incubated and frozen groups of the 37 °C and 22 °C PMCA.
PK titration	Optimization step- An attempt to identify the optimal enzyme concentration that would observation of band patterns after PK digestion.	A PK titration was performed on a 222 μ M solution of A β ₄₂ fibrils in PBS. The concentrations of PK tested were: 50 μ g/ml, 40 μ g/ml, 30 μ g/ml, 20 μ g/ml, 10 μ g/ml, 1 μ g/ml, 750 ng/ml, 500 ng/ml, 250 ng/ml, 125 ng/ml, 31 ng/ml, 62 ng/ml and 15 ng/ml. Fibrils were incubated with PK for 30 minutes at 37 °C prior to their analysis on SDS-PAGE gels	Unlike α -syn, regardless of the high concentration of fibrils and the wide range of PK dilutions used, it was not possible to detect a protease-resistant banding pattern for any of the samples analysed.

4.8 Discussion

4.8.1 Monomer solubilization

In this chapter, synthetic A β peptides sources from two different suppliers were tested under an array of conditions with the purpose of acquiring an understanding of the misfolding kinetics of the monomers prior to performing an antibody discovery campaign.

Following the successful identification of α -syn polymorphs using PMCA and human derived samples; at the start of the experiments, the aim was to use this condition with another protein, A β ₄₂. Initially, monomeric A β ₄₂ was purchased as a lyophilized powder from Gencust. The synthetic peptide possessed the aminoacidic sequence: "DAEFRHDSGYEVHHQKLVFFAEDVGSNKGAIIGLMVGGVVIA"; with no modification at either the C or N-terminus. The best methodology to solubilize this highly hydrophobic peptide was identified. Particular attention was placed to this step as the A β ₄₂ peptide is notorious for its difficulty to be solubilized as a monomer in aqueous solutions. Historically, the commonly used methodology involves the initial resuspension of the peptides in an organic solvent, hexafluoroisopropanol (HFIP); following by the removal of the solvent through freeze drying, and then resuspension in dimethyl sulfoxide (DMSO) [292]. Although this method has been validated and used by several research groups, it is not without criticism. It has been documented that the use of HFIP and DMSO can produce highly variable (and in some instances irreproducible) results, due to slight variations in the conditions used to prepare the different batches of monomers (such as buffers, temperatures and concentrations) [293]. The use of HFIP has also been found to alter the structure of the β -sheets in solution by disrupting hydrophobic interactions and stabilizing the formation of α -helices in the peptides [246]. Due to the limitations recorded in the literature, an alternative method to solubilize the peptides in this study was sought. Following the advice provided by the supplier, A β was resuspended by using a strong alkali solution. This method was found to be valid in the literature as solutions of NH₄OH and NaOH were recorded to be capable of not only solubilizing the lyophilized peptide in an aqueous solution, but also to inhibit the spontaneous aggregation of this peptides into oligomers and fibrils [244]. Initial experiments followed the standardized solubilisation procedures provided by the supplier. This methodology consisted in the use of small volume of 1% NH₄OH solution in PBS (80 μ l) to dissolve 1mg of lyophilized peptide. Once all the powder was dissolved, the solution was then brought up to 1mg/ml by adding 920 μ l of PBS 1x. The resulting solubilized peptide was then analysed using both TEM and CD to assess the level of monomers in solution. The analysis of the resuspended peptide revealed unexpected results as both NS-TEM images (figure 4.1, A) and CD

spectra (figure 4.1, B) showed clear evidence for the presence of fibrils in solution. This could be explained by the fact that a 1% NH₄OH solution in PBS might not be alkali enough to inhibit the formation of fibrils and thus allowed the majority of the monomers in solution to spontaneously misfold and produce *de novo* aggregates. The fibrils produced in this way were preserved as positive controls, for future experiments.

The implementation of the methodologies described by Teplow *et al.*, 2006 [246], and Ryan *et al.*, 2012 [245] and 2013 [244] allowed for the stable solubilization of monomers, as no fibril formation was observed with real time misfolding analysis with ThT at 5 μ M (figure 4.2, A), with higher monomer concentrations (figure 4.2, B) or with human seeding (figure 4.2 ,C, D). This was crucial for future data interpretation as the stability of the monomers guaranteed that any potential fibrils found after amplification steps (such as sonication or shaking), were the result of the propagation of whatever seed is found within the samples themselves, rather than spontaneously formed fibrils in the monomeric substrate. Additionally, as ThT fluorescence seemed to be unaltered by the concentration of the monomers in solution, it was decided to perform future experiments using 20 μ M of A β 42 , this value was chosen with the aim of working within the critical micellar concentration of this peptide, estimated to be at around 20-25 μ M [293]. Higher concentrations were avoided as they could introduce artefacts through spontaneous formation of protein micelles and amorphous aggregates.

4.8.2 PMCA misfolding of Gencust monomers

With the identification of a suitable methodology to resuspend monomers in solution, PMCA was attempted. A thorough research of the literature revealed no records of PMCA (with sonication) being implemented to enhance fibril formation, therefore Initial experiments were designed to pinpoint the optimal settings (in terms of amplitude and sonication time) that would allow for the minimal *de novo* misfolding in non-seeded samples while promoting fibril formation in seeded samples (seeded with preformed fibril or human samples). Interestingly, the variation of amplitude (figure 4.3) and sonication time (figure 4.4) did not seem to have a major impact in the process of fibril formation, as evidenced by the similarities between ThT binding patterns within experiments. A 10% amplitude was

chosen, as non-seeded samples possessed the least *de novo* misfolding levels; and 20 second sonication as an in-between point of all the different time-setting analysed. Regardless of the conditions tested, 10% (v/v) preformed fibril seeded reactions always produced the highest ThT binding values, followed by 1% (v/v) seeding. The implementation of human brain seed in the reactions was ineffective in the promotion of fibril formation (figure 4.5 and figure 4.11); diluting the brain (and therefore any potential fibril-forming inhibitory compounds found within the CNS [270]) did not seem to alter this, as a 10-fold dilution was unable to promote fibril formation, although samples seeded with more diluted brains seemed to possess marginally higher ThT emissions. Different fibril-stabilizing compounds were then added to the PMCA reaction, with the aim of stabilizing the fibrillar elements within the human seeds and therefore promoting the templated misfolding of the synthetic peptides into human-derived conformers. The additives used were heparan sulphate, saponin, digitonin, dextran sulphate, α -crystallin and heparin; all molecules with known abilities to enhance PMCA sensitivity for prion amplification [284-291, 294, 295]. Nevertheless, these additives lacked an effect within the context of the tested experiments (figure 4.6 and figure 4.7), with only a handful of human seeded samples actively misfolding during the PMCA experiment. Further study of human seeded, and non-seeded PMCA revealed that the increase in ThT observed within the human seeded samples was irreproducible, as there seemed to be a stochastic component to the increase in ThT seen in both human seeded and non-seeded samples (figure 4.8).

In order to better understand the role of PMCA in the fibril forming process for the only seeded sample with consistent, high ThT emission (reactions using 10% [v/v] preformed fibril seed), PMCA was compared with incubation (figure 4.9). This experiment revealed that incubation had a similar ability to produce fibrils *in vitro*. Even more surprising still, non-amplified seeded samples possessed only slightly less ThT emission than their PMCA or incubated counterparts. This was further confirmed with NS-TEM microscopy, as non-treated samples possessed low levels of small fibril-like structures; incubated samples were characterized by the presence of long-unreached fibrils reaching lengths of around 1 μ M and sonicated fibrils were seen with high amount of shorter fibril-like structures (figure

4.10). These findings strongly suggested that, firstly, most of the ThT emitted in the previously observed 10% (v/v) preformed fibril seeded reactions, comes from the seeds themselves, as evidenced by the non-amplified samples possessing slightly lower (but not statistically significant) ThT values than 3-day sonicated or incubated samples (figure 4.10). Incubation seemed to promote the formation of fibrils, with the highest ThT emission values seen within this group. The fibrils seen in the incubated samples closely matched the canonical fibril morphology, with long-unbranched structures. PMCA promoted the extensive fragmentation of fibrils, resulting in shattered structures with decreased length. Evidence suggested that rather than promoting fibril formation, PMCA only served to promote the shattering of the fibrils introduced by the seeds; the slight increase in ThT fluorescence after 3 days of PMCA would then most likely derive from the 29:40 minute incubation period of the fibrils in excess monomer, hence the similar results to the incubated samples.

4.8.3 RT-QUIC assays and the misfolding of monomers from two different suppliers

The ability to test synthetic A β peptides from a different supplier, shed new light on the behaviour of the monomers observed in the previous experiments. Peptides were pre-processed and solubilized with the same method; any differences seen within the monomeric populations would therefore be tied to the way in which each peptide was produced by the different suppliers.

The analysis of equimolar solutions of Genscript and Gencust peptides revealed distinct results. Analysis of the real time fibril formation kinetics through ThT revealed that while Gencust m/o/pr lacked the ability to misfold (evidenced by a flat ThT curve), Genscript monomers possessed an initial lack of fluorescence, followed by a rapid exponential growth of β -sheets in solution (sigmoidal pattern), evidenced by the increase of ThT binding (figure 4.12, A). An in-depth analysis of each solution with CD revealed that the lack of misfolding seen in the Gencust population was likely due to the solution containing an array of A β peptides at different aggregation states. Genscript monomers, on the other hand, displayed a typical random coil spectra in solution [277, 278], strongly suggesting that during the first 6 hours of the incubation assay, Genscript peptides were mostly monomeric. These monomers would then convert to fibrils as the incubation proceeded (figure 4.12, B). CD data

was further confirmed with analysis by native PAGE (figure 4.12, C), as Genscript samples were seen to resolve as a smear between 4.5 kDa and 14 kDa, indicative of structures ranging from monomers to trimers, respectively. Gencust m/o/pr, while presenting the same smear between 4-14 kDa shared with Genscript monomers, also possessed other higher molecular elements in solution, evidenced by the additional protein smear ranging from the middle to the top of the gel (representing small oligomers and protofibrils) and culminating on a band in the well itself, containing structures too large to be resolved by the gel (larger oligomers, protofibrils and potentially fibrils).

With Genscript monomers showing promising results, the peptide misfolding kinetics were further tested by the implementation of a modified RT-QUIC protocol originally developed by Salvadores *et al.*, 2014 [166] (figure 4.13). Through this assay, it was possible to appreciate the non-seeded samples possessing a sigmoidal increase of ThT over time, signifying the formation of fibrils as reported by Salvadores *et al.* [166] but also other research groups working with A β monomers in the field of antibody discovery [177, 179, 180]. Through shaking, the lag phase observed in the non-seeded sample was reduced by 24 hours (72-hour lag phase) compared to the incubated sample seen in figure 4.13, A, indicating that RT-QUIC could have an effect in accelerating the formation of fibrils in solution. Seeding with 1% (v/v) Genscript fibrils further accelerated this process, reducing the lag phase by a further 24 hours (48-hour lag phase), but still forming the characteristic sigmoidal curve indicative of fibrils. Surprisingly, the end ThT values at the plateau of the 1% seeded samples were lower than those in the non-seeded samples, this could be explained by non-seeded samples possessing a slightly different conformation to seeded samples, similarly to what was observed for α -syn monomers seeded with different synucleinopathies [274] and considering that A β is a highly polymorphic compound [142, 150, 154]. Regardless, both seeded and non-seeded samples possessed higher ThT values than the fibril control sample, suggesting at the end of the fibril forming process, all monomers were transformed into fibrils and that the number of fibrils in solution from both the seeded and non-seeded sample were greater than the controls.

4.8.3.1 Misfolding of biotinylated monomers

Biotinylated fibrils and monomers were a required material to perform antibody discovery using phage display of VHH antibodies. As both populations were needed, RT-QUIC was performed to measure the misfolding kinetics of the biotinylated monomers compared to the unmodified peptides (figure 4.14). While the unmodified Genscript peptide was seen to misfold following the expected pattern, this time with a 48 hour lag phase (most likely due to small variations in the monomer pre-processing that results in slightly different kinetics), chemical biotinylation of the monomers also produced a sigmoidal curve, but with faster misfolding kinetics and lower endpoint ThT emission values. This alteration in the misfolding kinetics could be attributed to a different A β conformer being generated due to biotinylation, as the fibrils that would result from a biotinylated monomer are likely to be different, due to the steric burden brought by the covalent binding of this group. The biotinylated monomers seemed to be stable for 24 hours (duration of the lag phase of these samples). Therefore, the chemical modification of the monomers resulted in a stable monomeric population that would misfold after 24 hours, producing biotinylated fibrils. Gencust m/o/pr behaved according to previously recorded data, with no misfolding being observed in both modified and unmodified forms.

4.8.4 Fibril fragmentation

The final step in the study of A β misfolding, was the fragmentation of the fibrils, in anticipation of antibody discovery efforts. This procedure aimed to replicate the findings previously reported in figure 4.10, where full length fibrils were effectively shattered through sonication. Fragmented fibrils are an appealing target for antibody discovery as reports have found that smaller fibrils have a higher cytotoxic effect than their full length counterparts; it is also thought that fragmentation of fibrils are more effectively spread *in vivo* [133, 282, 296]. Having fully characterized the kinetics of monomer misfolding, the end point fibrils developed through RT-QUIC or incubation were fragmented as described in section 2.5.4. Fragmentation was confirmed through analysis by gel electrophoresis and NS-TEM (figure 4.15), which revealed the expected shattered fibrils.

Overall, in this chapter different methodologies to produce A β 42 fibrils *in vitro* were tested. From the different techniques analysed, RT-QUIC was successful in controlling of the misfolding kinetics of monomers. Peptides from two suppliers were tested, revealing Genscript monomers were able to produce a predominantly monomeric population after resuspension, which could be induced to self-aggregate through several cycles of incubation and agitation. Gencust peptides, on the other hand, could not be produced as a solely monomeric solution with the techniques implemented in this work, but were able to form fibrils. Together, both Genscript and Gencust fibrils would be implemented for the next step of this project, antibody discovery.

Chapter 5. Discovery of A β fibril-specific binders through phage display

5.1 Introduction

Phage display is a very versatile methodology, that allows for the discovery of monoclonal binders towards virtually any kind of purified antigen [227]. The technology is centred around the filamentous M13 phage, and the ability of this viral vector to be genetically modified to express small antibody molecules (scFv, VHH, Fab, etc) on the coat proteins surrounding the viral DNA [228]. To identify specific antibody binders towards a particular target, high diversity libraries (with a diversity of around 10^6 to 10^{11} clones [226, 297]) are used and clones with the highest affinity isolated through several rounds of biopanning [225-227]. Due to the relative low costs associated with this technique and the high affinity antibodies obtained through the process of biopanning, phage display is a very appealing methodology for the identification of antibody binders to complex molecules such as A β fibrils [177, 179, 180]. Several research groups have been successful in the identification of scFv [173, 180, 231, 232, 234] and VHH [177] antibodies with the ability to directly bind A β peptides in different aggregation states [173, 177, 179, 180, 230-233] or to indirectly influence the processing of A β through the targeting of other proteins related with AD onset and progression, such as BACE [235]. Antibodies discovered through this methodology were also seen to reduce fibril formation *in vitro* [173, 177, 180, 230, 231] and reduce disease burden in treated transgenic (Tg) animal models [231-233]. Additionally, it was through the phage display of Fab antibodies that Gantenerumab was discovered, which is a promising therapeutic drug currently in phase III clinical trials [210].

In this chapter, phage display was implemented for the discovery of antibodies with the ability to bind A β fibrils produced from monomers obtained from different suppliers. This was achieved using a naïve VHH library and peptides supplied by both Genscript and Gencust. A nanobody library was chosen as VHH molecules have the ability to bind small structural epitopes [298], an ideal quality for a fibril-binding antibody. The best binders were identified via several biopanning rounds targeting fibrils and non-specific binders were minimized through a subtraction step to A β monomers and an unrelated mix of proteins. Fibril specific binders were identified through ELISA and the antibody sequences obtained with Sanger sequencing. This data was then used to produce VHH-human Fc complexes

either in monomeric (VHHscFc) or dimeric (VHHFc) forms. Both formats of the fibril specific binders were expressed, purified and then assessed through ELISA, in order to highlight potential differences in the binding patterns. Binding kinetics were also recorded in real time through the use of BLI. Results indicate that through the panning of a naïve VHH phage display library, 23 unique antibodies with the ability of binding A β fibrils were identified.

5.2 Biopanning with a naïve VHH phage display library

Biopanning was performed using the previously characterized biotinylated fibrils from both Genscript and Gencust. The successful biotinylation of the fibrils was paramount for the success of the biopanning experiment, as phage display was performed in solution (refer to section 2.21 for methods), in order to preserve the structural integrity of the fibrils [224]. As seen in previous experiments, biotinylated fibrils can be formed from biotinylated Genscript monomers, but not Gencust m/o/pr, due to the heterogeneity of the A β compounds in solution. Therefore, both Gencust and Genscript fibrils were labelled with biotin to provide targets for antibody panning. Confirmation of the biotinylation state of the fibrils was obtained through BLI (figure 5.1). Genscript and Gencust fibrils (200 μ l at 250 μ g/ml) were compared to two different unrelated proteins in solution: protein I (200 μ l 13.25 μ g/ml) and protein II (200 μ l at 26 μ g/ml); non-biotinylated fibrils were also used as controls, to measure potential non-specific binding. To measure the levels of biotinylated compound in solution, Streptavidin (SA) biosensors were used. From this assay, it was revealed that chemical biotinylation of both fibrils was successful, evidenced by a clear strong association rate, producing a shift of around 3 nm for fibrils from both suppliers. Control proteins I and II also bound to the SA biosensors, with slower on rates as their concentrations were lower than in the fibril samples. The unmodified fibrils did not bind to the biosensors. The observed binding was stable, as evidence by the lack of dissociation and as expected by the strong interaction between streptavidin and biotin.

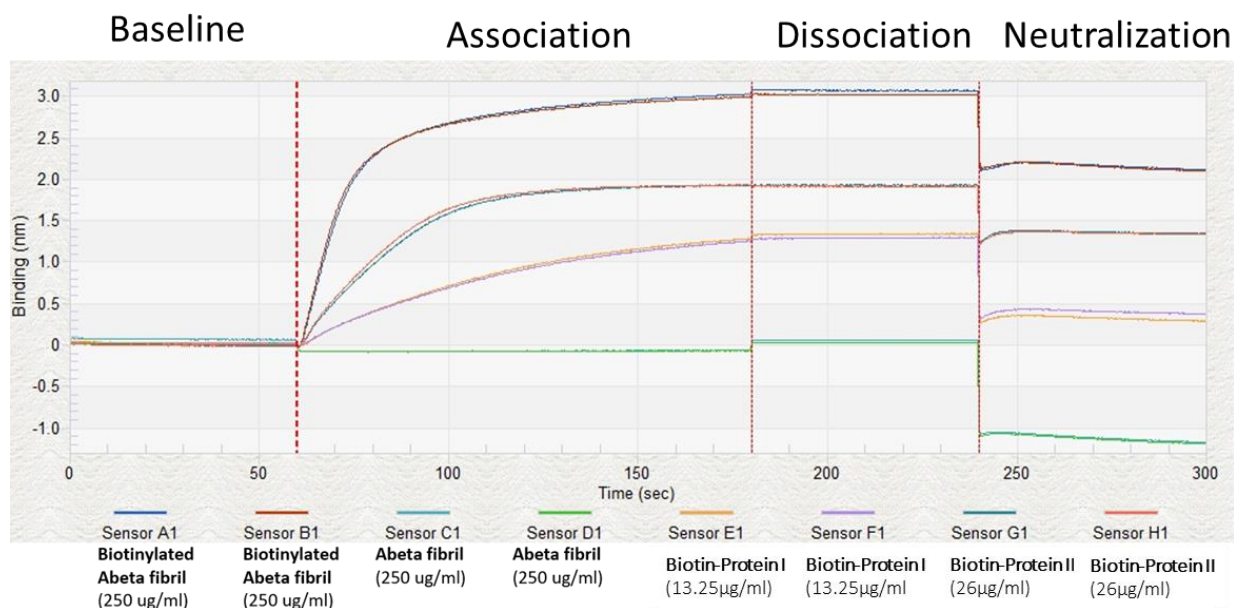


Figure 5-1: Biotinylation test on modified fibrils

Biotinylated Gencust fibrils (Sensor A1), Genscript fibrils (sensor B1); unmodified Gencust (sensor C1), Genscript fibrils (sensor D1) and two repeats of a control biotinylated protein “I” (sensor E1 and F1) and “II” (sensor G1 and H1) were tested with SA tips. Biotinylated fibrils and control proteins were seen to bind to the sensor, as evidenced by the binding shift (in nm) in the sensogram during the association step. Fibrils were seen to have the most binding as they were the most concentrated protein (250 $\mu\text{g/ml}$), followed by protein II (26 $\mu\text{g/ml}$) and finally, protein I (13.25 $\mu\text{g/ml}$). As expected, unmodified fibrils were not seen to bind to the tips. The biotinylated compounds remained strongly bound to the biosensors even during the dissociation step, highlighting stable binding. Neutralization of the fibrils was achieved using a 1% SDS solution.

With the targets (biotinylated fibrils) confirmed to possess stable biotin tags, the next step was to perform phage display. For this, a naïve library generated within UCB Celltech was used. The library used for these experiments was generated by mixing 10 sub-libraries obtained from 10 different llamas (estimated diversity of 7×10^9 clones).

5.2.1 Panning experiment 1 (P1)

Phage display was performed over three rounds of biopanning, following the procedures described in section 2.18. Experiment P1 was performed using biotinylated Gencust fibrils as targets; for each round 10 μg of target were used; the quantity of fibrils added per round did not change, as fibril concentration was an estimate based on the amount of converted monomer used, and therefore may not be accurate and potentially overestimating the effective quantities of fibrils in solution. During round 2, a subtraction of non-specific binders was achieved with 10 μg of Genscript monomers and

10 µg of a mix of non-related biotinylated proteins. At the end of each round, the cfu were recorded to check for enrichment (table 5.1).

Table 5-1: cfu values throughout three rounds for experiment P1

Round 1 (cfu)	Round 2 (cfu)	Round 3 (cfu)
0.3x10 ⁵ cfu	1.5x10 ⁵ cfu	4.2x10 ⁵ cfu

After the third round of panning was concluded, colonies were picked and assessed with ELISA. Each clone was tested against biotinylated Gencust fibrils, biotinylated Genscript monomers, a mix of unrelated biotinylated proteins (at 2 µg/ml) and streptavidin (at 5 µg/ml), and the strength of binding measured by absorbance at 630 nm. The absorbance values were then compared for each condition, a clone was deemed to be fibril specific when the absorbance at 630 nm (OD630) measure was at least three times higher in the fibril wells compared to the monomer, protein mix and streptavidin wells [299]. Through this approach, 6 colonies (out of 48) possessed the required criteria to be fibril-specific (figure 5.2).

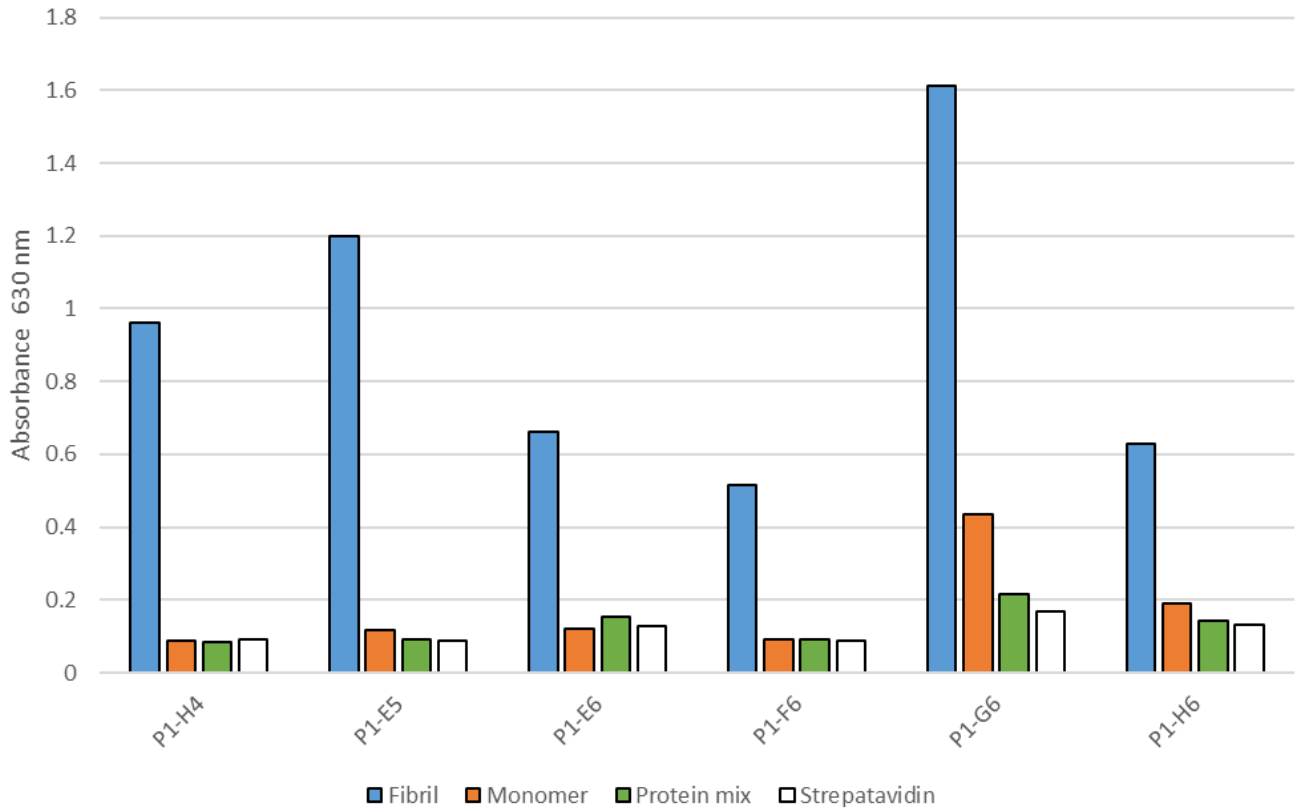


Figure 5-2: Analysis of panning experiment 1 (P1), targeting Gencust fibrils

Three rounds of panning were performed on a single selection of the naïve VHH library. For this, 10 µg of Aβ fibril were introduced at the end of each round. During round 2, a subtraction step with Genscript monomers and protein mix was performed to remove non-specific binders. From 48 colonies picked, 6 antibodies displayed specificity for fibrils (with clones which possessed signals at least 3x higher to the target compared than to the controls). For the labelling of each clone, the prefix (P1) indicates the experiment, and the suffix the well from the monoclonal colony plate of which the antibody was obtained. Screening was performed measuring each clone once.

5.2.2 Panning experiment 2 (P2)

Following the initial success of the first biopanning experiment, a new experiment was set up. The experimental design for experiment P2 was identical to P1, with the only difference being the implementation of Gencust m/o/pr instead of Genscript monomers for subtraction in round 2; and biopanning was performed for two rounds instead of 3. An ELISA was performed on 95 colonies at the end of round 2 to screen for fibril-specific binders. Through the rounds, enrichment was observed (table 5.2). Although binders were identified, no clone matched the selection criteria for fibril specificity, and the round 2 screening was therefore discarded.

Table 5-2: cfu values for the two rounds of panning for experiment P2

Round 1 (cfu)	Round 2 (cfu)
4.8×10^6	7.2×10^8

5.2.2.1 Panning experiment 2.5 (P2.5)

In an attempt to preserve the potential fibril-specific antibodies identified in round 1 of experiment P2; round 1 phage was rescued and the subtraction step re-attempted using Genscript monomers. This time, biopanning was performed for a third round, to ensure further antibody enrichment. In addition to this, from experiment P2.5, two selections were used: one labelled as “subtracted” (or S) and the other labelled as “non-subtracted” (or NS); both selections were treated identically, with the only difference being the omission of the subtraction step in round 2 for the NS selection (therefore acting as a control to avoid loss of antibody due to subtraction, as seen in P2). The colonies from the titration plates were counted in order to calculate the cfu for each round (table 5.3) and again, enrichment was observed.

Table 5-3: cfu values for the three rounds of panning for experiment P2.5

Selection	Round 1 (cfu)	Round 2 (cfu)	Round 3 (cfu)
S	4.8×10^6 *	8×10^8	6×10^8
NS	4.8×10^6 *	11×10^8	7.12×10^8

* From experiment P2

Following three rounds of panning, 95 colonies were picked and binding for each monoclonal antibody tested through ELISA. Like experiment P1, monoclonal phage ELISA was performed to measure binding to biotinylated Gencust fibrils, Genscript monomers, a control protein mix (all at 2 µg/ml) and streptavidin (at 5 µg/ml). Fibril-specific antibodies were identified: 2 antibodies were identified from selection S, and 7 from selection NS (figure 5.3)

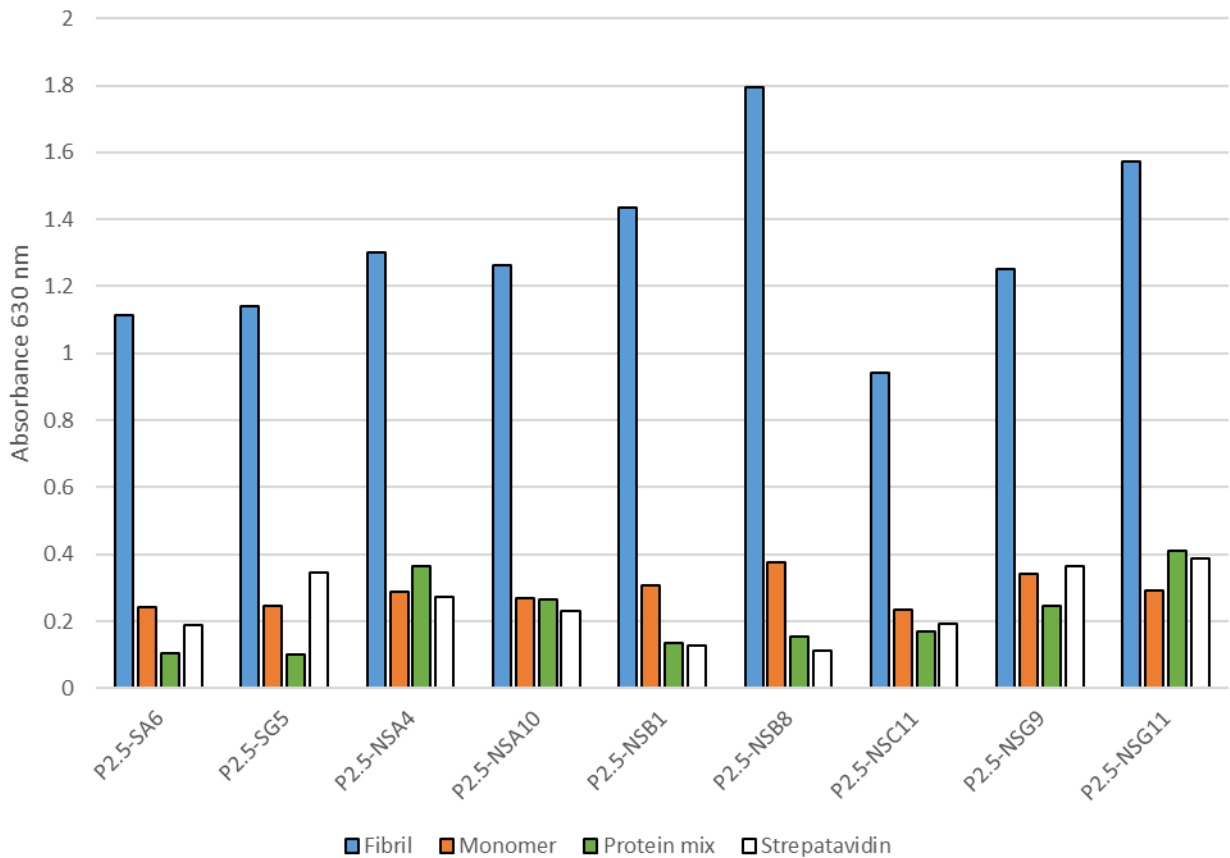


Figure 5-3: Analysis of panning experiment 2.5 (P2.5), targeting Gencust fibrils

Following the unsuccessful P2 experiment, the round 1 output was rescued and the panning experiment restarted from the beginning of round 2. This time, Genscript monomers were used instead of Gencust m/o/pr for subtraction, together with a control protein mix. For each round, 10 µg of fibrils were used as target. For binding analysis, 95 colonies were picked per selection. A total of 9 antibodies from subtracted (S) and non-subtracted (NS) selections were specific binders. For the labelling of each clone, the prefix (P2) indicates the experiment, and the suffix the indicates the selection (S or NS) followed by well from the monoclonal colony plate of which the antibody was obtained. Screening was performed measuring each clone once.

5.2.3 Panning experiment 3 (P3)

A final panning experiment aiming to obtain fibril specific antibodies was performed. Biopanning was performed targeting 10 µg of Genscript fibrils instead of the previously used Gencust fibrils. Three rounds of panning were performed, with a subtraction step in round 2 to remove non-specific binders to Genscript monomers and an unrelated protein mix. Like before, two selections were carried out, S and NS; with selection NS not undergoing subtraction in round 2. For each round, cfu were calculated by counting the colonies in the titration plates (table 5.4); enrichment was observed.

Table 5-4: cfu values for the three rounds of panning for experiment P3

Selection	Round 1 (cfu)	Round 2 (cfu)	Round 3 (cfu)
S	1.2×10^7	3.4×10^8	2.2×10^8
NS	1×10^7	8×10^8	2.58×10^9

From each selection, 95 colonies were picked and tested with ELISA, using biotinylated Genscript fibrils, monomers, a mix of unrelated biotinylated proteins (all at 2 µg/ml) and streptavidin (at 5 µg/ml) to coat maxisorp plates. Monoclonal antibodies were tested against all compounds and binding values assessed with absorbance of TMB at 630 nm. The analysis of all antibodies revealed three fibril specific binders from selection S and seven binders from selection NS which possessed fibril absorbance values at least three times higher than the negative controls [299] (figure 5.4).

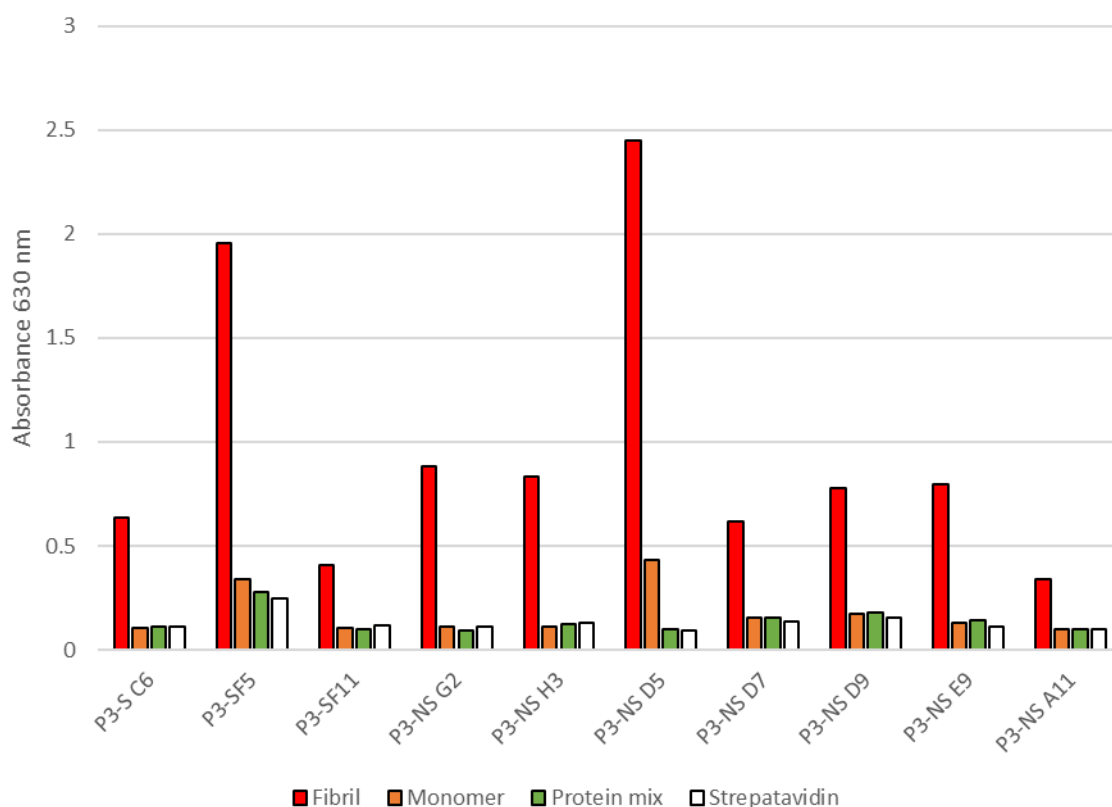


Figure 5-4: Analysis of panning experiment 3 (P3), targeting Genscript fibrils

Biopanning targeting Genscript fibrils was performed. Three rounds were implemented to isolate antibody binders against 10 µg of Genscript fibrils. During round 2, a subtraction step was done to remove non-specific binders towards Genscript

monomers and a control protein mix. Colonies from both the subtracted (S) and non-subtracted (NS) selections (for a total of 95 colonies each) were picked and binding assessed through ELISA. Binders were tested against Genscript fibrils and monomers, the control protein mix and streptavidin. A total of 10 fibril specific antibodies were identified. Screening was performed measuring each clone once.

5.3 Sanger sequencing and antibody gene synthesis

With the identification of a total of 25 fibril-specific binders, through three successful biopanning experiments, the next step was to characterize the antibodies through sequencing. This was performed by isolating and amplifying the phagemid DNA through PCR. For this, small volumes (less than 1 μ l) of the monoclonal colonies were added to the reaction mix (25 μ l per sample, as described in paragraph 2.18.6); Yol 13 and Yol 22 were used as forward and reverse primers respectively, as they would allow the propagation of the VHH sequence within the vector. Yol 13 bound a region around 230 bp upstream of the pelBSS leader sequence, and Yol 22, a region around 44 bp downstream the VHH sequence (refer to figure 2.3); together, these primers produced an amplicon of around 700 bp long, containing the VHH sequence (figure 5.5).

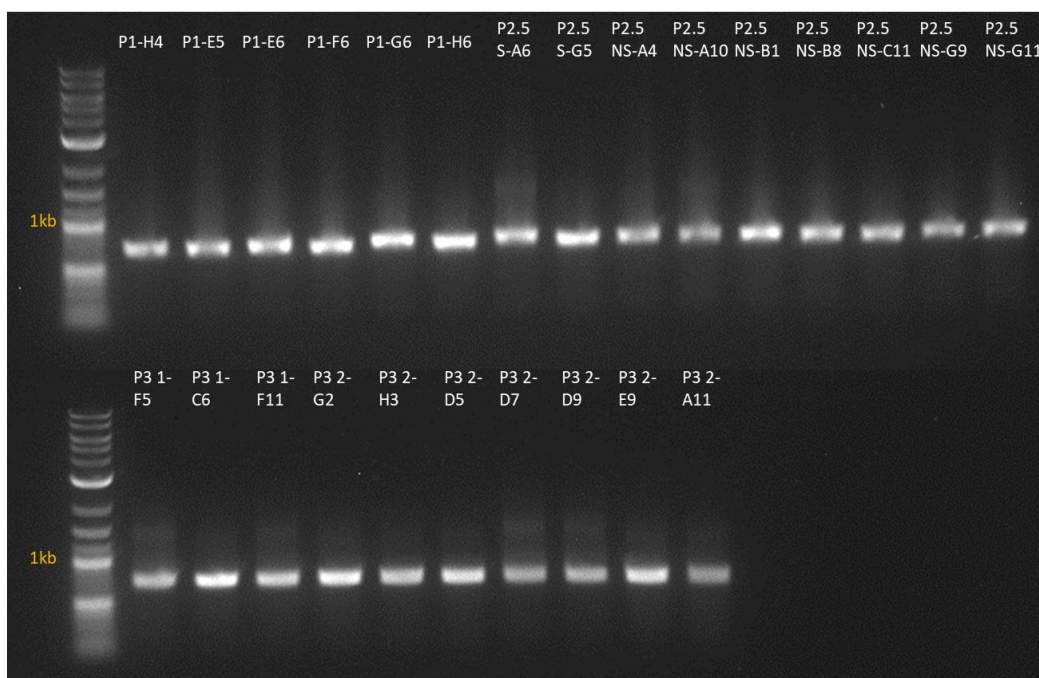


Figure 5-5: Fibril-specific binder PCR

The DNA from the VHHs with fibril specificity PCR. This was achieved by mixing small volumes (around 1 μ l) of the colonies expressing the antibodies of interest with the PCR mix (20.75 μ l DEPC-treated water, 2.5 μ l 10x standard Taq buffer, 0.5 μ l dNTP, 0.5 μ l Yol13 forward primer, 0.5 μ l Yol22 reverse primer and 0.25 μ l Taq DNA polymerase, for a total of 25 μ l per reaction), as described in section 2.21.6. Only the VHH domain was expanded. PCR products were run on a 1% (w/v) agarose

gel in TAE buffer and visualized with SYBR™ Safe DNA gel stain. Quick-Load® purple 1 kb plus DNA ladder was used as molecular weight standard (Mw). Illustra™ Exostrar™ was used to removed unused dNTPs and primers before Sanger sequencing.

The amplicons were sequenced by an external company, Macrogen using the primer LMB3. Once delivered, the chromatogram of each sequence was checked for errors, and where possible, corrections were applied. Two sequences were excluded (P2.5-SA6 and P3-NSD7) as their sequences were of poor quality and could not be corrected (figure 5.6).

All sequences were aligned and translated (applying +1 frame); further corrections were made to the DNA sequences to ensure all antibodies were in frame. From this, 23 protein sequences were obtained (table 5.5), corresponding to the fibrils specific VHH antibodies.

Table 5-5: Protein sequences of fibril-specific antibodies

ID	Antibody	Protein sequence
1	P1-H4	EVQLVESGGGLVQPGGSLRLSCAASGVSRSIGALGWYRRAPGKRRRLVAATRDGNTYYADSVKGRFAISRDNAKNTIVLQMNNLKPEDTAVYYCSAEIQSDAGWDDYWGQGTQTVSS
2	P1-E5	EVQLVESGGGLVQAGGSLRLSCAASGNTYNINNMRWYRQAPGKQRELVAIVSSGGGTYYADSVRGRFTISRDNNAKMMVYLQMNLDKPDPTAVYHCYTFVRRDYWGRGTLTVSS
3	P1-E6	EVQLVESGGGLVQAGDSLRLSCAASGRTFSYHSMGWFRQAPGKEREFVSVINRSGGRTWYADAVKGRFTISRDNKNTLTEMNSLKPEDTAMYYCKGRNTNGFSFQNKGGGTQTVSS
4	P1-F6	QVQLVESGGGLVQPGGSLRLSCAASGRRFSVSTMGWYRQVPGEQRELVAIVSNRGTYYGEPVKGRFTISRDNKNSVYLDMDNLKSEDPTAVYYCRVGTRIKGGTQTVSS
5	P1-G6	QVQLVESGGGLVQPGGSLRLSCAASGSTFSINAMGWYRQAPGKRELVAIVTRYGTTYADSVKGRFTISRDNNAKIVYLQMDSLRPEDTAVYYCYARAGRIVGLGDYWGQGTQTVSS
6	P1-H6	EVQLVESGGGLVQAGDSLRLSCAASGRTFSRMGWFRQAPGKEREFVAIVSRNGRTYYADSVKGRFTVSRDNAKNTVYLQMNSLKPEDTAVYYCNAHRYWGGGTQTVSS
8	P2.5-SG5	QVQLVESGGGWVQPGGSLRLSCAASGRISNINMAWYRQTPGKQRELVAIVMRSGGTTYADSVKGRFTISRDNNAKTVYLQMNSLKPEDTAVYYCNAQTYGLNLYWGQGTQTVSS
9	P2.5-NSA4	EVQLVESGGGLVQPGGSLRLSCAASGRTFSNRAMGWFRQAPGKERTFVAIVSKSGRTYYADFSKGRFTISRDNANNIVYLQMNSLKPEDTAVYYCAAAYQRSAPPSTDYKYWGQGTQTVSS
10	P2.5-NSA10	EVQLVESGGGLVQAGGSLRLSCAASGRTFSRRVSWFRQAPGKERIVAGVSGSGRTYYADSVKGRFTISRDNANNTVFLQMNNLAPEDTAVYYCAAGFGTVSMGVRVYWGKGLTVTVSS
11	P2.5-NSB1	EVQLVESGGGLVQAGGSLRLSCAASGATDTRATMIGWYRQAPGKREHVALMARNGGATYYADSVKGRFTISRDNKNTIYLEMSSLKPEDTAVYYCVATTGFSSRWSDWKEWEHWGGGTQTVSS
12	P2.5-NSB8	QVQLVESGGGSVQAGGSLRLSCAASGSIFSIDAMGWYRQAPGKQRELVAIVMTSGGSTYYADSVKGRFTISKDNKNTVYLQMNSLKPEDTAVYYCNAHGRNRLWPGVKREYDYWGQGTQTVSS
13	P2.5-NSC11	EVQLVESGGGLVQAGKSLRLSCAASGSTFRVNVMGWYRQAPGKQRELVAIVSRGGNTYYADSVKGRFTISRDNNAKIVYLQMDSLRPEDTAVYYCYARAGRIVGLGDYWGQGLTVTVSS
14	P2.5-NSG9	EVQLVESGGGLVQAGGFLRLSCEASGTIFRINTMGWYRQAAGEQREVVAIVTITRSGSAYADSVKGRFTISKDNKNTVYLQMNSLKPEDTAVYYCNAHGRNRLWPGVKREYDYWGQGTQTVSS
15	P2.5-NSG11	EVQLVESGGGLVQPGGSLRLSCAASGRTFSNRAMGWFRQAPGKERTFVAIVSKSGRTYYADFSKGRFTISRDNANNIVYLQMNSLKPEDTAVYYCAAAYQRSAPPSTDYKYWGQGTQTVSS
16	P3-SC6	EVQLVESGGGLVQGGSLRLSCAASGRTFRNYAMAWFRQAPGKEREFVAIVVRRGGSTYYADSVKGRFTISRDNKNTLYLQMNSLKPEDTAVYYCAATPACTTRHMDEYKYWGHGTQTVSS
17	P3-SF5	QVQLVESGGGSVQAGDSLRLSCTTSSGRSIHRTMGWFRQAPGKEREMVAIVAWRDSATAYADSVKGRFTISRDNKNTVSLQMTSLKPEDTAVYYCAAGPKRSADRRAIDYWGQGTQTVSS
18	P3-SF11	EVQLVESGGGSVRTGGSLRLSCAASGRTFSSTVVGWFRQAPGTERDFVAIVKWRPRTSHYADSLKGRFTISRDKDKMMVYLEMNNLKPEDTAVYYCAARPGSGRSDRPRAYEYWGHTQTVSS
19	P3-NSG2	EVQLVESGGGLVQAGESLRLSCAASGRVFNSTMGWFRQAPGKEREFVAVVYWSGSAAYADSVQGRFAVSRDANENTVYLQMNSLKPEDTAVYYCAVASRNLGIVSRKREKNYDYWGQGTQTVSS
20	P3-NSH3	EVQLVESGGGLVQAGGSLRLSCAASGRTLSSYAMGWFRQAPGKEREFVAIVSRSGSTYYADSVKGRFTISRDNKNTVFLQMTSLNLPEDTAVYYCAARDSIVLRTSAGAWTYWGQGTQTVSS
21	P3-NSD5	QVQLVESGGGLVQAGGSLRLSCTASGRTFSSYHMGWFRQAPGKEREFVAIVTRSGRNQYSDSVKGRFTVARDNAKNTAGLLMNSLKPEDTAVYYCAADVHGLGSSVSRYEYWGQGTQTVSS
23	P3-NSD9	EVQLVESGGGLVQAGASLRLSCAASGRTFSRYAVGWFRQAPGKEREFVAIVSWSEGSTYYADSVKGRFTISRDNKNTVTLQMNSLKPEDTAVYYCNVRRKKGIMRQSEYWGQGTQTVSS
24	P3-NSE9	QVQLVESGGGLVQAGDSLRLSCTTSSGRTRSWYTVGWFRQFPGQERQFIGASARRGGRTVVDVSKRFAISRDKNTVYLQMNALQVEDTAVYYCAASHSSGRAYSDDEYWGQGLTVTVSS
25	P3-NSA11	EVQLVESGGGWVQAGGSLRLSCAASGRTFRSYAMGWFRQAPGKEREFVAIVSRSGDNTLGDVSKGRFTISRDNKNNMYYLQMNSLKLEDTAVYYCAANRRIFSGSVYKDSSEYDYWGQGTQTVSS

CDR1 evidenced in Green; CDR2 evidenced in blue and CDR3 in red

Next, the sequences were sent to Twist Bioscience to produce the fibril-specific antibody DNA. The 23 antibodies were ordered in two different formats: VHHC, consisting of a dimeric molecule with two subunits of VHH-human FC domains (figure 5.7, A); and VHHscFC (standing for VHH single chain FC) in which a monomeric VHH domain is expressed joined with two linked human FC domains (figure 5.7, B). This was performed by Twist through the cloning of the antibody protein sequence in proprietary vectors developed by UCB. Genes were delivered as lyophilized compounds or as glycerol stocks containing bacteria transformed with the antibody vectors. Antibodies were ordered with a nomenclature that highlighted their format (VHHC or scFC) followed by their sequence ID (from 1 to 25, as seen in table 5.5). Alongside the antibodies discovered through phage display, several control antibodies with proven recombinant A β fibril-binding properties as described by Munke *et al.*, 2017 [180] were also ordered, in scFv-scFC and scFv-FC (consisting of two scFv subunits linked to two human Fc domains) formats (table 5.6).

Table 5-6: control scFv antibody sequences

Antibody	scFv sequence, as seen in Munke <i>et al.</i> , 2017
I2	VHSEVQLLESGGGLVQPGGSLRLSCAASGFTFSSYAMSWVRQAPGKLEWVSGIYNYGYTTNYADSVKGRFTISRDNKNTLYLQMNSLRAEDTAVYY CAKTAYGFDYWGQGLTVTVSSGGGGSGGGGGGGGGSTDIQMTQSPSSLSASVGDRTITCRASQSISSYLNWYQQKPKGKAPKLLIYNASTLQSGVPSR FSGSGSGTDFTLTISLQPEDFATYYCQNNSSPTTFGQGTKVEIKAAA
I48	VHSEVQLLESGGGLVQPGGSLRLSCAASGFTFSSYAMSWVRQAPGKLEWVSGINTTGSNTSYADSVKGRFTISRDNKNTLYLQMNSLRAEDTAVYY CAKSDSDFDYWGQGLTVTVSSGGGGSGGGGGGGGGSTDIQMTQSPSSLSASVGDRTITCRASQSISSYLNWYQQKPKGKAPKLLIYDASSLQSGVPSR FSGSGSGTDFTLTISLQPEDFATYYCQSNATPATFGQGTKVEIKAAA
I68	VHSEVQLLESGGGLVQPGGSLRLSCAASGFTFSSYAMSWVRQAPGKLEWVSGIDYTGTSAYADSVKGRFTISRDNKNTLYLQMNSLRAEDTAVYY CAKSDNDFDYWGQGLTVTVSSGGGGSGGGGGGGGGSTDIQMTQSPSSLSASVGDRTITCRASQSISSYLNWYQQKPKGKAPKLLIYTASALQSGVPSR FSGSGSGTDFTLTISLQPEDFATYYCQYNNGPATFGQGTKVEIKAAA
J46	VHSEVQLLESGGGLVQPGGSLRLSCAASGFTFSSYAMSWVRQAPGKLEWVSTISNYGVQNTNYADSVKGRFTISRDNKNTLYLQMNSLRAEDTAVYY CAKRLHRFDYWGQGLTVTVSSGGGGSGGGGGGGGGSTDIQMTQSPSSLSASVGDRTITCRASQSISSYLNWYQQKPKGKAPKLLIYRASSLQSGVPSR FSGSGSGTDFTLTISLQPEDFATYYCQQRGHPPTFGQGTKVEIKAAA
J57	VHSEVQLLESGGGLVQPGGSLRLSCAASGFTFSSYAMSWVRQAPGKLEWVSAINKGGYKTYADSVKGRFTISRDNKNTLYLQMNSLRAEDTAVYY CAKTPKPFDYWGQGLTVTVSSGGGGSGGGGGGGGGSTDIQMTQSPSSLSASVGDRTITCRASQSISSYLNWYQQKPKGKAPKLLIYGASVLQSGVPSR FSGSGSGTDFTLTISLQPEDFATYYCQANTKPATFGQGTKVEIKAAA

VHHFc and scFc sequences were aligned to highlight similarities between the different antibodies; interestingly, from this analysis it was possible to identify sequences 12 and 14 possessing the same CD3; as were the pair 13/5 and 15/9 (figure 5.7, A and B).

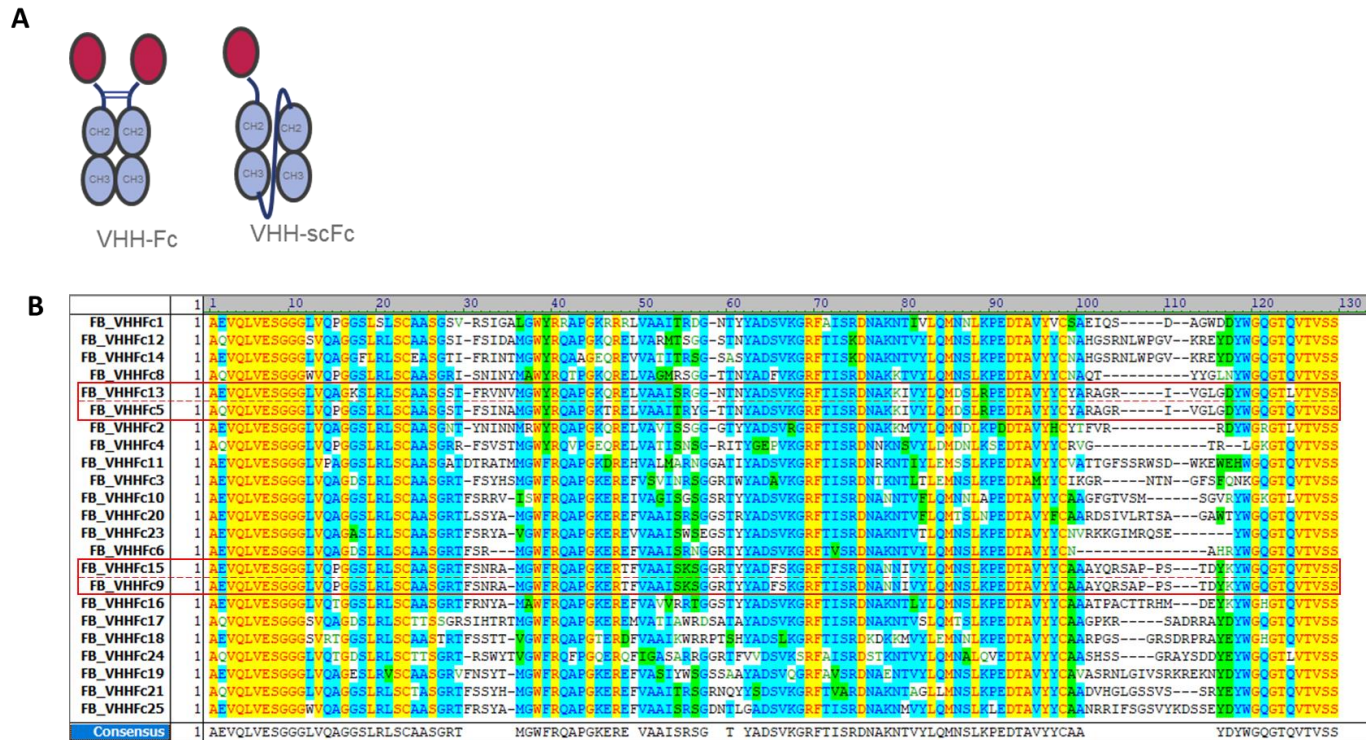


Figure 5-7: Different antibody formats and sequence alignment

The DNA was translated into protein sequences. **A:** These sequences were then used to order the VHH antibodies in two different formats: VHHFc, where two VHH domains are joined together by two human-Fc domains and VHH-scFc, with a single antibody domain bound to a human-Fc dimer joined by a linker. **B:** Sequences were aligned to show sequence homology. Identical sequences are highlighted with red boxes. The addition of an alanine at the start of the sequence was a necessary step for protein expression. The VHH sequence for the 23 antibodies ordered was identical in both formats. FB: fibril binder.

Non-similar regions evidenced by black characters and white background; conservative regions are evidenced with blue characters over a light-blue background; blocks of similar regions were evidenced with black characters over a green background; identical regions were highlighted with red characters over a yellow background and weakly similar regions were evidenced with green characters over a white background.

5.4 Antibody expression, purification and testing

DNA produced by Twist was used to transfect Expi293 cells, in order to produce the fibril-specific and control antibodies (following the methods described in section 2.20). After a 6-day incubation after the addition of Enhancer solution I and II, protein expression of all antibodies was tested through Octet. Crude expression supernatants were diluted 1:4 in kinetic buffer (PBS + 0.05% Tween 20). For this assay, kinetic anti-human FC biosensors (AHC) were chosen. These make use of anti-Fc antibodies

within the bilayer of the sensor that would bind to the FC domain of the expressed antibodies in both formats, therefore allowing for the assessment of antibody expression. Following a 60 second baseline step in kinetic buffer, antibodies were bound to the tips through a 10 minute association step and stability of the assay assessed through a 5 minute dissociation in kinetic buffer. The analysis of the sensogram analysis revealed that all of the antibodies tested (n= 57 from 23 VHHFc antibodies, 23 scFc antibodies, 5 control scFc antibodies, 6 control scFv antibodies [with the addition of I57, not ordered in scFc format due to issues with the supplier] and a mock control) expressed, albeit with varied expression levels (evidenced by the fluctuations in the association of the different antibodies to the tips between 1 nm and 6 nm). Mock supernatant did not possess any binding (figure 5.8). This variation in the expression levels likely depended on a series of factors, such as cell passage, pipetting errors or efficiency of transfection.

Figure 5-8: Expression test of VHHFc, scFc and control antibodies using AHC tips

Lyophilized DNA (1 µg) was transfected into Expi293 cells and incubated for 7 days in order to produce antibodies. At the end of the transfection, protein expression was assessed using Octet. Crude supernatant was diluted 1:4 in kinetic buffer, and following a 60 second baseline, AHC tips were introduced to the diluted supernatant for a 10 minute association. Following association, dissociation was measured in kinetic buffer. The obtained sensogram reveals that the antibodies were successfully expressed in the Expi293 system, as evidenced by the increase in binding (nm) values during the association step. Expression varied between samples, as some were seen to possess a binding of 6 nm while others a binding of 1. Mock supernatant was used as a blank control, which failed to show any binding to the AHC tips, as expected. Samples A1-G3 were VHHscFc samples, in increasing numerical order: with A1 being scFc 1 and G3 scFc 25; from well H3 to F6, VHHFc samples were assessed in increasing numerical order: with sample H3 being VHHFc 1 and F6 VHHFc25. Well G6-C7 contained control scFc antibodies, with scFc I2 in well G6; scFc I48 in well H6; scFc I68 in well A7; scFc J47 in well B7 and scFc J7 in well C7. Well D7-A8 contained control scFv antibodies, with scFv I2 in well D7; scFc I48 in well E7; scFc I68 in well F7; scFc J47 in well G7; scFc J7 in well H7 and scFv I57 in well A8. Mock supernatant was placed in well B8.

With the successful expression of both fibril-binding and control antibodies in both formats, the same crude supernatant (diluted 1:4 in mPBS) was used to re-assess the binding patterns of each antibody in the different formats, against a range of relevant molecules. Like before, 2 µg/ml of biotinylated Genscript fibrils and monomers; biotinylated Gencust fibrils and Gencust m/ o/pr were used bound to streptavidin coated plates, leaving empty wells for streptavidin binding controls (at 5 µg/ml). Fibril

binders (FB) were used as a 1:4 dilution in 3% (w/v) mPBS and target binding was evidenced with HRP conjugated anti-human Fc secondary antibodies. Following the addition of TMB, wells were incubated for 5 minutes and the intensity of the signal measured with absorbance at 630 nm. Absorbance values were plotted to compare the binding patterns of VHHFc and scFc antibodies (figure 5.9). Interestingly, while some antibodies possessed similar binding patterns between formats, like antibody 1 and 2, others showed clear distinctions in the binding patterns to the chosen molecules, like antibody 11 and 24. Almost all of the control antibodies in either format did not seem to possess binding to the chosen molecules within our experiment settings. The only exception was J7 scFc, with strong binding to Gencust fibrils.

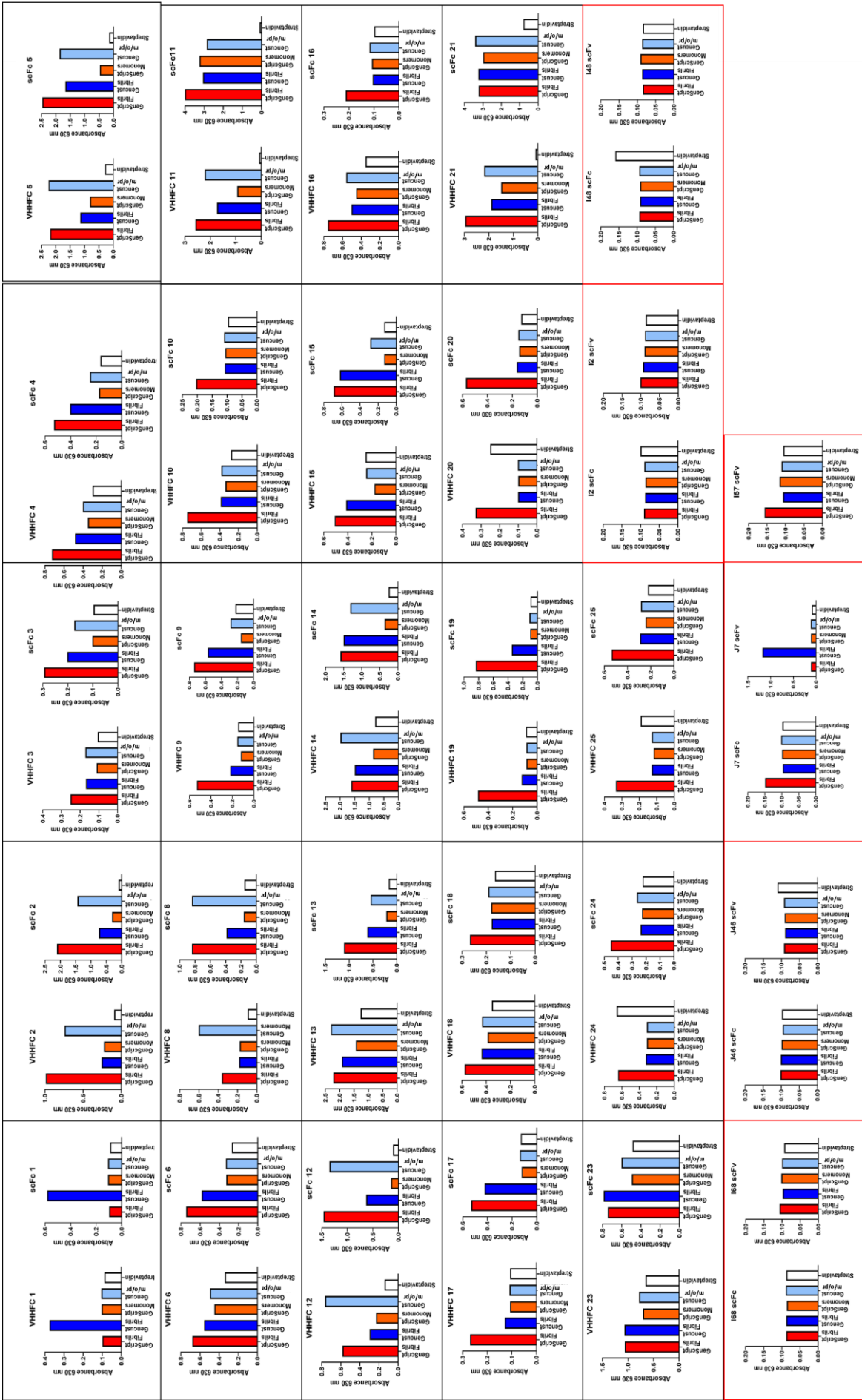


Figure 5-9: Binding pattern comparison between VHHFCs and scFcFs with ELISA

Expressed antibody supernatants were diluted 1:4 with 3% (w/v) mPBS, as used a primary binding antibody for a series of ELISA experiments. All 23 fibril binding antibodies (black boxes), expressed antibody supernatants were assessed together with a series of control recombinant A β fibril binding antibodies (red boxes) against Gencust Fibrils (red bar), Gencust fibrils (blue bar), Gencust monomers (orange bar), Gencust m/o/pr, oligomers and protofibrils [m/o/pr] (light blue bar) and streptavidin (white bar). Being a dilution of crude antibody-rich supernatant, the exact dilution of each antibody tested was unknown. Both fibrils and monomers were added to the streptavidin coated maxisorp wells at a concentration of 2 μ g/ml. The histograms represent the absorbance values at 630 nm following TMB addition. Overall, most binding patterns seem to be consistent between formats, even though some showed marked differences. For the control antibodies, only the J7 scFv seemed to possess strong binding, and only to Gencust fibrils.

Next, antibodies were purified in preparation of more refined binding kinetic assessments with BLI and binding pattern confirmation using equimolar antibody preparations.

Antibodies were purified using the methods described in section 2.21; using proprietary protocols developed for UCB by PhyNexus. From 1 ml of crude supernatant, around 100 μ l of pure product were obtained. Purified antibodies were resolved on 4-12% gels to assess level of purity; usually within 90-95% pure (figure 5.10),

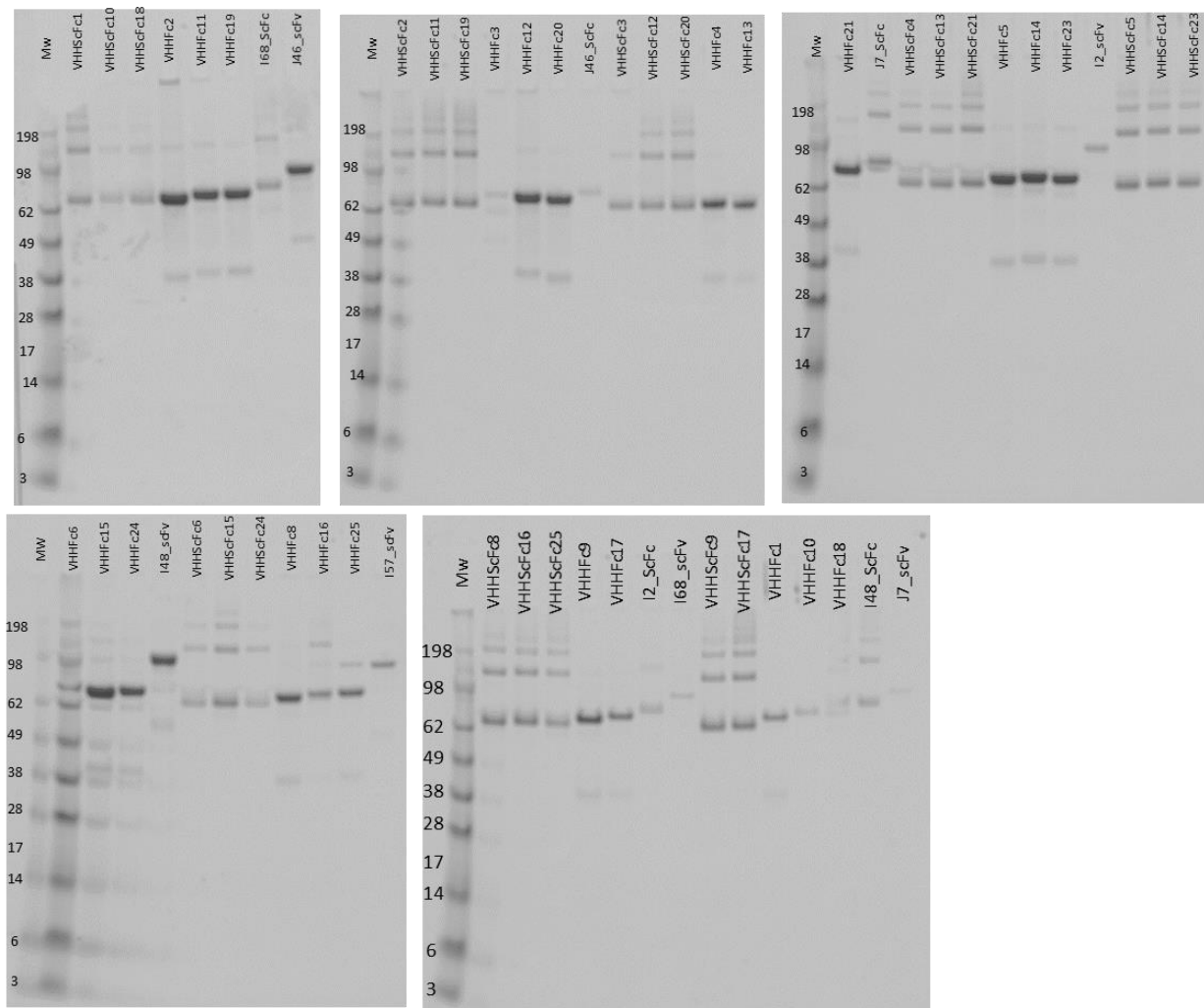


Figure 5-10: Examples of purification of fibril binding antibodies

Harvested supernatants were purified using the PhyNexus system. Small volumes of the end product (around 2 μ l out of the 100 μ l of pure antibody) were then run on gels to assess the presence of potential contaminants still in solution. VHHFc antibodies possessed an estimated molecular weight of 75-80 kDa; VHH-scFc antibodies, an estimated value of 65-70 kDa. On the other hand, controls scFv-Fc possessed an estimated molecular weight of 100-105 kDa and scFv-scFc antibodies, an estimated value of 77-82 kDa. Molecular weight marker used was Seeblue Plus 2 (Mw). Multiple bands present due to batch-to batch variations in purification efficacy.

Protein concentration was measured using a Nanodrop, with a “simple” concentration estimation function (1 Abs=1 mg/ml), obtaining the results listed in table 5.7.

Table 5-7: Fibril-binding and control antibody concentration measured with Nanodrop

VHHFc antibodies	A280 mg/ml	VHHscFc antibodies	A280 mg/ml	Control antibodies	A280 mg/ml
VHHFc1	0.364	VHHscFc1	1.075	scFc I2	0.135
VHHFc2	4.199	VHHscFc2	0.662	scFc I48	0.128
VHHFc3	0.121	VHHscFc3	0.357	scFc I68	0.491
VHHFc4	1.007	VHHscFc4	0.493	scFc J46	0.056
VHHFc5	2.252	VHHscFc5	0.797	scFc J7	0.511
VHHFc6	0.596	VHHscFc6	0.262	scFc I2	0.182
VHHFc8	1.338	VHHscFc8	0.986	scFv I48	1.796
VHHFc9	0.395	VHHscFc9	1.077	scFv I57	0.392
VHHFc10	0.095	VHHscFc10	1.508	scFv I68	0.069
VHHFc11	2.447	VHHscFc11	1.279	scFv J46	2.171
VHHFc12	2.793	VHHscFc12	0.562	scFv J7	0
VHHFc13	1.165	VHHscFc13	0.567		
VHHFc14	2.311	VHHscFc14	0.758		
VHHFc15	2.691	VHHscFc15	0.668		
VHHFc16	0.504	VHHscFc16	0.159		
VHHFc17	0.366	VHHscFc17	1.389		
VHHFc18	0.082	VHHscFc18	0.415		
VHHFc19	2.399	VHHscFc19	1.269		
VHHFc20	1.97	VHHscFc20	0.719		
VHHFc21	1.312	VHHscFc21	0.873		
VHHFc23	2.324	VHHscFc23	0.748		
VHHFc24	1.553	VHHscFc24	0.215		
VHHFc25	0.738	VHHscFc25	0.469		

The concentration range of the antibodies varied significantly between samples. Especially after purification, with some antibodies possessing concentration as high as 4.199 mg/ml (VHHFc2) while others possessing very low amounts of antibody in solution (scFv I68) or none at all (scFv J7). This expression and purification process was repeated until enough antibody was obtained to run the different assays.

5.4.1 Binding pattern analysis in ELISA using purified antibodies

In an attempt to define the different binding patterns of the antibodies to either fibrils and monomers from both suppliers; an ELISA experiment was designed with equimolar solutions of purified antibodies (8 µg/ml, as this was the highest concentration possible with the available antibody stocks).

An array of antibodies that displayed interesting and distinct binding patterns from the previously run ELISA with crude supernatant (figure 5.9) were chosen for this assay; these binding patterns were: Genscript fibril specific, Gencust fibril specific, Fibril specific (binding to both Genscript and Gencust aggregates), Genscript fibril specific, Gencust m/o/pr (monomer/oligomer/protofibril) specific, and binders to all conditions tested. This experiment was performed with purified and equimolar solutions of antibody to ensure that the binding patterns observed in the experiment were the result of relative differential antibody affinity rather than other factors such as antibody concentration. Together with the fibril-specific binder scFc J7, two commercial fibril-specific polyclonal antibody binders were also used as controls. Fibril binders and J7 control were run in duplicate, to validate the potential binding patterns identified through this process (figure 5.11).

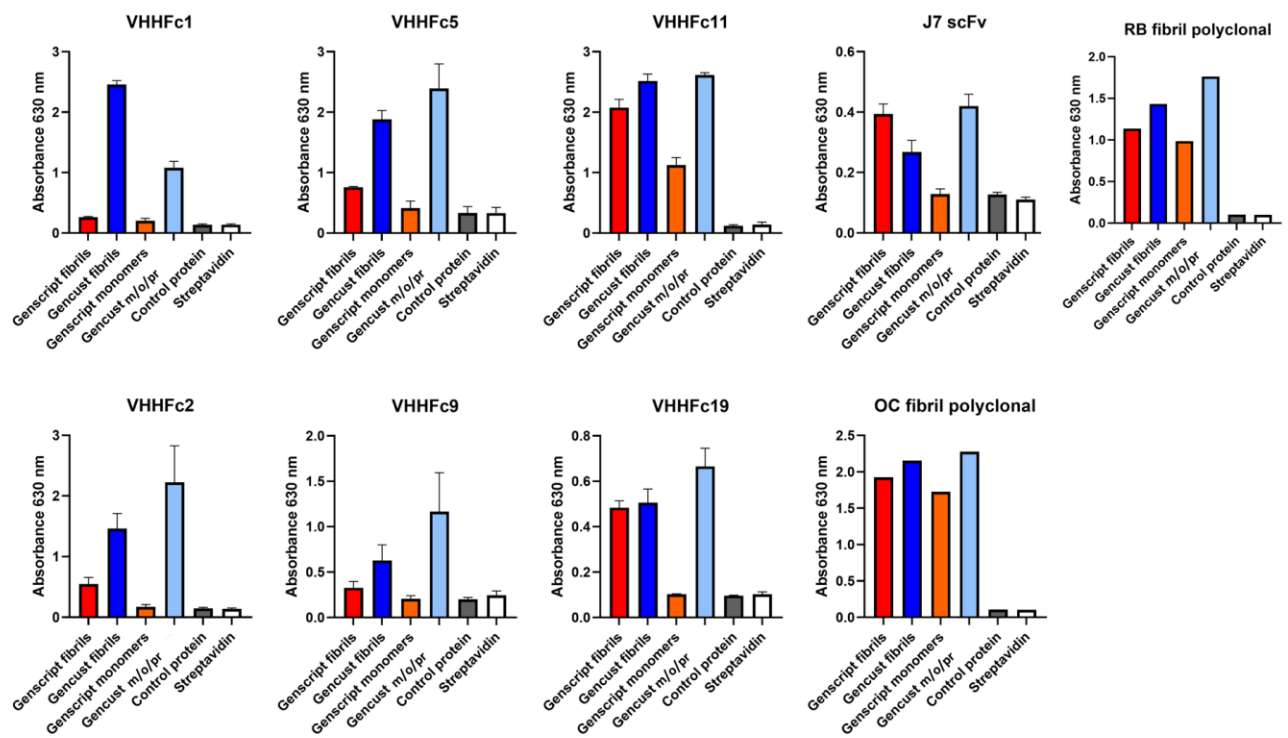


Figure 5-11: In-depth binding pattern analysis of fibril binders of interest

Equimolar solutions of fibril binding antibodies (8 µg/ml) with distinct binding patterns were re-assessed with ELISA, in order to confirm the patterns seen in previous experiments. These patterns of interest were: Binding to Genscript fibrils only (VHHFc 19); Binding Gencust fibrils only (VHHFc 1); Binding both fibrils (VHHFc 9); Binding both fibrils and Gencust monomer/oligomer/protofibril [m/o/pr] (VHHFc 5); Binding Genscript fibrils and Gencust monomer/oligomer/protofibril (VHHFc 2); Binding all forms (VHHFc 11). Alongside fibril binders, J7 scFv was also assessed as a control, at the same concentration to the fibril binding antibodies. Rb fibril polyclonal and OC fibril polyclonal were also assessed as commercially sourced fibril binder antibodies (used at 1:10000 and 1:1000 in 3% (w/v) mPBS respectively). Binding was assessed towards

Genscript fibrils, Gencust fibrils, Genscript monomers, Gencust monomers/oligomers/protofibrils [m/o/pr], a control protein and streptavidin. While the expected binding patterns were not preserved in all samples, it was still possible to distinguish differences in the binding of the different antibodies tested.

Interestingly, only the expected binding patterns seen in figure 5.9 for VHHFc-11 and VHHFc-5 were present when testing the selected antibodies under the new conditions. All of the antibodies seemed to bind to Gencust m/o/pr, invalidating the previously observed specificity for fibrils for VHHFc 19, VHHFc 2 and VHHFc 9; only VHHFc 1 maintained its higher specificity for Gencust fibrils, although binding to Gencust m/o/pr was also present. Surprisingly, scFc J7, which previously showed high specificity for Gencust fibrils was seen to possess strong affinity for Genscript fibrils and Gencust m/o/pr also. VHHFc 11, which was previously seen to bind to all forms of A β maintained its general binding tendencies; as did VHHFc 5, with specificity to Gencust m/o/pr and fibrils. Commercial antibodies displayed binding to all tested form of A β within the contexts of the experiments performed forms.

5.5 Identification of best fibril binders through BLI

The expressed and purified antibodies were tested with BLI. For this, each purified antibody (23, in both formats) was diluted to 30 $\mu\text{g/ml}$ (where possible) in kinetic buffer and tested with both SA and AHC tips. Both tips were used as each one would allow the analysis of the binding kinetics of the antibodies from different orientation; SA tips would allow the broad identification of the binders with the most affinity, as antibodies interact with the fibrils bound to the tips, while AHC would allow for the in-depth analysis of the binding behaviour as antibodies are bound to the tips and interacting with fibrils through a high avidity interaction.

5.5.1 BLI binding assessment with SA tips

Initial experiments were performed with SA tips. Non-specific interactions between the biosensors and the antibodies were measured before the introduction of biotinylated fibrils (figure 5.12)

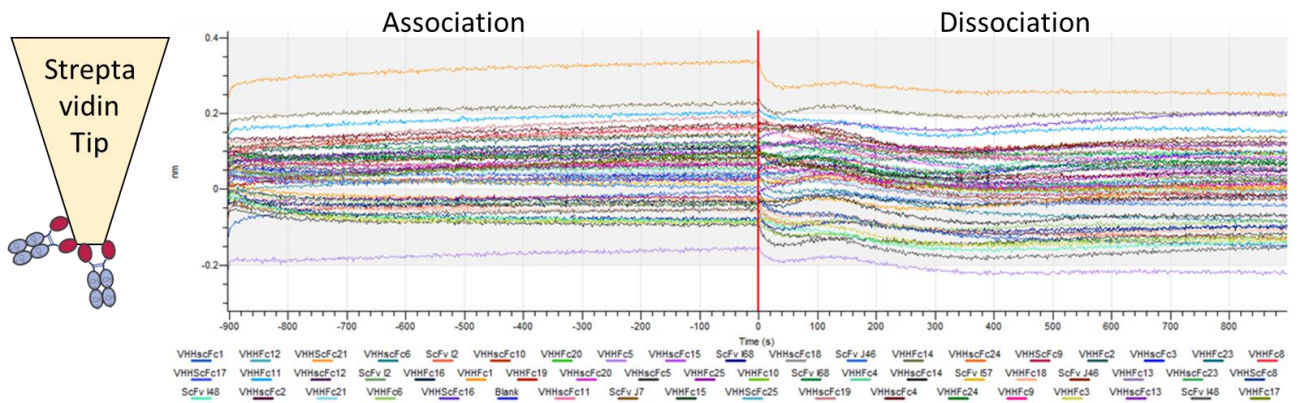


Figure 5-12: BLI experiments measuring SA tip background binding

Purified fibril binding and control antibodies (30 $\mu\text{g/ml}$) were exposed to SA tips. The diagram on the left indicates a schematic representation of what the sensorgram on the right shows. No major non-specific binding was identified.

Analysis of background binding revealed negligible non-specific binding. All traces were subtracted to a negative (blank) well, with no antibody, therefore obtaining the flat lines observed in the image above.

Next, Genscript fibrils were diluted in kinetic buffer (at 25 $\mu\text{g/ml}$) and bound to SA tips, these loaded tips were introduced to solutions of diluted antibodies (30 $\mu\text{g/ml}$). Interestingly, out of all of the antibodies tested, only three seemed to possess specificity to Genscript fibrils in this assay: VHHFc 8, scFc 8 and the control scFc J7 (figure 5.13)

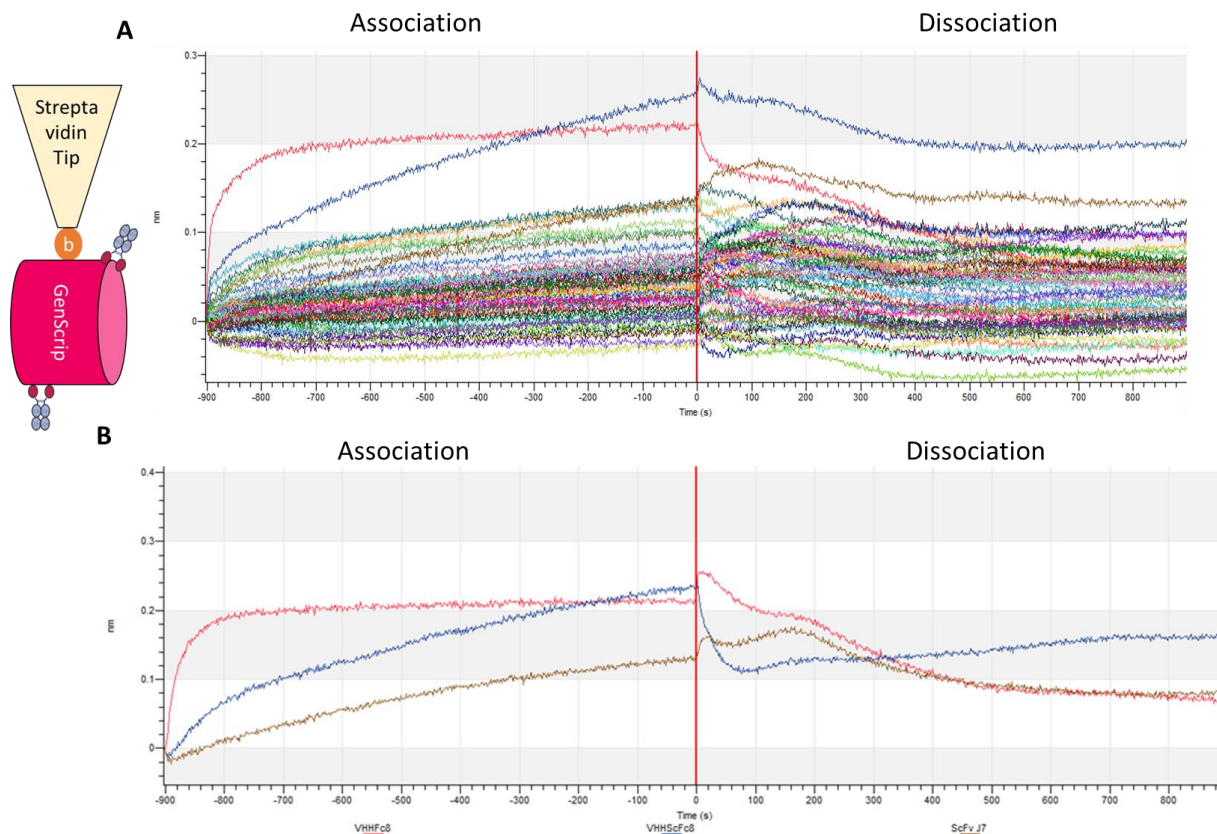


Figure 5-13: BLI experiments-SA tip immobilised Genscript fibril binding to antibodies.

A: SA tips were conjugated to biotinylated fibrils in solution (25 $\mu\text{g}/\text{ml}$). The loaded tips were then submerged in a solution containing purified antibody (30 $\mu\text{g}/\text{ml}$), represented in the diagram to the left. As the antibodies bound to the fibrils, an optical shift occurred in the tip, resulting in the binding (nm) values evidenced in the sensogram. **B:** All fibril binding and control antibodies were tested, but very little binding was observed, with only VHHFc8, VHH scFc8 and J7 possessing distinguishable binding.

Once bound, both formats of fibril-binder 8 and control J7 seemed to present very slow dissociation, but due to the low binding signal, the off-rates were not very pronounced.

Further testing was performed with the second fibrillar target used during biopanning; Gencust fibrils (at 25 $\mu\text{g}/\text{ml}$). Interestingly, antibodies seemed to react in a completely different way to fibrils sourced from this supplier: BLI tests with SA tips revealed as many as ten antibodies with the ability to bind these aggregates (figure 5.14). From these selected binders, three were already highlighted in the previous BLI run (VHHFc8, scFc8 and scFc J7), the other seven binders identified were VHHFc 12, VHHFc 5, VHHFc 14, VHHFc 2, VHHFc 11, VHHFc 13 and VHHFc 21. Different affinity was recorded for each of the antibodies of interest, with VHHFc 8 being the antibody with the highest affinity to Gencust fibrils

(as evidenced by the 1 nm binding observed in the sensogram) and VHHFc 11 being the antibody with the lowest affinity observed in the group. Additionally, the binding kinetics seemed to be different for J7, scFc 8 and VHHFc 11, as their traces seemed to increase in a linear manner, without reaching saturation. The 10 antibodies highlighted through this assay were deemed the best binders in this orientation (figure 5.14), as all other antibodies tested did not show binding (figure 5.15). On and off-rates were not calculated as the binding kinetics were complex due to the dimeric nature of the VHHFc format, and therefore not explained with 1:1 binding model. Similarly, to what was observed in the previous run with Genscript fibrils, the dissociation of the antibodies from the fibrils seemed to be slow, evidenced by the almost flat dissociation curved seen in the sensogram.

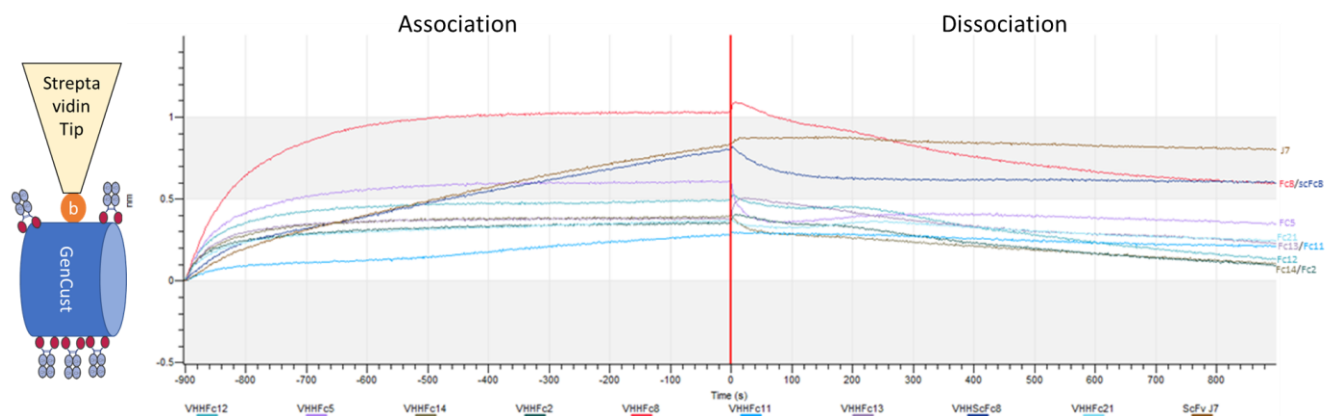


Figure 5-14: BLI experiments-SA Gencust fibril binding

SA tips were conjugated to biotinylated fibrils in solution. The loaded tips were then submerged in a solution containing purified antibody (30 µg/ml), represented in the diagram to the left. The analysis of the sensogram (right) indicate a number of antibodies (VHHFc 12, VHHFc 5, VHHFc 14, VHHFc 2, VHHFc 8, VHHFc 11, VHHFc 13, VHHFc 21, VHHscFc 8, VHHscFc, 8 and scFv J7) with the ability to bind to Gencust fibrils and produce a bigger shift (in nm) to Genscript fibrils, ranging from 0.3 nm seen in VHHFc 11 to 1 nm from VHHFc8.

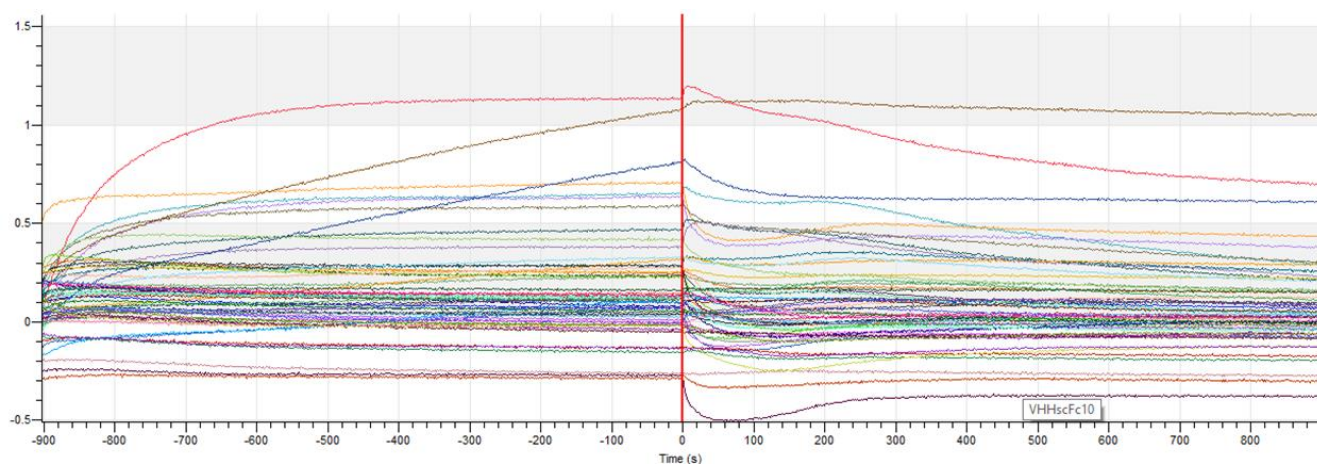


Figure 5-15: Traces of all antibodies tested with SA tips and Gencust fibrils

Sensogram showing the binding of both fibril-specific and control antibodies to Gencust fibrils, using SA tips. No further binding was observed beyond the ten antibodies observed and described in figure 5-14.

5.5.2 BLI binding experiments with AHC tips

Following the identification of the best binders in the SA biosensor-fibril-antibody orientation, the antibodies were further tested using AHC tips, changing the binding orientation. The experimental design was identical to that of the SA tips, only that this time, an initial load step was performed to allow the different antibodies to bind to the biosensors (one antibody type per sensor, at 30 $\mu\text{g}/\text{ml}$) prior to the introduction of the loaded tips to fibrils in solution (25 $\mu\text{g}/\text{ml}$). For this assay, only Gencust fibrils were tested, as the use of this kind of fibrils revealed the most binders in the previous run. Testing the antibodies in this orientation revealed that most of the binders identified with SA tips were also able to bind fibrils in this orientation (VHHFc 12, VHHFc 5, VHHFc 14, VHHFc 2, VHHFc 8, VHHFc 11, VHHFc 21 and VHHFc 13); but also, that this orientation allowed for the identification of other antibodies, previously undetected (VHHFc 20, VHHFc 10, VHHFc 4 and scFc 14). Interestingly, scFc J7, which was found to be a binder in the previous orientation, lacked any kind of binding once linked to AHC tips, highlighting the importance of testing different orientation when assessing antibody binding (figure 5.16).

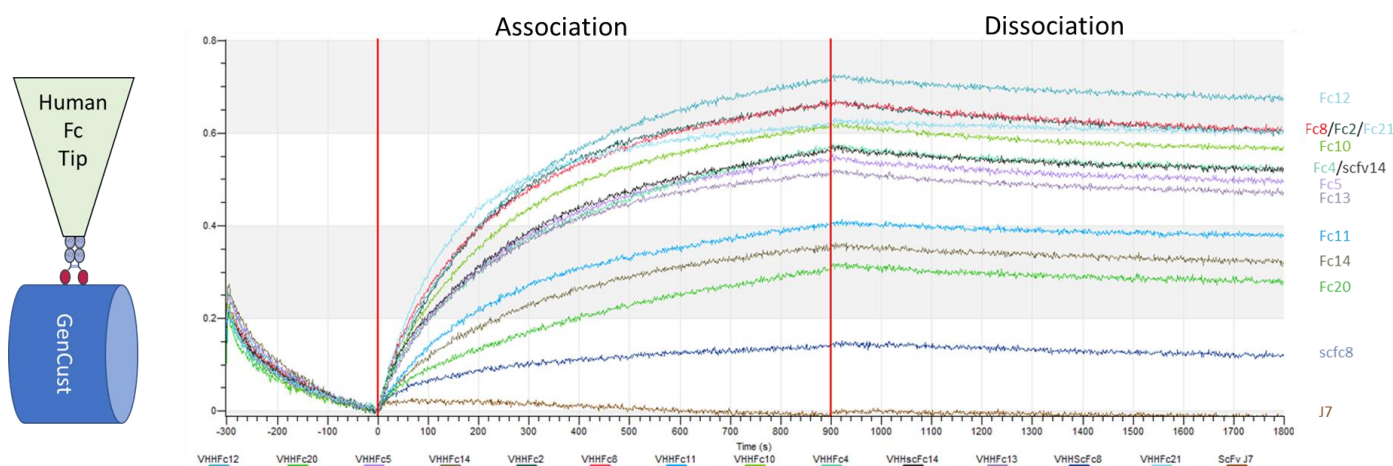


Figure 5-16: BLI experiments-AHC Gencust fibril binding

Purified antibodies (30 µg/ml) were loaded onto AHC tips; the tips were then introduced to solutions of Gencust fibrils at 25 µg/ml (represented in diagram to the left). Both fibril binding and control antibodies were tested in both formats. The association curves revealed the presence of 12 antibody binders: VHHFc12, VHHFc 20, VHHFc 11, VHHFc 13, VHHFc 5, VHHFc 4, VHHFc 10, VHHFc 21, VHHFc 2, VHHFc 8, VHHFc 14 and VHHscFc 14. The association and dissociation curves of VHHscFc8 and J7 were also evidenced, as they were seen to be good binders with SA tips but interestingly the latter two antibodies did not possess much binding in this orientation.

Similar to what was observed with SA tips, most of the binders identified through BLI seemed to be in the VHHFc format, most likely due to avidity effect of the antibodies (being dimeric molecules) and/or fibrils in solution (as repetitive epitopes are present in solution, and are able to interact with the antibodies bound to the tips). Owing to the dimeric nature of the VHHFc antibodies, binding could only be explained with a complex 2:1 interaction model within the Fortebio Data analysis software. This model outputs two kD affinity values (one for each VHH molecule) making the interpretation of binding data complex, kinetic measurements were therefore omitted. Interestingly, once the fibrils were bound onto the antibody-tip complex, they seemed to form a stable interaction as virtually no dissociation was observed, also most likely due to avidity effect.

Finally, fibril binders identified through SA and AHC biosensors were tested with Genscript monomers, to assess non-specific binding. This was carried out using the AHC tips, as this orientation seemed to be the most sensitive to the binding of antibodies. The twelve antibodies identified in the previous run with Gencust fibril were tested (figure 5.17). While most antibodies did not present any signs of

binding, J7 and VHHFc 21 (respectively one of the worst and best binders to Gencust fibrils, as seen in figure 5.17) were seen to possess non-specific affinity to monomers.

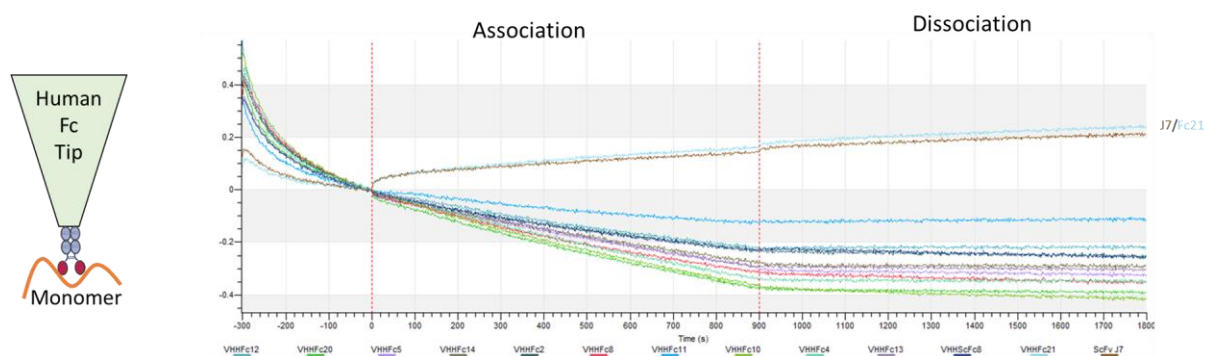


Figure 5-17: BLI experiments-AHC Genscript monomer binding

Purified antibodies (30 $\mu\text{g}/\text{ml}$) were loaded onto AHC tips; the tips were then introduced to solutions of Genscript monomers at 25 $\mu\text{g}/\text{ml}$ (represented in diagram to the left). For this assay, particular emphasis was made with the best binders identified through the analysis of Gencust FB in the AHC and SA tip orientation. These antibodies were VHHFc 12, VHHFc 20, VHHFc 5, VHHFc 14, VHHFc 2, VHHFc 8, VHHFc 11, VHHFc 10, VHHFc 4, VHHFc 13, VHHFc 21, VHHscFc 8 and scFv J7. Only J7 and VHHFc 21 were seen to possess non-specific binding to monomers

5.6 Discussion

The discovery of a therapeutic antibody through phage display is a very appealing prospect for future hopes of identifying a cure for AD. With the discovery of Gantenerumab [210] and the ever evolving field of antibody engineering [228], the ambitions of discovering a disease modifying drug is higher than ever. In this chapter, the fully characterized synthetic A β fibrils and monomers produced in the previous chapter were implemented for the discovery of fibril-specific binders through phage display. The use of VHH libraries to develop antibodies against A β fibrils is a relatively novel approach, even though VHH antibodies would be an ideal format to target fibril forming proteins, due to its compact size, solubility and specificity for conformational targets [176, 235, 298]. Currently, only a few research papers describing the discovery of potentially therapeutic VH antibodies have been published, these are: Heibicht *et al.*, 2007, in which a synthetic VHH library is used to discover a conformational antibody capable of binding synthetic A β fibrils and oligomers [176] and, similarly, by Medicago *et al.*,

2010 in which an IgG VH-pIII library is generated from mice immunized with A β peptides [231]. Indeed, most studies using phage display for the discovery of antibodies against A β fibrils/oligomer are either based on scFv [173, 177, 180, 230-234] or *in silico* designed antibodies [179].

In this chapter, initial experiments focused on understanding the stability of the chemical biotinylation of both Genscript and Gencust fibrils. This was achieved by the loading of the modified fibrils on SA tips (figure 5.1). Modified fibrils at a higher concentration were compared with two control biotinylated proteins. This revealed that fibrils were stably modified as the traces recorded in the sensogram showed fibrils were binding to the biosensors with high affinity, much like the control proteins. The kinetics of binding were different depending on the concentration of the protein used, henceforth fibrils (being at the higher concentration) reached saturation quicker than biotin-protein I (at a lower concentration). The bond between modified proteins and biosensor was found to be stable, as a dissociation step in kinetic buffer produced no changes in the traces of the sensogram. This was an important step to confirm as biopanning would be performed in solution, and the stable biotinylation of fibrils/monomers would be a determining factor in the success of the method, as magnetic streptavidin-coated beads were implemented for isolation/subtraction of phage. This method for antibody discovery was chosen as biopanning in solution allows for the preservation of the structural integrity of the fibrils and avoids the potential masking of hydrophobic sites that would occur through the binding of the target to a solid surface [224].

With the confirmation of the stability of the modified fibrils in solution through BLI, biopanning with UCB Celltech's naïve VHH library was carried out. Phage display was performed targeting Gencust fibrils and Genscript fibrils. Each successful experiment consisted of three rounds, with subtraction to monomers applied in round 2 for some panning experiments. The first panning experiment (P1) was performed targeting Gencust fibrils, in this instance only one subtracted selection was implemented. From P1, six antibody binders were identified (figure 5.2). Fibril specificity was confirmed through monoclonal phage ELISA, in binders that showed 3x times more OD630 in the fibril wells compared to

all other compounds tested. Following the initial success of this assay, the next panning experiment (P2) was designed to target Gencust fibrils, with subtraction of monomers from the same supplier in round 2. This was performed with the aim of eliminating any potential aspecific supplier-specific binders that could remain if using Genscript monomers for subtraction. Surprisingly, subtracting with Gencust m/o/pr completely wiped out any fibril specificity from the picked colonies in monoclonal phage ELISA. This was most likely the result of the A β aggregate contamination seen within Gencust “monomeric” population (figure 4.12, C) pulling out the fibril specific binders isolated during the first round of panning during the subtractions step. Interestingly, rescuing round 1 phage from experiment P2 and re-performing the subtraction with Genscript monomers resulted in the identification of FBs (figure 5.3) in experiment P2.5. Within this same experiment an additional non-subtracted selection was also implemented. In total, an additional nine fibril-specific antibodies were identified. From these antibodies, two were from the subtracted selection and seven from the non-subtracted selection; indicating that the subtraction step was indeed pulling out fibril binders from the libraries. From the cfu count throughout the three rounds of panning, it was possible to appreciate an enrichment effect, indicating the selection of higher affinity antibodies throughout several rounds of biopanning [226, 227].

For the final panning experiment (P3), with the aim of obtaining a more strictly fibrillar-specific antibody, Genscript fibrils were targeted and Genscript monomers were subtracted in round 2. Like with experiment P2 before, this was done with the aim of removing monomer binders. This time, 10 distinct antibody binders were identified; three of which derived from the subtracted selection and the other seven from the non-subtracted selection (figure 5.4). As with the previous experiments, the analysis of the cfu throughout the three rounds of panning showed enrichment, with the non-subtracted selection possessing a higher number of colonies than the subtracted selection.

In total, from three biopanning experiments, 25 fibril-specific antibodies were identified. The DNA sequences from these antibodies were propagated through PCR (figure 5.5) and sequenced. From this

process two sequences were eliminated as the sequencing data was of poor quality (figure 5.6). This resulted in 23 unique antibody sequences (listed in table 5.5) which were used to produce antibody-human Fc construct in two formats: VHHFc and scFc. This was done with the aim of observing the avidity (or chelate) effects at play when the different FBs were tested against fibrils [180, 300]. Interestingly, when the different antibody sequences were aligned (figure 5.7) it was revealed that some of the fibril-specific antibodies possessed the same CD3 domain, mainly with the pairs: 12 (P2.5-NSB8)/14 (P2.5-NSG9); 13 (P2.5-NSC11)/5 (P1-G6) and 15 (P2.5-NSG11)/9 (P2.5-NSA4). This interesting detail found only in the experiments targeting Gencust fibrils hinted to the possibility that during biopanning, these sequences bound a single epitope more than once and independently. Curiously, this phenomenon was also observed in sequences belonging to two different experiments altogether (P2.5 and P1), signifying that this same CDR3 was isolated twice in two independent and unrelated experiments targeting the same protein.

Antibodies, in both formats were ordered alongside an array of control antibodies described by Munke *et al.*, 2017 [180], to have a point of reference against proven anti-fibril antibody binders discovered through similar methods. FBs and control antibodies were successfully transfected and expressed in the Expi293™ system (figure 5.8). Crude supernatants (diluted 1:4 in PBS) were used to perform an initial screening of the antibodies (figure 5.9) to assess the specificity of each antibody in both formats. Binding was tested with an array of potential targets, such as fibrils and monomers from both suppliers, always measuring the binding to streptavidin alone to control for non-specific interactions. OD630 values for each antibody revealed the presence of different binding patterns:

- Genscript fibril specific (e.g., antibody 19)
- Gencust fibril specific (e.g., antibody 1)
- Specific to both fibril types (e.g., antibody 9)
- Specific to fibrils and Gencust m/o/pr (e.g., antibody 5)
- Specific to Genscript fibrils and Gencust m/o/pr (e.g., antibody 2)

- Specific to all A β targets (e.g., antibody 11)

The presence of these distinct binding patterns suggested that the different antibodies discovered through phage display could possess different specificities as they target different epitopes within the A β peptides. Additionally, the side by side comparison of VHHFc and scFc antibodies revealed that while most antibodies possessed similar binding patterns regardless of the different formats (like antibody 1, 4, 9, 10, 11, 12, etc), some possessed very different binding profiles, like antibody 8, showing more specificity to Genscript fibrils in scFc format, or 17 displaying more specificity to Gencust fibrils in scFc format, possibly an effect of epitope accessibility or antibody format (dimeric or monomeric). Additionally, the analysis of crude supernatants did not reveal any uniform artificial increase in the binding of the different antibodies to the targets from the avidity effect, as both formats possessed similar absorbance values (with scFc antibodies possessing stronger binding than VHHFc in some instances). Further still, the analysis of the control antibodies revealed no binding, regardless of the format tested for all binders, apart from J7 scFc, which showed high specificity to Gencust fibrils. This could be a reflection of these control antibodies possessing affinity for the recombinant proteins used for their discovery [180] rather than the synthetic fibrils used for the experiments described in this chapter.

It is important to mention that the four characteristics described above for the ELISA results shown in figure 5.9 (distinct binding patterns between antibodies, format-dependant binding variability within the same antibodies, lack of uniform increased binding in VHHFc due to avidity effect and lack of binding in the control antibodies) could partly be attributed to concentration variabilities within the samples tested. Indeed, these results were produced using diluted crude supernatant; from the expression test with BLI, it is possible to appreciate the different antibodies possessing different binding values (within 1 and 6 nm). As BLI was performed with AHC tips, differential binding can be solely attributed to the differential expression of each antibody within the supernatant, therefore the different antibodies were purified and retested with equimolar concentrations of antibodies to

validate the findings describe above. Purification was achieved using the PhyNexus automated system, obtaining the concentrations listed in table 5.7 and gels shown in figure 5.10. The measured concentrations matched the intensity of the bands resolved with SDS-PAGE.

Binding pattern re-assessment was performed with an ELISA using purified antibodies (at 8 µg/ml). For this assay, only VHHFc were used, to assess if the binding patterns were linked to the antibody sequence themselves rather than the format (figure 5.11) together with commercial polyclonal antibody controls. This repeat with equimolar solutions of antibody revealed a more accurate representation of the binding patterns. Some antibodies, like VHHFc1 maintained the previously observed affinities, while others, displayed completely different profiles to the expected patterns (like VHHFc 9 and 19). Regardless of this, all of the tested antibodies displayed a higher specificity to Gencust “monomers” than previously observed. This could most likely be attributed to the presence of higher molecular weight contaminants in the Gencust “monomer” population, as Genscript monomers were devoid of signal. From the analysis of the six antibodies tested, three binding patterns emerged:

- Gencust fibril and Gencust m/o/pr specific (VHHFc 1, 5, 2 and 9)
- Fibril (both sources) and Gencust m/o/pr specific (VHHFc 19)
- Binder to all A β forms (VHHFc11)

Interestingly, J7 scFc, which previously only showed specificity for Gencust fibrils in the ELISA using crude antibody, displayed binding to both fibril types and Gencust m/o/pr. Control polyclonal antibodies clearly bound all A β forms, confirming the validity of the synthetic peptide in producing relevant aggregates. This data likely suggests the presence of three binding sites: one present in all misfolded forms of A β tested and shared with monomers; one present in all misfolded forms of A β tested but not shared with monomers; and one present only in misfolded Gencust A β . Further epitope characterization assays would be needed to confirm this.

Having better characterized the different antibodies and their binding properties through ELISA, the next step was to perform a distinct binding assay to confirm the interaction of the different antibodies to the fibrillar targets. As seen throughout the results above, the signal in an ELISA is strongly dependant on the concentration of the antibody used, therefore determination of the effective binding affinities to the antigens using BLI [249, 254] used purified antibodies and targets at a set concentration. Antibodies were diluted to 30 $\mu\text{g/ml}$ in kinetic buffer, as that was maximal concentration in which all antibodies could be tested, given the concentration values after purification. As for fibrils, they were measured at 25 $\mu\text{g/ml}$ (around 5.5 μM) as loading experiment with SA tips revealed that to be the minimal concentration that would allow for sufficient saturation of the biosensor. Initial experiments were performed with SA tips, and tests confirmed no non-specific interaction between the antibodies and the biosensors (figure 5.12). Next, both Genscript (figure 5.13) and Gencust (figure 5.14 and 5.15) fibrils were assessed, revealing that all of the antibodies tested showed very little binding to Genscript fibrils, with only VHHFc8, scFc 8 and scFc J7 showing tendencies to bind this target with very small 0.2 nm and 0.1 nm shifts respectively. In contrast, the use of Gencust fibrils allowed for the identification of 10 antibody binders. On-rates varied considerably between antibodies, as during association the antibodies reached shifts ranging from 0.2 to 1 nm. Interestingly, the same three antibodies that were previously identified using Genscript fibrils (VHHFc8, scFc8 and scFc J7) were also binders to Genscript fibrils, suggesting these antibodies possessed the ability to recognize structural epitopes in different kinds of fibrils. Another interesting aspect of the analysis of the association traces of the different antibodies, was the fact that scFc binders seemed to possess a different binding kinetic to VHHFc8, this was best exemplified by scFc8 and scFc J7 posing a more linear trace compared to the other VHHFc8. This could be the result of an avidity effect, causing the dimeric antibodies to bind better than their monomeric counterpart [249]. Analysing the off-rates during the dissociation step revealed that once bound, the antibodies do not seem to come off the fibrils (or possessed very slow dissociation curves). This was present for both VHHFc and scFc formats and could

indicate a stable bond between antibodies and targets, an encouraging finding for potential therapeutic antibodies.

Following the initial discoveries with SA tips, the binding orientation was switched with AHC biosensors. In this instance, only Gencust fibrils were tested, as they were the target that revealed the best results in the previous orientation. This time, 12 binders were identified, some of which were already highlighted as binders with SA tips, but also new ones that were found to bind only in this orientation. Likewise, binders that were previously seen to be very successful with SA tips were found to be lacking in this orientation, with scFc8 and J7 possessing very little (or no) binding. Analysing the association curves for each antibody did not reveal major difference between binders, with VHHFc8 and scFc8 possessing similar patterns. As all antibodies were tested at the same concentration, differences in on-rates could only be attributed to variations in affinity by the antibodies to the target. Like what was observed before, dissociation of the antibodies was almost non-existent. This could indicate a strong interaction between the antibodies and their targets due to high affinity, but also the repetitive nature of the epitopes within fibrils in solution could be causing an increased avidity effect resulting in the lack of dissociation. Finally, the analysis of these same binders with Genscript monomers instead of Gencust fibrils revealed no non-specific monomer interaction, apart from J7 and VHHFc 21, which were seen to bind with low affinities to these peptides (figure 5.16).

In summary, fully characterized A β fibrils and monomers were used to discover fibril specific antibodies through phage display. This methodology was applied to discover binders to both Genscript and Gencust fibrils. Binding and specificity were confirmed with ELISA. The different fibril-specific antibodies were then sequenced and ordered as human-Fc fusions in either dimeric (VHHFc) or monomeric (scFc) form. Ordered antibodies were further tested with ELISA, revealing the presence of different binding patterns. Alongside ELISA, BLI was also used to confirm binding. From these efforts it was discovered that some of the FBs were indeed specific to fibrils, with a predilection to Gencust fibrils over Genscript fibrils. This binding was specific as minimal binding to Genscript monomers was

observed. The identification of fibril-specific binders with distinct binding characteristics and likely distinct epitopes provided a panel of antibodies to screen for their ability to disrupt A β fibrillation *in vitro*.

Chapter 6. Discovery of fragmented A β fibril-specific binders through phage display and functional assay optimization

6.1 Introduction

Fibril fragmentation is the process through which a fully formed fibril is shattered into several smaller pieces, either through mechanical stimulation, handling, or as a biological process in living tissue [154]. Through fragmentation, a fibril is broken into smaller segments and in this fragmented state, fibril propagation is thought to accelerate due to the increased number of nucleation sites present in solution [154, 171]. Fibril growth and propagation are thought to be regulated by three processes (known as secondary pathways [301]): secondary nucleation; in which the fibril surface is able to catalyse the formation of soluble aggregates; elongation, in which monomers are added to the ends of fibrils, increasing the length of the fibril itself; and further fragmentation, where the overall number of fibrils is increased [250, 302, 303]. These processes are distinct from primary nucleation, which only involves the crystallization of monomers into small soluble oligomers, and then fibrils [250, 301-304] (figure 6.1). Several studies have found a direct link between fibril fragmentation and disease progression [147, 151, 296]. In addition fragmented fibrils are also responsible for cell death as a correlation between fragmentation and cytotoxicity through the disruption of cell membranes has been found for fibril forming proteins [133].

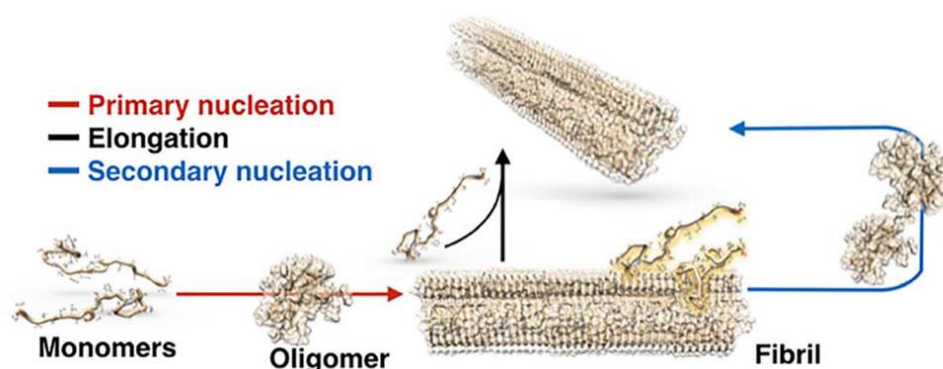


Figure 6-1: Model of Aβ aggregation

Model describing the aggregation process of Aβ. The red arrow indicates the process of Primary nucleation (monomers aggregate to form soluble oligomers and then fibrils). Secondary nucleation (oligomers catalysed by fibril surface) is described with by the blue arrow. Finally, elongation (recruitment of monomers onto fibril surface) is indicated with the black arrow. Although not shown in image, fragmentation (division of fibril into smaller fragments) also contributes to fibril propagation. Image modified from Aprile *et al.*, 2017 [304], licence under the CC BY 4.0.

Fragmented fibrils are therefore a very attractive target for antibody discovery as, the inhibition of secondary nucleation sites could not only potentially halt disease progression, but also decrease neurotoxicity. Several research groups aimed at discovering antibodies with the ability of targeting these sites, such as the scFv antibodies developed by Munke *et al* [180] or the rationally designed antibodies developed by Limbocker *et al.*, [179], with varied success. In this chapter, biotinylated fragmented fibrils were used for the discovery of monoclonal binders specific to secondary nucleation sites (fragmented fibril specific sites). The discovered antibodies were then ordered as human-Fc constructs, expressed and purified in order to measure binding with ELISA and affinity kinetics with BLI. Through 3 rounds of biopanning, 34 unique antibody sequences with the ability to bind fragmented fibrils were identified. Additionally, the initial establishment for future functional and cytotoxicity assays were developed, showing preliminary results indicating some antibodies may inhibit fibril formation.

6.2 Biopanning against fragmented fibrils

Prior to the start of the biopanning experiments, the effective biotinylation of the Genscript fragmented fibrils (FF) were assessed in duplicate with BLI. Biotinylated FF (at 125µg/ml) were compared with Genscript biotinylated fibrils (125 µg/ml), unmodified Gencust fibrils (125 µg/ml) and a biotinylated unrelated protein as positive control for biotinylation (15 µg/ml). BLI was performed using SA tips; after a 60 second baseline, fibrils were loaded onto the tips during a 7-minute association. FF were successful in the binding to the biosensors, reaching a shift value of around 2.5 nm and displaying high affinity for streptavidin as the traces were quick to reach saturation. Biotinylated Genscript fibrils and unrelated proteins also bound to the biosensors, as expected. Unbiotinylated fibrils were non-reactive. Following the association steps, the bound fibrils were subjected to a 60 second dissociation in kinetic buffer, where no alterations in binding patterns was observed. Finally, the fibrils were neutralized in 1% SDS for 3 minutes (figure 6.2)

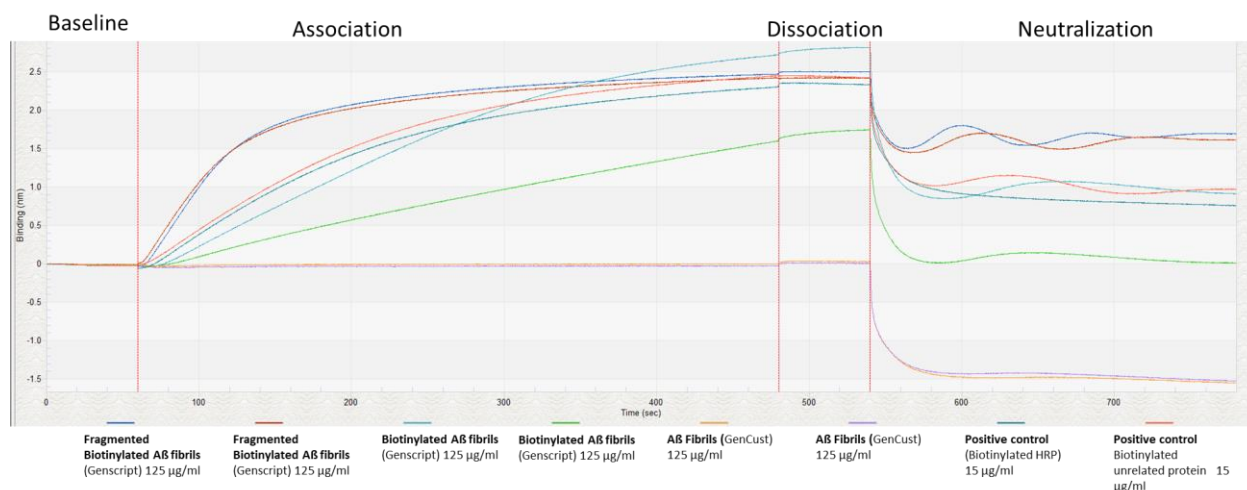


Figure 6-2: Fragmented fibril biotinylation test

Fragmented fibrils were biotinylated with Lightning-Link® Biotin conjugation kit (type B). Effectiveness of biotinylation was assessed with BLI. SA tips were used to measure binding of biotinylated fragmented Genscript fibrils (125 µg/ml), biotinylated Genscript fibrils (125 µg/ml), Gencust fibrils (125 µg/ml) and an unrelated biotinylated protein (15 µg/ml), acting as positive control (all measured in duplicate). Fragmented fibrils were found capable of binding the biosensors, indicating a successful biotinylation. Additionally, the affinity of the fragmented fibrils to the biosensors seemed to be the greatest out of all the other molecules tested, evidenced by the prompt saturation of the signal in the sensogram. Biotinylated fibrils were seen to possess less affinity, but the ability to induce a bigger shift than their fragmented counterparts. No binding was observed in unbiotinylated fibrils. Finally, control biotinylated proteins were seen to bind with similar kinetics to fragmented fibrils. Dissociation highlighted the stability of the link between biosensors and bound modified molecules. Traces were highly variable in the neutralization step as 1% SDS was used.

With confirmation of the effective biotinylation of the target, biopanning could commence. Phage display was performed using the same methodologies implemented for the discovery of FB (section 2.21). Discovery of fragmented fibril binders (FFB) was achieved using Genscript FF as targets, with subtraction to Genscript fibrils and monomers. The same supplier was implemented for all steps of the process in order to reduce the risk of obtaining non-specific binders. Additionally, the same batch of Genscript monomers was used to make each component needed for the discovery of antibodies, to reduce batch variability between Aβ aggregates.

For the discovery of FFB, a single biopanning experiment was done, using three selections:

- 1: Non subtracted selection, using 10 µg of FF per round for 3 rounds of panning.

2: Monomer-subtracted selection, using 10 µg of FF per round for 3 rounds; with subtraction in round 2 to remove non-specific binders using 10 µg of monomers and 10 µg of an unrelated biotinylated protein.

3: Fibril-subtracted selection, using 10 µg of FF per round for 3 rounds; with subtraction in round 2 to remove non-specific binders using 10 µg of full length fibrils, 10 µg of monomers and 10 µg of an unrelated biotinylated protein.

At the end of each round, colonies from the titration plates were counted (table 6.1); enrichment was observed for all selections

Table 6-1: cfu per round of biopanning against FF

Selection	Round 1 (cfu)	Round 2 (cfu)	Round 3 (cfu)
1	8×10^3	9.6×10^6	2×10^7
2	4×10^4	8×10^6	8×10^7
3	18×10^4	10×10^6	0.2×10^7

After round 3, 95 colonies were individually picked for each selection. The monoclonal antibodies within each colony were then tested with phage ELISA to establish any specificity for FF. Each selection was assessed separately, using an array of biotinylated targets bound to streptavidin-coated plates, such as FF (2 µg/ml), Genscript fibrils (2 µg/ml), Genscript monomers (2 µg/ml), an unrelated protein (2 µg/ml) or no protein to measure binding to streptavidin (5 µg/ml). From the 95 colonies tested per selection, 16 FFB were found in selection 1 (Figure 6.3), 16 from selection 2 (figure 6.4) and 17 from selection 3 (figure 6.5). As with FB beforehand, FFB were deemed specific to their target when the OD630 from the FF wells were at least 3 times higher than the absorbance for all the other compounds tested.

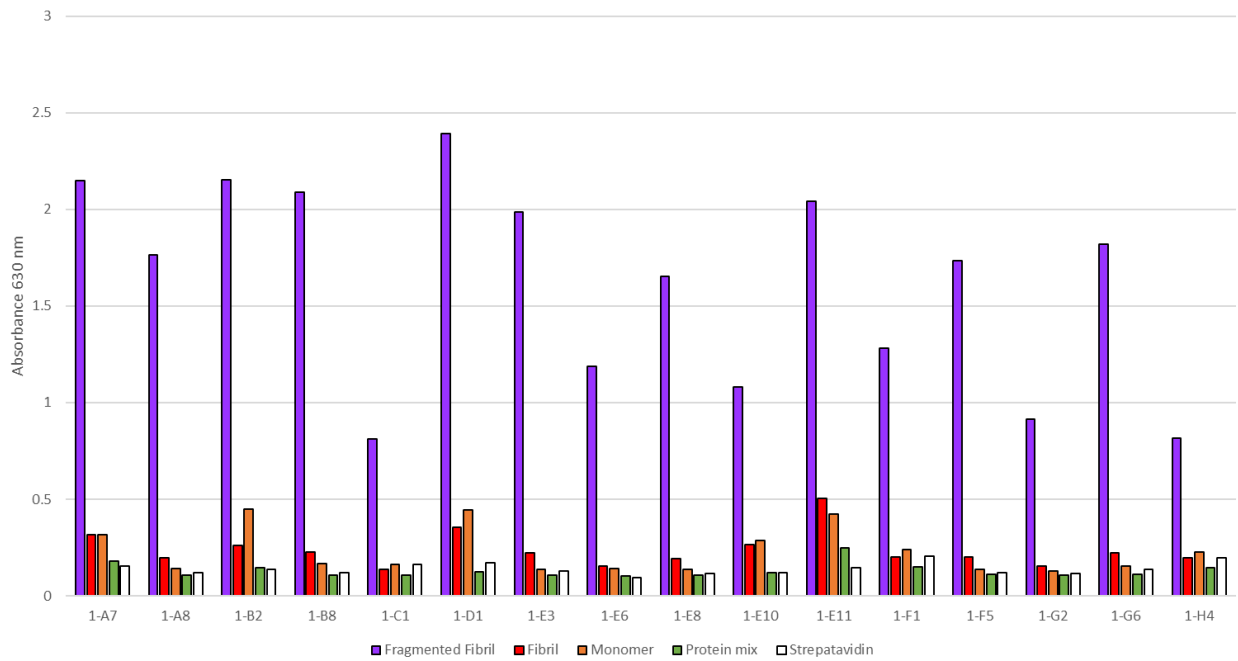


Figure 6-3: Fragmented fibril biopanning, selection 1, monoclonal ELISA screening of phage antibodies

Monoclonal phage ELISA values of the FF-specific binders from selection 1 (non-subtracted). ELISA screening was performed by binding 2 µg/ml solutions of biotinylated Genscript Fragmented fibrils, Genscript fibrils, Genscript monomers and a mix of unrelated proteins onto streptavidin coated plates (5 µg/ml). A well was left blank to measure background binding. A total of 95 colonies were screened, from which 16 binders were identified as specific for FF. Binding was assessed by measuring OD₆₃₀ within each well after the addition of TMB. Each antibody was labelled with the selection number (1) following the well from which the monoclonal antibody was obtained from the master-plate. Screening was performed measuring each clone once.

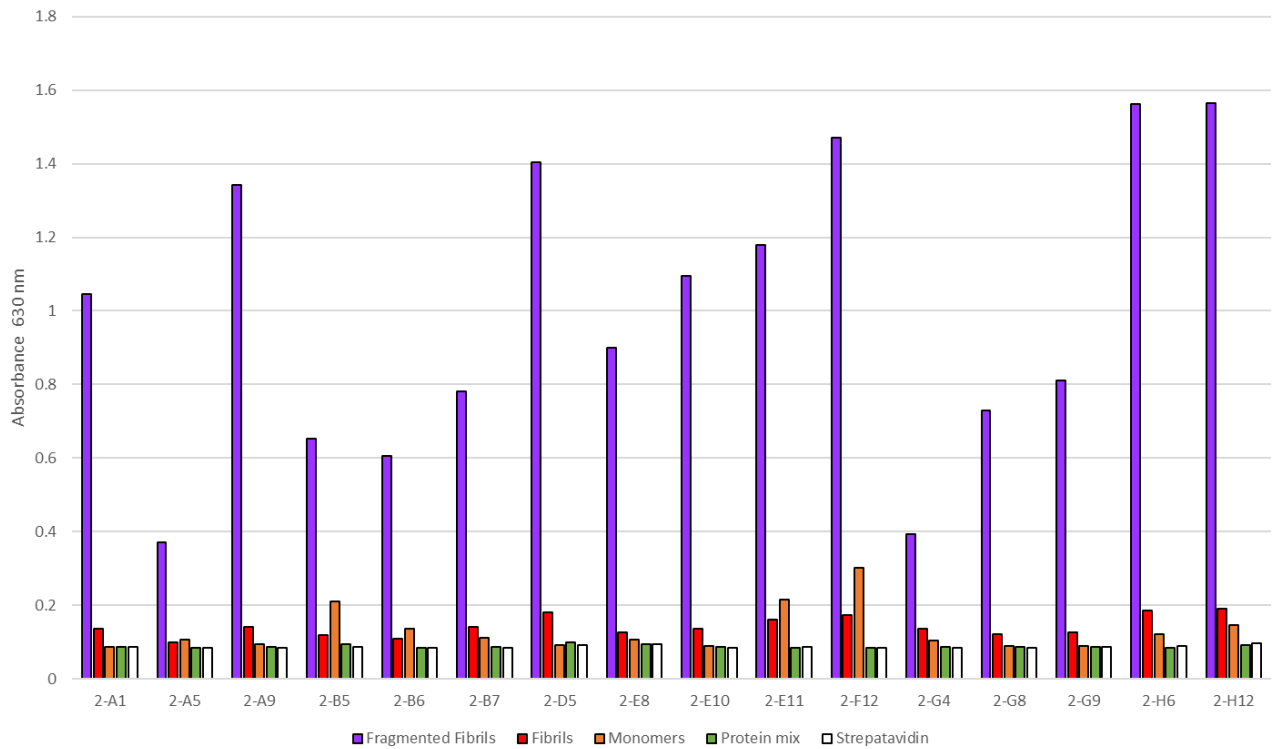


Figure 6-4: Fragmented fibril biopanning, selection 2, monoclonal ELISA screening of phage antibodies

Monoclonal phage ELISA values of the FF-specific binders from selection 2 (biotinylated monomer and unrelated biotinylated protein subtracted). ELISA screening was performed by binding 2 $\mu\text{g}/\text{ml}$ solutions of biotinylated Genscript Fragmented fibrils, Genscript fibrils, Genscript monomers and a mix of unrelated proteins onto streptavidin coated plates (5 $\mu\text{g}/\text{ml}$). A well was left blank to measure background binding. A total of 95 colonies were screened, from which 16 binders were identified as specific for FF. Binding was assessed by measuring OD630 within each well after the addition of TMB. Each antibody was labelled with the selection number (2) following the well from which the monoclonal antibody was obtained from the master-plate. *Screening was performed measuring each clone once.*

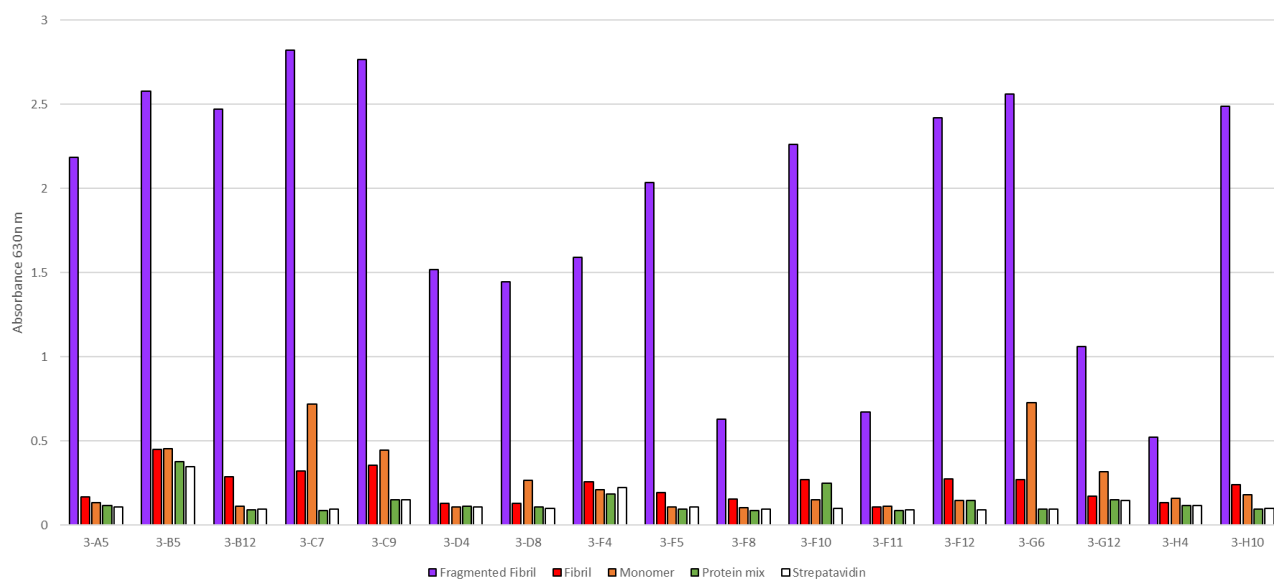


Figure 6-5: Fragmented fibril biopanning, selection 3, monoclonal ELISA screening of phage antibodies

Monoclonal phage ELISA values of the FF-specific binders from selection 3 (biotinylated Genscript fibril, biotinylated monomer and unrelated biotinylated protein subtracted). ELISA screening was performed by binding 2 µg/ml solutions of biotinylated Genscript Fragmented fibrils, Genscript fibrils, Genscript monomers and a mix of unrelated proteins onto streptavidin coated plates (5 µg/ml). A well was left blank to measure background binding. A total of 95 colonies were screened, from which 17 binders were identified as specific for FF. Binding was assessed by measuring OD630 within each well after the addition of TMB. Each antibody was labelled with the selection number (3) following the well from which the monoclonal antibody was obtained from the master-plate. N.B most clones possessed similar binding (or no binding) to multiple forms of Aβ, such as fibrils and monomers, Aβ coating was assumed to be similar between all forms of Aβ. Screening was performed measuring each clone once.

From the 3 different selections, a total of 49 FFB were identified. Next, the VHH domains were amplified with PCR (figure 6.6) and DNA sequences were obtained through Sanger sequencing through Macrogen, using the LMB3 primer. Sequences were reviewed and if issues were detected, manually corrected whenever possible using DNA Dynamo. A total of 9 sequences were excluded due to poor quality of the sequencing (table 6.2), reducing the number of unique sequences identified to 40.

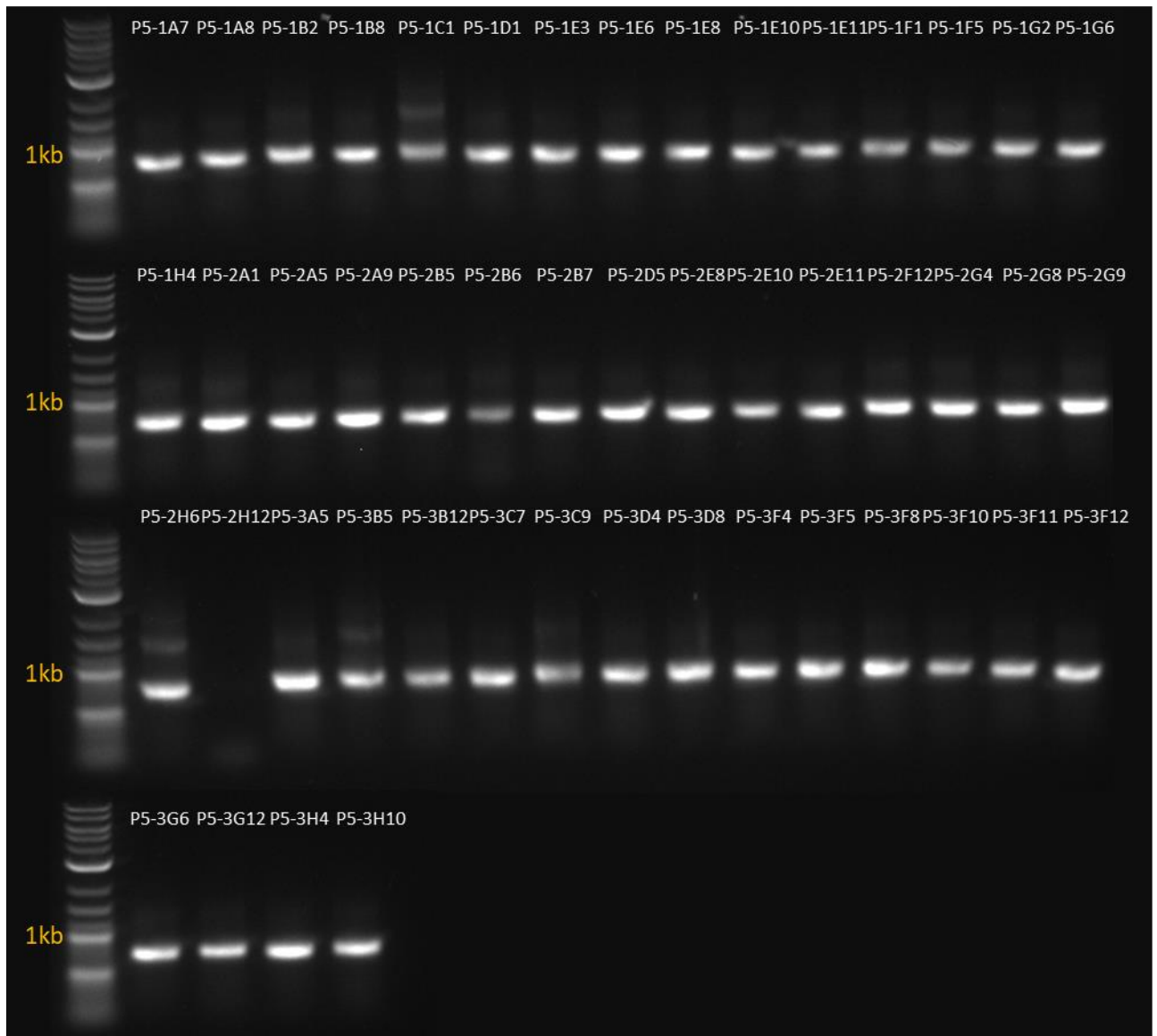


Figure 6-6: Antibody DNA sequence amplification through PCR

The 49 FF-specific antibodies identified through three rounds of biopanning were amplified through PCR. This was achieved by mixing small volumes (around 1 μ l) of the colonies expressing the antibodies of interest with the PCR mix (20.75 μ l DEPC-treated water, 2.5 μ l 10x standard Taq buffer, 0.5 μ l dNTP, 0.5 μ l Yol13 forward primer, 0.5 μ l Yol22 reverse primer and 0.25 μ l Taq DNA polymerase, for a total of 25 μ l per reaction), as described in section 2.18.6. Only the VHH domain was amplified. PCR products were run on a 1% (w/v) agarose gel in TAE buffer and visualized with SYBRTM Safe DNA gel stain. Quick-Load[®] purple 1 kb plus DNA ladder was used as molecular weight standard (Mw). IllustraTM ExostrarTM was used to remove unused dNTPs and primers before Sanger sequencing. N.B. Sample P5-2H12 is missing from this gel, but it was indeed sequenced.

Table 6-2: FFB amino acid sequences

Antibody	Sequence status	Protein sequence
P5-1A7	Corrected	EVQLVESGGGLVQAGGSLRLSCAASGRRFSRYTMGWFRQVPGKEREFVAAISSRSGSSTYYADSVKGRFTISRDNKNTMYLEMNSLKPEDTADYYCAADRSYSGSYTDRRAYEYWGQGTQVTVSS
P5-1A8	Intact	EVQLVESGGGLVQAGGSLRVSCAVSGRSFATSVMAWFRQAPGKQREFVASTGRPGTYADSVKGRFAISRDNKNTVYLEMNSLKPEDTAVYYCAAKSGGYRYSDFNDYRYWGQGTQVTVSS
P5-1B2	Intact	EVQLVESGGGFGQTGGSLRLSCTASGRTFSRRAMAWFRQAPGKEREIFVAISQSAFNTYYAESVKGRFIISRDNKSNMVFQMNSLKPEDTAVYYCAANSYHRSGLDLSQYLYRYWGQGTQVTVSS
P5-1B8	Intact	EVQLVESGGGLVQAGGSLRVSCAASGRTFSRYFMGWFRQAPGKEREFVATISRSGSTYYTDSVKGRFTISRDNKNAVYLQMNSLKPEDTAVYYCAADITRRVGVSRAGYGYKWPGGTQVTVSS
P5-1C1	Excluded	
P5-1D1	Intact	EVQLVESGGGLVQAGGSLRLSCAASGRTFSKVMGWFRQAPGKQRELVAISRSGSSTSYADPVKGRFTISRDNKNTMYLQNSLKPEDTAVYYCAARRYSRSTNFESDYPYWGQGLTVTVSS
P5-1E3	Intact	EVQLVESGGGLVQAGASRRLTCKASGRTFSRRPMGWFRQAPGKEREFVAVIDRRGTTTDTADSVKGRFTISRDNKNTMYLQNSLKPEDTAVYYCAARSYSGIAYLPNEYIYWGGGTQVTVSS
P5-1E6	Intact	EVQLVESGGGLVQAGGSLRLSCATSGRTFSKVMGWFRQAPGKEREFVAISGSGGRTWYADSVKGRFTISRDNKNTGYLQMNSLKPEDTAIYYCTASASLSTIVSGEGAYWGQGTQVTVSS
P5-1E8	Intact	EVQLVESGGGLVQAGGSLRVSCAVSGRSFATSVMAWFRQAPGKQREFVASTGRPGTYADSVKGRFAISRDNKNTVYLEMNSLKPEDTAVYYCAAKSGGYRYSDFNDYRYWGQGTQVTVSS
P5-1E10	Intact	EVQLVESGGGLVQAGGSLRVSCAASGRTFSRRTMGWWRAPGKEREFVAAINWNGERTWYADSVKGRFTISRDNKNTLYLQMNSLKPEDTAVYYCMTESGRYKGGGTQVTVSS
P5-1E11	Excluded	
P5-1F1	Excluded	
P5-1F5	Intact	EVQLVESGGGLVQAGASRRLTCKASGRTFSRRPMGWFRQAPGKEREFVAVIDRRGTTTDTADSVKGRFTISRDNKNTMYLQNSLKPEDTAVYYCAARSYSGIAYLPNEYIYWGGGTQVTVSS
P5-1G2	Intact	QVQLVESGGGLVQSGGSLRLSCAASGRTFSYTMGWFRQAPGKEREFVAISGSGGATYYADSVKGRFTISRDNKNTVYLQMNLSLKPEDTAVYYCARGGTWWSRLLGDYDRGGGTQVTVSS
P5-1G6	Intact	EVQLVESGGGLVQAEGSLRLSCASGRTFSRRDMGWFRQTPGEEREFVAHISRSGESTHYADSVKGRFTISRDNKNTVYLQMNLSLKPEDTAVYYCASARYGTQHFTTPGDYVYWGRTGLTVTVSS
P5-1H4	Intact	QVQLVESGGGLVQAGGSLRLSCAASGRTSRRYAMGWFRQAPGKEREFVASISRNNGTTVYDNPKEGRFTISRDNKNTVYLQMNLSLKPEDTAVYYCVADRRTAQDMAFRVRTDYDSWGQGTQVTVSS
P5-2A1	Intact	EVQLVESGGGLVQAGGSLRLSCAASGRTFSRRTMGWWRAPGKEREFVAAINWNGERTWYADSVKGRFTISRDNKNTLYLQMNSLKPEDTAVYYCMTESGRYKGGGTQVTVSS
P5-2A5	Intact	EVQLVESGGGLVQAGGSLRLSCTASGRRFSVSTMGWYRQVPGKERELVATISNIGRITYGEPVKGRFTISRDNKNTVYLDMDNLKSEDTAVYYCRVGTSLGKGLTVTVSS
P5-2A9	Intact	EVQLVESGGGLVQAGGSLRVSCAASGRTFSRRTMGWWRAPGKEREFVAAINWNGERTWYADSVKGRFTISRDNKNTLYLQMNSLKPEDTAVYYCMTESGRYKGGGTQVTVSS
P5-2B5	Corrected	EVQLVESGGGLAQPGGSLRLSCAASSTLRNYAMGWFRQAPGKEREFVAAFWSGSSTYYADSVKGRFTISKDNKNSLYLQMNLSLKPEDTAVYYCAAASPWRIRGQYDRGGGTQVTVSS
P5-2B6	Intact	EVQLVESGGGMVQAGGSLRLSCAQSGGTFNSYVMTWFRRAPGKEREFVAGISRRGSSSEYTDVSKGRFTISRDNKNTVSLMNNLKPEDTAIYYCAVYTSRHRYSDFKNDPEYGYWGQGTQVTVSS
P5-2B7	Intact	EVQLVESGGDLVQPGGSLRLSCASGIFSTNAMGWYRQAPGKQREFVARISTGGTITKYADVVKGRFTISRDNKNTVYLQMNLSLKPEDTAVYYCNAAGTSHLRPGPLWGQGTQVTVSS
P5-2D5	Intact	EVQLVESGGGLVQAGDSLRLSCAASGRTFSTRTMGWFRQAPGQREFVAAISWNGRSTAYADSVRGRFTISRDNKNTVYLEMNSLKPEDTAVYYCAARPFSSYTTREDGYRYWGQGTQVTVSS
P5-2E8	Intact	EVQLVESGGGLVQAGGSLRLSCAASGRTFSRFMGWFRQAPGKQRELVALTSIGTIVYADSVKGRFTISRDNKNTVYLQMNLTLPKPEDTGYYCAARRYGLGRIFDSDYWGQGLTVTVSS
P5-2E10	Intact	EVQLVESGGGLVQAGASRRLTCKASGRTFSRRPMGWFRQAPGKEREFVAVIDRRGTTTDTADSVKGRFTISRDNKNTMYLQNSLKPEDTAVYYCAARSYSGIAYLPNEYIYWGGGTQVTVSS
P5-2E11	Intact	EVQLVESGGDLLQPGGSLRLSCASGIFSTNAMGWYRQAPGKQREFVARISLGGTITKYADSVKGRFTISRDNKNTVYLQMNLSLKPEDTAVYYCNAAGTSHLRPGPLWGQGTQVTVSS
P5-2F12	Corrected	EVQLVESGGGLVQAGDSLRLVSCAASGRVFNYSYTMGWFRQAPGKEREFVASIYWSGSSAAYADSVQGRFAVSRDNTVYVYLQMNLSLKPEDTAVYYCAVASRNLGIVSRKREKNYDYWGQGTQVTVSS
P5-2G4	Corrected	QVQLVESGGGLVQAGGSLRVSCATASGIFSTNAMGWYRQAPGKQREFVARISTGGTITKYADSVKGRFTISRDNKNTVYLQMNLSLKPEDTAVYYCNAAGTSLRPGPLWGQGTQVTVSS
P5-2G8	Excluded	
P5-2G9	Intact	EVQLVESGGGLVQAGDSLTLSCAASERIFKTKTMGWFRQAPGKEREFVAAISKSGSTFSADSVKGRFTISRDNHNTVYLQMNLSLKPEDTAVYYCAAKSILRYNDRDSYAYWGQGTQVTVSS
P5-2H6	Excluded	
P5-2H12	Excluded	

P5-3A5	Intact	EVQLVESGGGLVQAGGSLRLSCAASGRTFSNRAVGWFRQAPGKEREFVAAITKNGQTTYADSVKGRFTISRDNKSMVYLQMDLSLP EDTANYYCAAGRFGTFSRYESGYRYWGQGTQVTVSS
P5-3B5	Intact	QQQLVESGGGLVQAGGSLRLSCAASGRTFSRRTVGWFRQAPGKEREWVSSITSNGGITPYADSVKGRFTISRDNKNTLYLQMNLDLKP EDTAVYYCAVARYCTSSPDSHYDYWGQGTQVTVSS
P5-3B12	Intact	EVQLVESGGGLVQAGASRRLTCKASGRTFSSRPMGWFRQAPGKEREFVAVIDRRGTTTDTADSVKGRFTISRDNKMMVYLQMNLSLK PEDTAVYYCAARSYSYGIAYLPNEYIYWGGQGTQVTVSS
P5-3C7	Intact	EVQLVESGGGLVQAGGSLRLSCEASGFSDVPIGWFRQAPGKQREFVARISTGGTITKYADSVKGRFTISRDNKNTVYLQMNLSLKPE DTAVYYCNAGTSHLRPGPLWGQGTQVTVSS
P5-3C9	Intact	EVQLVESGGGLVQAGGSLRVSCGASGRTFSRKAMGWFRQAPGKEREFVARISSRGGSTYYADSVKGRFTISRDNKNNMVSLLQMNLSLK DEDTAVYYCAAARNGRFWTSTSQFQDVNEYPYWGQGTQVTVSS
P5-3D4	Excluded	
P5-3D8	Corrected	QQQLVESGGGVVQAGASLKLSCAASGRTVSTYGMWFRQAPGKEREFVGAIRRSGETTYADSVKGRFTISRDNPKNTVYLQMTNLKS EDTAVYYCAADHERRWTIATRSSEYGSWGQGTQVTVSS
P5-3F4	Intact	EVQLVESGGGLVEAGGSLRLSCAASGRAFRSYAMGWFRQAPGKEREFVAAISRSGGRTSYADSVKGRFTISRDNKNTVYLQDLALPK EDTAVYYCAARHGSGRSDSPRAYEYWGQGTQVTVSS
P5-3F5	Corrected	EVQLVESGGGLVQAGASRRLTCKASGRTFSSRPMGWFRQAPGKEREFVAVIDRRGTTTDTADSVKGRFTISRDNKMMVYLQMNLSLK PEDTAVYYCAARSYSYGIAYLPNEYIYWGGQGTQVTVSS
P5-3F8	Corrected	EVQLVESGGGLVQAGGSLRLSCAASGRTFNNTYTMWFRQAPGKEREFVSVINRSRGTWYADSVTGRFTISRDNKNNMVSLLQMNLDL KPEDTAVYYCTRRRSGGSWLDQDPYWGQGTQVTVSS
P5-3F10	Corrected	EVQLVESGGGLVQPGGSLRLSCAASGRTFSRRNMGWFRQAPGKEREFVAGISWDGRITHYADAVKGRLLISRDNKSTVDLQMNLSLK PEDTAVYYCAARYGGIVDYTTNVDRWRYWGQGTQVTVSS
P5-3F11	Corrected	EVQLVESGGGLVQAGGSLKLSQASGFASRYWMHWVRQAPGKPEWVSSINSSGERTYRDSVKGRFTISRDNKNTLYLQMNLSL KSEDTAVYYCAKSGGSYLRGYEYDSWGQGTQVTVSS
P5-3F12	Corrected	EVQLVESGGGLVQAGGSLRLSCAASRRTFSPRFMAWFRQAPGKEREFVASISRSTYYADSVKGRFTISRDNKMYLQMTSLKPEDTA VYYCAARMKSDGTFIDWGQGTQVTVSS
P5-3G6	Excluded	
P5-3G12	Excluded	
P5-3H4	Intact	EVQLVESGGGLVQPGGSLRLSCQASGFASSTMYWVRQTPGKLEWVSSITRGGTNTYYRDSVKGRFTISRDDAKNTLFLQMTNLKP EDTALYYCAKARGVGVYFAGYDYWGQGTQVTVSS
P5-3H10	Intact	EVQLVESGGGLVQAGGSLKLSVCSGRTFSRRAMGWFRQAPGKEREFITGSRSSGRIFYADSVKGRFTISRDNVKTVYLQMNLSLKPE DTAVYYCAAQFGPTFDPRADEYNYWGQGTQVTVSS

Further analysis of the sequences revealed the presence of homologous antibodies (table 6.3), further reducing the number of unique antibody sequences to 35. From the sequences analysed, two particular antibodies shared almost identical amino acid chains, save for a single residue (V and L from sequence 3 and 4 respectively in table 6.3). This was treated as a consequence of sequencing variability and sequence 4 was chosen to be carried over for the next steps, excluding 3.

Table 6-3: identification of sequence homologies within the discovered FFB

Sequence	Hit number
EVQLVESGGGLVQAGASRRLTCKASGRTFSSRPMGWFRQAPGKEREFVAVIDRRGTTTDTADSVKGRFTISRDNKMMVYLQMN SLKPEDTAVYYCAARSYSYGIAYLPNEYIYWGGQGTQVTVSS	5
EVQLVESGGGLVQAGGSLRVSCAASGRTFSRRTMGWWRAPGKEREFVAAINWNGERTWYADSVKGRFTISRDNKNTLYLQ MNSLKPEDTAVYYCMTESGRYKQGTQVTVSS	2
EVQLVESGGGLVQAGGSLRVSCAVSGRSFATSVMAWFRQAPGKQREFVASTGRPGTYADSVKGRFAISRDNKNTVYLEMN SLKPEDTAVYYCAAQSGGRYSDFNDYRYWGQGTQVTVSS	1
EVQLVESGGGLVQAGGSLRLSCAVSGRSFATSVMAWFRQAPGKQREFVASTGRPGTYADSVKGRFAISRDNKNTVYLEMN SLKPEDTAVYYCAAQSGGRYSDFNDYRYWGQGTQVTVSS	1
EVQLVESGGGLVQAGGSLRLSCATSGRTFSTKVMGWFRQAPGKEREFVAAISGGRTWYADSVKGRFTISRDNVKTGYLQMN SLKPEDTAIYYCTASASLSTIVSGEGAYWGQGTQVTVSS	1

EVQLVESGGDLVQPGGSLRLSCASGSIFFSTNAMGWYRQAPGKQREFVARISTGGTITKYADVVKGRFTISRDNKNTVYLQMNSL KPEDTAVYYCNAAGTSHLRPGPLWGQGTQVTVSS	1
EVQLVESGGGLAQPGGSLRLSCAASTTLRNYAMGWFRQAPGKEREVFAAFSWSGSSTYYADSVKGRFTISKDNAKNSLYLQMNSL KPEDTAVYYCAAASPWRLIRGQYDYRGQGTQVTVSS	1
EVQLVESGGDLLQPGGSLRLSCASGSIFFSTNAMGWYRQAPGKQREFVARISLGGTITKYADSVKGRFTISRDNKNTVYLQMN LKPEDTAVYYCNAAGTSHLRPGPLWGQGTQVTVSS	1
EVQLVESGGGLVEAGGSLRLSCAASGRAFRSYAMGWFRQAPGKEREVFAAISRSRGGRTSYADSVKGRFTISRDNKNTVYLQDAL KPEDTAVYYCAARHGSGRSDSPRAYEYWGQGTQVTVSS	1
EVQLVESGGGFGQTGGSLRLSCTASGRTFSRRAMAWFRQAPGKEREIVAAISQSAFNYYAESVKGRFIISRDNSKNMVFLOMNG LKPEDTAVYYCAANSYHRSGDLSQYLYRYWGQGTQVTVSS	1
EVQLVESGGGLVQAGGSLRLSCEASGFSFDDVPIGWFRQAPGKQREFVARISTGGTITKYADSVKGRFTISRDNKNTVYLQMN KPEDTAVYYCNAAGTSHLRPGPLWGQGTQVTVSS	1
EVQLVESGGGLVQAEGLRLSASGRTFSSRDIMGWFRQTPGEEREFVAHISRSGESTHYADSVKGRFTISRDNKNTVYLQMN KPEDTAVYYCASARYGTQHFTTPGDYVYWGRTLVTVSS	1
EVQLVESGGGLVQPGGSLRLSCAASGRTFSRRNMGWFRQAPGKEREVAGISWDGRITHYADAVKGRLIISRDNAKSTVDLQMN NLKPEDTAVYYCAARYGGIVDYTTNVDWRWYWGQGTQVTVSS	1
EVQLVESGGGMVQAGGSLRLSQAQSGGTFSNYVMTWFRAPGKEREVAGISRRGGSSEYTDVSKGRFTISRDNKNTVLSLEMN NLKPEDTAVYYCAVYTSRRHYRDSFKNPDEYGYWGQGTQVTVSS	1
QVQLVESGGGLVQAGGSLRLSCAASGRTSRRYAMGWFRQAPGKEREVVASISRNGGTTVYDNPVKGRFTISRDNKNTVYLQMN SLKPEDTAVYYCVADRRTAQDMAFRVRTDYDSWGQGTQVTVSS	1
QVQLVESGGGLVQSGGSLRLSCAASGRTFSYTMGWFRQAPGKEREVFAAISGSGGATYYADSVKGRFTISRDNKNTVYLQMN SLKPEDTAVYYCARGGTWGSRRLLGDYDYRGQGTQVTVSS	1
EVQLVESGGGLVQAGDLSRLSCAASGRTFSTRIMGWFRQAPGQEREVFAAISWNGRSTAYADSVRGRFTISRDNKNTVYLEMN SLKPEDTAVYYCAARPFSSYTTREDGYRYWGQGTQVTVSS	1
EVQLVESGGGLVQAGGSLRLSCAASRRFTSPRFMAWFRQAPGKEREVVASISRSYTYADSVKGRFTISRDNKNTVYLQMTSLKPED TAVYYCAARMKSDGTFIDWGQGTQVTVSS	1
EVQLVESGGGLVQAGDLSRVSCAASGRVFNSTYTMGWFRQAPGKEREVVASIYWSGSSAAYADSVQGRFAVSRDNAENTVYLQMN NSLKPEDTAVYYCAVASRNLGIVSRKREKNYDYWGQGTQVTVSS	1
EVQLVESGGGLVQAGDLSLSCAASERIFKTKTMGWFRQAPGKEREVFAAISKSGGSTFADSVKGRFTISRDNHNTVYLQMN KPEDTAVYYCAAASSILRYNDRDSYAYWGQGTQVTVSS	1
EVQLVESGGGLVQAGGSLRLSCTASGRRFSVSTMGWYRQVPGKERELVATISNSGRITYGEPVKGRFTISRDNKNTVYLQMDNL KSEDTAVYYCRVGTSLGKGLTVTVSS	1
EVQLVESGGGLVQAGGSLKLSQASGFASFYWMHWVWRQAPGKGPVWVSSINSSGERTYRDSVKGRFTISRDNKNTVYLQMN NSLKSEDTAVYYCAKSGSSYLRYEYDSWGQGTQVTVSS	1
EVQLVESGGGLVQAGGSLRVSCAASGRTFSSYFMGWFRQAPGKEREVATISRSGSTTYTDSVKGRFTISRDNKNTVYLQMN LKPEDTAVYYCAADITRRVGSVRAGYGYKWGPGTQVTVSS	1
EVQLVESGGGLVQAGGSLKLSQASGRTFSSRRAMGWFRQAPGKEREVITGISRSSGRIFYADSVKGRFTISRDNKNTVYLQMN PEDTAVYYCAAQFGPTFDPRRADEYNYWGQGTQVTVSS	1
EVQLVESGGGLVQAGGSLRVSCGASGRTFSRKAMGWFRQAPGKEREVVARISSRGGSTYYADSVKGRFTISRDNKNTVYLQMN SLKDEDTAVYYCAAARNGRFWTSTSQFDVNEYPYWGQGTQVTVSS	1
EVQLVESGGGLVQAGGSLRLSCAASGRRFSRYTMGWFRQVPGKEREVFAAISRSRSGSTYYADSVKGRFTISRDNKNTVYLEMN SLKPEDTADYYCAADRSYSGSYTYDTRRAYEYWGQGTQVTVSS	1
EVQLVESGGGLVQPGGSLRLSQAASGFASFSSSTMYWVWRQTPGKLEWVSSITRGGTNTYRDSVKGRFTISRDDAKNTLFLQMTN LKPEDTALYYCAKARGVGVYFAGYDYWGQGTQVTVSS	1
EVQLVESGGGLVQAGGSLRLSCAASGRTFNNTYMAWFRQAPGKEREVSVINRSGIRTWYADSVTGRFTISRDNKNTVYLQMN DLKPEDTAVYYCTRRSGGSWLDLDPDYWGQGTQVTVSS	1
QVQLVESGGGLVQAGGSLRLSCAASGRTFSRRVGMWFRQAPGKEREWVSSITSGGITPYADSVKGRFTISRDNKNTVYLQMN LKPEDTAVYYCAVARYCTSSPDSSHIDYWGQGTQVTVSS	1
EVQLVESGGGLVQAGGSLRLSCAASGRTFSRFRMGWFRQAPGKQRELVASLTSIGTIVYADSVKGRFTISRDNKNTVYLQMN KPEDTGYYCAARRYGLGRIFDSDYWGQGTQVTVSS	1
QVQLVESGGGLVQAGGSLRVSTASGSIFFSTNAMGWYRQAPGKQREFVARISTGGTITKYADSVKGRFTISRDNKNTVYLQMN LKPEDTAVYYCNAAGTSHLRPGPLWGQGTQVTVSS	1
EVQLVESGGGLVQAGGSLRLSCAASGRTFSNRAVGMWFRQAPGKEREVFAAITKNGQTTYADSVKGRFTISRDNKNTVYLQMN LSPEDTANYCAAGRFGTFSRYESGYRYWGQGTQVTVSS	1
QVQLVESGGGVQAGASLKLSCAASGRTVSTYGMWFRQAPGKEREVGAIRRSRTTYADSVKGRFTISRDNKNTVYLQMTN LKSEDTAVYYCAADHERRWTIATRSSEYGSWGQGTQVTVSS	1
EVQLVESGGGLVQAGGSLRLSCAASGRTFSRRTMGWWRAPGKEREVFAAINWNGERTWYADSVKGRFTISRDNKNTVYLQMN NSLKPEDTAVYYCMTESGRYKGGQGTQVTVSS	1
EVQLVESGGGLVQAGGSLRLSCAASGRTFSSKVMGWFRQAPGKQRELVAVISRSGSSTYADVPKGRFTISRDNKNTVYLQMN LKPEDTAVYYCAARRYSRSTNFESDYPYWGQGTQVTVSS	1

Finally, with the consideration of the sequence homologies, a total of 34 unique FFB were discovered (table 6.4).

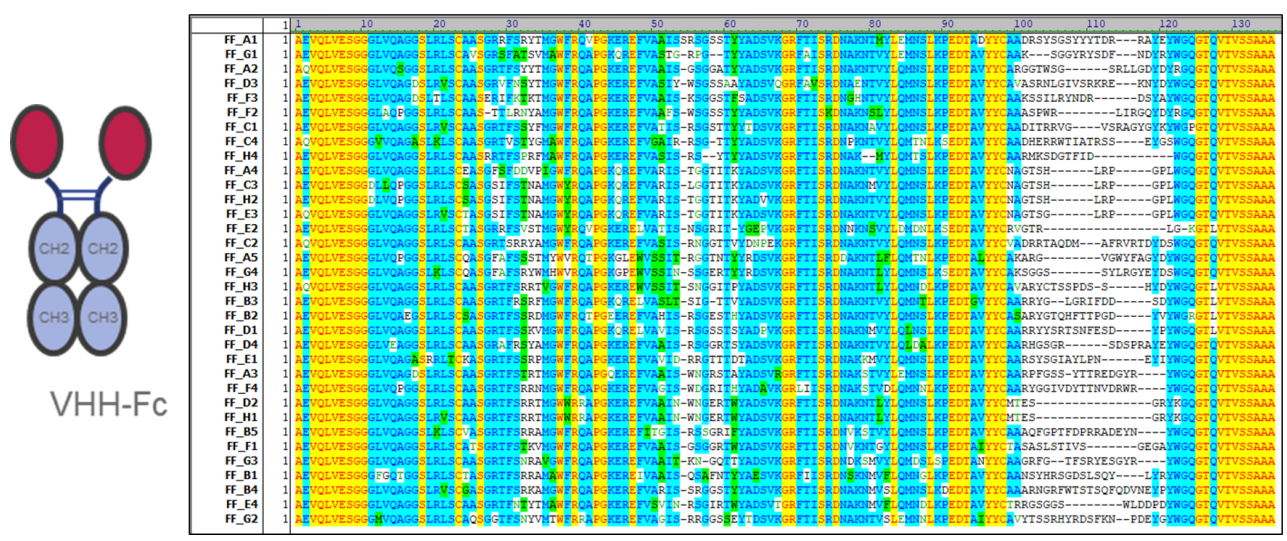
Table 6-4: Unique FFB sequences

Antibody ID*	Sequence
A1	EVQLVESGGGLVQAGGSLRLSCAAS GRFRSRYT MGWFRQVPQKEREVFAA ISRSGSST YYADSVKGRFTISRDNNAKNTMYLEMNSLKPEDTADYY CAADRSYSGSYITDRRAYEYW GGGTQVTVSS
B1	EVQLVESGGGFGQGGSLRLSCTAS GRTFSRRR MAWFRQAPGKEREVAA ISQSAFNT YYAESVKGRFIISRDNKNMVFLOMNSLKPEDTAVYYC AAANSYHRSGDLSQLYRYW GGGTQVTVSS
C1	EVQLVESGGGLVQAGGSLRVSCAAS GRTFSRYF MGWFRQAPGKEREVAT ISRSGSTT YYTDSVKGRFTISRDNNAKNAVYLQMNLSLKPEDTAVYYC AADITRRVGVSRAGYGYKYW GGGTQVTVSS
D1	EVQLVESGGGLVQAGGSLRLSCAAS GRTFSKYM MGWFRQAPGKQRELVAA ISRSGSST SYADPVKGRFTISRDNNAKNTMYLQNSLKPEDTAVYYC AARRYSRTSNFESDYPIW GGGTQVTVSS
E1	EVQLVESGGGLVQAGASRRLTCKAS GRTFSRRP MGWFRQAPGKEREVAV IDRRGTTT DTADSVKGRFTISRDNNAKNTMYLQMNLSLKPEDTAVYYC AARSYGGIAYLPNEYIYW GGGTQVTVSS
F1	EVQLVESGGGLVQAGGSLRLSCTAS GRTFSTKY MGWFRQAPGKEREVFAA ISGSGGRT WYADSVKGRFTISRDNVKNVYLGQMNLSLKPEDTAVYYC TASASLSTIVSDEGAYW GGGTQVTVSS
G1	EVQLVESGGGLVQAGGSLRLSCAVS GRSFATSY MAWFRQAPGKQREFVA ITGRPGT YYADSVKGRFAISRDNNAKNTVYLEMNSLKPEDTAVYYC AAKSGGYRYSDFNDRYVW GGGTQVTVSS
H1	EVQLVESGGGLVQAGGSLRVSCAAS GRTFSRRT MGWWRAPGKEREVFAA INWNGERT WYADSVKGRFTISRDNNAKNTLYLQMNLSLKPEDTAVYYC MTESGRYK GGGTQVTVSS
A2	QVQLVESGGGLVQAGGSLRLSCAAS GRTFSYTY MGWFRQAPGKEREVFAA ISGSGGAT YYADSVKGRFTISRDNNAKNTVYLMNSLKPEDTAVYYC CARGGTWGSRLLDGDIYW GGGTQVTVSS
B2	EVQLVESGGGLVQAGGSLRLSCTAS GRTFSRRD MGWFRQTPGEEREVFA HSRSGESTH YADSVKGRFTISRDNNAKNTVYLMNSLKPEDTAVYYC ASARYGTHFTTPGDYVYW GRGLTVTVSS
C2	QVQLVESGGGLVQAGGSLRLSCAAS GRTFSRYA MGWFRQAPGKEREVFA ISRRGGT TVYDNPVKGRFTISRDNNAKNTVYLMNSLKPEDTAVYYC WADRRTAQDMAFRVTDYDWS GGGTQVTVSS
D2	EVQLVESGGGLVQAGGSLRLSCAAS GRTFSRRT MGWWRAPGKEREVFAA INWNGERT WYADSVKGRFTISRDNNAKNTLYLQMNLSLKPEDTAVYYC MTESGRYKGG GGGTQVTVSS
E2	EVQLVESGGGLVQAGGSLRLSCTAS GRFRSVST MGWYRQVPQKEREVAT ISNSGRIT YGEVPKGRFTISRDNNAKNTVYLDMDNLKSEDTAVYYC RVGTRL GGKGLTVTVSS
F2	EVQLVESGGGLVQAGGSLRLSCTAS TLRNYA MGWFRQAPGKEREVFAA ISWGSST YYADSVKGRFTISKDNNAKNTLYLQMNLSLKPEDTAVYYC AAASPWRLRIGQDYR GGGTQVTVSS
G2	EVQLVESGGGMVQAGGSLRLSCTAS GGTFSNYY MTWFRAPGKEREVFA ISRRGSSEY YDTSVKGRFTISRDNNAKNTVLEMMNSLKPEDTAVYYC AVYTSRHYRDSFKNPDEYVW GGGTQVTVSS
H2	EVQLVESGGDLVQPGGSLRLSCTAS GSIFSTNA MGWYRQAPGKQREFVAR ISTGGTIT KYADSVKGRFTISRDNNAKNTVYLMNSLKPEDTAVYYC NAGTSHLRPGPLW GGGTQVTVSS
A3	EVQLVESGGGLVQAGGSLRLSCTAS GRTFSTRT MGWFRQAPGQEREVFAA ISWNGRST AYADSVRGRFTISRDNNAKNTVYLEMNSLKPEDTAVYYC CAARPGSSYITREDGRIYW GGGTQVTVSS
B3	EVQLVESGGGLVQAGGSLRLSCTAS GRTFSRRP MGWFRQAPGKQRELVAA LSIGTIT YYADSVKGRFTISRDNNAKNTVYLMNTLKPEDTAVYYC AARYGLGRIFDSDIYW GGGTQVTVSS
C3	EVQLVESGGDLVQPGGSLRLSCTAS GSIFSTNA MGWYRQAPGKQREFVAR ISLGGTIT KYADSVKGRFTISRDNNAKNTVYLMNSLKPEDTAVYYC NAGTSHLRPGPLW GGGTQVTVSS
D3	EVQLVESGGGLVQAGGSLRVSCAAS GRVFNSTY MGWFRQAPGKEREVFA ISWGSST AYADSVQGRFAVSRDIAENTVYLMNSLKPEDTAVYYC AVASRNLIIVSRKREKNDYDYG GGGTQVTVSS
E3	QVQLVESGGGLVQAGGSLRVSCAAS GSIFSTNA MGWYRQAPGKQREFVAR ISTGGTIT KYADSVKGRFTISRDNNAKNTVYLMNSLKPEDTAVYYC NAGTSHLRPGPLW GGGTQVTVSS
F3	EVQLVESGGGLVQAGDSLRLSCTAS GRIFKTKT MGWFRQAPGKEREVFAA ISKSGGST FADSVKGRFTISRDNHNTVYLMNSLKPEDTAVYYC AAKSSILRYNDRDSYAYW GGGTQVTVSS
G3	EVQLVESGGGLVQAGGSLRLSCTAS GRTFSNRA VGWFRQAPGKEREVFAA ITKNGQT YYADSVKGRFTISRDNNAKNTVYLMNSLKPEDTAVYYC AAGRFGTFSRYESGYRYW GGGTQVTVSS
H3	QVQLVESGGGLVQAGGSLRLSCTAS GRTFSRRT VGWFRQAPGKEREVSS ITSNGGIT PYADSVKGRFTISRDNNAKNTVYLMNSLKPEDTAVYYC AVARYCTSSPDSHYDIW GGGTQVTVSS
A4	EVQLVESGGGLVQAGGSLRLSCEAS GSFDDVPI GWFRQAPGKQREFVAR ISTGGTIT KYADSVKGRFTISRDNNAKNTVYLMNSLKPEDTAVYYC NAGTSHLRPGPLW GGGTQVTVSS
B4	EVQLVESGGGLVQAGGSLRVSCGAS GRTFSRKA MGWFRQAPGKEREVFA ISRRGSST YYADSVKGRFTISRDNNAKNTVYLMNSLKPEDTAVYYC AAARNGRFTSTSQFDVNEYPIYW GGGTQVTVSS
C4	QVQLVESGGGVVQAGASLRLSCTAS GRTVSTYG MAWFRQAPGKEREVFA IGARRSGTT YYADSVKGRFTISRDNNAKNTVYLMNSLKPEDTAVYYC AADHERRWTIATRSSEYGSW GGGTQVTVSS
D4	EVQLVESGGGLVEAGGSLRLSCTAS GRAFRSYA MGWFRQAPGKEREVFAA ISRSGGRTS YADSVKGRFTISRDNNAKNTVYLDALKPEDTAVYYC AARHGSGRSDSPRAYEYW GGGTQVTVSS
E4	EVQLVESGGGLVQAGGSLRLSCTAS GRTFNITY MAWFRQAPGKEREVSV INRSGRIT WYADSVTGRFTISRDNNAKNTVYLMNSLKPEDTAVYYC TRRSGSGSWLDDPDYW GGGTQVTVSS
F4	EVQLVESGGGLVQPGGSLRLSCTAS GRTFSRRN MGWFRQAPGKEREVFA ISWDGRIT HYADAVKGRLLISRDNNAKNTVYLDQMNLSLKPEDTAVYYC AARYGGIVDYTTNVDWRWRYW GGGTQVTVSS
G4	EVQLVESGGGLVQAGGSLKLSQAS GFAFSRYW MHWVFRQAPGKPEWVSS INSSGERT YYRDSVKGRFTISRDNNAKNTLYLQMNLSLKPEDTAVYYC AKSGSSYLRYGYEYDYSW GGGTQVTVSS
H4	EVQLVESGGGLVQAGGSLRLSCTAS RRTFSRRP MAWFRQAPGKEREVFA ISRSY YYADSVKGRFTISRDNNAKNTVYLMNSLKPEDTAVYYC AARMSDGTGFIW GGGTQVTVSS
A5	EVQLVESGGGLVQPGGSLRLSCTAS GFAFSST MYWVRQTPGKLEWVSS TRGGTNT YYRDSVKGRFTISRDNNAKNTLFLQMNLSLKPEDTAVYYC ARGVGVWYFAGDYIYW GGGTQVTVSS
B5	EVQLVESGGGLVQAGGSLKLSVCA GRTFSRRR MGWFRQAPGKEREVFA ISRSSGRI FYADSVKGRFTISRDNNAKNTVYLMNSLKPEDTAVYYC AAQFGPTFDPRADEYVYW GGGTQVTVSS

*Antibody ID determined by position in Twist order with Lyophilized DNA. This was done to distinguish FFB from FB.

Within the different sequences, CDR1 is highlighted in green, CDR2 highlighted in blue and CDR3 highlighted in red.

These FFB sequences were used as the basis to order human-Fc constructs from Twist using proprietary vectors and cloning protocols. This time, antibodies were only ordered in VHHC format, as previous analysis of fibrils binders revealed this format to usually possess the most effective binding to the target. Upon ordering, antibody sequences were aligned (figure 6.7) to reveal further similarities between the sequences, such as identical CDR3 regions in antibodies A4, C3 and H2. The 34 sequences were preserved regardless of CDR3 homology as the sequence did vary in structural or other CDR regions.



the variability (and responsibility for binding) found in the different antibodies [298]. The comparison of all anti-A β antibodies revealed that 2 CDR3 sequences were homologous in both FB and FFB (figure 6.8), indicating that for these molecules the CDR3 sequence was positively selected twice in two different experiments.

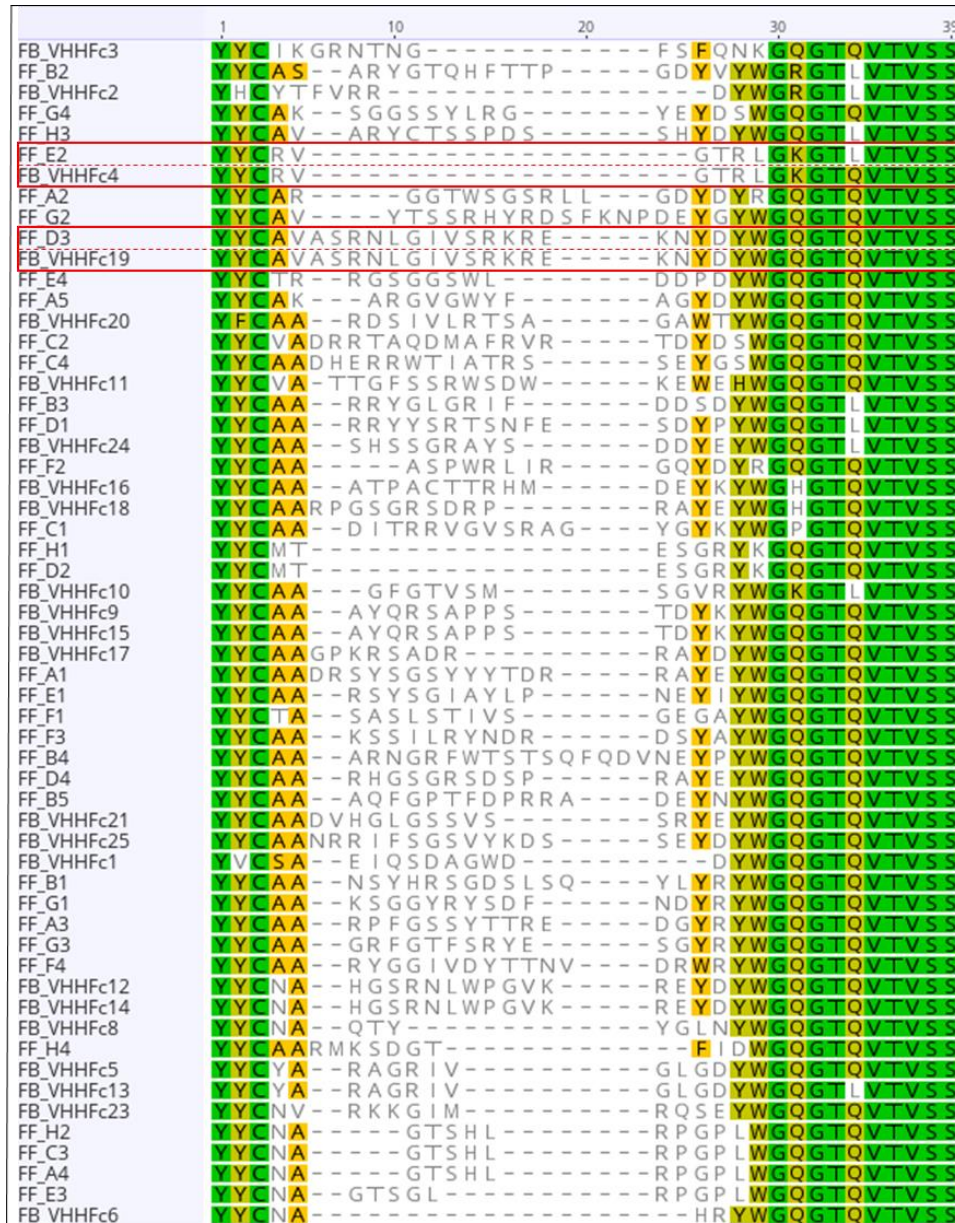


Figure 6-8: Alignment of FFB and FB CDR3 sequences

FFB and FB C-terminal sequences were aligned. CDR3 sequence homology between binders from independent biopanning experiments and targeting different forms of A β were highlighted. Homologous CDR3 sequences were evidenced by red boxes. Sequences were considered identical if all but a single amino acid was different. FF indicated fragmented fibril binders while FB, fibril binders. Green boxes indicate 100% homology between sequences, Dark yellow boxes indicate 80-100% homolog, bright yellow boxes indicate 60-80% homology and grey residues with white background indicate less than 60% homology between sequences.

6.3 Antibody expression and purification

The 34 FFB VHHFc sequences were delivered as lyophilized DNA powder from Twist. The different sequences were resuspended to a final volume of 0.5 $\mu\text{g}/\mu\text{l}$ in ultrapure water. This was used to transfect Expi™293 cells following the methodologies described in section 2.20. Antibodies were incubated for 6 days following the addition of both enhancer solutions and the supernatant harvested at the 7th day of transfection. From this, around 2 ml of crude supernatant was obtained. Protein expression was then tested with BLI, using 1:4 diluted crude supernatant and measuring the binding of the different antibodies to AHC biosensors (figure 6.10). From this analysis it was possible to determine that all 34 antibodies were effectively expressed, albeit with different efficiencies, as evidenced by the different binding values observed during the association step. Mock supernatant did not bind to the biosensors. As seen during the expression of FB, the variability could be attributed to different factors such as cell passage, pipetting errors or inefficient transfection.

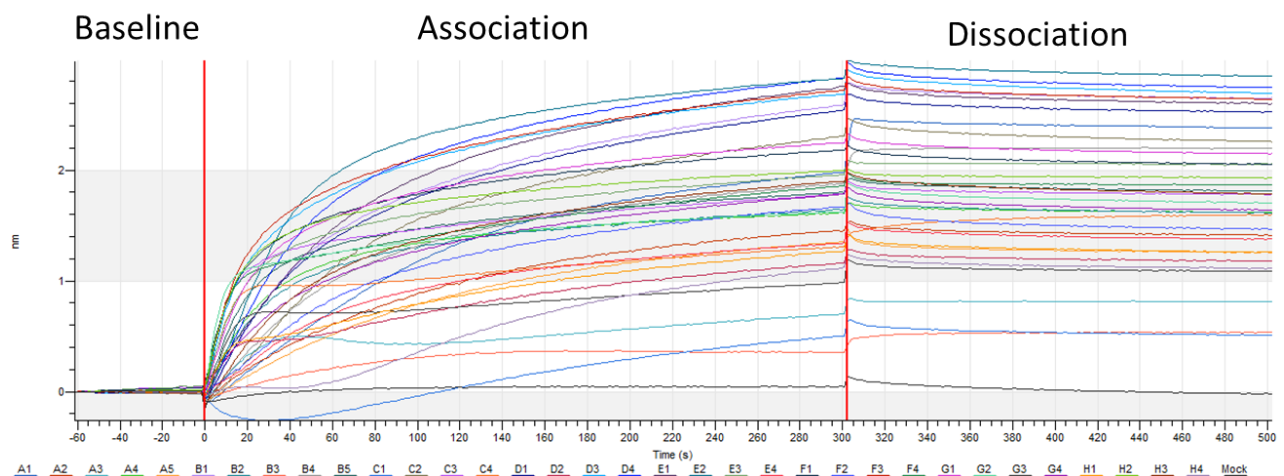


Figure 6-10: Antibody expression test with BLI

Lyophilized FFB VHHFc antibody DNA (1 μg) was transfected into Expi™293 cells and incubated for 7 days in order to produce antibodies. At the end of the transfection, protein expression was assessed using Octet. Crude supernatant was diluted 1:4 in kinetic buffer, and following a 60 second baseline, AHC tips were introduced to the diluted supernatant for a 5 minute association. Following association, dissociation was measured in kinetic buffer. The obtained sensogram revealed that the antibodies were successfully expressed in the Expi™293 system, as evidenced by the increase in binding (nm) values during the association step. Expression varied between samples, as some were seen to possess a binding of 2.5 nm while others a binding of 0.1. Mock supernatant was used as a blank control, which failed to show any binding to the AHC tips, as expected. Overall protein expression of FF-binders was lower than that of F binders.

Following the confirmation of the expression of the different antibodies, FFB were directly purified using the PhyNexus system, as described in section 2.21. From the small-scale purification of 1 ml of supernatant, 100 μ l of pure product were obtained; from this 2 μ l were resolved on 4-12% Bis-Tris Gels, to assess the level of antibody purity (figure 6.11). SDS-PAGE confirmed the antibodies to be of high purity in solution, with the expected molecular weight from the bands matching the expected weight from the amino acid sequences (around 75-80 kDa)

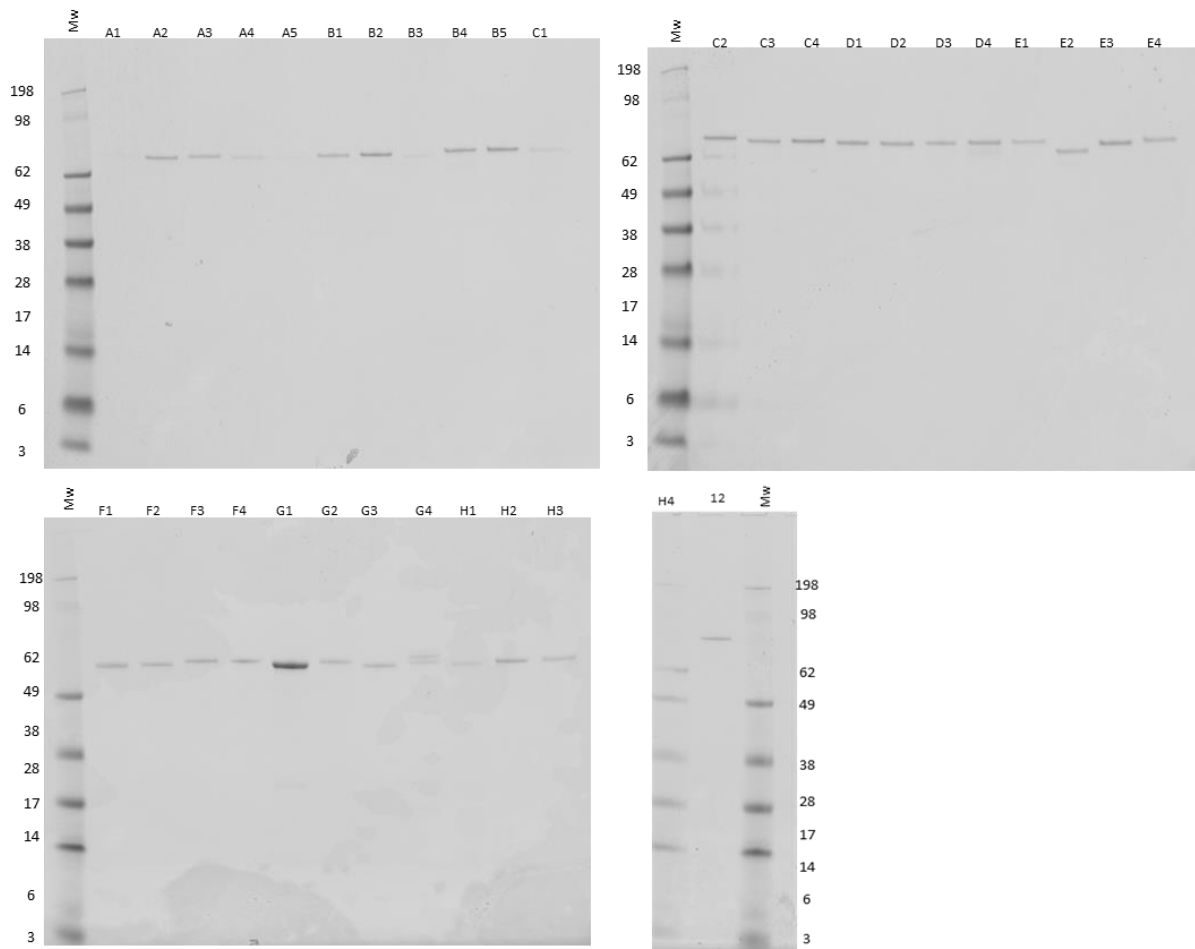


Figure 6-11: FFB small scale purification with PhyNexus system

SDS-PAGE of purified VHHFc antibodies (around 75-80 kDa) obtained from PhyNexus system. It is possible to see all bands matching the expected molecular weight. Variations in intensity depend on the concentration of protein purified. Antibody 12 was an unrelated control scFv antibody. Band purity was greater for this experiment compared to previous runs (as seen in figure 5.10) due to batch-to batch variations in the purification protocol.

Effective protein concentration was measured using a Nanodrop™ system. In order to obtain the most accurate values possible, the molecular weight and extinction coefficient (ϵ) were calculated

based on the protein sequences, using the ExPASy protoparm webtool

(<https://web.expasy.org/protparam/>). VHHFc parameters were calculated inputting a construct with

2x the VHH sequences belonging to each antibody and 2x human FC sequences

(DKTHTCPPCPAPPELLGGPSVFLFPPKPKDTLMISRTPEVTCVVVDVSHEDPEVKFNWYVDGVEVHNAKTKPREEQ

YNSTYRVVSVLTVLHQDWLNGKEYKCKVSNKALPAPIEKTISKAKGQPREPQVYTLPPSRDELTKNQVSLTCLVKGF

YPSDIAVEWESNGQPENNYKTTTPVLDSDGSFFLYSKLTVDKSRWQQGNVFCFSVMHEALHNHYTQKLSLSLSPGK)

to mimic a VHHFc molecule. The calculated extinction coefficient and molecular weight (in kDa) were

then used as input to measure the effective concentration of each antibody, using the “Other

protein ($\epsilon + MW$)” option within the nanodrop software interface and obtaining the concentration

shown in table 6.5.

Table 6-5: Calculation of the extinction coefficient and Molecular weight (Mw) of each VHHFc FFB

Antibody	Extinction coefficient (ϵ)	$\epsilon/1000$	Mw	kDa	mg/ml	nM
A1	129580	129.58	80197.97	80	0.013	162
A2	120640	120.64	78286.06	78	0.037	473
A3	125680	125.68	79102.81	79	0.077	973
A4	105740	105.74	77163.1	77	0.029	376
A5	139660	139.66	78452.49	78	0.012	153
B1	117660	117.66	79535.67	80	0.028	352
B2	114680	114.68	79216.91	79	0.069	871
B3	111700	111.7	78272.52	78	0.029	371
B4	122700	122.7	80130.13	80	0.037	462
B5	111700	111.7	79341.58	79	0.082	1034
C1	120640	120.64	79003.12	79	0.047	595
C2	111700	111.7	79639.66	80	0.074	929
C3	108720	108.72	77253.42	77	0.080	1036
C4	125680	125.68	78930.88	79	0.247	3129
D1	117660	117.66	78973.17	79	0.111	1406
D2	130720	130.72	76998.98	77	0.159	2065
D3	128660	128.66	79437.31	79	0.117	1473
D4	114680	114.68	78346.1	78	0.053	676
E1	114680	114.68	79017.4	79	0.017	215
E2	97720	97.72	75695.66	76	0.101	1334
E3	108720	108.72	76810.78	77	0.081	1055
E4	130720	130.72	78588.52	79	0.231	2939
F1	119720	119.72	77673.58	78	0.167	2150
F2	128660	128.66	78088.06	78	0.135	1729
F3	111700	111.7	78596.53	79	0.280	3562
F4	133700	133.7	79515.75	80	0.231	2905
G1	120640	120.64	78228.07	78	0.026	332
G2	117660	117.66	79909.71	80	0.516	6457
G3	114680	114.68	78452.16	78	0.232	2957
G4	142640	142.64	78734.49	79	0.126	1600
H1	130720	130.72	76970.93	77	0.064	831
H2	108720	108.72	77165.19	77	0.215	2786
H3	125805	125.805	78608.47	79	0.119	1514
H4	111700	111.7	77157.37	77	0.068	881

With low protein yields from a single transfection and purification experiment, the process was repeated until enough pure antibody was produced for the characterization assays, resulting in products ranging from 0.15 to 0.6 mg of pure protein.

6.4 Binding characterization

6.4.1 Binding pattern assessment with ELISA

With the identification, expression and purification of FFB, the next step was to assess the different binding patterns of each antibody through ELISA. This was performed using a set concentration of purified antibody (8 µg/ml) for each binding tested, and an array of targets which included biotinylated FF, biotinylated Genscript fibrils, biotinylated Gencust fibrils, biotinylated Genscript monomers, biotinylated Gencust m/o/pr (all added to streptavidin coated wells at 2 µg/ml) and streptavidin (at 5 µg/ml). For this assay the complete collection of FFB were tested alongside with two commercial anti-A β antibodies, acting as controls: anti fibril OC and anti-Beta-Amyloid rabbit polyclonal antibodies (previously referred as RB fibril polyclonal antibody), diluted at 1:1000 and 1:10000, respectively. Binding patterns were assessed by measuring the OD630 of each well after the addition of TMB. Each antibody was tested in the different conditions within the same plate, to avoid plate variability. Binding patterns analysis revealed (figure 6.12) that most FFB tested possessed high affinity for FF, Genscript fibrils, Gencust fibrils and Gencust m/o/pr, but not Genscript monomers or streptavidin. This higher affinity for aggregated A β elements was reflected differently in the different monoclonal binders, as some antibodies possessed higher affinities for Gencust m/o/pr (i.e. A1 and A2), Genscript fibrils (i.e. B5 and A4) or fragmented fibrils (i.e. F3). Other patterns observed were binders to Genscript fragmented fibrils and fibrils (i.e. E3) and Genscript fragmented fibrils, fibrils and Gencust m/o/pr (i.e. F1). In addition, some of the FFB were seen to bind to all A β elements tested (i.e. G4). Other antibodies were seen to possess high background binding (i.e. E4 and G2). Control antibodies were seen to have widely different binding affinities, with OC being able to bind all A β components with high affinity while RB fibril polyclonal was seen to have a preference to Gencust fibrils, Genscript monomers and Gencust m/o/pr.

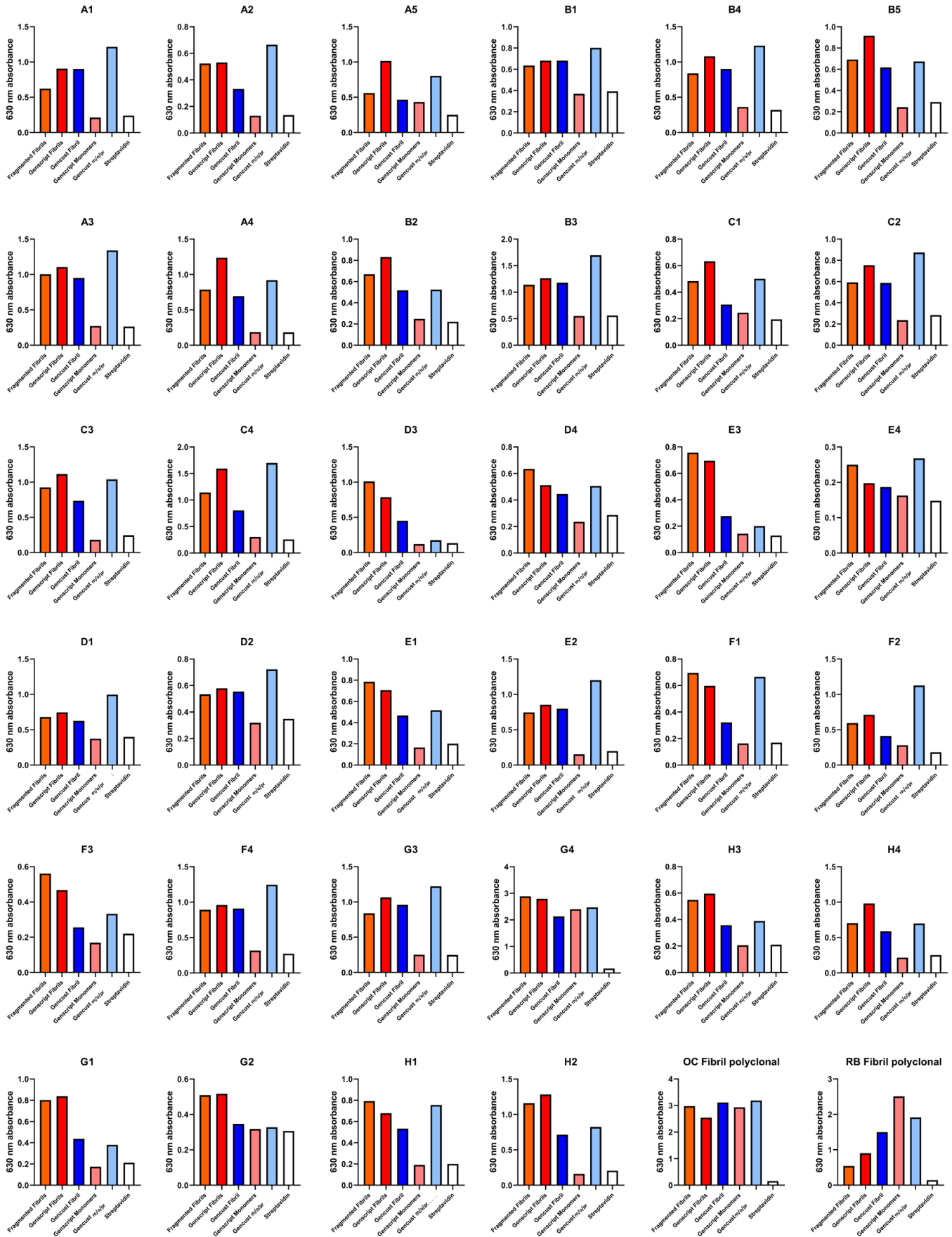


Figure 6-12: Monoclonal ELISA with purified antibodies.

Binding of the purified FF antibodies was tested at a set concentration (8 $\mu\text{g}/\text{ml}$). An array of biotinylated targets were used: fragmented Genscript fibrils, Genscript fibrils, Gencust fibrils, Genscript monomers and Gencust m/o/pr; all at 2 $\mu\text{g}/\text{ml}$. Blank wells without A β coating (Streptavidin) were also implemented as controls (at 5 $\mu\text{g}/\text{ml}$). Binding was assessed by the implementation of secondary-HRP conjugated antibodies and TMB substrate and measuring absorbance at 630 nm.

6.4.2 Identification of best FFB through BLI

As with the FB in section 5.5, binding and affinity were also tested with BLI. Initial experiments were performed using AHC tips, as FB experiments revealed this biosensor assay format was able to detect more antibody binding compared to the SA tip assay format. The AHC BLI protocol consisted in the loading of a 30 $\mu\text{g}/\text{ml}$ solution of purified FFB antibodies into each different biosensor, followed by a 60 second baseline in kinetic buffer, then a 15 minute association step where the loaded tips were submerged solutions containing A β (monomers, fibrils or fragmented fibrils at 25 $\mu\text{g}/\text{ml}$), and a 15 minute dissociation in kinetic buffer. Traces were aligned to baseline and compared together; an unrelated VHHFc antibody (here defined as '12') was used as a negative control to measure background binding of the fibrils to the biosensors; the signal from 12 was subtracted from all the other traces to obtain the final results.

In order to quantify the binding of the different antibodies, initial experiments measured the binding of the different antibodies to Genscript monomers (figure 6.13). No binding to monomers was observed

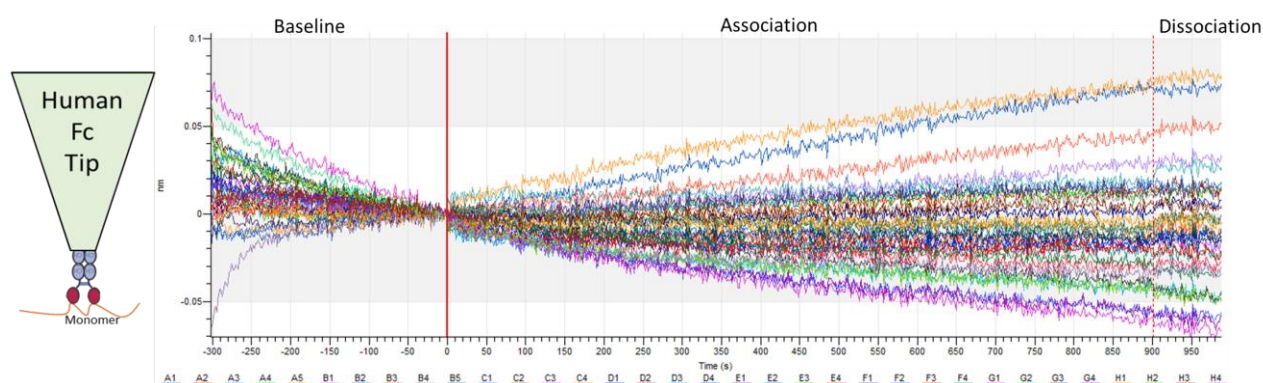


Figure 6-13: Genscript monomer binding with AHC tips

FFB (30 $\mu\text{g}/\text{ml}$) were loaded into AHC biosensors, as shown in the diagram on the left. Biosensors were then introduced to solutions of Genscript monomers (25 $\mu\text{g}/\text{ml}$). No binding was observed for any of the tested binders after a 15 minute association

FFB were then introduced to a solution containing Genscript fibrils (figure 6.14), surprisingly no binding was recorded to this type of A β aggregate.

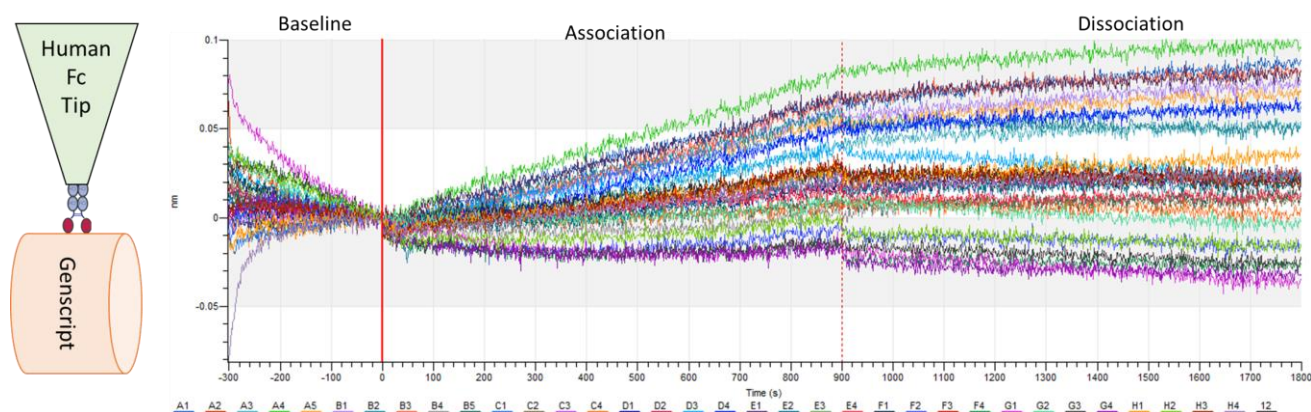


Figure 6-14:Genscript fibril binding with AHC tips

FFB (30 $\mu\text{g}/\text{ml}$) were loaded into AHC biosensors (as indicated in the diagram to the left), and then introduced to solutions of Genscript fibrils (25 $\mu\text{g}/\text{ml}$). No binding was observed for any of the tested binders after a 15 minute association.

Next, antibodies were tested against Genscript fibrils, to assess potential binding to different polymorphs of A β fibrils. Interestingly, binding was observed between some antibodies and the fibrils in solution (figure 6.15). As expected, FFB were observed to possess a complex binding kinetic to the fibrils themselves, explained with a 2:1 binding model given the divalent nature of the VHHFc particles. As before, due to this high level of complexity of this model, the association and dissociation constants were not calculated. Within this complex binding kinetics, some antibodies were seen to possess a good affinity to the tested target, with antibodies such as E2, B2 and A3 inducing a shift of around 0.7 nm. Remarkably, dissociation did not seem to occur in bound antibodies, potentially due to avidity effect.

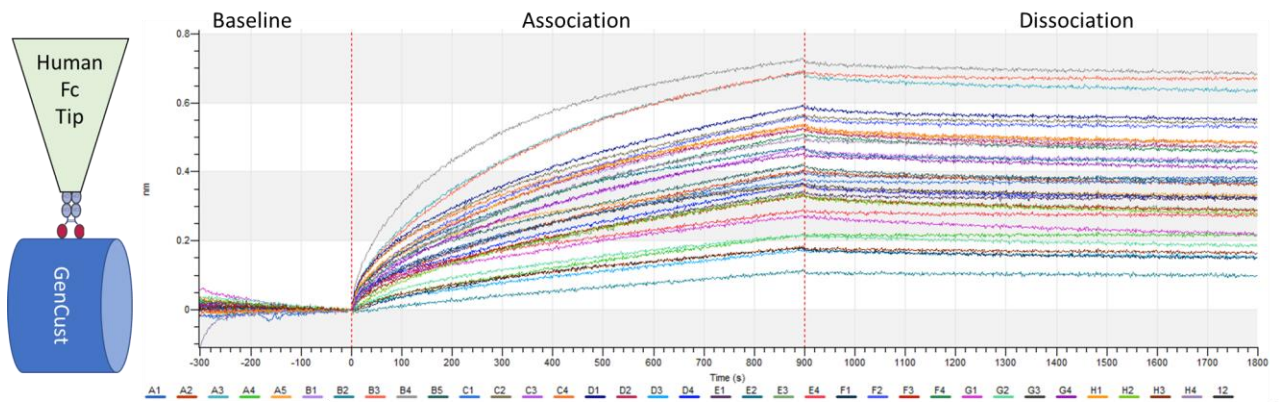


Figure 6-15:Gencust fibril binding with AHC tips

FFB (30 $\mu\text{g/ml}$) were loaded into AHC biosensors, and then introduced to solutions of Gencust fibrils (25 $\mu\text{g/ml}$), as indicated in the diagram to the left. Binding was confirmed for most binders. Antibodies possessed an array of on-rates, with B4 possessing the highest affinity and reaching a binding of 0.7 nm and E2 the lowest affinity, causing a shift of 0.1 nm. As seen with the FB, the antibodies did not seem to dissociate once bound to the fibrils in solution.

During the final assay with AHC tips, the different antibodies were introduced to biotinylated fragmented Genscript fibrils. During the association step, binding was observed in all antibodies tested. The shift (in nm) observed for each antibody varied in values that ranged from 0.2 nm in the antibodies with less affinity to the target, to 1 nm in the antibodies with the highest affinities towards fragmented fibrils (figure 6.16). FFB F3, H1, D4, G4 and C1 could be distinguished as the best binders with values between 0.8 and 1 nm. As seen with Gencust fibrils, the binding kinetics of the VHHFc antibodies were quite complex due to the format of the human-Fc construct, with a 2:1 kinetic model better explaining the binding traces of each one of the antibodies. Dissociation to fragmented fibril binders was also absent, most likely due to avidity effect.

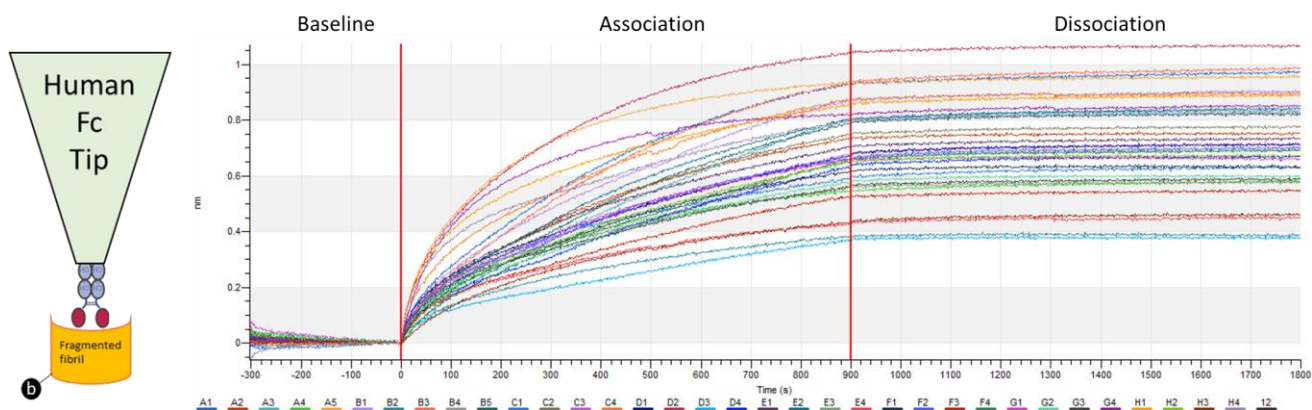


Figure 6-16: biotinylated fragmented Genscript fibril binding with AHC tips

FFB (30 $\mu\text{g}/\text{ml}$) were loaded into AHC biosensors, and then introduced to solutions of biotinylated fragmented Genscript fibrils (25 $\mu\text{g}/\text{ml}$), as illustrated in the diagram to the left. All of the antibodies tested were able to bind the target, albeit with different affinities, which ranged between 0.2 nm (D3) and 1 nm (F3). Like it was observed for Gencust fibrils, FFB seemed to form a stable bond with the target showing little to no dissociation.

With the successful binding of all VHHFc antibodies to biotinylated fragmented fibrils, the next step was to assess binding by switching the binding orientation. This was achieved by using SA tips, and loading the biotinylated FF (at 25 $\mu\text{g}/\text{ml}$) to the biosensors. Following a 60 second baseline, the loaded tips were introduced to solutions containing the antibodies diluted in kinetic buffer (at 30 $\mu\text{g}/\text{ml}$) for a 15-minute association. The assay was then concluded with a 15-minute dissociation in kinetic buffer. The implementation of SA tips revealed surprising results, as with this orientation, almost no binding was observed by any of the FFB tested; only a single antibody, G4 was seen to interact with the biotinylated FF in the biosensors (figure 6.17). This antibody possessed a good affinity for the target, inducing a shift of 0.7 nm and reaching high levels of biosensor saturation fairly quickly during the association phase. Following this step, the antibodies seemed to dissociate with fairly slow dissociation rates. As before, although a distinct association and dissociation curve could be observed, the exact kinetics for this antibody were not calculated due to the dimeric nature of the VHHFc particles and indeed, a 2:1 model needed to be used to explain the binding. The complexity of the kinetics of G4 could be better exemplified by the association curve never reaching a true plateau, and the dissociation curve never truly dissociating from the biosensors (reaching 0 nm).

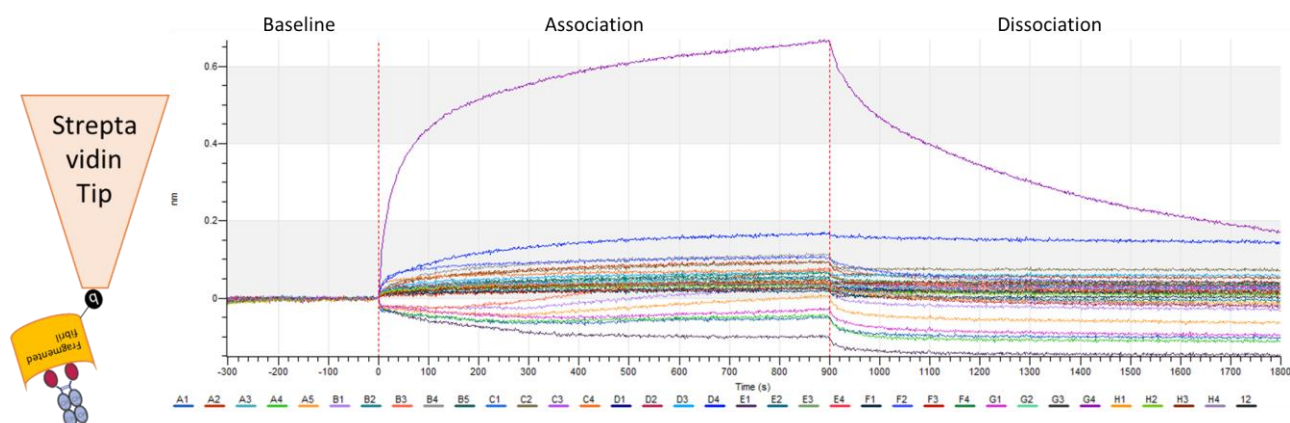


Figure 6-17: biotinylated fragmented Genscript fibril binding with SA tips

FFB (30 $\mu\text{g}/\text{ml}$) tested with SA tips, switching the orientation of binding. In this system, biotinylated fragmented Genscript fibrils (25 $\mu\text{g}/\text{ml}$) were loaded into SA biosensors (as indicated in the illustration to the left). Bound fibrils were then introduced to the antibodies in solution. Out of all of the antibodies tested, only one seemed to bind the target in this orientation, G4. The binding kinetics of this particular antibody perfectly matched the 2:1 model, as expected of the antibody format.

6.5 Functional assays

With the successful identification of antibody binders to fragmented and full length fibrils, the final step in the antibody characterization process was to assess the functionality of the antibodies themselves; this was tested with RT-QUIC. Preliminary functional assays consisted in the implementation of the already optimized $\text{A}\beta$ misfolding assay with shaking (see paragraph 2.5.3). This time, $\text{A}\beta$ monomers were incubated in the presence of increasing concentrations of antibody binders to assess if either the FFB or FB could prevent the formation of fibrils; RT-QUIC was performed for 72 hours. For this assay, 10 μM of Genscript $\text{A}\beta$ monomers were incubated as is or with the addition of increasing concentrations (1 μM , 5 μM and/or 10 μM , depending on the amount of antibody available at the time of this assay) of FFB A5, C1, E3 F4, and FB VHHFc1, VHHFc5 VHHFc11 and VHHFc19. These antibodies were chosen as they were the only ones with sufficient pure antibody to allow testing, after a new run of protein expression and purification. A total of 10 non seeded samples were used as non-seeded controls, to assess the effective misfolding of the monomers without the presence of antibodies in solution. ThT emission revealed comparable misfolding kinetics for all repeats (figure

6.18, A). Commercial anti-A β polyclonal antibody OC was used as a positive control, as this antibody was able to completely inhibit fibril formation when diluted 1:1000 in PBS (figure 6.18, B).

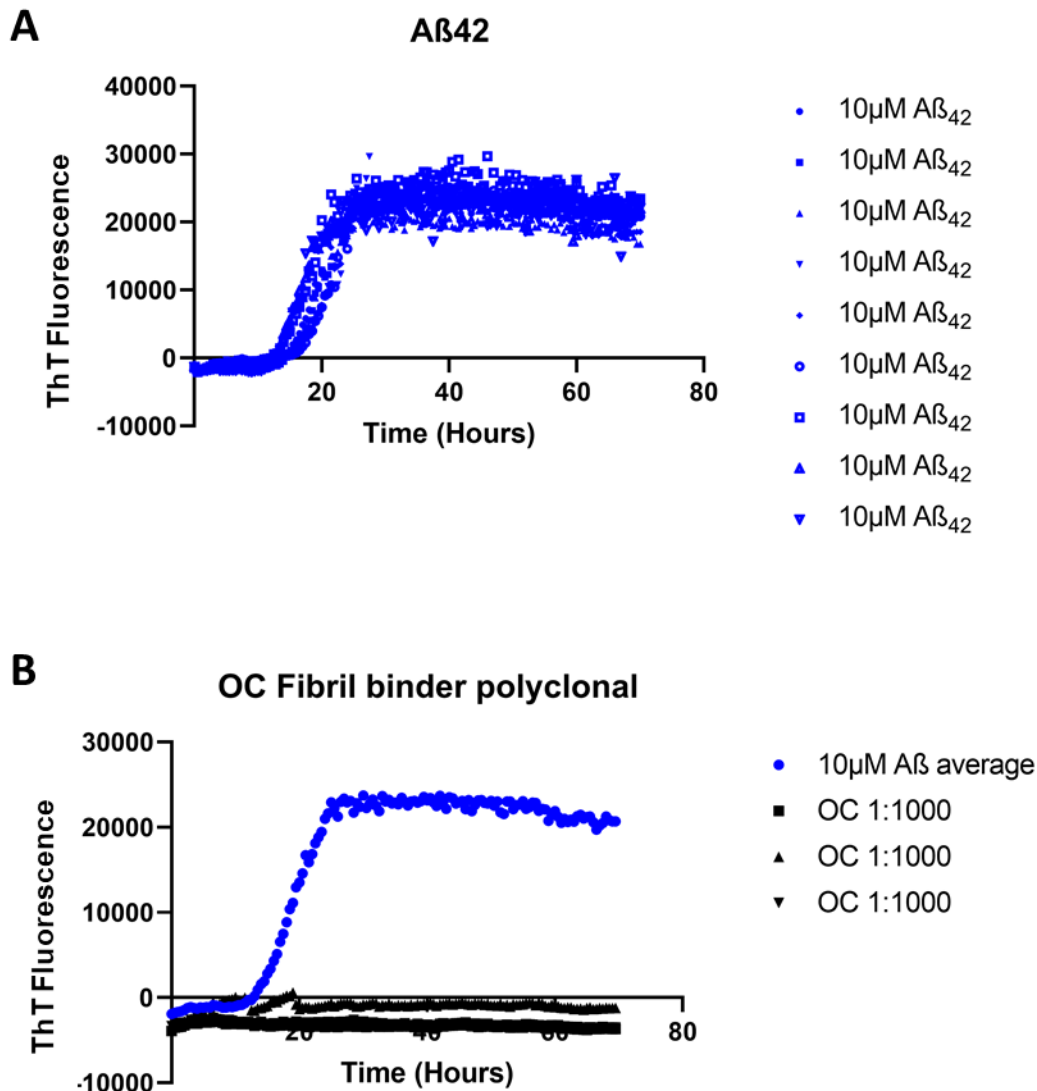


Figure 6-18: Functional assay- Assessment of monomer misfolding and control antibody inhibition

RT-QUIC was performed on freshly resuspended Genscript monomers. A: Multiple repeats (n=10) of monomer solutions (10 μ M) were placed in different wells and measured for 72 hours. The misfolding kinetics of the synthetic monomers within the different wells were highly reproducible. The different monomer solution within the wells were indicated by different symbols; B: An average of the different monomer repeats were taken and used as non-seeded controls (10 μ M average, blue line). This was compared to three-repeats of the same 10 μ M A β solution but with the addition of 1:1000 of a commercial polyclonal anti A β fibril (OC), indicated by the black lines. The presence of the commercial antibody completely inhibited any fibril formation.

The analysis of the some of the FFB and FB revealed an influence of the binders in the misfolding kinetic of the monomers, as all antibody solutions resulted in overall lower ThT emissions in the

treated samples compared to an average of the 10 non-treated controls (figure 6.18). Furthermore, some antibodies were seen to actually delay the fibril forming process at lower concentrations (such as A5, C1, E3, F4, G4, VHHFc5, and VHHFc11) and effectively inhibit fibril formation at higher concentrations (C1, E3 VHHFc11 and VHHFc19). Interestingly, while some antibodies were seen possessing a dose-dependent inhibition of the misfolding kinetics of A β , others seemed to be more random in their effects, such as G4, with 10 μ M antibody samples possessing delayed but higher ThT values than 1 and 5 μ M samples. Additionally, VHHFc1 and VHHFc19 accelerated the formation of fibrils at 1 μ M (figure 6.19).

Although promising, an unrelated-antibody control was not used in the functional assay. More repeats are needed to be performed in order including such controls to confirm the effective function of the discovered antibodies. This will also need to be repeated for the full panel of fibril binders.

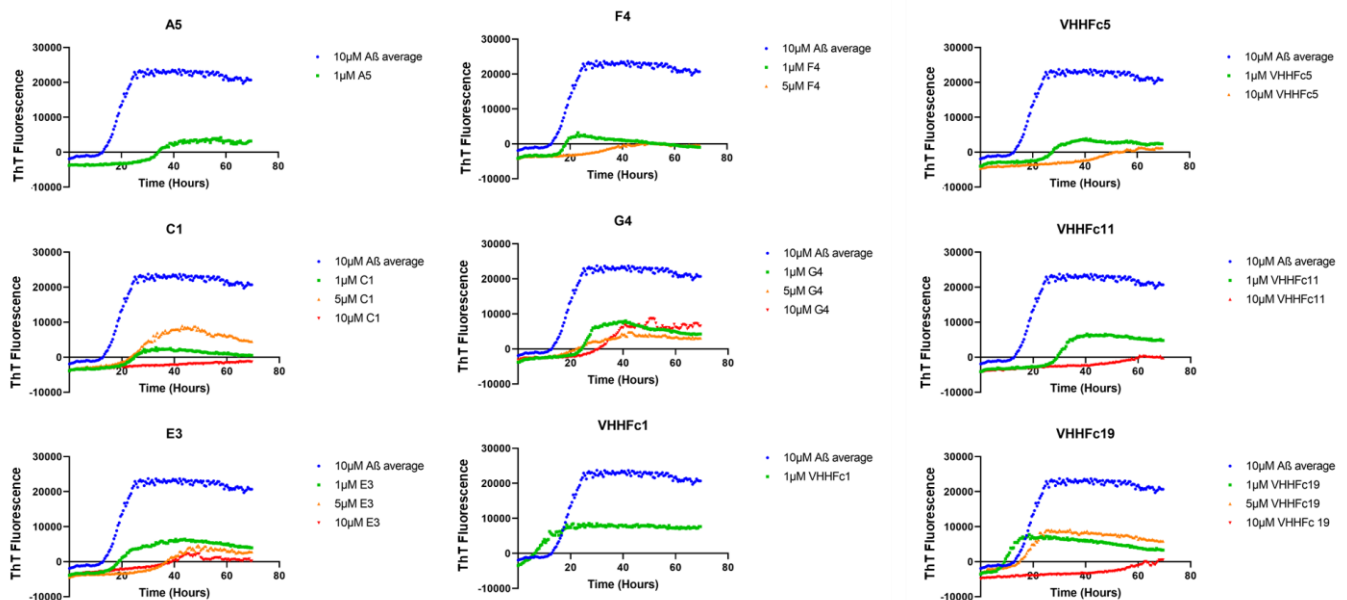


Figure 6-19: Functional assay- inhibition of fibril forming process through the use of FFB and FB

The assay was performed on freshly resuspended monomers (10 μ M) treated with an array of both FFB and FB, at different concentrations. Inhibition was monitored by comparing the fibril forming kinetics in the treated samples compared to the 10-repeat average of non-seeded samples (blue line). Depending on the antibody availability, the concentration used were 1 μ M (green line), 5 μ M (yellow line) or 10 μ M (red line). Misfolding kinetics were measured over 72 hours with ThT. The

presence of antibodies always resulted in lower ThT emissions than the untreated controls and in most cases (apart from VHHFc1 and VHHFc19) this also translated in slower kinetics, with the 1 μ M and 5 μ M treated samples possessing a longer lag phase than the untreated controls. A dose-dependent inhibition of fibrils could be seen with some antibodies (E3, F4, VHHFc5, VHHFc11 and VHHFc 19), but not in others (C1, G4). Using equimolar concentrations of fibrils and monomers (10 μ M) always resulted in the delay of the fibril forming process, and in some instances (C1, VHHFc11 and VHHFc19), antibodies were able to completely inhibit the formation of fibrils.

6.6 Discussion

6.6.1 Discovery and characterization of FFB

In a similar fashion to the discovery of FB using a VHH naïve library, this chapter focused on the implementation phage display methodologies for the discovery of antibodies with the ability to bind an alternative target, biotinylated fragmented fibrils. The aim was to discover antibodies able to bind secondary nucleation sites, as seen in other works such as Munke *et al.*, 2017 [180]. Indeed, fibril formation is a highly complex phenomenon that is characterized by several contributing microscopic factors: i) primary nucleation, in which monomers interact to form small soluble oligomers, followed larger oligomers, protofibrils and then fibrils; ii) secondary nucleation, where the surface end of formed fibrils is able to promote the formation of soluble aggregates; iii) fragmentation, whereby fibrils break into smaller segments and iv) elongation, where monomers are recruited at the end of fibrils to increase the length of the fibril itself [250, 301-304]. Secondary processes (elongation, fragmentation and secondary nucleation) are important to the pathological progression of the disease, as they underly fibril propagation and toxicity [133, 147, 151, 296] (figure 6.1), and as such, they are a prime candidate for antibody discovery efforts.

Initial experiments aimed at confirming that fragmented Genscript fibrils could indeed undergo successful chemical biotinylation after sonication. Results with BLI confirmed this through the use of SA biosensors (figure 6.2). With this confirmation obtained, biopanning could commence. The knowledge gained through 4 previous biopanning experiments were implemented to perform a single phage display assay for to discovery VHH binders towards fragmented fibrils. For this, three selections were used, all targeting biotinylated fragmented fibrils:

- Selection 1: Three rounds of panning with no subtraction step- aimed at obtaining the most antibodies with the ability to bind the targets (figure 6.3).
- Selection 2: Three rounds of panning with monomer and unrelated biotinylated protein subtraction- aiming at eliminating non-specific binders, and only obtaining antibodies with the ability to recognize fibrils and fragmented fibrils (figure 6.4).
- Selection 3: Three rounds of panning with fibril, monomer and unrelated biotinylated protein subtraction- with all A β elements deriving from the same batch of monomer produced by the same supplier (Genscript) and processed in the same way, the aim of this selection was to obtain only antibody binders with the ability to recognize secondary nucleation sites, at the edges of the fragmented fibrils themselves (figure 6.5).

From these three selections, a total of 49 monoclonal binders were identified through phage ELISA as binding preferentially to FF compared to monomer or non-fragmented fibrils. The DNA from these binders were propagated through PCR (figure 6.6) and the sequences obtained from an external supplier, Macrogen. The sequences were analysed and samples with poor sequence quality were eliminated from the sample group (table 6.2). Further analysis revealed the presence of homologous sequences within the discovered antibodies. Overall, a total of 34 unique sequences were obtained (table 6.4). This data was used to order the discovered binders as human-Fc constructs from Twist; the VHHFc format was chosen as previous results with FB revealed this antibody format was more likely to produce binding to the desired targets. FFB VHHFc sequences were aligned together, to reveal further similarities between CDR3 regions shared by some antibodies while preserving their differences in either structural or CDR1/CDR2 amino acids (figure 6.7).

Further analysis was performed on both FB and FFB sequences, as the CDR3 regions of all of the discovered antibodies were aligned to reveal shared sequences that developed independently thorough completely different biopanning experiments to different fibril targets (figure 6.8). These results suggest the presence of shared epitopes between fibrils and fragmented fibrils (as is to be

expected), but more importantly, it highlighted the effectiveness of the phage display methodology implemented in the discovery of antibody binders towards this particular target. A more in-depth view of the relationships between the different antibodies, revealed with the generation of a phylogenetic tree (figure 6.9), allowed for a close inspection of the potential similarities or differences between sequences within this theoretical grouping technique.

With the delivery of the lyophilized VHHFc DNA, the constructs were transfected into Expi™293 expression system. Antibody production levels were assessed through BLI (figure 6.10) showing a variability in expression level found for each antibody. FFB were purified and that the antibodies matched the expected molecular weight (figure 6.11). The concentration of each antibody was measured using a Nanodrop™, and an accurate concentration measurement was obtained through the inputting of the extinction coefficient and molecular weight values calculated with the ExPASy toolkit (table 6.5). Purified antibodies were then used to characterize the binding pattern and relative affinities of the different FFB against a range of targets. This was performed through ELISA and BLI.

ELISA studies used antibody solutions at a set concentration to test the binding to biotinylated fragmented Genscript fibrils, biotinylated Genscript fibrils, biotinylated Gencust fibrils, biotinylated Genscript monomers and biotinylated Gencust m/o/pr bound to the wells of a streptavidin coated maxisorp plate. Data revealed the presence of several binding patterns (figure 6.12):

1. Binders to fragmented fibrils, fibrils (from both suppliers) and Gencust m/o/pr. Within this group, while still possessing the ability to target all compounds mentioned above, it was also possible to see binders with relatively higher affinity for:
 - a. Gencust m/o/pr (e.g. E2)
 - b. Genscript fibrils (e.g. B5)
 - c. Both fragmented fibrils and Genscript fibrils (e.g. E3)
2. Greater affinity for fragmented fibrils, Genscript fibrils and Gencust m/o/pr (e.g. F1)
3. Greater affinity for Genscript fibrils and Gencust m/o/pr (e.g. C4)

4. Binders to all targeted compounds (e.g. G4)
5. Binders aspecific affinity for streptavidin (background) e.g. E4

Overall, binding to Genscript monomers was relatively very low, suggesting the high specificity of the discovered antibodies to binding aggregated forms of A β .

Interestingly, the comparison of the FFB and FB sequences with homologous CDR3 regions (VHHFc19/D3, VHHFc4/E2) revealed slightly different binding patterns (see image 6.12 and 5.11). This difference in binding could be explained by the fact that although the CDR3 regions were homologous between the FFB and FB; and thus hinting at the convergent identification of specific epitopes (most likely structural), other differences remained in the binder's sequence that made it such that the resulting antibodies possessed different binding patterns while preserving the same CDR3 region.

The analysis of control antibodies also revealed different binding patterns, highlighting the presence of different antibodies with different affinities within the polyclonal reagents.

Having identified potential binding patterns of interest through ELISA, binding and affinity were further tested with BLI. Initial experiments were done with AHC biosensors, as previous studies with FB demonstrated an increased sensitivity of these tips to detect binding; most likely due to, the size of the bound antibodies compared to fibrils in solution, avidity of the dimeric antibodies or repeated epitopes present within the fibrils in solution being able to interact more easily with bound antibodies on the tips. Through BLI, FFB were confirmed to be unreactive to Genscript monomers (figure 6.13) and Genscript fibrils (figure 6.14). Most FFB were seen to be cross-reactive with Gencust fibrils, and a high proportion of these antibodies were seen to bind this target (figure 6.15). The FFB with the highest affinities to Gencust fibrils (E2, B2 and D3) were also able to detect this target during ELISAs; but unexpectedly, ELISA results also showed these antibodies possessing higher affinity for Genscript fibrils, even though BLI assays confirmed minimal binding to aggregates from this supplier. This discrepancy could be explained by ELISA and BLI being different assays although they are used to

measure similar phenomenon, and the implementation of both assays is paramount for the a more thorough characterization of antibody binders.

The analysis of biotinylated FF revealed all FFB possessed the ability to bind this desired target, albeit with different affinities, as indicted by the different on-rates seen during the association phase (figure 6.16). Remarkably, switching the binding orientation of the BLI assay through the use of SA biosensors revealed very different results when measuring the binding of FFB to biotinylated FF. In this configuration, only one antibody was seen to bind to the target: G4 (figure 6.17). Interestingly, G4 possessed a characteristic association and dissociation curve, but due to the dimeric nature of the VHHFc molecule (and avidity effect) the association and dissociation constants for this molecule could not be accurately measured. This considerable variation in results depending on the orientation of the assay could hint at a differential sensitivity of the BLI methodology depending on the binding configuration. The implementation of AHC biosensors seems to allow a more accurate representation of the effective interaction between the different binders to big targets such as fibrils, possibly due to the fact that fibrils can then interact freely with the bound antibodies using different orientations. Additionally, the size differences between antibodies and fibrils means that it would be much easier to detect a shift when big targets such as fibrils bind to relatively smaller molecules such as antibodies within the tips. Finally, the AHC orientation would allow to more clearly see the potential avidity effects incurred I the VHHFc antibodies.

SA tips, on the other hand, require the loading of the fibrils to the biosensors thus presenting the structures in a set orientation (potentially masking epitopes) prior to measuring the shift induced by the interaction with FFB, therefore resulting in less overall binding. Furthermore, the size difference between the bound fibrils and antibodies could possibly translate in less sensitivity, as antibodies would produce a relative smaller shift.

Overall, through a single biopanning experiment targeting biotinylated fragmented Genscript fibrils, 34 unique FFB antibodies were identified. These antibodies were sequenced and ordered as VHHFc

construct. Antibodies were then expressed and purified for further testing with ELISA and BLI. Through this methodology unique binding patterns were revealed and interesting properties from the antibodies were highlighted. Although the discovered antibodies possess an undisputable ability to bind the desired targets, further research needed to be performed in order to assess the functionality of these binders, and to confirm their ability to bind secondary nucleation sites through functional assays. Furthermore, the UCB naïve VHH library was successful in allowing the discovery of antibody binders towards fibrils and fragmented fibrils. Each antibody binder was then tested using both ELISAs and BLI measurements with different biosensors, to further characterize the binding properties of each molecule (summarized in table 6.6).

Table 6-6: Summary of binding properties of all FB and FFB identified through phage display.

Fibril binders (VHHFc only)					
Antibody	ELISA OD630 purified antibody (8 µg/ml)	BLI association: SA tips (nm)-GS fibrils vs VHHFc in solution	BLI association: SA tips (nm)-GC fibrils vs VHHFc in solution	BLI association: AHC tips (nm)-VHHFc vs GC fibrils in solution	
1	Gencust fibrils and Gencust m/o/pr	No	No	No	
2	Gencust fibrils and Gencust m/o/pr	No	Yes	Yes	
5	Gencust fibrils and Gencust m/o/pr	No	Yes	Yes	
9	Gencust fibrils and Gencust m/o/pr	No	No	No	
11	All forms of Aβ	No	Yes	Yes	
19	Fibrils (both sources) and Gencust m/o/pr	No	No	No	
Fragmented fibril binders (VHHFc only)					
Antibody	ELISA OD630 purified antibody (8 µg/ml)	BLI association: SA tips (nm)-GS fragmented fibrils vs VHHFc in solution	BLI association: AHC tips (nm)-VHHFc vs GS fragmented fibrils solution	BLI association: AHC tips (nm)-VHHFc vs GC fibrils in solution	BLI association: AHC tips (nm)-VHHFc vs GS fibrils in solution
A1	Fragmented fibrils, Fibrils (both sources) and Gencust m/o/pr	No	Yes	Yes	No
A2	Fragmented fibrils, Fibrils (both sources) and Gencust m/o/pr	No	Yes	Yes	No
A3	Fragmented fibrils, Fibrils (both sources) and Gencust m/o/pr	No	Yes	Yes	No
A4	Fragmented fibrils, Fibrils (both sources) and Gencust m/o/pr	No	Yes	Yes	No
A5	Fragmented fibrils, Fibrils (both sources) and Gencust m/o/pr	No	Yes	Yes	No
B1	Fragmented fibrils, Fibrils (both sources) and Gencust m/o/pr	No	Yes	Yes	No
B2	Fragmented fibrils, Fibrils (both sources) and Gencust m/o/pr	No	Yes	Yes	No
B3	Fragmented fibrils, Fibrils (both sources) and Gencust m/o/pr	No	Yes	Yes	No

B4	Fragmented fibrils, Fibrils (both sources) and Gencust m/o/pr	No	Yes	Yes	No
B5	Fragmented fibrils, Fibrils (both sources) and Gencust m/o/pr	No	Yes	Yes	No
C1	Fragmented fibrils, Fibrils (both sources) and Gencust m/o/pr	No	Yes	Yes	No
C2	Fragmented fibrils, Fibrils (both sources) and Gencust m/o/pr	No	Yes	Yes	No
C3	Fragmented fibrils, Fibrils (both sources) and Gencust m/o/pr	No	Yes	Yes	No
C4	Fragmented fibrils, Fibrils (both sources) and Gencust m/o/pr	No	Yes	Yes	No
D1	Fragmented fibrils, Fibrils (both sources) and Gencust m/o/pr	No	Yes	Yes	No
D2	Fragmented fibrils, Fibrils (both sources) and Gencust m/o/pr	No	Yes	Yes	No
D3	Fragmented fibrils and Fibrils (both sources)	No	Yes	Yes	No
D4	Fragmented fibrils, Fibrils (both sources) and Gencust m/o/pr	No	Yes	Yes	No
E1	Fragmented fibrils, Fibrils (both sources) and Gencust m/o/pr	No	Yes	Yes	No
E2	Fragmented fibrils, Fibrils (both sources) and Gencust m/o/pr	No	Yes	No	No
E3	Fragmented fibrils and Genscript fibrils	No	Yes	Yes	No
E4	All forms of A β	No	Yes	Yes	No
F1	Fragmented fibrils, Fibrils (both sources) and Gencust m/o/pr	No	Yes	Yes	No
F2	Fragmented fibrils, Fibrils (both sources) and Gencust m/o/pr	No	Yes	Yes	No
F3	Fragmented fibrils, Genscript fibrils and Gencust m/o/pr	No	Yes	Yes	No
F4	Fragmented fibrils, Fibrils (both sources) and Gencust m/o/pr	No	Yes	Yes	No
G1	Fragmented fibrils, Fibrils (both sources) and Gencust m/o/pr	No	Yes	Yes	No
G2	All forms of A β	No	Yes	Yes	No
G3	Fragmented fibrils, Fibrils (both sources) and Gencust m/o/pr	No	Yes	Yes	No
G4	All forms of A β	Yes	Yes	Yes	No
H1	Fragmented fibrils, Fibrils (both sources) and Gencust m/o/pr	No	Yes	Yes	No
H2	Fragmented fibrils, Fibrils (both sources) and Gencust m/o/pr	No	Yes	Yes	No
H3	Fragmented fibrils, Fibrils (both sources) and Gencust m/o/pr	No	Yes	Yes	No
H4	Fragmented fibrils, Fibrils (both sources) and Gencust m/o/pr	No	Yes	Yes	No

As a final characterization assay, a selection of antibodies were tested for their ability to alter the misfolding kinetics of the monomers in a series of functional assays.

6.6.2 Functional assay optimization

In order to verify if the FFB and FB discovered through phage display possessed the ability to inhibit fibril formation, a functional assay was designed. This method was based on RT-QUIC and the predictable manner in which A β monomers can be induced to misfold through agitation and incubation cycles. For this, 10 μ M of Genscript A β monomers were subjected to 72 hours of RT-QUIC either alone or treated with increasing concentrations of different antibodies. The aim of this protocol was to monitor the formation of fibrils in real time and assess the effects of antibody binders in the fibril forming kinetics. Initially, non-treated samples were compared to OC polyclonal antibody-treated samples. For the non-treated samples, 10 repeats were assessed in order to control inter-well variability (figure 6.18, A) in misfolding. All untreated repeats seemed to misfold within the same timeframe and following similar kinetics. The introduction of 1:1000 diluted OC polyclonal commercial antibody prevented the formation of fibrils, and thus this antibody was used as a positive control for fibril inhibition (figure 6.18, B). Within the same experiment, a selection of FFB (A5, C1, E3, F4 and G4) were tested together with a selection of FB (VHHFc 1, 5, 11 and 19) at increasing molar concentrations: 1 μ M, 5 μ M or 10 μ M, depending on antibody availability. This revealed very promising results as all antibodies tested reduced the ThT emission levels (figure 6.19). Additionally, some antibodies induced a dose-dependent delay in the fibril formation process. This was seen for antibodies E3, F4, G4, VHHFc 5 and VHHFc 11. This was not always the case though, as some antibodies were seen to actually accelerate the formation of fibrils (such as VHHFc1 and VHHFc 19). Furthermore, some FFB (C1 and G4) seemed to induce stochastic variations to the ThT emission patterns as monomers treated with 5 μ M (in the case of C1) or 10 μ M (in the case of G4) seemed to possess higher ThT emission values than samples treated at lower concentrations. Notwithstanding, the use of stoichiometric amounts of monomer and antibody (10 μ M) almost always resulted in the complete inhibition of the fibril forming process, apart from antibody G4.

These results helped to unveil further insight into the functionality of the discovered antibodies, as most of the FFB and FB tested seemed to induce a dose-dependent decrease of ThT emission in treated samples. But further experiments are needed to confirm this. Firstly, a negative control (unrelated antibody) should be implemented, to assess the misfolding kinetics of A β with the presence of another protein in solution, such as an IgG, scFv or VHH; then, antibodies in PBS (no A β) should also be assessed as controls, in order to confirm that the increase of ThT binding is only due to the conversion of A β monomers into fibrils, and not a non-specific interaction generated from the antibodies. Next, further repeats with higher concentrations of all antibodies should also be tested to confirm the effective dose-dependent decrease in the rate of fibril formation within the observed samples. Finally, a mathematical model should be implemented to interpret ThT fluorescence data in order to infer how our antibodies are changing the kinetics of fibril formation (in terms of inhibiting primary nucleation, secondary nucleation, elongation or more of these components at the same time), as seen in Aprile *et al.*, 2017 [304] and Munke *et al.*, 2017 [180]. Moreover, assays such as CD or TEM could also be implemented in parallel, to compliment the ThT data. This could be implemented by measuring the spectral shift from random coil (negative band at 195 nm) to β -sheet (negative peak at 218 nm and positive peak at 195 nm) [277, 278] in A β samples treated with different concentrations of antibodies, in the case of CD; or the effective presence (or lack) of fibrils in treated samples with TEM, as some A β polymorphs have been recorded to be ThT insensitive [184].

Overall, the basis for a protocol to test the functionality of antibodies has been established. Further experiments could apply these methods into working protocols to assess the effectiveness of all the discovered antibodies.

Chapter 7. Conclusions and future prospects

7.1 α -syn polymorph generation

Recombinant α -syn was induced to misfold using PMCA, with human derived PD and control brain samples as templates to direct fibrillization. Through this method, for the first time, two distinct α -syn fibril conformers (High and Low) were discovered; the High conformer was present in human seeded samples and Low conformer was from *de novo* fibrils, and each displayed distinct biophysical characteristics. This approach is relatively novel, as few studies have used PMCA (with sonication) with the scope of producing α -fibrils [106, 163, 261, 271, 275], in spite of the advantages this method can provide.

As previously discussed, prion biology demonstrates that PMCA-produced aggregates have a higher pathogenicity than fibrils produced with alternative methods, such as RT-QUIC [276]; and therefore are better-suited to model pathogenic fibril formation *in vitro*. Future work could apply antibody discovery techniques such as phage display to identify antibodies that can inhibit this PMCA produced α -syn fibril formation. Such antibodies would target the end-point fibril conformer most likely found in humans. Applying phage display to produce anti- α -syn binders has already been validated by Emadi *et al.* 2009 [174] and De Genest *et al.* 2010 [172] in studies where VHH and scFv libraries, respectively, were applied to the discovery of antibodies with the ability to bind α -syn monomers.

In addition, the versatility of the PMCA methodology could allow the implementation of a wide array of different seeds to potentially produce disease specific polymorphs, rather than the unique human-derived conformer found from both PD and control seeding, as described throughout this work. This could potentially be achieved through the use of SDS or Urea insoluble fractions derived from brains, which have been shown to possess higher numbers of α -syn aggregates in PD subjects compared to controls [305]. Indeed, as seen in figure 3.8, the cytosolic brain extracts used for our experiments lacked major distinctions in terms of α -syn burden in both PD and HC, so further studies with seeds known to possess different properties could result in different polymorphs being generated.

Regardless, further studies are needed to confirm the pathological relevancy of the High and Low conformers. An interesting approach to validate this would be the implementation of *in vitro* assays using cell lines to measure the toxicity of the different polymorphs of α -syn, or the establishment of a chronic infection in α -syn overexpressing SH-SY5Y cells, as described by Herva *et al.*, 2014 [163], to confirm efficacy of infection and toxicity over several cell passages. SH-SY5Y cells have found great success in these assays, given the similarities of the neuroblastoma cells with the dopaminergic neurons which are the main target of PD, as described in the reviews by Xie *et al.*, 2010 [306] and Xicoy *et al* 2017 [307]. Effectively, the SH-SY5Y model has been implemented by several research groups trying to understand the effects of α -syn fibrils in this *in vitro* system [93, 308, 309].

In conclusion, this thesis sets the basis for future developments in the field of α -syn misfolding and polymorph characterization by studying one of the first ever instances of human-seeded polymorphs generated through the misfolding of recombinant α -syn with PMCA. Further investigation is paramount to develop a deeper understanding of the intrinsic mechanisms that regulate the generation of aggregates through templated misfolding.

7.2 A β misfolding and fibril characterization

Having identified the appropriate parameters to manipulate the misfolding kinetics of a fibril forming protein (α -syn), the next step of the project focused on the implementation of similar techniques to understand the behaviour of another aggregation prone peptide, synthetic A β 42. Synthetic peptides were used as opposed to recombinant proteins given the availability of these compounds from commercial sources. The decision to use synthetic peptides was also supported by previous studies confirming the pathological relevancy of these synthetic aggregated peptides when infecting a susceptible host [310, 311].

Initial studies aimed to assess if the methodology optimized for α -syn misfolding could be replicated with A β 42 peptides, as (to my knowledge) there is currently no recorded evidence of A β misfolding using PMCA with sonication. These preliminary studies were performed using monomers produced by

a single source, Gencust. This approach failed to produce significant results, in terms of fibril formation in both seeded and non-seeded samples, potentially due to the aggressive nature of PMCA, with ultrasonic-induced free radical being generated during sonication [312] and the inherent instability of the A β 42 peptides in aqueous buffers [157, 244, 246, 292]. A promising result was found with static incubation (but further tests at the University of Nottingham were halted due to the COVID-19 lab lockdowns).

Research resumed in UCB Celltech where PMCA could not be performed due to lack of the necessary equipment. An alternative method was sought in RT-QUIC, following the guidelines described by Salvadores *et al.*, 2014 [166]. As previously seen with α -syn, questions remain regarding the effective pathological relevance of RT-QUIC produced fibrils [276]. Notwithstanding, RT-QUIC was successfully implemented for the misfolding of A β 42 peptides sourced from Genscript, with clear distinctions between lag phase, exponential growth and plateau at the end of the aggregation process as measured with ThT; all clear indications of the successful formation of fibrils in solution [85, 166, 180]. Interestingly, the same phenomenon could not be seen with Gencust monomers, as a persistent contamination of oligomers and protofibrils was observed within the monomeric population when the optimized pre-solubilization methods were used. This prevented the misfolding of monomers into fibrils with RT-QUIC; but fibrils could still be generated by adding PBS directly to the lyophilized peptides without any pre-treatment. This lack of reproducibility between synthetic peptides produced by different companies is in agreement with the known variability present in commercially available synthetic peptides [313, 314], highlighting the importance of assessing multiple sources of monomers when attempting misfolding assays with synthetic peptides. The lack of misfolding seen in the Gencust peptides could be due to the implementation of a different solubilization method in UCB as opposed to the one optimized at the University of Nottingham (N₂ drying and not freeze-drying), but further comparison would be needed to confirm this, mainly a side-by-side test of monomers pre-treated in both ways. This information would be paramount for further understanding the behaviour of differentially sourced monomers in our methodological procedures.

Regardless, the methods described in this thesis provide a solid and reliable foundation for studying A β misfolding kinetics. Overall, 5 distinct populations of A β at different aggregation rates were produced: 1) fragmented Genscript fibrils, 2) Genscript fibrils, 3) Gencust fibrils, 4) Genscript monomers and 5) Gencust m/o/pr. As concluded with α -syn, future experiments could include the assessment of the toxicity of A β fibrils (both in their full-length and fragmented form) in the SH-SY5Y model [133, 315].

Finally, it would also be interesting to test the misfolding kinetics of a third commercially available source of synthetic A β to determine if this again produces distinct misfolding. Also, assessing recombinant A β misfolding may produce distinct results as studies have shown recombinant peptides possess higher stabilities and thus result in higher fidelity and robustness when assessing misfolding kinetics [316, 317].

In conclusion, the study of synthetic A β 42 peptides sources from two different suppliers allowed for the optimization of a method to consistently produce either monomers or fibrils in a controlled manner; but further studies (mainly in terms of toxicity or structural characterisation) are needed to fully understand the fibril polymorphs targeted by antibody discovery.

7.3 Antibody discovery using UCB's naïve VHH library

The UCB naïve VHH library was implemented to discover antibodies against: Genscript fibrils, Gencust fibrils and Genscript fragmented fibrils. These forms of A β were targeted as the distinct misfolding kinetics between Gencust and Genscript fibrils most likely indicated these aggregates belonged to different A β polymorphs, and fragmented fibrils were implemented to target secondary nucleation sites. Antibodies were then ordered as either monomers or dimers conjugated to a human FC domain, to allow purification and testing. This novel approach was successful in the identification of VHH antibodies with the ability to bind A β fibrils in solution, and the implementation of two different antibody formats granted the possibility to see the effects of avidity and affinity within each VHH, in order to distinguish the antibodies with the best binding kinetics. Binding patterns were assessed

through ELISAs using both crude HEK supernatant and purified protein to reveal a strong concentration-dependence of the binding of each clone to the different A β forms tested. For that reason, binding was reassessed with a different assay, BLI, which provided confirmation of binding using different antibody-target orientations. Finally, some of the binders identified through ELISA and BLI were tested in an initial functional assay, providing preliminary data suggesting that FB VHHFc 1, VHHFc 5, VHHFc 11 and VHHFc 19 (respectively targeting Gencust fibrils and Gencust m/o/pr in the case of antibody 1 and 5, and both fibril polymorphs together with Gencust m/o/pr for antibody 11 and 19) together FFB C1 and F4 (preferentially targeting fragmented fibrils, both fibril polymorphs and Gencust m/o/pr); A5 (preferentially binding to Genscript fibrils and Gencust m/o/pr); E3 (preferentially binding fragmented fibrils and Genscript fibrils) and G4 (targeting all forms of A β tested) could have an inhibitory effects in the formation of Genscript fibrils in solution.

As previously discussed, the implementation of VHH libraries is not often seen in the literature, although there are some examples [172, 176, 177, 231]. This thesis aimed to provide the basis for further studies using VHH antibodies. Indeed, the implementation of VHH antibodies for the developing of therapeutics is a promising field, due to the ease of expression, small size, CDR3 length (and flexibility) and ease of genetic engineering to conjugate with other molecules, all properties which is intrinsic to nanobodies [318, 319].

7.4 Future prospects

Future work should include further implementation of the functional assays with the appropriate repeats and controls either through the measurement of ThT emission or through measuring the protection against the neurotoxic effects of fibrils in cell line models, mainly the SH-SY5Y system [172, 174, 175, 177, 179, 180, 231, 300]. This could be used to effectively demonstrate the ability of our synthetic fibrils to elicit a neurodegenerative process, and through the addition of antibodies the model could highlight any neuroprotective effects of the antibodies themselves, as described by several authors [174, 177, 179, 231, 300]. SH-SY5Y toxicity assays would also be particularly interesting to prove that fibril fragmentation does indeed increase the toxicity of A β fibrils [133], therefore further

validating the choice of identifying FFB through phage display. In addition, further experiments with NS-TEM or cryo-electron microscopy [113, 142, 144, 155, 167, 184, 281, 320] could be implemented to further evidence the morphological differences (if any) found in Genscript fibrils, Gencust fibrils and Genscript fragmented fibrils. This would not only provide crucial information about the molecules used for antibody discovery, but any structural information could be correlated with ELISA and BLI binding data to further understand the behaviour of the different antibodies described throughout this thesis. In addition, should these assays be successful in the identification of functional inhibitory antibodies, further studies could then focus on assessing the inhibition of the fibril forming process from monomers supplied by different vendors or across batches [313, 314], together with recombinant monomers; in order to confirm the wider applicability of the FB and FFB to other fibril conformers or their restriction to only bind the polymorphs identified in this work.

Additionally, further studies could be performed to identify the epitopes of the best binders highlighted through the functionality tests, most likely using an array of overlapping A β derived peptide sequences for epitope mapping assays [173, 175, 210]. This would also allow the comparison of the mapped epitopes with ThT inhibition assays, to assess function [180]. Further still, an additional method to measure the effectiveness of the antibodies discovered through this work would be the implementation of immunohistochemical staining of patient and control brain sections [171, 176, 210, 231, 232, 300]. In this way, the ability of our VHH antibodies to cross-react with *in vivo* human derived samples would be confirmed.

Following this validation, another focus could be the engineering of the VHHs for *in vivo* pharmacokinetic and efficacy studies. For this purpose, initial studies could aim to understand if a human-Fc conjugation is the best approach to undertake when utilizing VHH molecules: Due to the small size of VHHs (15 kDa) these molecules tend to have a fast clearance from the bloodstream of treated subjects [318, 321-323], making them less ideal as therapeutic agents; therefore the conjugation of the nanobody with a molecules (such an Fc, an anti-albumin nanobody, or PEG) is

generally used to increase the half-life of the nanobodies themselves [318], depending on the therapeutic needs. Next, humanization efforts should take place to ensure the discovered nanobodies can be studied *in vivo*. In terms of humanization, VHHs have the advantage of sharing many similarities with human VH domain [319, 321], with the main differences being the length of the CDRs and the presence of more hydrophilic amino acids in framework 2 (most commonly Y37, E44, R45 and G47, according to Kabat amino acid numbering) [318, 324, 325] which are important to confer the VHH particle its increase hydrophilicity, low tendency to dimerize and have also been seen to possibly be involved in antigen binding [318, 322-324]. These similarities could allow for a straightforward humanization process, using a VH framework to accept the CDR3 grafts from the VHH sequences, and then back-mutate important camelid amino acids to stabilize the resulting molecule [326].

The humanization of the VHH molecule would serve the ultimate purpose of testing these compounds as potential therapeutic molecules. Therapeutic efficacy could be measured through the implementation of transgenic animal models expressing human A β , such as the PS2APP strain described in Bohrmann *et al.*, 2016 [210]. This way, a therapeutic effect through A β clearance and rescue of normal behaviour could be directly linked to the discovered antibodies in treated animals.

Should the VHH antibodies possess a high affinity for native A β fibrils but fail to demonstrate a therapeutic effect, they could still be tested as potential diagnostic tools. Indeed, VHH molecules have been conjugated with radionucleotides. These elements are characterized by possessing unstable nuclei, and therefore to emit radiation over time. Diagnostic tools such as positron emission tomography are able to detect these faint radioactive signals and are routinely used to detect tumours or, in our case, A β deposition *in vivo* [171, 298]. The high tissue penetrance of nanobodies (due to their small size) together with the reduced half-life incurred by the lack of an FC domain make VHHs an extremely appealing candidate for antibody-mediated imaging and to date, several nanobodies have been engineered as radioactive tracers, mainly in the field of oncology [327-333].

In conclusion, antibody binders to fibrils and fragmented fibrils have been identified using UCB's naïve VHH library; although different binding patterns were identified through ELISA and affinities inferred through BLI, further characterization work should be performed in order to understand the functionality and efficacy of these antibodies in halting (or altering) the misfolding of A β 42. Regardless, the antibodies discovered throughout this thesis have laid the groundwork for future experimental research in this topic, with the identification of potential first of a kind therapeutic molecules.

References

1. Hartl, F.U., *Molecular chaperones in cellular protein folding*. Nature, 1996. **381**(6583): p. 571-9.
2. Bellotti, V. and M. Stoppini, *Protein misfolding diseases*. The Open Biology Journal, 2009. **2**: p. 228-234.
3. Polymeropoulos, M.H., et al., *Mutation in the alpha-synuclein gene identified in families with Parkinson's disease*. Science, 1997. **276**(5321): p. 2045-7.
4. Spillantini, M.G., et al., *Alpha-synuclein in Lewy bodies*. Nature, 1997. **388**(6645): p. 839-40.
5. Glenner, G.G., *The pathobiology of Alzheimer's disease*. Annu Rev Med, 1989. **40**: p. 45-51.
6. Prusiner, S.B., *Prions*. Proc Natl Acad Sci U S A, 1998. **95**(23): p. 13363-83.
7. Dobson, C.M., *Getting out of shape*. Nature, 2002. **418**(6899): p. 729-30.
8. Dobson, C.M., *Protein folding and misfolding*. Nature, 2003. **426**(6968): p. 884-90.
9. Ferreira, M. and J. Massano, *An updated review of Parkinson's disease genetics and clinicopathological correlations*. Acta Neurol Scand, 2017. **135**(3): p. 273-284.
10. Aaseth, J., P. Dusek, and P.M. Roos, *Prevention of progression in Parkinson's disease*. Biometals, 2018. **31**(5): p. 737-747.
11. Kalia, L.V. and A.E. Lang, *Parkinson's disease*. Lancet, 2015. **386**(9996): p. 896-912.
12. Ghatak, S., et al., *Parkinson's disease: what the model systems have taught us so far*. J Genet, 2018. **97**(3): p. 729-751.
13. Blandini, F., et al., *Functional changes of the basal ganglia circuitry in Parkinson's disease*. Prog Neurobiol, 2000. **62**(1): p. 63-88.
14. DeLong, M.R. and T. Wichmann, *Circuits and circuit disorders of the basal ganglia*. Arch Neurol, 2007. **64**(1): p. 20-4.
15. Graybiel, A.M., *The basal ganglia*. Curr Biol, 2000. **10**(14): p. R509-11.
16. Surmeier, D.J., et al., *D1 and D2 dopamine-receptor modulation of striatal glutamatergic signaling in striatal medium spiny neurons*. Trends Neurosci, 2007. **30**(5): p. 228-35.
17. Soukup, S.F., R. Vanhauwaert, and P. Verstreken, *Parkinson's disease: convergence on synaptic homeostasis*. EMBO J, 2018. **37**(18).
18. Shendelman, S., et al., *DJ-1 is a redox-dependent molecular chaperone that inhibits alpha-synuclein aggregate formation*. PLoS Biol, 2004. **2**(11): p. e362.
19. Zhou, W., et al., *The oxidation state of DJ-1 regulates its chaperone activity toward alpha-synuclein*. J Mol Biol, 2006. **356**(4): p. 1036-48.
20. Lane, C.A., J. Hardy, and J.M. Schott, *Alzheimer's disease*. Eur J Neurol, 2018. **25**(1): p. 59-70.
21. Serrano-Pozo, A., et al., *Neuropathological alterations in Alzheimer disease*. Cold Spring Harb Perspect Med, 2011. **1**(1): p. a006189.
22. Masters, C.L., et al., *Alzheimer's disease*. Nat Rev Dis Primers, 2015. **1**: p. 15056.
23. Liu, P.P., et al., *History and progress of hypotheses and clinical trials for Alzheimer's disease*. Signal Transduct Target Ther, 2019. **4**: p. 29.
24. Walker, L.C., *Prion-like mechanisms in Alzheimer disease*. Handb Clin Neurol, 2018. **153**: p. 303-319.
25. Selkoe, D.J. and J. Hardy, *The amyloid hypothesis of Alzheimer's disease at 25 years*. EMBO Mol Med, 2016. **8**(6): p. 595-608.
26. Eichenbaum, H., A.P. Yonelinas, and C. Ranganath, *The medial temporal lobe and recognition memory*. Annu Rev Neurosci, 2007. **30**: p. 123-52.
27. Braak, H. and E. Braak, *Frequency of stages of Alzheimer-related lesions in different age categories*. Neurobiol Aging, 1997. **18**(4): p. 351-7.
28. Castellani, R.J., G. Plascencia-Villa, and G. Perry, *The amyloid cascade and Alzheimer's disease therapeutics: theory versus observation*. Lab Invest, 2019. **99**(7): p. 958-970.

29. LaFerla, F.M., K.N. Green, and S. Oddo, *Intracellular amyloid-beta in Alzheimer's disease*. *Nat Rev Neurosci*, 2007. **8**(7): p. 499-509.
30. Jack, C.R., Jr., et al., *Brain beta-amyloid load approaches a plateau*. *Neurology*, 2013. **80**(10): p. 890-6.
31. Ingelsson, M., et al., *Early Abeta accumulation and progressive synaptic loss, gliosis, and tangle formation in AD brain*. *Neurology*, 2004. **62**(6): p. 925-31.
32. Hervy, J. and D.J. Bicut, *Dynamical decoration of stabilized-microtubules by Tau-proteins*. *Sci Rep*, 2019. **9**(1): p. 12473.
33. Strang, K.H., T.E. Golde, and B.I. Giasson, *MAPT mutations, tauopathy, and mechanisms of neurodegeneration*. *Lab Invest*, 2019. **99**(7): p. 912-928.
34. Butler, V.J., et al., *Tau/MAPT disease-associated variant A152T alters tau function and toxicity via impaired retrograde axonal transport*. *Hum Mol Genet*, 2019. **28**(9): p. 1498-1514.
35. Rosenberg, R.N., et al., *Genomics of Alzheimer Disease: A Review*. *JAMA Neurol*, 2016. **73**(7): p. 867-74.
36. Muller, U.C., T. Deller, and M. Korte, *Not just amyloid: physiological functions of the amyloid precursor protein family*. *Nat Rev Neurosci*, 2017. **18**(5): p. 281-298.
37. Thinakaran, G., *The role of presenilins in Alzheimer's disease*. *J Clin Invest*, 1999. **104**(10): p. 1321-7.
38. Zhao, N., et al., *Apolipoprotein E, Receptors, and Modulation of Alzheimer's Disease*. *Biol Psychiatry*, 2018. **83**(4): p. 347-357.
39. Aguzzi, A., A.K.K. Lakkaraju, and K. Frontzek, *Toward Therapy of Human Prion Diseases*. *Annu Rev Pharmacol Toxicol*, 2017.
40. Connolly, B.S. and A.E. Lang, *Pharmacological treatment of Parkinson disease: a review*. *JAMA*, 2014. **311**(16): p. 1670-83.
41. Yiannopoulou, K.G. and S.G. Papageorgiou, *Current and future treatments for Alzheimer's disease*. *Ther Adv Neurol Disord*, 2013. **6**(1): p. 19-33.
42. Poewe, W., et al., *Parkinson disease*. *Nat Rev Dis Primers*, 2017. **3**: p. 17013.
43. Rascol, O., et al., *Limitations of current Parkinson's disease therapy*. *Ann Neurol*, 2003. **53 Suppl 3**: p. S3-12; discussion S12-5.
44. Schapira, A.H.V., K.R. Chaudhuri, and P. Jenner, *Non-motor features of Parkinson disease*. *Nat Rev Neurosci*, 2017. **18**(8): p. 509.
45. Searl, T., C. Prior, and I.G. Marshall, *Acetylcholine recycling and release at rat motor nerve terminals studied using (-)-vesamicol and troxpyrrolium*. *J Physiol*, 1991. **444**: p. 99-116.
46. Brambilla, D., *Drug discovery, development and delivery in Alzheimer's disease*. *Pharm Res*, 2017. **35**(1): p. 3.
47. Scarpini, E., P. Scheltens, and H. Feldman, *Treatment of Alzheimer's disease: current status and new perspectives*. *Lancet Neurol*, 2003. **2**(9): p. 539-47.
48. Birks, J., *Cholinesterase inhibitors for Alzheimer's disease*. *Cochrane Database Syst Rev*, 2006(1): p. CD005593.
49. Kavirajan, H. and L.S. Schneider, *Efficacy and adverse effects of cholinesterase inhibitors and memantine in vascular dementia: a meta-analysis of randomised controlled trials*. *Lancet Neurol*, 2007. **6**(9): p. 782-92.
50. Goedert, M., *Alpha-synuclein and neurodegenerative diseases*. *Nat Rev Neurosci*, 2001. **2**(7): p. 492-501.
51. Jellinger, K.A., *Neuropathological spectrum of synucleinopathies*. *Mov Disord*, 2003. **18 Suppl 6**: p. S2-12.
52. Goedert, M., *Familial Parkinson's disease. The awakening of alpha-synuclein*. *Nature*, 1997. **388**(6639): p. 232-3.
53. Ottolini, D., et al., *Alpha-synuclein at the intracellular and the extracellular side: functional and dysfunctional implications*. *Biol Chem*, 2017. **398**(1): p. 77-100.

54. Sharon, R., et al., *alpha-Synuclein occurs in lipid-rich high molecular weight complexes, binds fatty acids, and shows homology to the fatty acid-binding proteins*. Proc Natl Acad Sci U S A, 2001. **98**(16): p. 9110-5.
55. Sharon, R., et al., *The formation of highly soluble oligomers of alpha-synuclein is regulated by fatty acids and enhanced in Parkinson's disease*. Neuron, 2003. **37**(4): p. 583-95.
56. Bartels, T., J.G. Choi, and D.J. Selkoe, *alpha-Synuclein occurs physiologically as a helically folded tetramer that resists aggregation*. Nature, 2011. **477**(7362): p. 107-10.
57. Selkoe, D., et al., *Defining the native state of alpha-synuclein*. Neurodegener Dis, 2014. **13**(2-3): p. 114-7.
58. Celej, M.S., et al., *Toxic prefibrillar alpha-synuclein amyloid oligomers adopt a distinctive antiparallel beta-sheet structure*. Biochem J, 2012. **443**(3): p. 719-26.
59. El-Agnaf, O.M., et al., *Alpha-synuclein implicated in Parkinson's disease is present in extracellular biological fluids, including human plasma*. FASEB J, 2003. **17**(13): p. 1945-7.
60. Periquet, M., et al., *Aggregated alpha-synuclein mediates dopaminergic neurotoxicity in vivo*. J Neurosci, 2007. **27**(12): p. 3338-46.
61. Beyer, K., *Alpha-synuclein structure, posttranslational modification and alternative splicing as aggregation enhancers*. Acta Neuropathol, 2006. **112**(3): p. 237-51.
62. Chen, L. and M.B. Feany, *Alpha-synuclein phosphorylation controls neurotoxicity and inclusion formation in a Drosophila model of Parkinson disease*. Nat Neurosci, 2005. **8**(5): p. 657-63.
63. Schreurs, S., et al., *In vitro phosphorylation does not influence the aggregation kinetics of WT alpha-synuclein in contrast to its phosphorylation mutants*. Int J Mol Sci, 2014. **15**(1): p. 1040-67.
64. Paleologou, K.E., et al., *Phosphorylation at S87 is enhanced in synucleinopathies, inhibits alpha-synuclein oligomerization, and influences synuclein-membrane interactions*. J Neurosci, 2010. **30**(9): p. 3184-98.
65. Giasson, B.I., et al., *Oxidative damage linked to neurodegeneration by selective alpha-synuclein nitration in synucleinopathy lesions*. Science, 2000. **290**(5493): p. 985-9.
66. Souza, J.M., et al., *Dityrosine cross-linking promotes formation of stable alpha -synuclein polymers. Implication of nitrative and oxidative stress in the pathogenesis of neurodegenerative synucleinopathies*. J Biol Chem, 2000. **275**(24): p. 18344-9.
67. Dorval, V. and P.E. Fraser, *Small ubiquitin-like modifier (SUMO) modification of natively unfolded proteins tau and alpha-synuclein*. J Biol Chem, 2006. **281**(15): p. 9919-24.
68. Hasegawa, M., et al., *Phosphorylated alpha-synuclein is ubiquitinated in alpha-synucleinopathy lesions*. J Biol Chem, 2002. **277**(50): p. 49071-6.
69. Tofaris, G.K., et al., *Ubiquitination of alpha-synuclein in Lewy bodies is a pathological event not associated with impairment of proteasome function*. J Biol Chem, 2003. **278**(45): p. 44405-11.
70. Lashuel, H.A., et al., *The many faces of alpha-synuclein: from structure and toxicity to therapeutic target*. Nat Rev Neurosci, 2013. **14**(1): p. 38-48.
71. Iwai, A., et al., *The precursor protein of non-A beta component of Alzheimer's disease amyloid is a presynaptic protein of the central nervous system*. Neuron, 1995. **14**(2): p. 467-75.
72. Burre, J., et al., *Alpha-synuclein promotes SNARE-complex assembly in vivo and in vitro*. Science, 2010. **329**(5999): p. 1663-7.
73. Devi, L., et al., *Mitochondrial import and accumulation of alpha-synuclein impair complex I in human dopaminergic neuronal cultures and Parkinson disease brain*. J Biol Chem, 2008. **283**(14): p. 9089-100.
74. Vicario, M., et al., *A split-GFP tool reveals differences in the sub-mitochondrial distribution of wt and mutant alpha-synuclein*. Cell Death Dis, 2019. **10**(11): p. 857.
75. Shavali, S., et al., *Mitochondrial localization of alpha-synuclein protein in alpha-synuclein overexpressing cells*. Neurosci Lett, 2008. **439**(2): p. 125-8.

76. Guardia-Laguarta, C., et al., *alpha-Synuclein is localized to mitochondria-associated ER membranes*. J Neurosci, 2014. **34**(1): p. 249-59.
77. Paillusson, S., et al., *alpha-Synuclein binds to the ER-mitochondria tethering protein VAPB to disrupt Ca(2+) homeostasis and mitochondrial ATP production*. Acta Neuropathol, 2017. **134**(1): p. 129-149.
78. Braak, H., et al., *Stanley Fahn Lecture 2005: The staging procedure for the inclusion body pathology associated with sporadic Parkinson's disease reconsidered*. Mov Disord, 2006. **21**(12): p. 2042-51.
79. Winklhofer, K.F., J. Tatzelt, and C. Haass, *The two faces of protein misfolding: gain- and loss-of-function in neurodegenerative diseases*. EMBO J, 2008. **27**(2): p. 336-49.
80. Burre, J., M. Sharma, and T.C. Sudhof, *alpha-Synuclein assembles into higher-order multimers upon membrane binding to promote SNARE complex formation*. Proc Natl Acad Sci U S A, 2014. **111**(40): p. E4274-83.
81. Goers, J., et al., *Nuclear localization of alpha-synuclein and its interaction with histones*. Biochemistry, 2003. **42**(28): p. 8465-71.
82. Kontopoulos, E., J.D. Parvin, and M.B. Feany, *Alpha-synuclein acts in the nucleus to inhibit histone acetylation and promote neurotoxicity*. Hum Mol Genet, 2006. **15**(20): p. 3012-23.
83. Goedert, M., et al., *Prion-like mechanisms in the pathogenesis of tauopathies and synucleinopathies*. Curr Neurol Neurosci Rep, 2014. **14**(11): p. 495.
84. Peng, C., R.J. Gathagan, and V.M. Lee, *Distinct alpha-Synuclein strains and implications for heterogeneity among alpha-Synucleinopathies*. Neurobiol Dis, 2018. **109**(Pt B): p. 209-218.
85. Shah Nawaz, M., et al., *Discriminating alpha-synuclein strains in Parkinson's disease and multiple system atrophy*. Nature, 2020. **578**(7794): p. 273-277.
86. Giehm, L., et al., *Low-resolution structure of a vesicle disrupting α-synuclein oligomer that accumulates during fibrillation*. Proc Natl Acad Sci U S A, 2011. **108**(8): p. 3246-51.
87. Chen, S.W., et al., *Structural characterization of toxic oligomers that are kinetically trapped during alpha-synuclein fibril formation*. Proc Natl Acad Sci U S A, 2015. **112**(16): p. E1994-2003.
88. Kim, H.Y., et al., *Structural properties of pore-forming oligomers of alpha-synuclein*. J Am Chem Soc, 2009. **131**(47): p. 17482-9.
89. Volles, M.J., et al., *Vesicle permeabilization by protofibrillar alpha-synuclein: implications for the pathogenesis and treatment of Parkinson's disease*. Biochemistry, 2001. **40**(26): p. 7812-9.
90. Fusco, G., et al., *Structural basis of membrane disruption and cellular toxicity by alpha-synuclein oligomers*. Science, 2017. **358**(6369): p. 1440-1443.
91. Cascella, R., et al., *The release of toxic oligomers from alpha-synuclein fibrils induces dysfunction in neuronal cells*. Nat Commun, 2021. **12**(1): p. 1814.
92. Campbell, B.C., et al., *The solubility of alpha-synuclein in multiple system atrophy differs from that of dementia with Lewy bodies and Parkinson's disease*. J Neurochem, 2001. **76**(1): p. 87-96.
93. Nonaka, T., et al., *Seeded aggregation and toxicity of {alpha}-synuclein and tau: cellular models of neurodegenerative diseases*. J Biol Chem, 2010. **285**(45): p. 34885-98.
94. Goedert, M., M. Masuda-Suzukake, and B. Falcon, *Like prions: the propagation of aggregated tau and alpha-synuclein in neurodegeneration*. Brain, 2017. **140**(2): p. 266-278.
95. Aguzzi, A. and L. Rajendran, *The transcellular spread of cytosolic amyloids, prions, and prionoids*. Neuron, 2009. **64**(6): p. 783-90.
96. Scheckel, C. and A. Aguzzi, *Prions, prionoids and protein misfolding disorders*. Nat Rev Genet, 2018. **19**(7): p. 405-418.
97. Aguzzi, A., M. Heikenwalder, and M. Polymenidou, *Insights into prion strains and neurotoxicity*. Nat Rev Mol Cell Biol, 2007. **8**(7): p. 552-61.
98. Woerman, A.L., et al., *Propagation of prions causing synucleinopathies in cultured cells*. Proc Natl Acad Sci U S A, 2015. **112**(35): p. E4949-58.

99. Prusiner, S.B., et al., *Evidence for alpha-synuclein prions causing multiple system atrophy in humans with parkinsonism*. Proc Natl Acad Sci U S A, 2015. **112**(38): p. E5308-17.
100. Giasson, B.I., et al., *Neuronal alpha-synucleinopathy with severe movement disorder in mice expressing A53T human alpha-synuclein*. Neuron, 2002. **34**(4): p. 521-33.
101. Mougenot, A.L., et al., *Prion-like acceleration of a synucleinopathy in a transgenic mouse model*. Neurobiol Aging, 2012. **33**(9): p. 2225-8.
102. Watts, J.C., et al., *Transmission of multiple system atrophy prions to transgenic mice*. Proc Natl Acad Sci U S A, 2013. **110**(48): p. 19555-60.
103. Yamasaki, T.R., et al., *Parkinson's disease and multiple system atrophy have distinct alpha-synuclein seed characteristics*. J Biol Chem, 2019. **294**(3): p. 1045-1058.
104. Peng, C., et al., *Cellular milieu imparts distinct pathological alpha-synuclein strains in alpha-synucleinopathies*. Nature, 2018. **557**(7706): p. 558-563.
105. Dhillon, J.S., et al., *Dissecting alpha-synuclein inclusion pathology diversity in multiple system atrophy: implications for the prion-like transmission hypothesis*. Lab Invest, 2019. **99**(7): p. 982-992.
106. Jung, B.C., et al., *Amplification of distinct alpha-synuclein fibril conformers through protein misfolding cyclic amplification*. Exp Mol Med, 2017. **49**(4): p. e314.
107. Lau, A., et al., *alpha-Synuclein strains target distinct brain regions and cell types*. Nat Neurosci, 2020. **23**(1): p. 21-31.
108. Peelaerts, W., et al., *alpha-Synuclein strains cause distinct synucleinopathies after local and systemic administration*. Nature, 2015. **522**(7556): p. 340-4.
109. Sacino, A.N., et al., *Non-prion-type transmission in A53T alpha-synuclein transgenic mice: a normal component of spinal homogenates from naive non-transgenic mice induces robust alpha-synuclein pathology*. Acta Neuropathol, 2016. **131**(1): p. 151-4.
110. Bousset, L., et al., *Structural and functional characterization of two alpha-synuclein strains*. Nat Commun, 2013. **4**: p. 2575.
111. Kim, C., et al., *Exposure to bacterial endotoxin generates a distinct strain of alpha-synuclein fibril*. Sci Rep, 2016. **6**: p. 30891.
112. Guo, J.L., et al., *Distinct alpha-synuclein strains differentially promote tau inclusions in neurons*. Cell, 2013. **154**(1): p. 103-17.
113. Petkova, A.T., et al., *A structural model for Alzheimer's beta -amyloid fibrils based on experimental constraints from solid state NMR*. Proc Natl Acad Sci U S A, 2002. **99**(26): p. 16742-7.
114. Chen, G.F., et al., *Amyloid beta: structure, biology and structure-based therapeutic development*. Acta Pharmacol Sin, 2017. **38**(9): p. 1205-1235.
115. Yan, R., et al., *Membrane-anchored aspartyl protease with Alzheimer's disease beta-secretase activity*. Nature, 1999. **402**(6761): p. 533-7.
116. Modarresi, F., et al., *Knockdown of BACE1-AS Nonprotein-Coding Transcript Modulates Beta-Amyloid-Related Hippocampal Neurogenesis*. Int J Alzheimers Dis, 2011. **2011**: p. 929042.
117. Baumketner, A., et al., *Amyloid beta-protein monomer structure: a computational and experimental study*. Protein Sci, 2006. **15**(3): p. 420-8.
118. Vivekanandan, S., et al., *A partially folded structure of amyloid-beta(1-40) in an aqueous environment*. Biochem Biophys Res Commun, 2011. **411**(2): p. 312-6.
119. Zhang, S., et al., *The Alzheimer's peptide a beta adopts a collapsed coil structure in water*. J Struct Biol, 2000. **130**(2-3): p. 130-41.
120. Sgourakis, N.G., et al., *The Alzheimer's peptides Abeta40 and 42 adopt distinct conformations in water: a combined MD / NMR study*. J Mol Biol, 2007. **368**(5): p. 1448-57.
121. Yang, Y., et al., *Cryo-EM structures of amyloid-beta 42 filaments from human brains*. Science, 2022. **375**(6577): p. 167-172.
122. Kollmer, M., et al., *Cryo-EM structure and polymorphism of Abeta amyloid fibrils purified from Alzheimer's brain tissue*. Nat Commun, 2019. **10**(1): p. 4760.

123. Gremer, L., et al., *Fibril structure of amyloid-beta(1-42) by cryo-electron microscopy*. Science, 2017. **358**(6359): p. 116-119.
124. Puzzo, D. and O. Arancio, *Amyloid-beta peptide: Dr. Jekyll or Mr. Hyde?* J Alzheimers Dis, 2013. **33 Suppl 1**: p. S111-20.
125. Yankner, B.A., L.K. Duffy, and D.A. Kirschner, *Neurotrophic and neurotoxic effects of amyloid beta protein: reversal by tachykinin neuropeptides*. Science, 1990. **250**(4978): p. 279-82.
126. Kamenetz, F., et al., *APP processing and synaptic function*. Neuron, 2003. **37**(6): p. 925-37.
127. Cirrito, J.R., et al., *Synaptic activity regulates interstitial fluid amyloid-beta levels in vivo*. Neuron, 2005. **48**(6): p. 913-22.
128. Puzzo, D., et al., *Picomolar amyloid-beta positively modulates synaptic plasticity and memory in hippocampus*. J Neurosci, 2008. **28**(53): p. 14537-45.
129. Lanni, C., et al., *Beta-amyloid short- and long-term synaptic entanglement*. Pharmacol Res, 2019. **139**: p. 243-260.
130. Cerf, E., et al., *Antiparallel beta-sheet: a signature structure of the oligomeric amyloid beta-peptide*. Biochem J, 2009. **421**(3): p. 415-23.
131. Townsend, M., et al., *Effects of secreted oligomers of amyloid beta-protein on hippocampal synaptic plasticity: a potent role for trimers*. J Physiol, 2006. **572**(Pt 2): p. 477-92.
132. Martins, I.C., et al., *Lipids revert inert Abeta amyloid fibrils to neurotoxic protofibrils that affect learning in mice*. EMBO J, 2008. **27**(1): p. 224-33.
133. Xue, W.F., et al., *Fibril fragmentation enhances amyloid cytotoxicity*. J Biol Chem, 2009. **284**(49): p. 34272-82.
134. Angelova, P.R. and A.Y. Abramov, *Alpha-synuclein and beta-amyloid - different targets, same players: calcium, free radicals and mitochondria in the mechanism of neurodegeneration*. Biochem Biophys Res Commun, 2017. **483**(4): p. 1110-1115.
135. Mungarro-Menchaca, X., et al., *beta-Amyloid peptide induces ultrastructural changes in synaptosomes and potentiates mitochondrial dysfunction in the presence of ryanodine*. J Neurosci Res, 2002. **68**(1): p. 89-96.
136. Mossmann, D., et al., *Amyloid-beta peptide induces mitochondrial dysfunction by inhibition of preprotein maturation*. Cell Metab, 2014. **20**(4): p. 662-9.
137. Holscher, C., et al., *Soluble beta-amyloid[25-35] reversibly impairs hippocampal synaptic plasticity and spatial learning*. Eur J Pharmacol, 2007. **561**(1-3): p. 85-90.
138. Echeverria, V., et al., *Altered mitogen-activated protein kinase signaling, tau hyperphosphorylation and mild spatial learning dysfunction in transgenic rats expressing the beta-amyloid peptide intracellularly in hippocampal and cortical neurons*. Neuroscience, 2004. **129**(3): p. 583-92.
139. Fein, J.A., et al., *Co-localization of amyloid beta and tau pathology in Alzheimer's disease synaptosomes*. Am J Pathol, 2008. **172**(6): p. 1683-92.
140. Ott, S., et al., *Pre-aggregated Abeta1-42 peptide increases tau aggregation and hyperphosphorylation after short-term application*. Mol Cell Biochem, 2011. **349**(1-2): p. 169-77.
141. Benilova, I., E. Karran, and B. De Strooper, *The toxic Abeta oligomer and Alzheimer's disease: an emperor in need of clothes*. Nat Neurosci, 2012. **15**(3): p. 349-57.
142. Tycko, R., *Amyloid Polymorphism: Structural Basis and Neurobiological Relevance*. Neuron, 2015. **86**(3): p. 632-645.
143. Petkova, A.T., et al., *Self-propagating, molecular-level polymorphism in Alzheimer's beta-amyloid fibrils*. Science, 2005. **307**(5707): p. 262-5.
144. Meinhardt, J., et al., *Abeta(1-40) fibril polymorphism implies diverse interaction patterns in amyloid fibrils*. J Mol Biol, 2009. **386**(3): p. 869-77.
145. Stohr, J., et al., *Distinct synthetic Abeta prion strains producing different amyloid deposits in bigenic mice*. Proc Natl Acad Sci U S A, 2014. **111**(28): p. 10329-34.

146. Paravastu, A.K., et al., *Seeded growth of beta-amyloid fibrils from Alzheimer's brain-derived fibrils produces a distinct fibril structure*. Proc Natl Acad Sci U S A, 2009. **106**(18): p. 7443-8.
147. Lu, J.X., et al., *Molecular structure of beta-amyloid fibrils in Alzheimer's disease brain tissue*. Cell, 2013. **154**(6): p. 1257-68.
148. Heilbronner, G., et al., *Seeded strain-like transmission of beta-amyloid morphotypes in APP transgenic mice*. EMBO Rep, 2013. **14**(11): p. 1017-22.
149. Watts, J.C., et al., *Serial propagation of distinct strains of Abeta prions from Alzheimer's disease patients*. Proc Natl Acad Sci U S A, 2014. **111**(28): p. 10323-8.
150. Rasmussen, J., et al., *Amyloid polymorphisms constitute distinct clouds of conformational variants in different etiological subtypes of Alzheimer's disease*. Proc Natl Acad Sci U S A, 2017. **114**(49): p. 13018-13023.
151. Cohen, M.L., et al., *Rapidly progressive Alzheimer's disease features distinct structures of amyloid-beta*. Brain, 2015. **138**(Pt 4): p. 1009-22.
152. Qiang, W., et al., *Structural variation in amyloid-beta fibrils from Alzheimer's disease clinical subtypes*. Nature, 2017. **541**(7636): p. 217-221.
153. Colletier, J.P., et al., *Molecular basis for amyloid-beta polymorphism*. Proc Natl Acad Sci U S A, 2011. **108**(41): p. 16938-43.
154. Tycko, R., *Physical and structural basis for polymorphism in amyloid fibrils*. Protein Sci, 2014. **23**(11): p. 1528-39.
155. Close, W., et al., *Physical basis of amyloid fibril polymorphism*. Nat Commun, 2018. **9**(1): p. 699.
156. Tywoniuk, B., et al., *Amyloid Fibril Design: Limiting Structural Polymorphism in Alzheimer's Abeta Protofilaments*. J Phys Chem B, 2018. **122**(49): p. 11535-11545.
157. Chakraborty, D., J.E. Straub, and D. Thirumalai, *Differences in the free energies between the excited states of Abeta40 and Abeta42 monomers encode their aggregation propensities*. Proc Natl Acad Sci U S A, 2020.
158. Gonzalez-Montalban, N., et al., *Highly efficient protein misfolding cyclic amplification*. PLoS Pathog, 2011. **7**(2): p. e1001277.
159. Morales, R., et al., *Protein misfolding cyclic amplification of infectious prions*. Nat Protoc, 2012. **7**(7): p. 1397-409.
160. Gough, K.C., et al., *The oral secretion of infectious scrapie prions occurs in preclinical sheep with a range of PRNP genotypes*. J Virol, 2012. **86**(1): p. 566-71.
161. Maddison, B.C., et al., *The interaction of ruminant PrP(Sc) with soils is influenced by prion source and soil type*. Environ Sci Technol, 2010. **44**(22): p. 8503-8.
162. Gough, K.C., C.A. Baker, and B.C. Maddison, *An in vitro model for assessing effective scrapie decontamination*. Vet Microbiol, 2017. **207**: p. 138-142.
163. Herva, M.E., et al., *Anti-amyloid compounds inhibit alpha-synuclein aggregation induced by protein misfolding cyclic amplification (PMCA)*. J Biol Chem, 2014. **289**(17): p. 11897-905.
164. Ji, K., et al., *Inhibition effects of tanshinone on the aggregation of alpha-synuclein*. Food Funct, 2016. **7**(1): p. 409-16.
165. Shahnawaz, M., et al., *Development of a Biochemical Diagnosis of Parkinson Disease by Detection of alpha-Synuclein Misfolded Aggregates in Cerebrospinal Fluid*. JAMA Neurol, 2017. **74**(2): p. 163-172.
166. Salvadores, N., et al., *Detection of misfolded Abeta oligomers for sensitive biochemical diagnosis of Alzheimer's disease*. Cell Rep, 2014. **7**(1): p. 261-8.
167. Au, D.F., et al., *Solid-state NMR reveals a comprehensive view of the dynamics of the flexible, disordered N-terminal domain of amyloid-beta fibrils*. J Biol Chem, 2019. **294**(15): p. 5840-5853.
168. Singh, S. and M.L. DeMarco, *In Vitro Conversion Assays Diagnostic for Neurodegenerative Proteinopathies*. J Appl Lab Med, 2019.

169. LeVine, H., 3rd, *Thioflavine T interaction with synthetic Alzheimer's disease beta-amyloid peptides: detection of amyloid aggregation in solution*. *Protein Sci*, 1993. **2**(3): p. 404-10.
170. Hackl, E.V., et al., *Effect of acidic and basic pH on Thioflavin T absorbance and fluorescence*. *Eur Biophys J*, 2015. **44**(4): p. 249-61.
171. Barr, R.K., et al., *Validation and Characterization of a Novel Peptide That Binds Monomeric and Aggregated beta-Amyloid and Inhibits the Formation of Neurotoxic Oligomers*. *J Biol Chem*, 2016. **291**(2): p. 547-59.
172. De Genst, E.J., et al., *Structure and properties of a complex of alpha-synuclein and a single-domain camelid antibody*. *J Mol Biol*, 2010. **402**(2): p. 326-43.
173. Droste, P., et al., *Structural differences of amyloid-beta fibrils revealed by antibodies from phage display*. *BMC Biotechnol*, 2015. **15**: p. 57.
174. Emadi, S., et al., *Detecting morphologically distinct oligomeric forms of alpha-synuclein*. *J Biol Chem*, 2009. **284**(17): p. 11048-58.
175. Emadi, S., et al., *Inhibiting aggregation of alpha-synuclein with human single chain antibody fragments*. *Biochemistry*, 2004. **43**(10): p. 2871-8.
176. Habicht, G., et al., *Directed selection of a conformational antibody domain that prevents mature amyloid fibril formation by stabilizing Abeta protofibrils*. *Proc Natl Acad Sci U S A*, 2007. **104**(49): p. 19232-7.
177. Kasturirangan, S., et al., *Nanobody specific for oligomeric beta-amyloid stabilizes nontoxic form*. *Neurobiol Aging*, 2012. **33**(7): p. 1320-8.
178. Kawasaki, T., K. Onodera, and S. Kamijo, *Selection of peptide inhibitors of soluble Abeta(1-42) oligomer formation by phage display*. *Biosci Biotechnol Biochem*, 2010. **74**(11): p. 2214-9.
179. Limbocker, R., et al., *Rationally Designed Antibodies as Research Tools to Study the Structure-Toxicity Relationship of Amyloid-beta Oligomers*. *Int J Mol Sci*, 2020. **21**(12).
180. Munke, A., et al., *Phage display and kinetic selection of antibodies that specifically inhibit amyloid self-replication*. *Proc Natl Acad Sci U S A*, 2017. **114**(25): p. 6444-6449.
181. Orner, B.P., et al., *Phage display affords peptides that modulate beta-amyloid aggregation*. *J Am Chem Soc*, 2006. **128**(36): p. 11882-9.
182. Biancalana, M. and S. Koide, *Molecular mechanism of Thioflavin-T binding to amyloid fibrils*. *Biochim Biophys Acta*, 2010. **1804**(7): p. 1405-12.
183. Kumar, H., et al., *Modulation of the extent of structural heterogeneity in alpha-synuclein fibrils by the small molecule thioflavin T*. *J Biol Chem*, 2017. **292**(41): p. 16891-16903.
184. Hatami, A., et al., *Familial Alzheimer's Disease Mutations within the Amyloid Precursor Protein Alter the Aggregation and Conformation of the Amyloid-beta Peptide*. *J Biol Chem*, 2017. **292**(8): p. 3172-3185.
185. Cohen, F.E. and J.W. Kelly, *Therapeutic approaches to protein-misfolding diseases*. *Nature*, 2003. **426**(6968): p. 905-9.
186. Lindstrom, V., et al., *Immunotherapy targeting alpha-synuclein, with relevance for future treatment of Parkinson's disease and other Lewy body disorders*. *Immunotherapy*, 2014. **6**(2): p. 141-53.
187. Lannfelt, L., N.R. Relkin, and E.R. Siemers, *Amyloid-ss-directed immunotherapy for Alzheimer's disease*. *J Intern Med*, 2014. **275**(3): p. 284-95.
188. Morgan, D., *Immunotherapy for Alzheimer's disease*. *J Intern Med*, 2011. **269**(1): p. 54-63.
189. Oertel, W. and J.B. Schulz, *Current and experimental treatments of Parkinson disease: A guide for neuroscientists*. *J Neurochem*, 2016. **139** Suppl 1: p. 325-337.
190. Schenk, D.B., et al., *First-in-human assessment of PRX002, an anti-alpha-synuclein monoclonal antibody, in healthy volunteers*. *Mov Disord*, 2017. **32**(2): p. 211-218.
191. Weihofen, A., et al., *Development of an aggregate-selective, human-derived alpha-synuclein antibody BIIB054 that ameliorates disease phenotypes in Parkinson's disease models*. *Neurobiol Dis*, 2019. **124**: p. 276-288.

192. Brys, M., et al., *Randomized phase I clinical trial of anti-alpha-synuclein antibody B1B054*. *Mov Disord*, 2019. **34**(8): p. 1154-1163.
193. Schofield, D.J., et al., *Preclinical development of a high affinity alpha-synuclein antibody, MEDI1341, that can enter the brain, sequester extracellular alpha-synuclein and attenuate alpha-synuclein spreading in vivo*. *Neurobiol Dis*, 2019. **132**: p. 104582.
194. Brundin, P., K.D. Dave, and J.H. Kordower, *Therapeutic approaches to target alpha-synuclein pathology*. *Exp Neurol*, 2017. **298**(Pt B): p. 225-235.
195. Wang, Z., et al., *Progress of immunotherapy of anti-alpha-synuclein in Parkinson's disease*. *Biomed Pharmacother*, 2019. **115**: p. 108843.
196. Fields, C.R., N. Bengoa-Vergniory, and R. Wade-Martins, *Targeting Alpha-Synuclein as a Therapy for Parkinson's Disease*. *Front Mol Neurosci*, 2019. **12**: p. 299.
197. Jamal, F., *Immunotherapies Targeting alpha-Synuclein in Parkinson Disease*. *Fed Pract*, 2020. **37**(8): p. 375-379.
198. Geylis, V., et al., *Human monoclonal antibodies against amyloid-beta from healthy adults*. *Neurobiol Aging*, 2005. **26**(5): p. 597-606.
199. Schenk, D., M. Hagen, and P. Seubert, *Current progress in beta-amyloid immunotherapy*. *Curr Opin Immunol*, 2004. **16**(5): p. 599-606.
200. Wilcock, D.M. and C.A. Colton, *Anti-amyloid-beta immunotherapy in Alzheimer's disease: relevance of transgenic mouse studies to clinical trials*. *J Alzheimers Dis*, 2008. **15**(4): p. 555-69.
201. Lannfelt, L., et al., *Perspectives on future Alzheimer therapies: amyloid-beta protofibrils - a new target for immunotherapy with BAN2401 in Alzheimer's disease*. *Alzheimers Res Ther*, 2014. **6**(2): p. 16.
202. Godyn, J., et al., *Therapeutic strategies for Alzheimer's disease in clinical trials*. *Pharmacol Rep*, 2016. **68**(1): p. 127-38.
203. Zampar, S. and O. Wirths, *Immunotherapy Targeting Amyloid-beta Peptides in Alzheimer's Disease*, in *Alzheimer's Disease: Drug Discovery*, X. Huang, Editor. 2020: Brisbane (AU).
204. Tolar, M., et al., *Aducanumab, gantenerumab, BAN2401, and ALZ-801-the first wave of amyloid-targeting drugs for Alzheimer's disease with potential for near term approval*. *Alzheimers Res Ther*, 2020. **12**(1): p. 95.
205. Vaz, M. and S. Silvestre, *Alzheimer's disease: Recent treatment strategies*. *Eur J Pharmacol*, 2020. **887**: p. 173554.
206. Rygiel, K., *Novel strategies for Alzheimer's disease treatment: An overview of anti-amyloid beta monoclonal antibodies*. *Indian J Pharmacol*, 2016. **48**(6): p. 629-636.
207. Dodart, J.C., et al., *Immunization reverses memory deficits without reducing brain Abeta burden in Alzheimer's disease model*. *Nat Neurosci*, 2002. **5**(5): p. 452-7.
208. Mably, A.J., et al., *Anti-Abeta antibodies incapable of reducing cerebral Abeta oligomers fail to attenuate spatial reference memory deficits in J20 mice*. *Neurobiol Dis*, 2015. **82**: p. 372-384.
209. Ostrowitzki, S., et al., *Mechanism of amyloid removal in patients with Alzheimer disease treated with gantenerumab*. *Arch Neurol*, 2012. **69**(2): p. 198-207.
210. Bohrmann, B., et al., *Gantenerumab: a novel human anti-Abeta antibody demonstrates sustained cerebral amyloid-beta binding and elicits cell-mediated removal of human amyloid-beta*. *J Alzheimers Dis*, 2012. **28**(1): p. 49-69.
211. Lord, A., et al., *An amyloid-beta protofibril-selective antibody prevents amyloid formation in a mouse model of Alzheimer's disease*. *Neurobiol Dis*, 2009. **36**(3): p. 425-34.
212. Ostenfeld, T., et al., *EVALUATION OF SAFETY, TOLERABILITY, PHARMACOKINETICS AND PHARMACODYNAMICS OF MEDI1814, A BETA-AMYLOID 42 (A β 42)-SPECIFIC ANTIBODY, IN PATIENTS WITH MILD-MODERATE ALZHEIMER'S DISEASE*. *Alzheimer's & Dementia*, 2017. **13**(7, Supplement): p. P574.

213. Pradier, L., et al., *SAR228810: an antibody for protofibrillar amyloid beta peptide designed to reduce the risk of amyloid-related imaging abnormalities (ARIA)*. *Alzheimers Res Ther*, 2018. **10**(1): p. 117.
214. Taupin, V., et al., *ANTI-AMYLOID ANTIBODIES AS A POTENTIAL THERAPEUTIC FOR ALZHEIMER'S DISEASE: NEUROPROTECTIVE ACTIVITY OF SAR228810 AGAINST AMYLOID-INDUCED NEUROTOXICITY IN VITRO*. *Alzheimer's & Dementia*, 2017. **13**(7, Supplement): p. P944.
215. Sevigny, J., et al., *The antibody aducanumab reduces Abeta plaques in Alzheimer's disease*. *Nature*, 2016. **537**(7618): p. 50-6.
216. Knopman, D.S., D.T. Jones, and M.D. Greicius, *Failure to demonstrate efficacy of aducanumab: An analysis of the EMERGE and ENGAGE trials as reported by Biogen, December 2019*. *Alzheimers Dement*, 2021. **17**(4): p. 696-701.
217. Lambracht-Washington, D. and R.N. Rosenberg, *Anti-amyloid beta to tau - based immunization: Developments in immunotherapy for Alzheimer disease*. *Immunotargets Ther*, 2013. **2013**(2): p. 105-114.
218. Li, C. and J. Gotz, *Tau-based therapies in neurodegeneration: opportunities and challenges*. *Nat Rev Drug Discov*, 2017. **16**(12): p. 863-883.
219. Goni, F., et al., *Anti-beta-sheet conformation monoclonal antibody reduces tau and Abeta oligomer pathology in an Alzheimer's disease model*. *Alzheimers Res Ther*, 2018. **10**(1): p. 10.
220. Herline, K., et al., *Immunotherapy to improve cognition and reduce pathological species in an Alzheimer's disease mouse model*. *Alzheimers Res Ther*, 2018. **10**(1): p. 54.
221. Kehoe, J.W. and B.K. Kay, *Filamentous phage display in the new millennium*. *Chem Rev*, 2005. **105**(11): p. 4056-72.
222. Ministro, J., A.M. Manuel, and J. Goncalves, *Therapeutic Antibody Engineering and Selection Strategies*. *Adv Biochem Eng Biotechnol*, 2020. **171**: p. 55-86.
223. Chan, C.E., et al., *The role of phage display in therapeutic antibody discovery*. *Int Immunol*, 2014. **26**(12): p. 649-57.
224. Ledsgaard, L., et al., *Basics of Antibody Phage Display Technology*. *Toxins (Basel)*, 2018. **10**(6).
225. Crosby, W.L. and P. Schorr, *Principles and applications of recombinant antibody phage display technology to plant biology*. *Methods Cell Biol*, 1995. **50**: p. 85-99.
226. Hoogenboom, H.R., *Overview of antibody phage-display technology and its applications*. *Methods Mol Biol*, 2002. **178**: p. 1-37.
227. Hoogenboom, H.R., et al., *Antibody phage display technology and its applications*. *Immunotechnology*, 1998. **4**(1): p. 1-20.
228. Reader, R.H., et al., *Advances in the Production and Batch Reformating of Phage Antibody Libraries*. *Mol Biotechnol*, 2019. **61**(11): p. 801-815.
229. van Wezenbeek, P.M., T.J. Hulsebos, and J.G. Schoenmakers, *Nucleotide sequence of the filamentous bacteriophage M13 DNA genome: comparison with phage fd*. *Gene*, 1980. **11**(1-2): p. 129-48.
230. Manoutcharian, K., et al., *Amyloid-beta peptide-specific single chain Fv antibodies isolated from an immune phage display library*. *J Neuroimmunol*, 2003. **145**(1-2): p. 12-7.
231. Medecigo, M., et al., *Novel amyloid-beta specific scFv and VH antibody fragments from human and mouse phage display antibody libraries*. *J Neuroimmunol*, 2010. **223**(1-2): p. 104-14.
232. Sebollela, A., et al., *A human scFv antibody that targets and neutralizes high molecular weight pathogenic amyloid-beta oligomers*. *J Neurochem*, 2017. **142**(6): p. 934-947.
233. Wang, J., et al., *Effects of an amyloid-beta 1-42 oligomers antibody screened from a phage display library in APP/PS1 transgenic mice*. *Brain Res*, 2016. **1635**: p. 169-79.
234. Marcus, W.D., et al., *Characterization of an antibody scFv that recognizes fibrillar insulin and beta-amyloid using atomic force microscopy*. *Nanomedicine*, 2008. **4**(1): p. 1-7.

235. Dorresteyn, B., et al., *Camelid heavy chain only antibody fragment domain against beta-site of amyloid precursor protein cleaving enzyme 1 inhibits beta-secretase activity in vitro and in vivo*. FEBS J, 2015. **282**(18): p. 3618-31.
236. Rauchenberger, R., et al., *Human combinatorial Fab library yielding specific and functional antibodies against the human fibroblast growth factor receptor 3*. J Biol Chem, 2003. **278**(40): p. 38194-205.
237. Williams, T., et al., *Nanobodies raised against monomeric alpha-synuclein distinguish between fibrils at different maturation stages*. J Mol Biol, 2013. **425**(14): p. 2397-411.
238. Iljina, M., et al., *Nanobodies raised against monomeric alpha-synuclein inhibit fibril formation and destabilize toxic oligomeric species*. BMC Biol, 2017. **15**(1): p. 57.
239. Vaikath, N.N., et al., *Generation and characterization of novel conformation-specific monoclonal antibodies for alpha-synuclein pathology*. Neurobiol Dis, 2015. **79**: p. 81-99.
240. Gupta, V., et al., *Fibrillar form of alpha-synuclein-specific scFv antibody inhibits alpha-synuclein seeds induced aggregation and toxicity*. Sci Rep, 2020. **10**(1): p. 8137.
241. Frenkel, D., M. Dori, and B. Solomon, *Generation of anti-beta-amyloid antibodies via phage display technology*. Vaccine, 2004. **22**(19): p. 2505-8.
242. Solomon, B., *Generation of anti-beta-amyloid antibodies via phage display technology towards Alzheimer's disease vaccination*. Vaccine, 2005. **23**(17-18): p. 2327-30.
243. Solomon, B., *Active immunization against Alzheimer's beta-amyloid peptide using phage display technology*. Vaccine, 2007. **25**(16): p. 3053-6.
244. Ryan, T.M., et al., *Ammonium hydroxide treatment of Aβ produces an aggregate free solution suitable for biophysical and cell culture characterization*. PeerJ, 2013. **1**: p. e73.
245. Ryan, T.M., et al., *Small amphipathic molecules modulate secondary structure and amyloid fibril-forming kinetics of Alzheimer disease peptide Aβ(1-42)*. J Biol Chem, 2012. **287**(20): p. 16947-54.
246. Teplow, D.B., *Preparation of amyloid beta-protein for structural and functional studies*. Methods Enzymol, 2006. **413**: p. 20-33.
247. Pollard, A.K., E.L. Craig, and L. Chakrabarti, *Mitochondrial Complex 1 Activity Measured by Spectrophotometry Is Reduced across All Brain Regions in Ageing and More Specifically in Neurodegeneration*. PLoS One, 2016. **11**(6): p. e0157405.
248. Sabir, J.S., et al., *Construction of naive camelids VHH repertoire in phage display-based library*. C R Biol, 2014. **337**(4): p. 244-9.
249. Choi, J.R., et al., *BLI-Based Functional Assay in Phage Display Benefits the Development of a PD-L1-Targeting Therapeutic Antibody*. Viruses, 2020. **12**(6).
250. Heller, G.T., et al., *Small-molecule sequestration of amyloid-beta as a drug discovery strategy for Alzheimer's disease*. Sci Adv, 2020. **6**(45).
251. Li, X., et al., *Screening, Identification, and Characterization of an Affinity Peptide Specific to MT1-MMP and Its Application in Tumor Imaging*. Bioconjug Chem, 2019. **30**(5): p. 1507-1517.
252. Muller-Esparza, H., et al., *Bio-Layer Interferometry Analysis of the Target Binding Activity of CRISPR-Cas Effector Complexes*. Front Mol Biosci, 2020. **7**: p. 98.
253. Ortega, P.A., et al., *Selection of a Single Domain Antibody, Specific for an HLA-Bound Epitope of the Mycobacterial Ag85B Antigen*. Front Immunol, 2020. **11**: p. 577815.
254. Ylera, F., et al., *Off-rate screening for selection of high-affinity anti-drug antibodies*. Anal Biochem, 2013. **441**(2): p. 208-13.
255. Emamzadeh, F.N., et al., *Effects of different isoforms of apoE on aggregation of the alpha-synuclein protein implicated in Parkinson's disease*. Neurosci Lett, 2016. **618**: p. 146-151.
256. Thorne, L., et al., *In vitro amplification of ovine prions from scrapie-infected sheep from Great Britain reveals distinct patterns of propagation*. BMC Vet Res, 2012. **8**: p. 223.
257. Sano, K., et al., *Prion-Like Seeding of Misfolded alpha-Synuclein in the Brains of Dementia with Lewy Body Patients in RT-QUIC*. Mol Neurobiol, 2018. **55**(5): p. 3916-3930.

258. Bernis, M.E., et al., *Prion-like propagation of human brain-derived alpha-synuclein in transgenic mice expressing human wild-type alpha-synuclein*. *Acta Neuropathol Commun*, 2015. **3**: p. 75.
259. Mason, D.M., et al., *Transmission of alpha-synucleinopathy from olfactory structures deep into the temporal lobe*. *Mol Neurodegener*, 2016. **11**(1): p. 49.
260. Tarutani, A., et al., *Potent prion-like behaviors of pathogenic alpha-synuclein and evaluation of inactivation methods*. *Acta Neuropathol Commun*, 2018. **6**(1): p. 29.
261. Becker, K., et al., *Detecting Alpha Synuclein Seeding Activity in Formaldehyde-Fixed MSA Patient Tissue by PMCA*. *Mol Neurobiol*, 2018. **55**(11): p. 8728-8737.
262. Nicot, S., et al., *Seeded propagation of alpha-synuclein aggregation in mouse brain using protein misfolding cyclic amplification*. *FASEB J*, 2019: p. fj201900354R.
263. De Luca, C.M.G., et al., *Efficient RT-QuIC seeding activity for alpha-synuclein in olfactory mucosa samples of patients with Parkinson's disease and multiple system atrophy*. *Transl Neurodegener*, 2019. **8**: p. 24.
264. Kovacs, G.G., et al., *An antibody with high reactivity for disease-associated alpha-synuclein reveals extensive brain pathology*. *Acta Neuropathol*, 2012. **124**(1): p. 37-50.
265. Thomzig, A., et al., *Transmissible alpha-synuclein seeding activity in brain and stomach of patients with Parkinson's disease*. *Acta Neuropathol*, 2021. **141**(6): p. 861-879.
266. Owen, J.P., et al., *Use of thermolysin in the diagnosis of prion diseases*. *Mol Biotechnol*, 2007. **35**(2): p. 161-70.
267. Owen, J.P., et al., *Molecular profiling of ovine prion diseases by using thermolysin-resistant PrP^{Sc} and endogenous C2 PrP fragments*. *J Virol*, 2007. **81**(19): p. 10532-9.
268. Tamguney, G. and A.D. Korczyn, *A critical review of the prion hypothesis of human synucleinopathies*. *Cell Tissue Res*, 2018. **373**(1): p. 213-220.
269. Melki, R., *Role of Different Alpha-Synuclein Strains in Synucleinopathies, Similarities with other Neurodegenerative Diseases*. *J Parkinsons Dis*, 2015. **5**(2): p. 217-27.
270. Paciotti, S., et al., *Are We Ready for Detecting alpha-Synuclein Prone to Aggregation in Patients? The Case of "Protein-Misfolding Cyclic Amplification" and "Real-Time Quaking-Induced Conversion" as Diagnostic Tools*. *Front Neurol*, 2018. **9**: p. 415.
271. Yoshinaga, S., et al., *Preserved proteinase K-resistant core after amplification of alpha-synuclein aggregates: Implication to disease-related structural study*. *Biochem Biophys Res Commun*, 2019.
272. Fairfoul, G., et al., *Alpha-synuclein RT-QuIC in the CSF of patients with alpha-synucleinopathies*. *Ann Clin Transl Neurol*, 2016. **3**(10): p. 812-818.
273. Groveman, B.R., et al., *Rapid and ultra-sensitive quantitation of disease-associated alpha-synuclein seeds in brain and cerebrospinal fluid by alphaSyn RT-QuIC*. *Acta Neuropathol Commun*, 2018. **6**(1): p. 7.
274. Singer, W., et al., *Alpha-Synuclein Oligomers and Neurofilament Light Chain in Spinal Fluid Differentiate Multiple System Atrophy from Lewy Body Synucleinopathies*. *Ann Neurol*, 2020. **88**(3): p. 503-512.
275. Wang, Z., et al., *Skin alpha-Synuclein Aggregation Seeding Activity as a Novel Biomarker for Parkinson Disease*. *JAMA Neurol*, 2020.
276. Haley, N.J. and J.A. Richt, *Evolution of Diagnostic Tests for Chronic Wasting Disease, a Naturally Occurring Prion Disease of Cervids*. *Pathogens*, 2017. **6**(3).
277. Greenfield, N.J., *Using circular dichroism spectra to estimate protein secondary structure*. *Nat Protoc*, 2006. **1**(6): p. 2876-90.
278. Kelly, S.M., T.J. Jess, and N.C. Price, *How to study proteins by circular dichroism*. *Biochim Biophys Acta*, 2005. **1751**(2): p. 119-39.
279. Murphy, M.P. and H. LeVine, 3rd, *Alzheimer's disease and the amyloid-beta peptide*. *J Alzheimers Dis*, 2010. **19**(1): p. 311-23.

280. Pitschke, M., et al., *Detection of single amyloid beta-protein aggregates in the cerebrospinal fluid of Alzheimer's patients by fluorescence correlation spectroscopy*. Nat Med, 1998. **4**(7): p. 832-4.
281. Schmidt, M., et al., *Comparison of Alzheimer Abeta(1-40) and Abeta(1-42) amyloid fibrils reveals similar protofilament structures*. Proc Natl Acad Sci U S A, 2009. **106**(47): p. 19813-8.
282. Xue, W.F., S.W. Homans, and S.E. Radford, *Systematic analysis of nucleation-dependent polymerization reveals new insights into the mechanism of amyloid self-assembly*. Proc Natl Acad Sci U S A, 2008. **105**(26): p. 8926-31.
283. Liu, J., et al., *Amyloid structure exhibits polymorphism on multiple length scales in human brain tissue*. Sci Rep, 2016. **6**: p. 33079.
284. Johnson, C.J., et al., *Highly efficient amplification of chronic wasting disease agent by protein misfolding cyclic amplification with beads (PMCAb)*. PLoS One, 2012. **7**(4): p. e35383.
285. Murayama, Y., et al., *Efficient in vitro amplification of a mouse-adapted scrapie prion protein*. Neurosci Lett, 2007. **413**(3): p. 270-3.
286. Murayama, Y., et al., *Sulfated dextrans enhance in vitro amplification of bovine spongiform encephalopathy PrP(Sc) and enable ultrasensitive detection of bovine PrP(Sc)*. PLoS One, 2010. **5**(10).
287. Matus, M.A.B., *Modelling Human Prion Replication in Cell-free Systems*. 2014.
288. Ellett, L.J., et al., *Glycosaminoglycan sulfation determines the biochemical properties of prion protein aggregates*. Glycobiology, 2015. **25**(7): p. 745-755.
289. Imamura, M., et al., *Heparan Sulfate and Heparin Promote Faithful Prion Replication in Vitro by Binding to Normal and Abnormal Prion Proteins in Protein Misfolding Cyclic Amplification*. J Biol Chem, 2016. **291**(51): p. 26478-26486.
290. Shaked, G.M., et al., *Reconstitution of prion infectivity from solubilized protease-resistant PrP and nonprotein components of prion rods*. J Biol Chem, 2001. **276**(17): p. 14324-8.
291. Stewart, K.L. and S.E. Radford, *Amyloid plaques beyond Abeta: a survey of the diverse modulators of amyloid aggregation*. Biophys Rev, 2017. **9**(4): p. 405-419.
292. Broersen, K., et al., *A standardized and biocompatible preparation of aggregate-free amyloid beta peptide for biophysical and biological studies of Alzheimer's disease*. Protein Eng Des Sel, 2011. **24**(9): p. 743-50.
293. Brender, J.R., et al., *Probing the sources of the apparent irreproducibility of amyloid formation: drastic changes in kinetics and a switch in mechanism due to micellelike oligomer formation at critical concentrations of IAPP*. J Phys Chem B, 2015. **119**(7): p. 2886-96.
294. Deleault, N.R., et al., *Protease-resistant prion protein amplification reconstituted with partially purified substrates and synthetic polyanions*. J Biol Chem, 2005. **280**(29): p. 26873-9.
295. Supattapone, S., *Prion protein conversion in vitro*. J Mol Med (Berl), 2004. **82**(6): p. 348-56.
296. Dean, D.N., et al., *Strain-specific Fibril Propagation by an A beta Dodecamer*. Scientific Reports, 2017. **7**.
297. Vaughan, T.J., et al., *Human antibodies with sub-nanomolar affinities isolated from a large non-immunized phage display library*. Nat Biotechnol, 1996. **14**(3): p. 309-14.
298. Bannas, P., J. Hambach, and F. Koch-Nolte, *Nanobodies and Nanobody-Based Human Heavy Chain Antibodies As Antitumor Therapeutics*. Front Immunol, 2017. **8**: p. 1603.
299. Kim, H. and M. Ho, *Isolation of Antibodies to Heparan Sulfate on Glypicans by Phage Display*. Curr Protoc Protein Sci, 2018. **94**(1): p. e66.
300. Brannstrom, K., et al., *A generic method for design of oligomer-specific antibodies*. PLoS One, 2014. **9**(3): p. e90857.
301. Cohen, S.I., et al., *From macroscopic measurements to microscopic mechanisms of protein aggregation*. J Mol Biol, 2012. **421**(2-3): p. 160-71.

302. Bunce, S.J., et al., *Molecular insights into the surface-catalyzed secondary nucleation of amyloid-beta40 (Abeta40) by the peptide fragment Abeta16-22*. *Sci Adv*, 2019. **5**(6): p. eaav8216.
303. Giorgetti, S., et al., *Targeting Amyloid Aggregation: An Overview of Strategies and Mechanisms*. *Int J Mol Sci*, 2018. **19**(9).
304. Aprile, F.A., et al., *Selective targeting of primary and secondary nucleation pathways in Abeta42 aggregation using a rational antibody scanning method*. *Sci Adv*, 2017. **3**(6): p. e1700488.
305. Bandopadhyay, R., *Sequential Extraction of Soluble and Insoluble Alpha-Synuclein from Parkinsonian Brains*. *J Vis Exp*, 2016(107).
306. Xie, H.R., L.S. Hu, and G.Y. Li, *SH-SY5Y human neuroblastoma cell line: in vitro cell model of dopaminergic neurons in Parkinson's disease*. *Chin Med J (Engl)*, 2010. **123**(8): p. 1086-92.
307. Xicoy, H., B. Wieringa, and G.J. Martens, *The SH-SY5Y cell line in Parkinson's disease research: a systematic review*. *Mol Neurodegener*, 2017. **12**(1): p. 10.
308. Ju, C., et al., *Neuroprotective effect of chondroitin sulfate on SHSY5Y cells overexpressing wildtype or A53T mutant alphasynuclein*. *Mol Med Rep*, 2017. **16**(6): p. 8721-8728.
309. Pieri, L., et al., *Cellular response of human neuroblastoma cells to alpha-synuclein fibrils, the main constituent of Lewy bodies*. *Biochim Biophys Acta*, 2016. **1860**(1 Pt A): p. 8-19.
310. Balducci, C., et al., *Synthetic amyloid-beta oligomers impair long-term memory independently of cellular prion protein*. *Proceedings of the National Academy of Sciences of the United States of America*, 2010. **107**(5): p. 2295-2300.
311. Gotz, J., et al., *Formation of neurofibrillary tangles in P301L tau transgenic mice induced by A beta 42 fibrils*. *Science*, 2001. **293**(5534): p. 1491-1495.
312. Haigh, C.L. and S.C. Drew, *Cavitation during the protein misfolding cyclic amplification (PMCA) method--The trigger for de novo prion generation?* *Biochem Biophys Res Commun*, 2015. **461**(3): p. 494-500.
313. Faller, P. and C. Hureau, *Reproducibility Problems of Amyloid-beta Self-Assembly and How to Deal With Them*. *Front Chem*, 2020. **8**: p. 611227.
314. Foley, A.R. and J.A. Raskatov, *Assessing Reproducibility in Amyloid beta Research: Impact of Abeta Sources on Experimental Outcomes*. *Chembiochem*, 2020. **21**(17): p. 2425-2430.
315. Datki, Z., et al., *Method for measuring neurotoxicity of aggregating polypeptides with the MTT assay on differentiated neuroblastoma cells*. *Brain Res Bull*, 2003. **62**(3): p. 223-9.
316. Finder, V.H., et al., *The recombinant amyloid-beta peptide Abeta1-42 aggregates faster and is more neurotoxic than synthetic Abeta1-42*. *J Mol Biol*, 2010. **396**(1): p. 9-18.
317. Stephens, A.D., et al., *Fast Purification of Recombinant Monomeric Amyloid-beta from E. coli and Amyloid-beta-mCherry Aggregates from Mammalian Cells*. *ACS Chem Neurosci*, 2020. **11**(20): p. 3204-3213.
318. Harmsen, M.M. and H.J. De Haard, *Properties, production, and applications of camelid single-domain antibody fragments*. *Appl Microbiol Biotechnol*, 2007. **77**(1): p. 13-22.
319. Vu, K.B., et al., *Comparison of llama VH sequences from conventional and heavy chain antibodies*. *Mol Immunol*, 1997. **34**(16-17): p. 1121-31.
320. Thacker, D., et al., *The role of fibril structure and surface hydrophobicity in secondary nucleation of amyloid fibrils*. *Proc Natl Acad Sci U S A*, 2020. **117**(41): p. 25272-25283.
321. Klarenbeek, A., et al., *Camelid Ig V genes reveal significant human homology not seen in therapeutic target genes, providing for a powerful therapeutic antibody platform*. *MAbs*, 2015. **7**(4): p. 693-706.
322. Muyldermans, S., *A guide to: generation and design of nanobodies*. *FEBS J*, 2021. **288**(7): p. 2084-2102.
323. Vincke, C., et al., *General strategy to humanize a camelid single-domain antibody and identification of a universal humanized nanobody scaffold*. *J Biol Chem*, 2009. **284**(5): p. 3273-3284.

324. Conrath, K., et al., *Antigen binding and solubility effects upon the veneering of a camel VHH in framework-2 to mimic a VH*. J Mol Biol, 2005. **350**(1): p. 112-25.
325. Muyldermans, S., et al., *Sequence and structure of VH domain from naturally occurring camel heavy chain immunoglobulins lacking light chains*. Protein Eng, 1994. **7**(9): p. 1129-35.
326. Almagro, J.C. and J. Fransson, *Humanization of antibodies*. Front Biosci, 2008. **13**: p. 1619-33.
327. D'Huyvetter, M., et al., *Radiolabeled nanobodies as theranostic tools in targeted radionuclide therapy of cancer*. Expert Opin Drug Deliv, 2014. **11**(12): p. 1939-54.
328. De Vos, J., et al., *Camelid single-domain antibody-fragment engineering for (pre)clinical in vivo molecular imaging applications: adjusting the bullet to its target*. Expert Opin Biol Ther, 2013. **13**(8): p. 1149-60.
329. Hrynachak, I., et al., *Nanobody-Based Theranostic Agents for HER2-Positive Breast Cancer: Radiolabeling Strategies*. Int J Mol Sci, 2021. **22**(19).
330. Huang, L., et al., *SPECT imaging with 99mTc-labeled EGFR-specific nanobody for in vivo monitoring of EGFR expression*. Mol Imaging Biol, 2008. **10**(3): p. 167-75.
331. Keyaerts, M., et al., *Phase I Study of 68Ga-HER2-Nanobody for PET/CT Assessment of HER2 Expression in Breast Carcinoma*. J Nucl Med, 2016. **57**(1): p. 27-33.
332. Schoonooghe, S., et al., *Novel applications of nanobodies for in vivo bio-imaging of inflamed tissues in inflammatory diseases and cancer*. Immunobiology, 2012. **217**(12): p. 1266-72.
333. Senders, M.L., et al., *Nanobody-Facilitated Multiparametric PET/MRI Phenotyping of Atherosclerosis*. JACC Cardiovasc Imaging, 2019. **12**(10): p. 2015-2026.